IDENTIFYING AND CHARACTERIZING MOLECULAR PARAMETERS THAT MODULATE THE ENDOSOMAL ESCAPE OF CATIONIC CELL- PENETRATING PEPTIDES: A STRUCTURE ACTIVITY APPROACH

A Dissertation

by

KRISTINA NAJJAR

Submitted to the Office of Graduate and Professional Studies of
Texas A&M University
in partial fulfillment of the requirement for the degree of
DOCTOR OF PHILOSOPHY

Chair of Committee,	Jean-Philippe Pellois
Committee Members,	Hays S. Rye
	James Sacchettini
	Robert Burghardt
Head of Department,	Gregory D. Reinhart

August 2017

Major Subject: Biochemistry

ABSTRACT

For over 20 years, cell-penetrating peptides (CPPs) have been used as delivery vectors transporting macromolecules (cargos) into live cells for cell biology manipulations and therapeutic applications. While the exact mechanism of cell penetration remains controversial, it is thought that CPPs are first internalized inside endocytic vesicles and have been reported to escape to the cytosolic space of cells. However, while the internalization of CPPs inside vesicles has proven to be highly efficient, their endosomal escape activity remains suboptimal and poorly understood. This is a severe limitation of the CPP-mediated delivery approach because the macromolecules' escape is essential if the cargo is to interact with its cytosolic/nuclear targets. Multiple approaches to enhance CPP's endosomolytic activity have been explored (summarized in Chapter 1). Multivalency has been proposed as a possible new approach, in which multiple copies of a molecule are attached as one functional unit. It has been hypothesized that the use of multivalent CPPs will result in an increase in their local concentration at the membrane; and as a consequence enhance their membrane disruption property.

In Chapter 2, I report on the generation of a multivalent CPP: dfTAT, a dimeric version of the most studied CPP, TAT. Similar to TAT, dfTAT enters cells via macropinocytosis. Interestingly, while monomeric TAT is extremely inefficient at escaping the endocytic pathway, I demonstrate that dfTAT escapes endosomes with an unprecedented level of efficiency. Cytosolic penetration of dfTAT can be achieved in

multiple cell lines and primary cells, without impacting the cell's physiology. Most importantly, dfTAT can efficiently deliver a wide variety of macromolecules and cell-impermeable small molecules efficiently into the cytosolic space of live cells.

In Chapter 3, I report on the role that chirality and protease-resistance have on the endosomal escape behavior of dfTAT. By inverting dfTAT's chirality from L to D stereochemistry, I generated a protease-resistant dfTAT (D-dfTAT). Interestingly, I show that while the mechanism of cellular entry remains the same, D-dfTAT's cellular internalization is substantially lower than dfTAT. Nonetheless, once in the endosome, D-dfTAT escapes with a higher efficiency than its L-counterpart. Finally, while dfTAT treatment is relatively innocuous to cells, D-dfTAT unexpectedly exerted a prolonged anti-proliferative activity.

The literature underscores the important role that arginine residues play in CPP cellular internalization. However, due to the low endosomolytic activity of most CPPs, residues vital for endosomal escape have not yet been established. In Chapter 4, I determined that the arginine residues are both necessary and sufficient for dfTAT endosomolytic activity. Interestingly, a minimum number of 12 arginine residues is required for sufficient endosomal escape.

Overall, this work identifies a novel endosomolytic agent and identifies some of the molecular features important for cellular permeation. In turn, my results lay the foundation for new and optimized versions of the dfTAT prototype that may find applications in a variety of delivery approaches.

DEDICATION

I would primarily like to dedicate this work to my parents and my four siblings, which have been a consistent loving and caring family and have unfailingly supported me throughout life. Each one of you has uniquely contributed to my growth and I am grateful to have you in my life. To my remarkable parents, I would specifically like to thank both of you for each uniquely instilling in me the qualities that have allowed me to pursue this work. Additionally, I would like to dedicate this work to my departed grandfather and would like to thank him for being an admirable role model for my entire family.

ACKNOWLEDGMENTS

I would like to thank Dr. Pellois, my advisor for his remarkable mentorship throughout this insightful journey also known as graduate school. I am grateful for his continuous patience, support, motivation, willingness to share his knowledge and making his laboratory an encouraging and nurturing environment to grow as a scientist. In addition, I would like to acknowledge Dr. Robert Burghardt, Dr. Hays Rye and Dr. James Sacchettini for serving as my committee members and for all their insight, helpful advice and contributions towards my studies throughout the years. I would like to thank in particular my two past lab members, Dr. Alfredo Erazo-Oliveras and Dr. Ting-Yi Wang. I am certain that I will remain immensely indebted to Alfredo. I am grateful for the multiple roles he has selflessly taken during this time: an inspirational mentor, a supportive and caring lab mate which ultimately has allowed me to find my life-long best friend. I want to also thank him for the countless times that he has encouraged me, persisted that I moved forward and no matter the situation remained reliably standing by my side. I would like to thank Ting-Yi for his consistent life and work-related advice, support and dear friendship throughout my graduate career and for continuously looking out for my best interest to this date. I would also like to express my deepest gratitude and appreciation to all former and current members of the Pellois laboratory, in particular, Dakota Brock, Helena Kondow and Jason Allen, who contributed uniquely to my growth during this time and have been extremely supportive over the years. I would like to thank all the undergraduates, in particular, Megan Whitlock, Ikram Rostane and Joseph Cinclair,

rotation students and high school students that have worked with me and allowed me to grow as a mentor and for their contribution to my work.

Finally, I would like to thank all my close friends, loving family, classmates, Biobio staff and academic advisor for their endless support and care. In particular, I would like to thank the Biochemistry Graduate Association for all the additional personal growth it has given me during graduate school.

NOMENCLATURE

Antp	antennapedia homeodomain
ATCC	American Type Culture Collection
BMP	bis(monoacylglycero)phosphate
BSA	bovine serum albumin
COI	cargo of interest
CPP	cell-penetrating peptide
DCM	dichloromethane
DIC	N,N-diisopropylcarbodiimide
DIEA	N,N-Diisopropylethylamine
DIGE	Differential in gel electrophoresis
DLS	Dynamic light scattering
DMEM	Dulbecco's modified eagle medium
DMF	dimethylformamide
DRBD	double-stranded RNA-binding domain
DSB	double stranded breaks
EGFP	enhanced green fluorescent protein

EIPA	5-(N-Ethyl-N-isopropyl)amiloride
ESI	electrospray ionization
FBS	fetal bovine serum
FITC	fluorescein isothiocyanate
Fl	carboxy-fluorescein
FACS	fluorescence activated cell sorting
FRET	Förster resonance energy transfer
GTPase	guanosine triphosphate hydrolase
HA2	haemagglutinin protein II
HBTU	2-(1H-Benzotriazole-1-yl)-1,1,3,3-tetramethyluronium hexafluorophosphate
HDF	human dermal fibroblast
HEPES	4-(2-hydroxyethyl)-1-piperazineethanesulfonic acid
HIV	Human immunodeficiency virus
HNF	human newborn fibroblasts
HPLC	high-performance liquid chromatography
HRP	Horse Radish Peroxidase
HSPG	heparin sulfate proteoglycan

IP	intra-peritoneal injection
IPTG	isopropyl -D-1-thiogalactopyranoside
ITC	isothermal calorimetry
kDa	kilo Dalton
L-15	Leibovitz's 15
MALDI	matrix-assisted laser desorption/ionization
MAP	model amphipathic peptide
mCPP	multivalent CPP
MOI	molecule of interest
MPTP	mitochondrial permeability transition pore
MTT	3-(4,5-Dimethylthiazol-2-yl)-2,5-diphenyltetrazolium bromide
MVB	multivesicular bodies
NLS	nuclear localization signal
NMR	nuclear magnetic resonance
ON	oligonucleotides
OVA	ovalbumin
p53	protein 53

PAD	pro-apoptotic domain
PBS	phosphate buffer saline
PCI	photochemical internalization
PCR	polymerase chain reaction
PG	proteoglycan
PNA	peptide nucleic acid
Ptd	phosphatidyl
Ptd-Ser	phosphatidyl serine
RBC	red blood cell
RNase A	ribonuclease A
SDS-PAGE	sodium dodecyl sulfate polyacrylamide gel electrophoresis
SPPS	solid-phase peptide synthesis
TAT	Trans-Activator of Transcription
TCEP	tris(2-carboxyethyl)phosphine
TFA	Trifluoroacetic acid
TMR	5(6)-carboxytetramethylrhodamine
WT	wild-type

CONTRIBUTORS AND FUNDING SOURCES

This work was supervised by a thesis committee consisting of Dr. Jean-Philippe Pellois (advisor), Dr. Hays Rye, Dr. James Sacchettini of the Department of Biochemistry and Biophysics and Dr. Robert Burghardt of the Department of Veterinary Biology.

The data for Chapter 2 was generated and analyzed in collaboration with Dr. Alfredo Erazo-Oliveras of the Department of Nutrition and Food Sciences and was published in 2014.

All other work conducted for the thesis (or) dissertation was completed by the student independently.

This work was made possible in part by National Institute of Health (NIH) Grant under Grant Number R01GM110137.Its contents are solely the responsibility of the authors and do not necessarily represent the official views of the NIH.

TABLE OF CONTENTS

Page

ABSTRACT ii

DEDICATION iv

ACKNOWLEDGMENTS v

NOMENCLATURE vii

CONTRIBUTORS AND FUNDING SOURCES xi

TABLE OF CONTENTS xii

LIST OF FIGURES xvi

LIST OF TABLES xxii

1. INTRODUCTION 1

1.1 Significance of the delivery of macromolecules into live cells 1
1.2 Cell-penetrating peptides as delivery vectors 2
1.2.1 History of cell-penetrating peptides 2
1.2.2 The importance of "arginine residues" in cellular penetration 5
1.2.3 *In cellulo* applications for the CPP TAT 7
1.2.4 *In vivo* applications for CPP TAT 13
1.2.5 CPP-mediated delivery challenges and limitations 16
1.3 Proposed mechanisms of cellular entry for TAT and its derivatives 17
1.3.1 CPP direct membrane translocation 18
1.3.2 Energy-dependent mechanisms: Endocytosis 21
1.3.3 Cell surface interaction 22
1.3.4 Endocytic internalization and trafficking 24
1.3.5 Endosomal escape: The bottleneck 33
1.4 Approaches to enhancing CPPs' endosomal escape properties 36
1.4.1 Multivalency: Enhancing endosomal escape 39
1.4.2 Approaches to and implications of cargo delivery 40
1.4.3 Limitations and challenges 44
1.5 Enhancing the chemical stability of CPPs 45
1.5.1 Classes of non-degradable CPPs 45
1.5.2 Limitations and challenges 49

1.6 Goal of this research 50

2. DELIVERY OF PROTEINS, PEPTIDES AND CELL-IMPERMEABLE SMALL MOLECULES INTO LIVE CELLS BY INCUBATING WITH THE HIGHLY ENDOSOMOLYTIC DELIVERY AGENT, dfTAT[157, 224] 52

2.1 Introduction 52
2.2 Results 53
2.2.1 Generation of dfTAT and its monomeric counterparts 54
2.2.2 dfTAT penetrates the cytosol of live cells efficiently 60
2.2.3 dfTAT penetrates the cells in a two-step process 68
2.2.4 dfTAT-mediated endosomal leakage is efficient 72
2.2.5 dfTAT-mediated delivery is not deleterious to cells 77
2.2.6 dfTAT delivers proteins by simple co-incubation 90
2.3 Discussion 105
2.4 Materials and Methods 111
2.4.1 Peptide design, synthesis and purification 111
2.4.2 Synthesis of acetamidated C(S-CH2CONH2)K(ε-NH-TMR)TATG (acfTAT) 113
2.4.3 Generation of dfTAT by dimerization of CK(TMR)TATG (fTAT) 113
2.4.4 Generation of nrdfTAT using fTAT 113
2.4.5 Cloning, overexpression and purification of TAT-Cre, TAT-mCherry, HOXB4 and TAT-HOXB4 114
2.4.6 Cell lines 116
2.4.7 Delivery of peptides inside live cells 117
2.4.8 Delivery of peptides and proteins inside live cells by co-incubation with dfTAT 118
2.4.9 Quantitative determination of peptide and macromolecule uptake inside cells 119
2.4.10 Quantitative analysis of TAT-HOXB4 and HOXB4 delivery with fTAT and dfTAT using a luciferase reporter 121
2.4.11 Cell viability assays 122
2.4.12 Whole-genome microarray analysis 123
2.4.13 Differential in gel electrophoresis (DIGE) proteomic analysis 124
2.4.14 Determination of dfTAT and EGFP interaction by FRET 125

3. AN L- TO D- AMINO ACID CONVERSION IN AN ENDOSOMOLYTIC ANALOG OF THE CELL-PENETRATING PEPTIDE TAT INFLUENCES PROTEOLYTIC STABILITY, ENDOCYTIC UPTAKE, AND ENDOSOMAL ESCAPE[264] 127

3.1 Introduction 127

3.2 Results 128
3.2.1 Generation of D-dfTAT: a protease resistance cell-penetrating peptide 131
3.2.2 D-dfTAT is protease resistant and capable of penetrating cells 135
3.2.3 Both dfTAT and D-dfTAT deliver macromolecules inside cells and access the cytosol of cells by using a similar endocytic route 141
3.2.4 L- to D- substitution negatively impacts endocytosis but favors endosomal escape 152
3.2.5 Endosomal scape is not toxic to cells, but intracellular retention of D-dfTAT inhibits cells proliferation and impacts transcription 170
3.3 Discussion 174
3.4 Materials and Methods 183
3.4.1 Peptide design, synthesis, and purification 183
3.4.2 Generation of D-dfTAT by dimerization of D-dfTAT 185
3.4.3 Cell culture and transfection 185
3.4.4 dfTAT and D-dfTAT degradation 186
3.4.5 Delivery of peptides and proteins into live cells 187
3.4.6 Quantitative determination of peptide uptake 190
3.4.7 Liposome Preparation and leakage assays 192
3.4.8 Cell proliferation assays 193
3.4.9 Whole genome microarray analysis 194

4. THE ENDOSOMAL ESCAPE PROPERTY OF POSITIVELY CHARGED CELL-PENETRATING PEPTIDES IS DEPENDENT ON THE NUMBER OF ARGININE RESIDUES PRESENT IN THE SEQUENCE 196

4.1 Introduction 196
4.2 Results 197
4.2.1 Generation of dfR_n and dfK_n reagents 197
4.2.2 The positive charge in dfTAT is necessary but not sufficient for its cell penetration activity 198
4.2.3 A peptide with the same number of arginine's found in dfTAT mimics its endosomolytic activity 205
4.2.4 Differences in endocytic uptake are not solely responsible for differences in cell penetration 210
4.2.5 A non-linear response for cell penetration of polyarginine peptides can be explained by the ability of the peptides to induce leakage of late endosomal compartments 216
4.3 Discussion 218
4.4 Material and Methods 220
4.4.1 Peptide design, synthesis, and purification 220
4.4.2 Generation of dfR_n and dfK_n peptides by dimerization reactions 222
4.4.3 Cell culture 222
4.4.4 Delivery of peptides into live cells 222

4.4.5 Determination of mechanism of cellular entry 224
4.4.6 Quantitative determination of peptide uptake 224
4.4.7 Liposome Preparation 225
4.4.8 Liposome leakage assays 226
4.4.9 Liposome binding assays 227

5. SUMMARY AND CONCLUSIONS 228

REFERENCES 243

APPENDIX A 268

LIST OF FIGURES

Page

Figure 1-1 Models proposed for CPP direct membrane translocation mechanism. 20

Figure 1-2 Model of the trafficking of a CPP-cargo conjugate through the endocytic pathway 26

Figure 1-3 CPP-cargo conjugate endosomal escape. 32

Figure 1-4 mCPP systems and their interactions with membranes. 42

Figure 2-1 Multivalent CPP system using disulfide bonds 55

Figure 2-2 Chemical structure of fTAT and dfTAT 56

Figure 2-3 Characterization of acfTAT 57

Figure 2-4 Characterization of nrfTAT 58

Figure 2-5 Characterization of dfTAT 59

Figure 2-6 Cytosolic delivery of dfTAT in live cells is efficient 61

Figure 2-7 Cytosolic and nuclear fluorescence distribution of dfTAT is concentration dependent 62

Figure 2-8 Delivery of dfTAT was achieved in multiple cell types 63

Figure 2-9 fTAT cellular localization after incubation with live cells depends on its concentration in the extracellular media 66

Figure 2-10 Delivery of nrdfTAT into live cells 67

Figure 2-11 Effect of endocytosis inhibitors on the cellular distribution of dfTAT 69

Figure 2-12 Fluorescence emission spectra of dfTAT (5 μM) before and after reduction with the reducing agent TCEP 70

Figure 2-13 Pulse-chase experiment showing the progressive cytosolic penetration of dfTAT 71

Figure 2-14 Structure and characterization of DEAC-K9 73

Figure 2-15 dfTAT causes the cytosolic release of molecules trapped inside endosomes 74

Figure 2-16 dfTAT displays a high endosomolytic activity when compared to acfTAT 76

Figure 2-17 Endosomolytic efficiency of dfTAT 78

Figure 2-18 SNAP-Surface 488 enters cells via endocytosis and does not escape endosomes in the absence of dfTAT 79

Figure 2-19 dfTAT is not toxic to cells under conditions where efficient endosomal escape is achieved 80

Figure 2-20 The cellular localization of acfTAT and dfTAT is different after incubation with live cells but cell morphology is not changed 81

Figure 2-21 dfTAT-mediated delivery does not significantly affect cell proliferation... 82

Figure 2-22 dfTAT-mediated delivery does not significantly affect cell division..... 83

Figure 2-23 dfTAT-mediated delivery does not significantly affect transcription in primary cells..... 85

Figure 2-24 mRNA expression analysis in the presence of staurosporine..... 86

Figure 2-25 Differential in gel electrophoresis (DIGE) proteomic analysis of HDF cells treated with dfTAT (5 μM) for 1 h 88

Figure 2-26 dfTAT-mediated delivery does not significantly affect endocytosis..... 89

Figure 2-27 Simultaneous delivery of SNAP-Surface 488 and DEAC inside cells using a one step protocol 91

Figure 2-28 Delivery of intact and functional EGFP using co-incubation with dfTAT . 92

Figure 2-29 Quantitation of the concentration of EGFP delivered into the cytosol of HDF and Neuro-2a..... 93

Figure 2-30 dfTAT and EGFP do not interact when co-incubated 95

Figure 2-31 dfTAT and EGFP do not interact 97

Figure 2-32 Effect of BSA, heparin and FBS on dfTAT cell penetration..... 99

Figure 2-33 Delivery of intact and functional Cre-recombinase using co-incubation with dfTAT 100

Figure 2-34 Delivery of an intact and functional antibody using co-incubation with dfTAT 102

Figure 2-35 The FITC-anti-ATP5a antibody co-localizes with a fluorescently labeled mitochondrial protein expressed in live cells after dfTAT-mediated delivery 103

Figure 2-36 dfTAT mediated delivery of HoxB4 and TAT-HoxB4 improves the expression of a luciferase reporter 104

Figure 2-37 The amount of DEAC-K9 delivered in the cytosol and nucleus of live cells can be titrated 106

Figure 2-38 Determination of the amount of DEAC-K9 delivered into cells 107

Figure 2-39 The induction of luciferase expression by dfTAT-medited delivery of HoxB4 into cells can be controlled 108

Figure 3-1 Schematic representation of the amino acid sequence of dfTAT and D-dfTAT 132

Figure 3-2 Characterization of dfTAT 133

Figure 3-3 Characterization of D-dfTAT 134

Figure 3-4 HPLC analysis of dfTAT and D-dfTAT before and after treatment with trypsin 136

Figure 3-5 Cellular distribution of dfTAT and D-dfTAT after 1 hr incubation 137

Figure 3-6 Cellular distribution of dfTAT and D-dfTAT immediately after delivery and after 24h 138

Figure 3-7 Analysis of peptide degradation by Tris-Tricine gel electrophoresis of cell lysates 140

Figure 3-8 dfTAT and D-dfTAT deliver Cre recombinase into live cells 142

Figure 3-9 Cytosolic penetration of D-dfTAT is blocked by expression of dominant-negative Rab7 144

Figure 3-10 D-dfTAT major route of cellular entry is via endocytosis followed by endosomal escape in a manner similar to dfTAT 146

Figure 3-11 Characterization of DEAC-k5 148

Figure 3-12 D-dfTAT causes the release of a peptide preloaded into endosomes but not that of peptide preloaded into lysosomes 149

Figure 3-13 D-dfTAT causes leakage of liposomes with a lipid composition mimicking that of late endosomes 151

Figure 3-14 Evaluation of the cytosolic delivery efficiency of dfTAT and D-dfTAT as a function of peptide concentration in incubation media 153

Figure 3-15 Quantification of whole cell uptake by dfTAT and D-dfTAT as a function of the peptide concentration in incubation media 155

Figure 3-16 The fluorescence emission of dfTAT and D-dfTAT increases upon reduction of the disulfide bond 158

Figure 3-17 Comparison of the cellular uptake of dfTAT and D-dfTAT 160

Figure 3-18 The uptake fluorescence intensity of dfTAT and D-dfTAT is not a consequence of extracellular membrane binding 162

Figure 3-19 Determination of the contribution of peptide export after dfTAT or D-dfTAT treatment 163

Figure 3-20 The number of endosomes present in cells treated with dfTAT is similar to that present in cells treated with D-dfTAT 165

Figure 3-21 Evaluation of the endosomal escape activity of dfTAT and D-dfTAT as a function of the total amount of peptide internalized by cells 166

Figure 3-22 A protease inhibitor cocktail protects dfTAT from proteolytic degradation prior to cytosol delivery 168

Figure 3-23 A protease inhibitor cocktail increases the penetration activity of dfTAT but not of D-dfTAT 169

Figure 3-24 D-dfTAT impacts cellular proliferation more dramatically than dfTAT after cytosolic delivery 171

Figure 3-25 Proliferation assay. dfTAT treated HDF cells proliferate at a similar rate to untreated cells 172

Figure 3-26 The effect of dfTAT and D-dfTAT treatment on cell growth was monitored by microscopy 173

Figure 3-27 RNA-seq analysis of HDF and MCH58 cells treated with D-dfTAT or dfTAT 175

Figure 3-28 Schematic representation modeling the similarities and differences observed in the cellular penetration of dfTAT and D-dfTAT 179

Figure 4-1 HPLC and ESI MS spectrum of dfK8 and dfRn series 199

Figure 4-2 Comparison of cellular distribution of the peptides after 1 h incubation 202

Figure 4-3 Quantification of total cellular uptake by dfTAT, dfR8 and dfK8 as a function of the peptide concentration in incubation media 203

Figure 4-4 dfR8 is cytotoxic at high peptide concentrations 204

Figure 4-5 Comparison of cellular distribution of the polyarginine peptides after 1 h incubation 206

Figure 4-6 dfR4, dfR5 and dfK8 co-localize with LysoTracker green, a marker of acidified endocytic organelles 207

Figure 4-7 Quantitative determination of the cytosolic delivery efficiency of dfRn constructs in comparison to dfTAT as a function of peptide concentration present in the incubation media 208

Figure 4-8 Comparison of the total cellular uptake of peptide as a function of the number of arginine 209

Figure 4-9 dfR6, dfR7 and dfR8 penetrate the cytosol by escaping from the endocytic pathway 212

Figure 4-10 The endocytic uptake does account for the difference observed in the endosomolytic activity of polyarginine peptide 215

Figure 4-11 The in vitro leakage activity of dfRn increases as a function of n 217

Figure 5-1 Model of dfTAT entry and escape from the endocytic pathway. 237

Figure 5-2 Design of future dfTAT analogues. 242

Figure A-1 D-dfTAT similar to dfTAT can efficiently delivery the DEAC-k5 peptide into the cytosolic space of MCH58 cells 268

Figure A-2 Comparison of the affinity of dfTAT and D-dfTAT to LE MLVs 269

Figure A-3 BMP-mediated partitioning of dfTAT and D-dfTAT into hexanes 270

Figure A-4 D-dfTAT does not impact cellular proliferation of HeLa cells after cytosolic delivery 271

Figure A-5 Images for the RNA-seq analysis of HDF and MCH58 cells treated with D-dfTAT or dfTAT 272

LIST OF TABLES

Page

Table 1-1 Origin and sequence of a subset of CPPs 4

Table 3-1 Table showing the list of names of gene transcripts related to cell death and proliferation that are affected after treatment with D-dfTAT..... 177

1. INTRODUCTION

1.1 Significance of the delivery of macromolecules into live cells

Delivering macromolecules such as RNAs and proteins to the inside of live cells is likely to have a huge impact on the fields of therapeutic and biomedical research. For example, delivery of transcription factors such as Oct4, Sox2, and Klf4 can be used to reprogram fibroblasts into pluripotent stem cells[1]. This delivery, however, is impeded by the presence of a selectively permeable plasma membrane that acts as a barrier blocking entry of large hydrophilic molecules to the cytosolic space of live cells. Therefore, overcoming this natural barrier is a crucial first step. Techniques such as scrape-loading, microinjection, and electroporation have all previously been used, but these fall short in terms of efficiency of delivery to a large population of cells[2-5]. This severely limits the application of these techniques, especially in areas such as drug delivery. Other approaches include the use of bacterial toxins, virus-like particles, cationic lipids for delivery of DNA/RNA, nanoparticles, and liposomes for the transport of well-known insoluble drugs and proteins[6-10]. Many of these approaches, however, suffer from high cell toxicity and undesirable immunogenic effects, are time-consuming, require a high level of expertise, or offer low delivery efficiency[11]. Therefore these methods, although useful, remain unsuitable for many applications. One promising approach that could circumvent many of these issues is the use of cell-penetrating peptides (CPPs); this method has attracted attention recently due to its non-invasiveness in cell-impermeable macromolecular delivery[12].

1.2 Cell-penetrating peptides as delivery vectors

1.2.1 History of cell-penetrating peptides

In 1988, Pabo and Loewenstein independently demonstrated that the trans-activator of transcription (TAT) protein from the human immunodeficiency virus type 1 (HIV-1) has the ability to cross the plasma membrane and activate gene expression of a reporter gene[13, 14]. Following this, work was aimed at understanding the mechanism by which this 86-amino acid protein, that is hydrophilic in nature, is able to enter cells. Several years later, it was reported that TAT enters cells by adsorptive endocytosis, and it was this report that underscored its possible use for the delivery of proteins into cells[15]. At this time, Lebleu and colleagues were interested in delineating the exact sequence responsible for TAT protein translocation[16]. Their research identified a cluster of basic amino acids extending from positions 48 to 60 that appeared to be unstructured and responsible for the protein's cellular internalization property. The sequence now known as the TAT peptide (amino acid sequence: RKKRRQRRR) was the first identified and continues to be the most well-studied cell-penetrating peptide (CPP)[17].

CPPs, sometimes also referred to as protein transduction domains (PTDs), are short peptide sequences composed of 5 to 30 amino acids. These peptides can be used to deliver biomolecules into live cells by a simple co-incubation protocol, or by covalently conjugating the peptide to the molecule of interest (MOI). CPPs can be further classified according to different properties, such as their physiochemical characteristics or, more commonly, their origin[18]. Regarding the latter, CPPs have been classified into three groups. Similar to the TAT peptide penetratin, VP22 and pVEC belong to peptides derived

from proteins[19, 20]. For example, penetratin is a 16-mer peptide derived from the third helix of Drosophila antennapedia homeodomain (Antp)[21]. The second group consists of chimeric peptides that originate from two fused constructs; these include Transportin, MPG, and Pep-1. Transportan (TP) was derived from fusion of the neuropeptide galanin to the wasp venom peptide mastoparan[22]. The third group is classified as synthetic peptides, which have since been identified based on the structural activity relationship of well-known CPPs. This class includes model amphiphatic peptide (MAP) MAP-17, GALA, R6W3, and the polyarginine peptide (which is characterized based on structure/function studies with the TAT peptide). Other well-known CPPs include CADY, Xentry, and PPTG1[17, 23-27].

From a physio-chemical standpoint, CPPs are classified as cationic, amphipathic, or hydrophobic in nature. Cationic CPPs include the TAT and synthetic polyarginine peptides. At a physiological pH, these are positively charged, due to enrichment of the basic amino acids arginine and lysine found in their sequence. MAP, GALA, and P28 are three examples of amphipathic peptides in which one face has a hydrophobic patch and the other is either cationic, anionic, or polar[28-30]. Residue substitution experiments have shown that even though many of these peptides are cationic, their translocation activity is a consequence of their amphiphilicity. Hydrophobic CPPs are the least-identified class; however, one emerging group is stapled peptides that involve a ring-closing olefin metathesis[31]. Interestingly, studies have shown that the staple itself, independent of the nature of the residue, contributes to the cellular internalization due to its higher affinity for the plasma membrane[18].

Peptide	Origin	Sequence
Derived from proteins		
TAT peptide	Tat(48-57)	GRKKRRQRRR
Penetratin	Antennapedia(43-58)	RQIKIWFQNRRMKWKK
pVEC	Cadherin(615-632)	LLIILRRRRIRKQAHAHSK
Chimeric peptides		
Transportin	Galanine/Mastopran	GWTLNSAGYLLGKINLKALAALAKKIL
MPG	HIV-gp41/SV40 T-antigen	GALFLGFLGAAGSTMGAWSQPKKKRKV
Pep-1	HIV-reverse transcriptase/ SV40 T-antigen	KETWWETWWTEWSQPKKKRKV
Synthetic peptides		
MAP	de novo	KLALKLALKALKAALKLA
GALA	pH dependent	WEAALAEALAEALAEHLAEALAEALEALAA
Polyarginine	derived from TAT peptide	R_n n>6
R6W3	derived from Penetratin	RRWWRRWRR

Table1-1 Origin and sequence of a subset of CPPs.

1.2.2 The importance of "arginine residues" in cellular penetration

Mutational analysis studies of the TAT peptide by Mitchell et al., Wender et al., and Futaki et al. have identified the crucial role that arginine plays in the activity of cationic peptides[32-34]. Wender et al. reported that truncation of the TAT peptide and individual mutations of its residues to alanine resulted in a significant decrease in the internalization of CPPs. Additionally, this work demonstrated that although TAT contains eight positive charges, its activity could be recapitulated by a peptide containing six or seven positive residues. Furthermore, peptides containing seven or more arginine residues exhibited a higher efficiency of internalization than TAT, as evaluated by flow cytometry[32]. Work done in the Rothbard laboratory showed that polyarginine peptides were internalized into T-cells more efficiently than polymers of lysine or ornithine of similar peptide lengths[33]. Altogether, these studies indicated that the cationic nature of the arginine residue was not the sole factor necessary for cell internalization.

Rothbard et al. showed that there was no strict requirement for side chain length or backbone chirality (L- vs. D-polyarginine); however, the guanidinium group on the arginine residue and other heptamers containing guanidinium did play a key role in cellular internalization[33]. This was clearly demonstrated by experiments where arginine was replaced with citrulline, an isostere of arginine that contains oxygen instead of nitrogen in the guanidino group. Thus, a urea group found in citrulline replaced the guanidinium group of arginine. A heptamer of citrulline showed no cellular internalization activity at concentrations up to 100 μM. Interestingly, the pKa of guanidinium is 12, while urea has a pKa of about 0.1; the difference results in the dramatic change in charge of the

molecule at a physiological pH. This makes the NH group of guanidinium an excellent hydrogen bond donor and allows for stable bidentate hydrogen bonds with anions such as the phosphates and sulfates found at the cell surface. This interaction will be discussed in the sections below.

It is important to note that all experiments in these two studies were performed using flow cytometry analysis. While flow cytometry is a useful tool that allows one to analyze the total fluorescence intensity found in cells, it cannot differentiate between cells that have a cytosolic fluorescence distribution, punctate distribution (i.e., peptides trapped inside endocytic vesicles), or peptides bound to the cell surface[35]. Futaki et al. used fluorescence microscopy to evaluate the internalization property of arginine-rich peptides, showing that arginine-rich peptides derived from many sources have the ability to reach the cytosolic space of a macrophage cell line: RAW264.2 cells. The authors also reported that a minimum number of approximately eight arginine peptides per chain were required for efficient cell translocation[34]. While microscopy is a technique that allows for differentiation of peptide localization, this study was performed after cellular fixation, which was reported to lead to experimental artifacts (i.e. artificial release of material from endosomes due to membrane permeabilization during fixation protocol) [35, 36]. This work ultimately led to the research conducted with live cell microscopy, which showed that polyarginine peptides could display a cytosolic fluorescence distribution[37, 38]. Such research underscores the remarkable difference in internalization properties of lysine and arginine residues in the context of live cell microscopy.

1.2.3 *In cellulo* applications for the CPP TAT

Cell-penetrating peptides provide a promising tool for the delivery of various biologics into live cells. In this section, I will provide examples of macromolecules (with a focus on proteins, and nucleic acids) being delivered into cells and describe the usefulness of this application. The examples were obtained from an extensive list of molecules internalized into live cells with the aid of CPP, which includes small molecule drugs, antibodies, peptide-based imaging agents, liposomes, and nanoparticles[39].

Protein Delivery

The transportation of proteins and hydrophilic peptides across a plasma membrane can be difficult, due to the barrier-like nature of the membrane. For more than 20 years, laboratory research has investigated the possibility of using cell-penetrating peptides to deliver a wide variety of peptides, proteins, and enzymes (i.e., cargo) to the insides of cells. Researchers have used methods such as covalently tagging the CPP to the cargo of interest (COI) or simple employment of a co-incubation protocol (CPP and COI incubated together, with no direct conjugation)[40]. Proteins delivered by CPPs can be classified into two groups: reporter peptides/proteins that give a simple readout upon delivery, and functional peptides/proteins that result in a change in the detectable cellular response pathway. As early as the 1990's, studies by Fawell et al. showed that TAT could be used to deliver reporter proteins such as β-galactosidase, horseradish peroxidase (HRP), a domain of Pseudomonas exotoxin A, and ribonuclease A (RNase A), by direct conjugation into a variety of cell lines including HeLa and primary human keratinocytes[11]. The authors compared the amount of β-galactosidase activity found in cells by the transfection method

or by protein delivery using TAT. Their results showed that the activity was observed on the time scale of minutes to hours for TAT; however, using transfection the activity occurred on a time scale of hours to overnight. Their conclusion was that the efficiency of delivery was far greater using the TAT peptide. However, these experiments lacked the controls that would account for variability attributed to the difference in expression level of each plasmid and the transfection efficiency. Unfortunately, while these experiments laid the foundation for protein delivery, they were performed using cellular fixation; this process overestimates the amount of protein that reaches the cytoplasm, due to artifacts of sample preparation.

In another example, Kim et al. described the use of TAT as a therapeutic and prophylactic vaccine. T-cells recognize the pathogen-derived peptides exposed on the major histocompatibility complexes class (MHC) I and II, upon macrophage infection by the pathogen. For this to occur, the protein or peptide exposed to the cell surface must reach the cytosolic space of the cells. At that time, protein-based vaccines failed to hijack the immune system because the protein was unable to cross the plasma membrane. In 1997, researchers conjugated TAT to ovalbumin (OVA), and showed the ability of this conjugate to stimulate the MHC class I responses in T-cells[41].

In 2004, to understand the mechanisms of CPP translocation, Dowdy and colleagues developed an assay that employs Cre recombinase. Cre recombinase is an enzyme that mediates the recombination of a region of a gene flanked by two *loxP* sites[42]. In this assay, a TAT- Cre fusion mediates the excision of the stop codon from a *loxP*-Stop-*loxP* upstream of the DNA sequence coding for EGFP. Therefore, for cells to express

EGFP, TAT-Cre must enter the cells and translocate to the nucleus to excise the stop codon. This assay is extremely valuable, since it allows for the characterization of the mechanism of CPP internalization in addition to efficiency in protein delivery, without the need for cellular fixation protocols. Using flow cytometry analysis, these researchers successfully delivered TAT-Cre to the cytosol of the cells. Interestingly, the majority of the TAT-Cre was shown to be entrapped in macropinosomes (endocytic vesicles formed as a result of macropinocytosis). This work highlights that while TAT can mediate cellular entry of a biologically active enzyme inside cells, the efficiency remains suboptimal due to the generally low endosomal escape efficiencies of TAT and cationic CPPs.

Transcription factors that can induce pluripotency have been delivered inside cells using CPPs. This has been used as an alternate approach to transfection of the cells with plasmid containing the genes that codes for these transcription factors. Kim et al. fused Oct4, Sox2, Klf4, and c-Myc (which had previously been shown to induce pluripotency by viral expression of transcription factors) to polyarginine and expressed the constructs in HEK293 cells. The cell extract from these cells were incubated with newborn human fibroblast (HNF)[43, 44]. Initial attempts at cell extract incubation were not successful, so the researchers reasoned that protein delivery needed to be repeated to observe the effect. In fact, treatment of HNF cells for multiple cycles (1 cycle = 16 hr protein treatment and six days of incubation with an essential media) resulted in formation of colonies with iPSC (induced pluripotent stem cells)-like morphology, and showed the expression of markers of pluripotency[43]. This indicated that CPPs could in the future be used for therapeutic applications such as organ transplants.

In 2014, work by Ramakrishna et al. reported the first use of the nonaarginine CPP 9R to deliver Cas9 and guide RNA into human cells[45]. The clustered, regularly interspaced, short palindromic repeat (CRISPR)-associated (Cas) system is an RNA-guided DNA cleavage process found in bacteria; it is important to their adaptive immunity[46, 47]. Research by the Doudna lab and others recognized the utility of this process in targeting and altering the genomes of various organisms. The guide RNA, which consists of CRISPR RNA (crRNA) and trans-activating crRNA (tracrRNA), are necessary to direct the endonuclease or Cas9 protein to a specific gene on the DNA that is complementary to the guide RNA (gRNA), thereby making double-stranded breaks (DSBs) at the specific genome locus. Typically, the Cas9 and guide RNA are expressed in cells following plasmid transfection or microinjection. However, plasmid-based delivery systems are notorious for problems such as uncontrolled integration of plasmid DNA into the host genome, and immunogenicity problems[48, 49].The authors showed the delivery of the modified Cas9 and gRNA into cells via a reporter assay, using an RFP-GFP reporter plasmid containing the guide RNA recognition site between the two genes. In this plasmid, the GFP was initially out of frame and the transfected cells only expressed RFP. Successful delivery of the Cas9/gRNA conjugated to TAT resulted in the non-homologous end joining of the DSB and a frameshift that resulted in GFP expression. Using flow cytometry, the researchers showed a 6.2% increase in the population of cells expressing GFP, and hence the positive delivery of Cas9/gRNA. They also reported reduced off-target effects, as compared to the plasmid-delivery approach. This can be attributed to the rapid degradation of the protein and RNA after delivery. Similar work

using CPPs has been performed to deliver other nucleases such as zinc fingers, and transcription activator-like effector nucleases[50, 51]. Interestingly, while these results are promising, they also indicate that more effective CPPs may need to be developed to achieve efficient delivery to a larger cell population.

One common characteristic of the proteins described above is the requirement that only a small amount be delivered to the cytosol for biological activity to be detectable. Many of these proteins are enzymes that upon successful cytosolic delivery can reach their target and exert their effect. These enzymes can, therefore, be either reused or alter a signal that can be further amplified, as is the case with TAT-Cre and amplified EGFP expressions. Unfortunately, however, these assays overestimate the efficiency of the CPP endosomal escape, a condition that will be described below.

Gene Delivery

Gene delivery to the nuclei of target cells to dysregulate disease-associated genes has proven to be a promising therapeutic tool [52]. However, due to its large size, it is often quite difficult to deliver highly negatively charged DNA to live cells because it does not efficiently permeate through the plasma membrane. Viral vectors have been used to overcome this barrier; they show promise in the integration of exogenous DNA into a wide variety of host genomes. However, they face major drawbacks, including immunogenicity, toxicity, and difficulties with largescale generation[53].Therefore, non-viral vectors such as CPPs are an ideal alternative approach.

RNAi, for example, is a valuable tool for manipulating cells and discovering new therapeutically relevant targets. SiRNA does not readily enter cells and approaches developed to delivery siRNA often results in low efficiency and high cellular toxicity[54]. Using cationic CPPs to deliver siRNA by direct conjugation leads to charge neutralization and, consequentially, inactivation of CPPs and limited siRNA delivery[52]. In 2009, Dowdy and colleagues reported the delivery of a TAT fusion with a double-stranded (ds) RNA-binding domain (DRBD) capable of binding siRNA with a high level of affinity[54]. In this work, the researchers showed efficient siRNA delivery and RNAi response in multiple cell lines (including several that are difficult to transfect) with no cellular toxicity. Additionally, they delivered various siRNA's, and claimed that their methodology could be implemented for a wide range of siRNA.

The use of oligonucleotides (ONs) is now of interest to the therapeutic industry. In brief, ONs are used to form RNA:DNA duplexes that can be sterically blocked or recognized by RNase H (termed "antisense"); essentially, they cleave the RNA and disrupt gene expression[55]. This class of therapeutic agent is designed to inhibit important genes involved in nuclear splicing and endogenous microRNA[56, 57]. ONs can be used to sterically block protein translation and are more advantageous, due to their greater specificity and lower number of off-target effects. These ONs can be synthetically generated, since they do not need to be recognized by RNase H. The generation of synthetic ONs opens the door to manipulation and optimization that may enhance their use in therapeutic applications.

One example of a synthetic ON analogue are peptide nucleic acids (PNAs), which were recently shown to be promising in gene inhibition. PNAs have a backbone composed

of N-(2-aminoethyl)-glycine units linked by amide or peptide bonds, instead of the deoxyribose or ribose sugar backbones found in DNA or RNA, respectively. The bases are linked to the backbones by a methylene and carbonyl groups. PNAs show very strong, sequence-specific RNA binding that can be attributed to less electrostatic repulsion, since PNAs do not contain a negatively charged phosphate backbone. Despite being uncharged, PNAs are still incapable of cellular entry. Therefore, CPPs have been used as a means of enhancing their delivery properties. Langel and colleagues were the first to demonstrate that the use of PNA-CPP conjugates blocked the expression of the galanin receptor mRNA in human Bowes cells by a 21-mer PNA coupled to Penetratin and Transportan[58]. Many other studies followed their lead, using a variety of CPPs including TAT, polyarginine, and Penetratin-PNA constructs; however, the results indicated that these constructs were inefficient at retaining their biological activity at low concentrations. According to fluorescence-activated cell sorting (FACS) and microscopy analysis, the conjugates were taken up by cells and remained trapped in the endocytic pathway. The efficacy of PNA delivery by CPP is enhanced by the addition of endosomolytic agents such as chloroquine and calcium ions[59, 60]. Therefore, as in many cases, endosomolytic entrapment of CPPs remains a limiting factor in delivery, and methods to enhance CPP activity will help advance this application.

1.2.4 *In vivo* applications for CPP TAT

The therapeutic *in vivo* use of proteins has previously been limited to extracellular target**s** and receptors. This is mainly because the proteins used must cross many barriers

(including the mucosal membrane and bloodstream) before reaching their target cells. CPP conjugation to such therapy can circumvent some of these issues. CPPs can be used to increase cellular absorption and protein bioavailability to organs known to be impenetrable. One early study that laid the foundation for the *in vivo* applications of CPPs was from the Dowdy lab. Their work reported on the *in vivo* delivery of β-galactosidase to various tissues in mice – including the brain – by intraperitoneal injection of TAT-β-galactosidase fusion protein[61]. Following this example, CPPs have been used to deliver proteins and peptides as a means of targeting diseases such as cancer, diabetes, and ischemia. These studies have also shown CPPs' success traversing epithelia and the blood-brain barrier.

The TAT peptide, for example, has been shown to be effective in cancer treatment by delivering various tumor suppressor proteins that are either altered or dysfunctional. The p53 tumor suppressor protein is known to induce growth arrest and apoptosis in response to cellular stress. More than 50% of all cancers show a mutation in the p53 gene; therefore, one approach to combating cancer is via restoration of p53 activity in affected cells. However, delivery of the p53 protein to human cells has proven to be challenging. While gene therapy could be a way of expressing exogenous p53 in cancer cells, this method is associated with a low level of efficiency and undesirable immune responses[62]. Strategies have been employed to restore endogenous p53 in cancer cells, because all cells have either wild-type or mutant p53. A peptide derived from the C-terminus of p53 (p53C') was shown to activate and restore function to the DNA binding of p53 by an unknown mechanism[63]. Many researchers have used CPPs to enhance the cellular uptake

of these p53 peptide constructs. For example, a proteolytically stable TATp53C' conjugate administered by intra-peritoneal injection (IP) to a peritoneal carcinomatosis mouse model was shown to induce apoptosis in cancerous cells. These researchers also identified specificity and dependency in the peptide to induce arrest in cells that specifically express p53. Cancerous and noncancerous cells deficient in p53 showed no response to peptide treatment[64]. Similarly, the p53C' mdm-2-binding domain of p53 and peptides derived from the p16 tumor suppressor have also been conjugated to other CPPs, and have shown efficacy *in vivo*[65-67].

Casein kinase 2 (CK2) is a protein dysregulated in many human cancers that allows for the survival of cancerous cells. A cyclic peptide, p15 was shown to inhibit the phosphorylation activity of CK2 *in vitro*[68]. In this work, the TAT peptide was directly conjugated to the cyclic p15 peptide and intratumorally administered to a TC-1 lung epithelial tumor implanted in a C57BL6 mouse model. Treatment with this peptide led to a decrease in tumor volume compared to a control peptide and phosphate-buffered saline administration. These results persisted even after cessation of the peptide treatment, indicating that this peptide displays anti-tumor properties.

Other areas in which CPPs have been used to deliver proteins *in vivo* include treatment of systemic and local inflammation by delivery of a suppressor of cytokine signaling[69], and cerebral ischemia attributed to proteins from the Bcl-2 family for reduction in cerebral infarction[70].The latter study and many others showed success in using CPP delivery of proteins across the highly restrictive blood-brain barrier (BBB). Interestingly, while many CPPs have been used in a variety of *in vivo* and human clinical

trials, there is currently no therapy approved by the Food and Drug Administration (FDA) that uses CPPs such as TAT[71]. Many Phase I and II clinical trials have been implemented with varied levels of success; this may in part be due to the challenges and limitations discussed below.

1.2.5 CPP-mediated delivery challenges and limitations

While it is evident that CPPs are useful vectors for delivery in a wide range of applications, CPPs have intrinsic limitations that must be addressed. Sensitive assays using CPPs show that while they are efficiently endocytosed into cells, their endosomal escape efficiency remains sub-optimal. CPPs conjugated with a fluorophore, for example, display a punctate peptide distribution when observed using fluorescence microscopy[72]. This distribution is consistent with peptide entrapment in the endocytic compartment. This step is necessary because it results in the cargo reaching its biological target (typically located in the cytosol or nucleus). While various approaches to enhancing the endosomolytic property of CPPs have been implemented and will be discussed in further detail below, this remains a bottleneck in the delivery field.

Another parameter affecting CPP activity is their susceptibility to degradation, due to their peptidic nature. This aspect is problematic for both *in cellulo* and *in vivo* applications. Researchers have employed, for example, unnatural amino acids to circumvent this problem. Proteolytic stability will be described below, as many *in vivo* models have implemented this approach as a means of improving CPP activity (as shown above with the p53C' peptide). Furthermore, till date, the lack of sensitive assays that can

be used to detect CPPs remains a limitation. For example, to understand the mechanisms by which CPPs hijack cells, it is important to track the CPPs upon delivery. This also aids in optimizing the delivery approach in failed applications. However, to date the favored means of tracking CPPs is by labeling them with a fluorophore, which has been shown to affect their membrane permeation activity[73]. Furthermore, target selectively is a major problem for CPPs. Most are not selective to specific cell types, tissues, or organs, which is a key drawback for therapeutic applications. However, promising work in this area has aimed at increasing CPP selectively by generating activatable (aCPPs) or stimuli-responsive CPPs, or by adding a localized sequence to direct them to a specific target. Roger Tsein first introduced aCPPs in 2004. His work detailed the generation of CPPs that remained inactive until exposed to a cancerous cell. The CPPs were engineered to have metalloprotease sequence recognition sites that were cleaved upon reaching the cancer cells (due to their secretion of metalloproteases). This cleavage resulted in a separation of the CPPs from their inactivator (polyglutamate sequences); the CPPs were then activated and capable of penetrating the specific cancer cells[74]. This work has, for example, been used for tumor imaging in a mouse model.

1.3 **Proposed mechanisms of cellular entry for TAT and its derivatives**

While it has been clearly established that CPPs are useful for delivering molecules to the interior of cells, the detailed mechanism of how these peptides promote cellular internalization remains controversial. For example, most early mechanistic studies using

arginine rich CPPs were performed on cells that were fixed. Results from such experiments indicated that the D-enantiomer version of the peptide showed similar translocation efficiency to the L-isomer CPP. This dismissed the involvement of membrane receptors in peptide internalization[32, 75]. Cellular fixation, however, was later found to result in many artifacts and difficulties in evaluating the data[35, 36]. Currently, these artifacts are avoided through the use of live cell microscopy. Additionally, differences in the nature of the cargo conjugated to the same CPP have resulted in variability in the reported routes of cellular entry. Therefore, a consensus view of the mechanism of cell penetration is that two major routes of cellular entry coexist for CPPs. The first is via a direct crossing of the plasma membrane, a mechanism that is known to be energy-independent. The second involves the endocytic pathway. In this scenario, the CPP reaches the cytosolic space of a cell via a two-step process: endocytic uptake followed by endosomal release. Studies have shown that the CPP internalization process is dependent upon multiple factors such as the sequence, concentration, cell type, cell differentiation state, and nature and size of the cargo/detection fluorophore[73, 76-82]. Work by Duchardt et al. highlights how three simultaneous mechanisms might occur in three well-known CPPs[83].

1.3.1 CPP direct membrane translocation

Evidence of direct membrane translocation was found by using fluorescence microcopy on live cells at 4°C (an energy depletion state) [34, 84]. In this research, it was shown that depleting the energy source did not diminish the uptake of the TAT peptide or

affect its intracellular localization. These results suggest an endocytic-independent route for TAT cellular entry and support the notion of a direct membrane mechanism for CPP translocation. Consequently, models have been proposed to explain how CPPs might cross this bilayer; three such models are the inverted micelle, carpet, and barrel stave or toroidal pore models[85].

Derossi et al. was the first to propose the "inverted micelle model." In this model, CPP interaction with the cellular membrane triggers a disruption, forming an inverted micelle in the bilayer. As a result, the peptide is located in the inner core of the micelle. This can be followed by the inverse mechanism whereby the CPP disturbs the micelle. Disruption of the membrane results in the peptide reaching the cytosolic space of the cell. NMR studies with the peptide Antp have shown that it can cause micelle formation[86]. This model explains how small hydrophilic molecules can translocate across the membrane; however, it fails to explain how large macromolecules can be trapped in the micelle membrane and then escape, due to their size limitations.

In the carpet model or "membrane thinning," the ability of CPPs to translocate across a plasma membrane is attributed to a major destabilization[87, 88]. This model was used to describe the translocation of CPPs at higher levels of concentration. First, the CPP binds to the membrane and covers the phospholipids on it in a carpet-like manner. This causes a secondary structure change

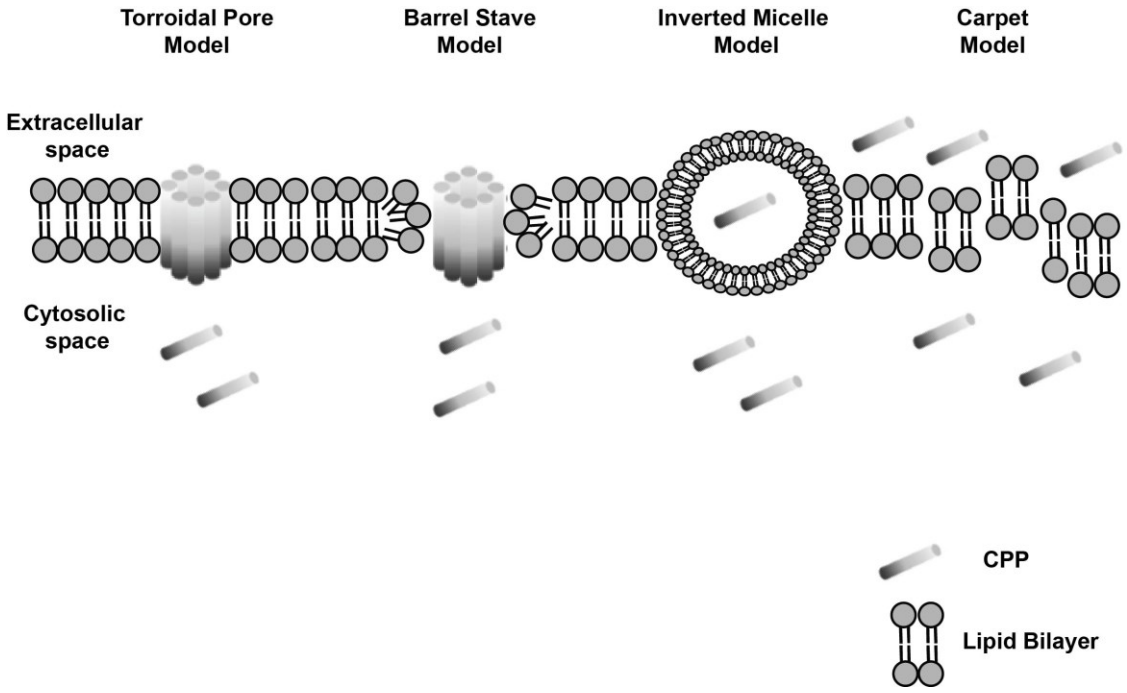

Figure 1-1 Models proposed for CPP direct membrane translocation mechanism. The Toroidal pore model: The CPP inserts into the lipid bilayer and induces a membrane curvature. The Barrel-stave model: the CPP inserts perpendicularly into the lipid bilayer to form a pore in the membrane. The inverted micelle model: The CPP induces the formation of inverted hexagonal structures (inverted micelles) in the lipid bilayer .The carpet model: the CPPs are adsorbed parallel onto the lipid bilayer, and at a threshold concentration this causes a membrane disruption similar to that of a detergent like effect.

in the CPPs, and a transient disruption of the bilayer structure. In membrane thinning, upon CPP interaction with the outer leaflet of the plasma membrane, rearrangements in the membrane cause a local surface tension that allows the CPPs to intercalate within the membrane. The carpet model depends heavily on the presence of hydrophobic amino acids that are not found in all CPPs.

In pore formation models such as "barrel stave" or toroidal pores, the peptide oligomerizes and inserts itself into the membrane[85, 89]. In a "barrel stave" model, the hydrophobic residues in the CPPs interact with the lipid tails, while the polar residues form a ring-structured lumen that is the pore. However, the toroidal model suggests that the CPPs interact exclusively with the polar head group of the phospholipid, which results in pore formation. While the pores formed are described as transient, they allow for sufficient entry of the CPPs into the cytosolic space of the cell.

Together, these models explain certain aspects of CPPs' ability to directly translocate across membranes. However, one of the major drawbacks is that they fail to explain how the uptake of a large hydrophilic cargo can be achieved, especially with no associated cellular toxicity. Therefore, it is apparent that while these models describe certain aspects of how the CPPs translocate, there is likely an additional mechanism by which CPPs and cargo are internalized.

1.3.2 Energy-dependent mechanisms: Endocytosis

It was necessary to reevaluate the work done on CPPs, as early experiments hinted at artifacts in the handling of the samples. Researchers tested whether endocytosis

remained a plausible mechanism by which CPPs might be internalized. Endocytosis is a naturally occurring phenomenon whereby cells internalize biomolecules, toxins, and many required nutrients[83, 90-92]. Endocytosis can be divided into two major classes: phagocytosis and pinocytosis. Phagocytosis, also referred to as "cell eating," is a cellular process that typically occurs in macrophages; it entails the engulfment of cell debris, bacteria, and other large particles[93]. Pinocytosis, or "cell drinking," involves the regulated internalization of smaller particles; it can be divided into the following sub-groups: macropinocytosis, clathrin-mediated, caveolae-mediated, clathrin, and caveolae-independent endocytosis[90, 94]. Regardless of the exact endocytic pathway, a CPP must interact with the cell's surface. This is followed by endosomal entrapment and escape sufficient to allow the cargo to reach its cytosolic target. The following sections will focus on these events.

1.3.3 Cell surface interaction

As mentioned earlier, the bidentate nature of the side chain of the arginine residue found in most CPPs is crucial in its cellular internalization properties. The guandinium moiety can form a hydrogen bond with anionic groups such as phosphates, sulfates, and the carboxylates found on the components of a cellular membrane[95, 96]. Such moieties can be located on proteoglycans (PGs), or proteins that are glycosylated and situated on the cell's surface. Two examples of PGs include the transmembrane syndecan and membrane lipid-linked glypicans[97]. Linear glycosaminoglycans (GAGs) are often substituted with sulfates and, to a lesser extent, carboxylates[98]. Heparin Sulfate PG (HSPG) plays an

important role in the uptake of many arginine-rich CPPs[99-102]. *In vitro* experiments performed using dynamic light scattering (DLS) and isothermal titration calorimetry (ITC) have shown that CPPs, including TAT and nona-arginine, have a high affinity for binding to GAGs. This affinity and multiple sites at which CPPs can bind to GAGs are mainly driven by electrostatic forces and, to some extent, hydrogen bonding. DLS measurements also show the ability of CPPs to form GAG clusters of approximately 2.1 x 10^5 heparin molecules per cluster.

In cellulo experiments have shown that the uptake of arginine-rich peptides was significantly reduced when heparin was incubated in the medium, or upon pre-treatment of cells with trypsin resulting in the removal of cell-surface PGs. Work by Raines and Chernomordik indicated that the internalization of TAT and nonaarginine was reduced in mutant cell types deficient in heparan sulfate (HS) [99, 103]. Interestingly, it was also demonstrated that HSPG and proteoglycans played an important role in the induction of F-actin organization and macropinocytosis[100, 104]. EIPA, an inhibitor of macropinocytosis, significantly reduced the internalization of arginine-rich CPPs in normal cells; however, the inhibitor had no effect on the lamellipodia or cellular uptake of the peptide in a proteoglycan-deficient CHO (Chinese-hamster ovary)-A745 cell line. The internalization of TAT in an HSPG-deficient cell line was 20% to 30% less than that of the wild type. Furthermore, the cellular uptake of R8 CPPs was further decreased in proteoglycan-deficient cell lines, as compared to those that were only HSPG-deficient. These results underscore the involvement of additional receptors (including HSPG) that play a role in the cellular uptake of arginine-rich CPPs. For example, Futaki and coworkers used a

photo- crosslinking approach to identify the membrane-associated receptors of arginine-rich CPPs. They identified specifically the HSPG Syndecan-4 as a binding partner for the photo-labeled octaarginine (R8) CPP[105]. Others have also reported that over-expression of both syndecan-2 and syndecan-4 results in an increased internalization of R8 and TAT.

HSPGs are known to be involved in many cellular processes, and have been reported to be instrumental in ligand catabolism[106, 107]. For example, some ligands that bind HSPGs are endocytosed, which allows them to enter the degradative cellular pathway. More importantly, both syndecans and glypicans are actively endocytosed inside cells[108, 109]. For example, assays show colocalization of TMR-R8 with syndecan-4 in endocytic vesicles. This advocates that HSPGs have the ability to play a role in CPP endocytosis. Moreover, two possible modes of CPP internalization via endocytosis and HSPG interactions has been suggested. In the first, CPPs bind to HSPGs (**Figure 1-1**), which then trigger endocytosis via possible interaction with other receptors ultimately resulting in CPP internalization in endocytic vesicles. In the second, HSPG's act as binding sites for CPPs that allow for piggybacking into cells.

1.3.4 Endocytic internalization and trafficking

Various studies have alluded to the ability of CPPs to hijack many pinocytosis pathways involving membrane ruffling[100]. Researchers have employed a variety of experimental approaches, such as: low temperature (4°C) incubation, incubation with drugs known to inhibit specific endocytic trafficking, colocalization experiments with

endosomal markers, and blocking of the endocytic pathway by overexpression of dominant negative (DN) protein markers[110]. Since endocytosis is an energy-dependent process, flow cytometry analysis of cells incubated with TAT have shown a dramatic reduction in the amount of CPP taken up by these cells after incubation at 4°C[99, 111]. Similar results were obtained by incubating cells using sodium azide and deoxyglucose, which depleted the cellular ATP pool[99]. Futaki and colleagues showed that these results could be generalized to various cationic CPPs, such as FITC-labeled arginine-rich peptides[112, 113].

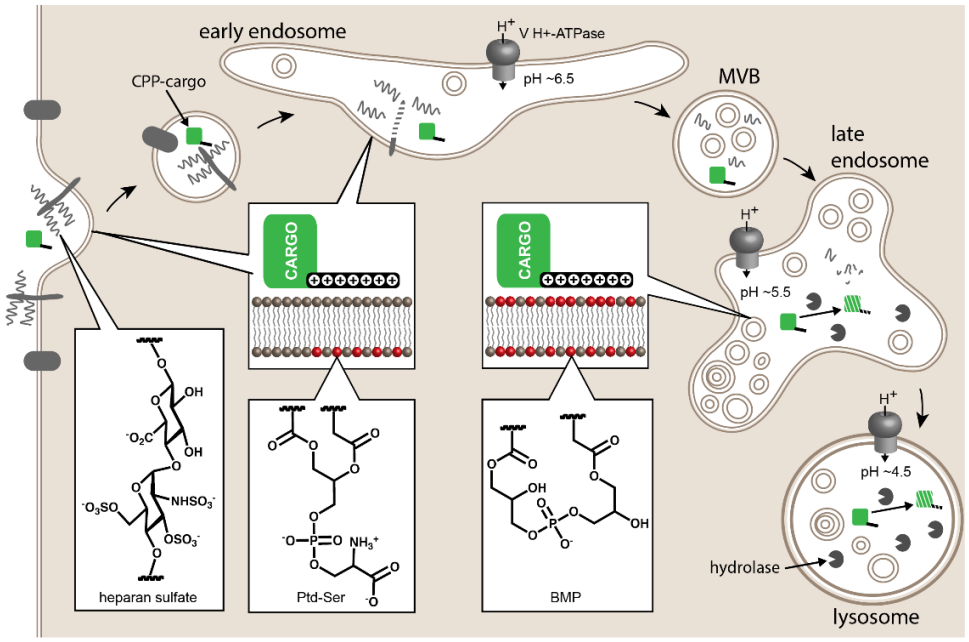

Figure 1-2 Model of the trafficking of a CPP-cargo conjugate through the endocytic pathway. From left to right: A CPP-cargo binds to heparin sulfate proteoglycans (HSPGs) on the cell surface and induces endocytosis. Endocytosis leads to uptake and entrapment of the CPP-cargo inside an endocytic vesicle. The endosomal membrane contains the lipid phosphatidylserine (Ptd-Ser) in its outer leaflet. During endosomal maturation, a vacuolar H+-ATPase acidifies the lumen of endocytic organelles. The CPP-cargo reaches early endosomes (pH~6.5). Concurrently, hydrolases partially degrade HSPGs and release HS fragments. Upon further maturation, the CPP-cargo reaches multivesicular bodies, late endosomes (pH~5.5), and lysosomes (pH~4.5). The membrane of the intraluminal vesicles of late endosomes is enriched with BMP. HS is further degraded to smaller fragments. The CPP-cargo is susceptible to degradation due to the low pH and lysosomal hydrolases. The figure is used with permission[114].

This approach does not allow for differentiation among different types of pinocytosis (i.e., macropinocytosis, clathrin-mediated, and caveolae-mediated endocytosis). However, researchers have attempted to decipher the exact mechanism. To do so, selective inhibitors of these endocytic pathways were used to shut down the pathway and evaluate the CPP penetration. It was demonstrated that cells treated with inhibitors of macropinocytosis, such as cytochalasin D and amiloride (as well as amiloride analogues), showed a dose-dependent decrease in TAT and TAT-cargo conjugate uptake[111, 115]. Experiments using such inhibitors, however, are not ideal, as many have been associated with cytotoxicity, which could have an impact on the results[77]. Additionally, within the CPP field the specificity of these inhibitors is an issue for debate. An alternative approach involves genetically engineering cells to knock down or knock out the expression of important endocytic regulators (eg. clathrin or caveolin) to decipher the exact mechanism of cellular entry[84].

Markers that probe for specific endocytic routes have been used to evaluate the pathway by which CPPs are internalized. These assays are typically evaluated by determining the colocalization efficiency between a fluorescently labeled marker and the CPPs. For example, an arginine-rich CPP was shown not to colocalize with transferrin, a marker for clathrin-mediated endocytosis, while penetratin showed colozalization with this marker[83, 112, 113]. Additionally, common fluid phase markers used for macropinocytosis have been employed, such as fluorescent dextrans molecules and FM4-64[115]. Results showed that TAT and TAT-cargo conjugates stimulated macropinocytosis by a dose-dependent increase in the uptake of dextran markers[111, 115]. While

macropinocytosis is the most recognized uptake mode for the TAT peptide (and will be the focus of the discussion below), it is important to note that research has alluded to the involvement of clathrin and caveoloe-mediated endocytosis[99, 116, 117]. Additionally, work by Duschardt and colleagues compared the internalization mechanisms of the above-mentioned CPPs, and noted that they simultaneously occur via all three endocytic pathways[83]. Together, these results suggest a dependence on the exact endocytic pathway, based on the physiochemical nature of CPPs. While all of the described mechanisms are plausible, the controversy might be explained by the different experimental conditions used in all of the experiments, including: cell lines, incubation times, and peptide concentrations.

Since CPPs have been described as a tool for the delivery of cargo to the insides of cells, it is important to note that the mechanism of cellular entry described for CPPs could be altered by the nature of the cargo[81]. While this adds to the complexity of the process, experiments have indicated the involvement of endocytosis over the direct membrane translocation mechanism suggested for CPP entry alone. The CPPs enter via the endocytic pathway, a process that involves multiple vesicles and maturation events. Macropinocytosis, for example, is a membrane ruffling that occurs in many cell types and typically is stimulated by growth (and other cellular factors)[90]. This ruffling is triggered by rearrangement of the cytoskeleton by actin[118, 119]. It has been shown that treatment of cells with an octa-arginine CPP results in significant rearrangement of the F-actin, similar to what is observed by epidermal growth factor (EGF), a substance that is known to induce this event[112]. Additionally, cytochalasin D, an inhibitor known to induce F-actin

depolymerization, leads to a significant decrease in peptide uptake. Similar results have been observed *in vitro*, using the TAT peptide[120]. In macropinocytosis, the distal edges of the membrane ruffles close up and engulf their extracellular material. A macropinsome is formed upon the constriction and closure of the ruffles and open cup-like structure of the cellular membrane. Occasionally, the ruffles will recede back into the cytoplasm without macropinosome formation. Macropinosomes vary in size from 0.2 to 10 μm in diameter, and their formation is not necessarily dependent upon a ligand-receptor interaction[121]. By comparison, the vesicles formed by clathrin and caveoloe-dependent endocytosis are smaller (50 and 100 nm, respectively)[122, 123]. The difference in vesicle size suggests that there may be an upper limit to the size of the cargo that can be delivered.

Irrespective of the exact endocytic internalization process, the CPP and its cargo are initially trapped inside the endocytic vesicles. The endocytic pathway involves a maturation process that includes an exchange of membrane components, movement toward the perinucleur membrane, vesicular fusion and sorting events, an intraluminal pH drop attributable to the presence of a vacuolar-type H^+ - ATPase (V-ATPase) that pumps protons across the membrane, acquisition of degradative enzymes and other proteins/lipids, and organelle morphology changes. In the first step, a cargo or CPP is internalized into early endosomes (EE). Early endosomes are known to be highly dynamic compartments, due to their homotypic fusion capacity[124]. EEs receive endocytic cargo through all types of endocytic pathways[91].These organelles are highly complex and typically consists of a cisternal region with a thin tubular structure (~60 nm), and a large

vesicle (~300-400 nm) that is multi-vesicular in nature[125]. This gives the EEs a cis-trans polarity and could give specificity to docking and fusion sites on the membrane.

The membrane structure is difficult to envision, as it involves a different curvature, composition and organization than that of the plasma membrane. This is due to the action of molecular machines that allow for the segregation of proteins and lipids in these membranes. The membranes are highly mosaic, with key components that regulate the membrane organization and protein transport found in functionalized domains. For example, the movement of these vesicles on actin cytoskeletons is regulated by small Rab GTPases. There are more than 60 members of the Rab family that are associated with different membranes via a geranylgeranyl group attached to the C-terminus of the GTPases[126]. Rab proteins are considered organelle markers, due to the restriction of their distribution on respective membranes. For example, Rab5 is typically found on EE membranes and is a major regulator for EE maturation. Intraluminal vesicle (ILV) formation occurs in EEs in the large vesicles mentioned above. Detachment of these vesicles from EEs results in formation of multi-vesicular bodies (MVB) that are typically 400 to 500 nm in diameter. The vesicles are known to serve as a transport intermediary between early and late endosomes (LE)[124]. While little is understood about the exact membrane lipid composition, it is recognized that MVBs vary between EEs and LEs. The lipids and proteins could be selectively sorted into such vesicles because of newly formed invaginations at the bilayer.

Maturation of MVBs results in the formation of LEs. These organelles can vary in size and morphology; however, similar to EEs, they have tubular and multi-vesicular

regions. They are characterized by a limiting membrane that contains proteins such as Rab7 and LAMP1 (or the lysosomal-associated membrane protein-1)[127]. Interestingly, late endosomes are highly enriched with a negatively charged lipid lysobisphosphatidic acid (LBPA is interchanged in this text with bismonoacylglycerophosphate (BMP))[128, 129]. BMP is, in particular, enriched in the ILV membranes of LEs, and is not found in upstream endocytic organelles. Interestingly, BMP has been implicated in the escape of some viruses into the cytosolic spaces of cells by a back-fusion mechanism[130, 131]. With respect to CPPs, it has been shown that TAT binds to BMP-enriched liposomes with a high level of affinity[132]. Furthermore, TAT can specifically promote the leakage and fusion of BMP-containing liposomes. The last step in this endocytic pathway is a "point-of-no-return." This involves LE fusion with lysosomes. At this stage, the cargo content of the LE is narrowed down to molecules that must be degraded. The lysosome compartment contains over 60 different acidic hydrolases that are necessary for macromolecular degradation and nutrient recycling[133]. It is crucial that CPPs escape the endocytic pathway before reaching this compartment, where the cargo would be degraded (**Figure 1-2**).

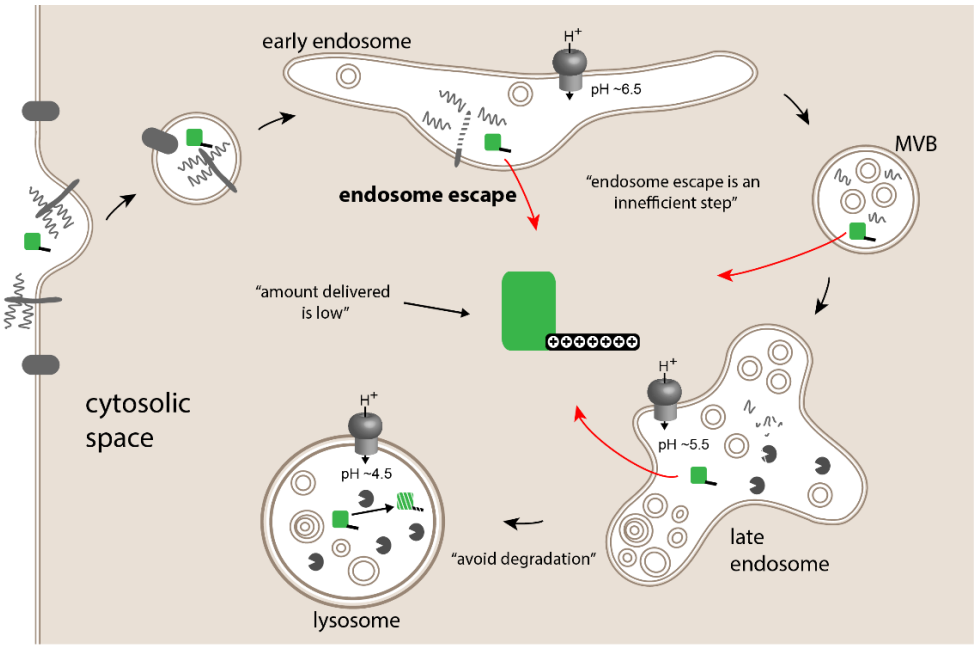

Figure 1-3 CPP-cargo conjugate endosomal escape. From left to right: A CPP-cargo binds to HSPGs on the cell surface and enter cells, which leads to entrapment of the CPP-cargo inside an endocytic vesicle. After the CPP-cargo reaches early endosomes, MVBs or late endosomes it can escape from the endocytic pathway (red arrows). This is the preferred point of exit for a CPP-cargo conjugate in order to avoid degradation. The CPP-cargo is susceptible to degradation and, in order to avoid degradation and inactivation, it needs to escape the endocytic pathway before it reaches lysosomes. The endosomolytic activity of CPPs is low and endosomal escape is inefficient. Consequently, the amount of CPP-cargo delivered into the cytosolic space of cells is very low. The figure is used with permission[114].

1.3.5 Endosomal escape: The bottleneck

For a cargo to achieve its biological function, it must reach its cytoplasmic or nuclear target. Therefore, after endocytic uptake of the CPP cargo, the CPP must display endosomal escape activity. As mentioned above, this must occur before the peptide reaches the lysosome in order to avoid CPP and/or cargo degradation. This step is crucial because it determines the amount of cargo released to the cytosolic space of the cells. The lumen of the endosome closely resembles the outside of the cell; no biological or phenotypic response is elicited in these vesicles. However, the endosomal escape property of many CPPs is suboptimal, which severely limits the application of many well-known CPPs[134]. Yet many studies have provided evidence that endosomal escape of CPPs does occur. For example, Dowdy and colleagues developed assays that employ the CRE recombinase system to distinguish between CPPs bound to the cell's surface (or are endocytosed) and cargo that escape from vesicles[115, 117]. As explained above, this illustrates that the incubation of T-cells with TAT-Cre excises the stop codon flanked by the loxP sites and induces the expression of EGFP in these cell lines. Similarly, Dowdy and colleagues also showed that a CPP fused to a double-stranded RNA binding domain was able to deliver siRNA and mediate an RNAi response in a variety of cell lines[54]. This research indicates that endosomal escape of these CPPs occurs; however, these are both non-stringent assays, since only a few molecules of Cre or siRNA need to escape the endocytic pathway for the phenotypic response to be observed. Conversely, many fluorescent or mass spectrometry-based approaches reveal (to different extents) that most of the CPPs remain trapped in the endocytic vesicles[135-138]. For example, TAT has been

conjugated to a ubiquitinated cargo that is designed to be cleaved upon reaching the cytosol due to the presence of the deubiquitanse enzymes[139]. However, the results show that while the conjugate was internalized by cells, the ubiquitin was not cleaved. This lead to the conclusion that the protein was unable to reach the cytosolic space at a detectable level. Additionaly, TAT has been conjugated to dipheria toxin-A (dtA) fragment, which is a known potent inhibitor of protein synthesis. This conjugate; however, showed no cytotoxicity. This indicates that while the TAT-dtA interacts with the cell surface, its escape from endosome hampers its ability to inhibit protein synthesis[140]. These examples highlight that while endosomal escape occurs, it is a highly inefficient process, which makes studying the mechanism of this process difficult.

Studies exploring how a CPP can directly cross the plasma membrane can also be applied to endosomal membranes. This is due to the notion that the peptide will encounter a similar membrane asymmetry at either the plasma membrane or inside the endocytic vesicle. For example, research has suggested that the crossing involves interaction of the CPPs with negatively-charged lipids[141, 142]. The outer leaflet of the plasma membrane (and to some extent, the inner leaflet of the endosomal membrane) is composed of zwitterionic phospholipid, while the inner leaflet (outer leaflet of endosomal membrane) contains negatively-charged lipids such as phosphatidyl serine (Ptd-Ser) [143-145]. It has been suggested that the CPP on the outer leaflet and the Ptd-Ser underneath it form a membrane capacitor that results in a transmembrane potential[146]. This potential is large enough to form electropores through which the CPP and its cargo can pass. Consistent with experiments by Tunnemann et al., this model also predicts that oligorarginines entering

cells must be superior to oligolysines, and that the more arginines present, the faster the transduction[147]. As explained above, oligolysines are not able to form the CPP-PS capacitor, and more arginines result in a higher transmembrane potential. Indeed, while this same mechanism could be used to explain CPP release from the endosomal vesicles, one must question why the CPP would not disrupt the first membrane it encounters, the plasma membrane. One possible explanation involves the interaction of CPPs with HSPGs. Such interaction at the cell surface decreases the overall pool of CPPs at the membrane. The model also suggests that pore formation depends on the concentration and cargo. As a CPP enters the endocytic pathway, it is still bound to the HSPG, limiting its ability to form pores. However, the HSPG is gradually hydrolyzed along the endocytic pathway. Once the CPP is no longer interacting with the HSPG, it is free to destabilize the endosomal membrane.

As mentioned above, the ILVs of late endosomes are highly enriched with negativelycharged lipid BMP. It has been shown that TAT binds to BMP-enriched liposomes with a high level of affinity[132]. Furthermore, TAT specifically promotes the leakage and fusion of BMP-containing liposomes. It has also been shown that both fluorescently labeled TAT and polyarginine peptides colocalize with Rab5+ and Rab7+ cells (Rab5/7+ cells are transfected with plasmids that code for GFP fusions of WT Rab5 and Rab7 proteins respectively)[136]. This suggests that these peptides travel along the endocytic pathway. Interestingly, the blocking of this pathway by an overexpression of a dominant negative Rab5 indicates that TAT escapes the pathway at a stage downstream of the early endocytic vesicles. Recently, using a similar approach our lab identified the

late endosome to be the escape point of a dimeric version of the TAT peptide. Using a combination of *in vitro* and *in cellulo* assays, we found this escape to be mediated by the interaction of dfTAT with BMP. Using liposomes as a model system, we demonstrated that dfTAT causes the leakage and fusion of BMP-containing membranes. These results are similar to the work published by Melikov et al. using monomeric TAT. Finally, we propose that dfTAT translocates and delivers cargo into the cytosolic space by a leaky fusion event occurring in the late endosomal compartment.

1.4 **Approaches to enhancing CPPs' endosomal escape properties**

Multiple approaches have been exploited to enhance CPPs' endosomal escape properties, including lysomotropic agents, pH-dependent membrane-active peptides (PMAPs), endosomal escape domains (EEDs), photochemical internalization (PCI), and multivalency[114, 148, 149]. Typically, lysomotropic agents are small molecules taken up into lysosomes. One of the most well-known lysosomotropic agents is chloroquine, a base that accumulates in endosomes and lysosomes upon protonation. Chloroquine's function is concentration-dependent; however, at high concentrations it results in endosome swelling by accumulation of counterions of protons in the endosomal lumen[150, 151]. It has been shown, for example, that increasing the concentration of chloroquine can result in enhanced delivery of TAT-Cre and TAT-PNA (two cargos mentioned earlier) conjugates into the cytosolic spaces of cells[115, 152, 153]. However, chloroquine has not seen significant success in *in vivo* applications, due to its high cytotoxity.

PMAP-CPP fusion proteins have been used to increase the endosomal escape of various cargos. PMAPs typically undergo a conformational change in the endocytic pathway as they become protonated; this is due to a decrease in the pH of the lumen of endosomes[154]. This conformational change results in the insertion of the PMAP into the membrane; that, in turn, leads to a preference for the lysis of the endosomal membrane, while keeping the plasma membrane intact[155]. One example is HA2, a peptide derived from the hemaglutinin protein of the influenza virus. Wadia et al. first reported the usefulness of HA2 for the endosomal escape of TAT-Cre. The TAT-HA2 caused an enhancement of TAT-Cre cytosolic delivery, as judged by an increase in EGFP expression[115]. This fusion construct has been demonstrated to be useful in certain therapeutic applications. A fusion of HA2 to p53 and the CPP R11 (HA2-p53-R11) yielded a more efficient reduction in the proliferation of cancer cells, when compared to p53-R11 alone[156]. While many of these concepts are easy to develop as fusion constructs, it is was shown that it was not necessary to fuse the cargo to TAT-HA2; a simple coincubation protocol of the cargo and TAT-HA2 can be performed[157]. This is important because the cargo of interest is directly conjugated to the PMAP-CPP, which in some instances may affect its activity. Similar to lysosomotropic agents, PMAPs have also been associated with toxicity and the retention of a PMAP-CPP-cargo conjugate at the endosomal membrane.

EEDs are hydrophobic peptides that can be fused to CPPs to enhance their endosomal escape. These domains were inspired by the notion that hydrophobic residues are important in virus-mediated endosomal escape. To show their usefulness, a split-GFP

fluorescence auto complementation assay was used that allows for a direct correlation of the amount of cargo delivered, without signal amplification[149]. As was reported in 2005, the removal of β-strand 11(β-11) from the GFP construct resulted in a non-fluorescent GFP [158, 159]. However, trans-coincubation of β-11 with this non-fluorescent fragment reconstitutes the fluorescent GFP protein. Using this assay, researchers showed that upon incubation of the EED GFWFG tagged TAT peptide fused to the GFP-β-11 in cells, stably transfecting the GFP-β1-10 fragment, resulted in an enhanced GFP signal (when compared to the GFP-β-11 conjugated to TAT alone). While some of the EEDs containing additional hydrophobic residues were toxic to cells, these researchers noted that the construct reported above was optimal for enhanced endosomal escape and low toxicity. Although this work appears to be a promising approach, further biophysical studies on these EEDs are required to delineate their mechanisms of action.

In an alternate strategy, photosensitizers have been used as a means of disrupting endocytic vesicles. In 2004, it was shown that fluorescein and Alexa-Fluor 633 labeled-CPPs initially entrapped in endosomes were released into the cytosolic spaces of cells, upon light irradiation with a 488 nm or a 633 nm laser[160]. This was also used for the delivery of proteins to the insides of cells. FITC-labeled CPP R11s conjugated to p53 were released from endosomes, upon light irradiation at 480 nm; they accumulated in the cytosolic and nuclear compartments[161]. Experiments using TMR-TAT indicated that the fluorescent CPPs produced singlet oxygen upon light irradiation[162]. Interestingly, it has been shown that while a nona-lysine peptide labeled with TMR, TMR-K9, accumulates in endosomes at a higher level than TMR-TAT, it remains trapped and cannot escape upon

light irradiation[163]. This suggests a synergistic affect between the CPP and the fluorophore, which transforms the fluorophore into an effective photolytic agent. In general, CPP-mediated photochemical internalization (PCI) and PCI have, however, also been associated with toxicity. While several reports have suggested that this strategy can occur without killing cells, many others have shown it to be independent of fluorescent peptide concentration[164]. For instance, plasma membrane permeabilization and blebbing were observed when light was used to release TMR-TAT from endosomes. Alternatively, CPP-mediated PCI has the potential for *in vivo* uses such as selective cell targeting (e.g., cancer cells), since this approach allows for both temporal and spatial control over the process[165].

Attachment of multiple copies of CPPs to the same structural unit, also known as multivalent CPPs, has also been used as a means of enhancing the endosomolytic activity of CPPs. As this is an approach I used in my thesis work, I will describe the research in this field in the section below.

1.4.1 Multivalency: Enhancing endosomal escape

Multivalency refers to the attachment of multiple copies of a functional element together to form a single multivalent unit. Multivalent interactions are observed in many biological systems, including in the viral and bacterial attachment to a host cell's surface components and the human immune response[166, 167]. Multivalent ligands can interact with multivalent or multiple monovalent (one-copy) receptors[168]. The central advantage of multi-valency is an increase in the avidity observed in the multivalent compound when

compared to the affinity of a monovalent molecule. This is due to an increase in the local concentration of the molecule, which is a consequence of the restriction in spatial configuration of each functional element. This phenomenon is referred to as the chelate or avidity effect[169].

1.4.2 Approaches to and implications of cargo delivery

Different methods have been exploited to generate multivalent CPPs (mCPPs), such as complexation, oligomerization/aggregation, and certain coupling mechanisms. These approaches have allowed for the pairing of multivalent peptides with cargos of interest[169]. For example, Torchillin et al. reported on the complexation of over 100 TAT peptide copies to a liposome modified with the PEGylated lipid p-nitophenylcarbonyl-PEG-phosphatifylethanolamine(pNP-PEG-PE)[170]. These TAT-conjugated liposomes have been used in the DNA transfection of mouse fibroblasts and Lewis Lung carcinoma cells[171, 172]. Additionally, it has been shown that various CPPs conjugated to liposomes can enhance their internalization properties in a manner dependent upon the number of CPPs per liposomal surface[173]. In another study, superparamagnetic nanoparticles were complexed with TAT peptides to achieve a multivalent CPP complex[174, 175]. These complexes demonstrated a dose-dependent increase in translocation efficiency as a function of the number of TAT copies, and have been used to track hematopoietic stem cells and antigen-specific T-lymphocytes[176, 177].

The cargos being delivered have in some instances been used to generate multivalent CPP systems. Such loads typically either oligomerize or are prone to

aggregation. For example, several CPPs have been fused to p53, the tumor suppressor, due to its ability to form a tetramer[178, 179]. Specifically, using solid-phase peptide synthesis TAT, decaarginine and decalysine have been fused to the N-terminus of the tetramerization domain of p53 (p53tet) (**Figure 1-3**), which corresponds to residues 325 to 355[180, 181]. The results showed that the tetravalent peptide displayed a 10- to 100-fold enhancement in internalization efficiency, when compared to a monomeric counterpart (an L334P mutation in the p53 tet resulted in the generation of mutants unable to form a tetramer known as p53 mono). These tetravalent compounds have also been used as a more

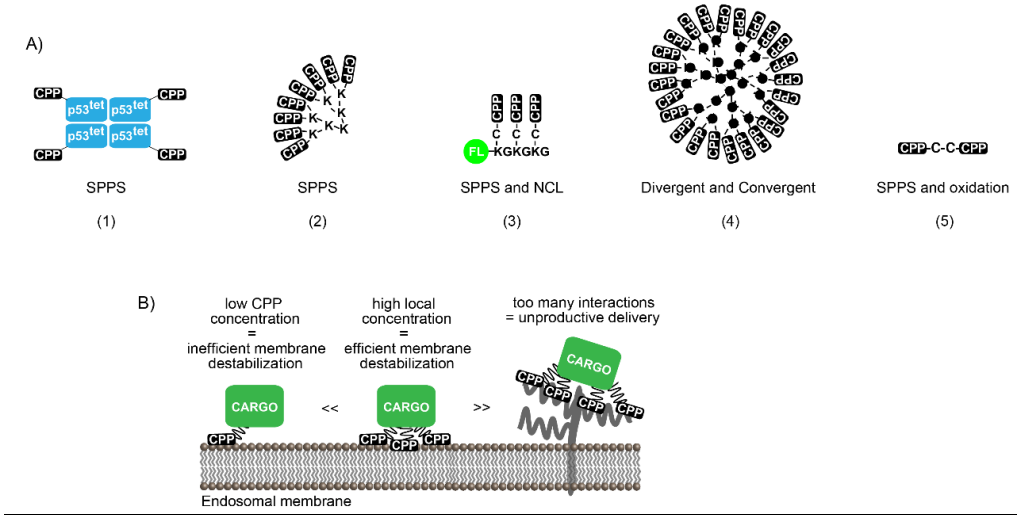

Figure 1-4 mCPP systems and their interactions with membranes. (a) Strategies used to generate mCPPs. From left to right: (1) The p53tet-CPP system involves connecting the tetramerization domain from the human tumor repressor protein p53 to a CPP. The peptide sequence is generated using SPPS. After purification of the peptide sequence, p53tet selfassembles into a tetramer producing a tetravalent CPP. (2) Loligomers are a "squid-like" mCPP system. The CPP is attached on the surface of a polylysine branch scaffold. The scaffold and the peptide are generated using SPPS. The number of branches of this mCPP system will depend on the number of Lys coupling steps. (3) The branched CPP system involves the generation of a peptide scaffold of Lys(ε-NH-Cys)Gly repeats to which a CPP-thioester is added using native chemical ligation (NCL). The peptides were generated using SPPS although production of recombinant peptide or protein thioesters is possible using intein fusions. A fluorophore was added on the *N*-terminal end of the scaffold peptide to serve as both an imaging agent and a small model cargo. (4) Dendrimers are mCPPs having a "tree-like" shape and are usually generated using divergent or convergent methods. CPPs have been attached to the surface of polyamidoamine (PAMAM), polypropylenimine (PPI) or polyethylenimine (PEI) dendrimers. The number of CPPs on dendrimers is among the highest observed for MCPPs. (b) A possible model for the mode of action of CPPs versus that of MCPPs. In this example, a CPP-cargo is present at the membrane of endosomes at a low local concentration, leading to poor endosomolytic activity. In contrast, a MCPP-cargo displays multiple copies of the CPP. This leads to efficient membrane interactions and a possible enhancement in membrane disruption. In some cases however, too many CPP copies might cause unproductive membrane interactions such as tight binding to HSPGs. This in turn might lead to poor cellular penetration. The figure is used with permission[114].

efficient means of delivering DNA into cells (as compared to monomeric forms), with the tetravalent decaargine (10R-p53tet) peptide being the most efficient at cellular entry. An additional example is fusion constructs of Antp or TAT with the Grb10 SH2 domain or the BH4 domain of Bcl-XL[182, 183]. These domains are predicted to form aggregates in a solution, due to a stretch of five or more amino acids that have a 50% probability of undergoing β-strand driven aggregation.

Another example of multivalent CPPs was generated through a branching system. For example, dendrimers are functionalized scaffolds to which multiple CPPs can be conjugated.[184-188] Dendrimers are highly branched molecules that have tree-like shapes. A specific example of a dendrimer is a "squid-like" construct known as a loligomer[189-192]. A loligomer contains eight CPP copies conjugated on a branched polylysine scaffold. These branched peptides have been successful at condensing DNA and increasing the efficiency of its internalization through the formation of a DNA-dendrimer conjugate[192]. Loligomers have also been conjugated to antigenic epitopes, and have successfully generated cytotoxic T-cell responses[191]. Other scaffolds have been created to generate mCPPs that display two, three, or four CPP copies. For example, a TAT peptide functionalized with a C-terminal thioester was conjugated to the cysteine of a (Lys(ε-NH-Cys)Gly)n scaffold by native chemical ligation[193, 194]. Also, CPPs modified by the addition of cysteine residues have been dimerized to form simple multivalent CPP systems with enhanced internalization properties[195, 196]. The latter will be the approach I use in this thesis to generate a simplistic multivalent CPP system.

1.4.3 Limitations and challenges

While multivalent CPP systems have been shown to enhance internalization properties, many challenges to this approach still exist. One of the major difficulties for mCPP is construct generation; such reagents are complex and difficult to synthesize compared to their monomer counterparts. This often leads to low yields, limitations on the size of the molecule generated, and homogeneity in the final product[194]. Additionally, the effectiveness of using branched CPPs for *in vivo* delivery systems is uncertain, due to their potential immunogenicity. Multivalent CPPs share common structural features with multiple antigenic peptides (MAPs). MAPs induce immune responses by their display of multiple copies of an antigen that can be recognized by T-cells. In a similar fashion, mCPPs may induce comparable undesirable immune responses *in vivo*. Moreover, it is not completely understood how multivalent CPPs are internalized or result in enhanced endosomal escape, as compared to their monomeric counterparts.

While some laboratories have reported an enhanced efficiency in dimeric CPPs, other research has shown that a scaffold with two TAT copies does not lead to enhanced cell penetration. Such results clearly highlight that the exact nature of the construct could affect the cell penetration properties. Therefore, structure activity relationship studies are necessary to understand how molecular parameters participate in CPP interaction with cell surfaces and internalization mechanisms. While some research has reported that mCPPs interact with heparan sulfate proteoglycans and are internalized via the endocytic pathway, many questions remain as to how these peptides escape from that pathway. Furthermore, many strategies have been developed to enhance their endosomal escape properties, as a

number remain suboptimal. These include combining the multivalency and with pH-responsive domain (as mentioned above). Lastly, as described for their monomeric counterpart, the effect of conjugated cargo on the internalization and overall mechanism of mCPPs remains unknown. Therefore, in-depth structure activity and mechanistic studies are important to finding the answers to many unanswered questions. This would allow for the optimization and generation of new and improved delivery agents.

1.5 **Enhancing the chemical stability of CPPs**

Despite their promising application as a drug delivery tool, the use of CPPs and branched CPPs has been limited due to their inherent chemical instability. Such peptides are prone to degradation by extracellular and intracellular proteases. This degradation can, ultimately, diminish CPP activity, since it may result in inactive compounds or a decreased concentration of the peptide exposed to the biological matrix. To avoid or slow down the kinetics of CPP degradation, stable or non-degradable CPPs have been generated.

1.5.1 Classes of non-degradable CPPs

Stereochemical modifications

One of the simplest approaches employed to improve CPP stability is changing the stereochemistry of the amino acid incorporated into them. The D-form of amino acids is not recognized by cellular proteases, and therefore peptides that are stable can be generated in this fashion. D-amino acids can be incorporated into the entire peptide

sequence, or at different positions within the sequence. Researchers have found success with several CPPs, such as polyarginine, pVEC, and penetratin[32, 75, 197]. Studies have also shown that the stability of a CPP can be modulated by changing the position and number of D-amino acids incorporated in its sequence[198]. As peptide chirality can play a role in the interaction of CPPs with the cell surface, altering the stereochemistry could affect the internalization efficiency and general mechanism. Additionally, the impact of the chirality of CPPs (e.g., R9 and penetratin) on cellular internalization has been reported to vary among different cell lines[199].

While the incorporation of D-amino acids could improve the stability of CPPs, it was reported that D-penetratin resulted in a decrease in uptake of some cargos, as compared to the L-counterpart[200]. To circumvent this problem, studies with human calcitonin (hCT)-derived CPPs have shown that substituting only the residues recognized by proteases will improve stability while maintaining the CPPs' internalization property[201]. In the 1980s, Chorev and Goodman hypothesized that exchanging the peptide sequence in all D-amino acids (*inverso*) and then reversing the order of the amino acid sequence (*retro*) would result in a peptide with side chains that would preserve the stereochemistry as the parent L-amino acid peptide[202, 203]. These peptides referred to as *retro inverso* (RI) peptides, have been implemented as a means of enhancing peptide stability in many applications, with a history of mixed success[204, 205]. Dowdy and colleagues used the RI construct of the TAT peptide conjugated to a p53 activating peptide (RI-TATp53C') to activate the p53 protein in cancer cells. They showed that the RI-TATp53C' could arrest the cell cycle at a substantially lower concentration than the L-

isomer peptide p53C'TAT. Additionally, a single treatment with the L-isomer resulted in the cells reentering the cell cycle after 24 h, while the RI peptide was able to maintain its activity for more than seven days[64]. Similar results have been observed for other CPPs, such as penetratin[206].

Incorporation of non-natural amino acids

Non-natural amino acids can be incorporated into the peptide chain as a way of avoiding recognition by proteases. For example, alternative alpha (α) amino acids with unnatural side chains or the amino group attached to a group other than the alpha carbon have been used. This approach maintains the peptide backbone topology, while generating unrecognized side chains. For example, α-amino isobutyric acid, a non-natural amino acid, is known to promote helix formation; this conformational constraint may increase peptide stability[207]. This approach was used to enhance the functionality of the CPP mitoparan[208]. Additionally, α-aminoxy acids have been employed as scaffolds to enhance the stability of analogous oligoarginine peptides[209]. Peptide hybrids were generated by alternating the α-aminoxy acids and a natural α-amino acid, resulting in peptides with enhanced stability, low cytotoxicity, and efficient cytosolic-penetrating CPPs[210].

Similarly, beta (β) and gamma (γ) amino acids have been incorporated solely or in addition to α-amino acids into peptide chains. In β-amino acids, the amino group is attached to the β-carbon instead of the α-carbon. These β-amino acids have been used to study the effects of the conformational stability and geometry of the guanidium group on polyarginine CPPs[211]. The β-amino acids' incorporation into CPPs resulted in more stable

conformers and CPPs with enhanced penetration efficiency, when compared to non-modified CPPs[212-214]. Similar results have been reported using γ-amino acids[215].

Cyclic and stapled peptides

Cyclic peptides were inspired by molecules observed in nature, such as cyclosporin. Cyclosporin is a natural product obtained from fungus that is known to be a stable cyclic peptide composed of modified D-amino acids. Encouraged by this peptide, N- to C-termini cyclization of many CPPs has been performed in an effort to enhance their proteolytic stability. For example, Tunneman et al. incorporated additional lysine and glutamic acid at respective TAT termini to allow for cyclization[216]. Results from this work showed that while cyclic and linear TAT entered cells with similar levels of efficiency, the kinetics of the entry were different. Cyclization of the peptide resulted in its entering cells at a faster rate (by 15 min) than linear TAT. While cyclization enhances the stability of CPPs, the authors also proposed that the conformational restriction that allows for maximal separation of the guanidinium groups aids in the enhanced internalization of cyclic CPPs[217]. Further examples of cyclic peptides include: macrocyclic CPPs, bicyclic CPPs, and cyclic cysteine knots (CCK), all of which have been reported to have enhanced stability, increased internalization and release properties, and lower cytotoxicity[218-220]. Bicyclic peptides can be used as a dual-function CPP, with one cycle responsible for internalization and the other for targeting purposes. This has been applied to intracellular targets such as Pin 1 isomerase and tyrosine phosphatase 1B. CCK's, or cyclic peptides that have six cysteines in their sequences for disulfide bond formation, were inspired by

nature. CCK scaffolds have been engineered and modified to be used in therapeutic applications[221].

Stapled peptides, as mentioned above, are peptides that have a stable α-helix structure. The α-helix can be stabilized via side chains cross-linking on the same side of the helix, including disulfide bridges or hydrocarbon stapling (click chemistry involving a ring-closing olefin metathesis, etc.). The increase in helicity of the stapled peptides depends on the amino acid sequence and exact position of the staple. While this conformational restriction aids in the proteolytic stability of the peptide, interest in stapled peptides has primarily been due to their intrinsic cell-penetrating properties. Even though stapling does not mean that a peptide becomes cell-permeable, most stapled peptides are[18]. This is thought to be due to the conformational restriction of the peptide, as seen with cyclic peptides. However, it remains unclear whether the staple itself, the increase in helicity or the exact residues play a bigger role in the cellular penetration activity of these peptides[18].

1.5.2 Limitations and challenges

Ways to improve peptide stability are regularly being researched[222]. Enhanced stability, however, may come at the cost of a decrease in biodegradability. Many stabilized CPPs are made of non-natural amino acids that cannot be reused for new protein synthesis. Additionally, it is important for a peptide to be degraded after achieving its biological response, since this may reduce cellular toxicity levels. Interestingly, it has been reported

that while RI peptides are more stable than their L-counterparts, they are associated with severe cytoxicity[223]. This toxicity is characterized for example by a loss of mitochondrial transmembrane potential, decreased metabolic activity, cellular morphology changes, and an induction of apoptosis. Additionally, while L- to D- conversion can enhance the stability of CPPs, it could also affect CPP cellular internalization[223]. For example, the RI form of M918 is a CPP derived from the tumor suppressor protein p14ARF, which exhibits lower internalization levels than its L-counterpart. While this is not the case for all CPPs, it raises the issue of whether the generation of new stabilized CPPs requires complete reevaluation of their internalization efficiency and mechanisms. Essentially, the effect on internalization could ultimately also affect endosomal escape. Assuming fewer CPPs are internalized, a lower CPP concentration at the endosomal membrane would result in less efficient membrane disruption.

1.6 **Goal of this research**

In this study, I used a multivalent approach to improve the endosomal escape property of CPPs. Many multivalent methods suffer from complexity in the synthesis, low yields, and high toxicity; I aim to overcome all of these complications. My work focuses on the generation of a multivalent CPP that combines the important parameters of an ideal delivery strategy: simplicity of synthesis and protocol, high delivery efficiency, low cellular toxicity, and the ability to deliver proteins to live cells. Due to the low level of efficiency previously seen in CPPs, it has been difficult to decipher the exact molecular parameters required to generate effective endosomolytic agents. With a highly efficient

multivalent system, I hope to answer two key questions: 1) What is the impact of peptide chirality and proteolytic degradation on cell penetration (Chapter 3)? and 2) What are the important residues in CPP sequence required for endosomal escape (Chapter 4)? Next-generation peptides based on the multivalent prototype were generated using solid phase peptide synthesis (SPPS) to asses these questions. Liposomes were used as an *in vitro* model membrane system, allowing for the assessment of these peptides and comparisons to be made in a controlled setting. These assays were complemented with *in cellulo* assays that allow me to distinguish the activity of the various peptide constructs in their cellular environment. The results of this work will aid in the development of new and improved delivery agents for both therapeutic and cell biology applications.

2. DELIVERY OF PROTEINS, PEPTIDES AND CELL-IMPERMEABLE SMALL MOLECULES INTO LIVE CELLS BY INCUBATING WITH THE HIGHLY ENDOSOMOLYTIC DELIVERY AGENT, dfTAT[157, 224]

2.1 Introduction

In this chapter, I aimed to generate a multivalent CPP system that enables the delivery of macromolecules inside live cells. Using a simple synthesis approach, I generate a dimeric fluorescent derivative of the CPP TAT, dfTAT, and determine its activity inside cells. I hypothesize that dfTAT will have an enhanced endosomolytic activity compared to the monomer TAT. This is based on the notion that multivalency increases the local concentration of CPPs at the membrane. Here, I demonstrate that dfTAT penetrates live cells by escaping from endosomes with a particularly high efficiency. By mediating endosomal leakage, dfTAT also delivers a variety of proteins to the cytosolic space of cells after a simple co-incubation protocol. I show that cytosolic delivery is achieved in several cell lines and primary cells, with relatively small amount of material remained entrapped inside endosomes. Delivery did not require a binding interaction between dfTAT and a protein, multiple copies could be delivered simultaneously, and delivery could be repeated.

---

*This chapter is reprinted with permission from "Protein delivery into live cells by incubation with an endosomolytic agent" by Erazo-Oliveras, A.[+]; Najjar, K.[+]; Dayani, L.; Wang, T.-Y.; Johnson, G.A. and Pellois, J.-P. *Nature Methods* **2014**, 11 861-867. doi: 10.1038/nmeth.2998. [+]authors contributed equally. Copyright (2014) by Kristina Najjar

* This chapter is in part a collaboration from Alfredo Erazo Oliveras Dissertation titled: "Cytosolic delivery of proteins, peptides and cell-impermeable small molecules into live cells utilizing virus-inspired multivalent cell-penetrating peptide: principles and mechanism".

Surprisingly, dfTAT-mediated delivery did not noticeably affect cell viability, cell proliferation or gene expression. dfTAT-based intracellular delivery should be useful for cell-based assays, cellular imaging applications and the *ex vivo* manipulation of cells.

2.2 **Results**

Protein transduction strategies are extremely useful for the investigation and manipulation of cellular processes. For example, proteins labeled with fluorophores, stable isotopes or reactive tags and delivered into live cells can, for instance, be used for imaging applications or *in cellulo* structure determination by NMR, respectively[225-227]. Despite the unique opportunities provided by protein transduction technologies, current protocols are often suboptimal[134, 228]. Proteins fused to a protein transduction domain (PTD) or CPP typically use the endocytic pathway as a route of cellular entry[229]. However, the majority of PTD-protein fusions endocytosed by cells typically remain trapped inside endosomes; as a result, the amount of protein that reaches the cytosol of cells is low, and the biological outcomes achieved are poor[230]. A possible solution to this problem is to increase the ability of proteins to escape from the endocytic pathway. This is possible with membrane-destabilizing agents that disrupt endosomes[231-233], but to date, the efficiencies of available reagents have remained low[234, 235]. Ideally, a delivery strategy should combine efficient endosomal escape, low cell toxicity and convenience. I aimed to develop an innocuous endosomolytic agent that efficiently delivers protein cargos into cells.

2.2.1 Generation of dfTAT and its monomeric counterparts

I used TAT as the template for my design of the dimeric delivery vehicle. The fluorescent peptide CK(ε-NH-TMR)-TAT (fTAT) was generated by SPPS using standard Fmoc protocols. I introduced a lysine at the N-terminus of TAT bearing a Mtt protecting group at the ε-NH_2. The lysine side chain protecting group was removed orthogonally with 2 % trifluoroacetic acid (TFA) and modified with TMR for fluorescence imaging. I added a cysteine at the N-terminus to permit dimerization by disulfide bond formation (**Figure 2-1**). Disulfide bonds are relatively stable inside endosomes but are cleaved following endosomal escape and upon entry into the reducing cytosolic space of cells[134, 236, 237]. TFA cleavage and preparative scale reverse phase HPLC purification afforded fTAT (**Figure 2-2 (A)**). Incubation in oxygenated medium and oxidation of the free cysteine thiol of fTAT generated the dimer (CK(ε-NH-TMR)TAT)2 (dfTAT; **Figure 2-2 (B)**). Alternatively, the thiol of CK(ε-NH-TMR)TAT was acetamidated to obtain a peptide (acfTAT) that cannot dimerize (**Figure 2-3**) or was reacted with bis(maleimido)ethane to obtain a nonreducible dimer (nrdfTAT) (**Figure 2-4**). dfTAT, acfTAT and nrdfTAT were purified by HPLC and their identities were evaluated by MALDI-TOF mass spectrometry (**Figure 2-3, 2-4 and 2-5**).

Figure 2-1 Multivalent CPP system using disulfide bonds. Peptides will be generated using SPPS, which should allow obtaining higher yields than before. The multivalent CPP, dfTAT, will be generated by a simple oxidation step with a peptide containing one Cys residue (top) then allowing the product of that reaction to react with itself to form the dimer product.

Figure 2-2 Chemical structure of fTAT and dfTAT. (a) fTAT contains the TAT sequence, a fluorescently- labeled Lys residue and Cys residue (Lys and Cys were conjugated to the N-terminus of TAT). (b) The thiol group in fTAT is oxidized to form a disulfide bond and generate dfTAT. The exact mass of each peptide is shown.

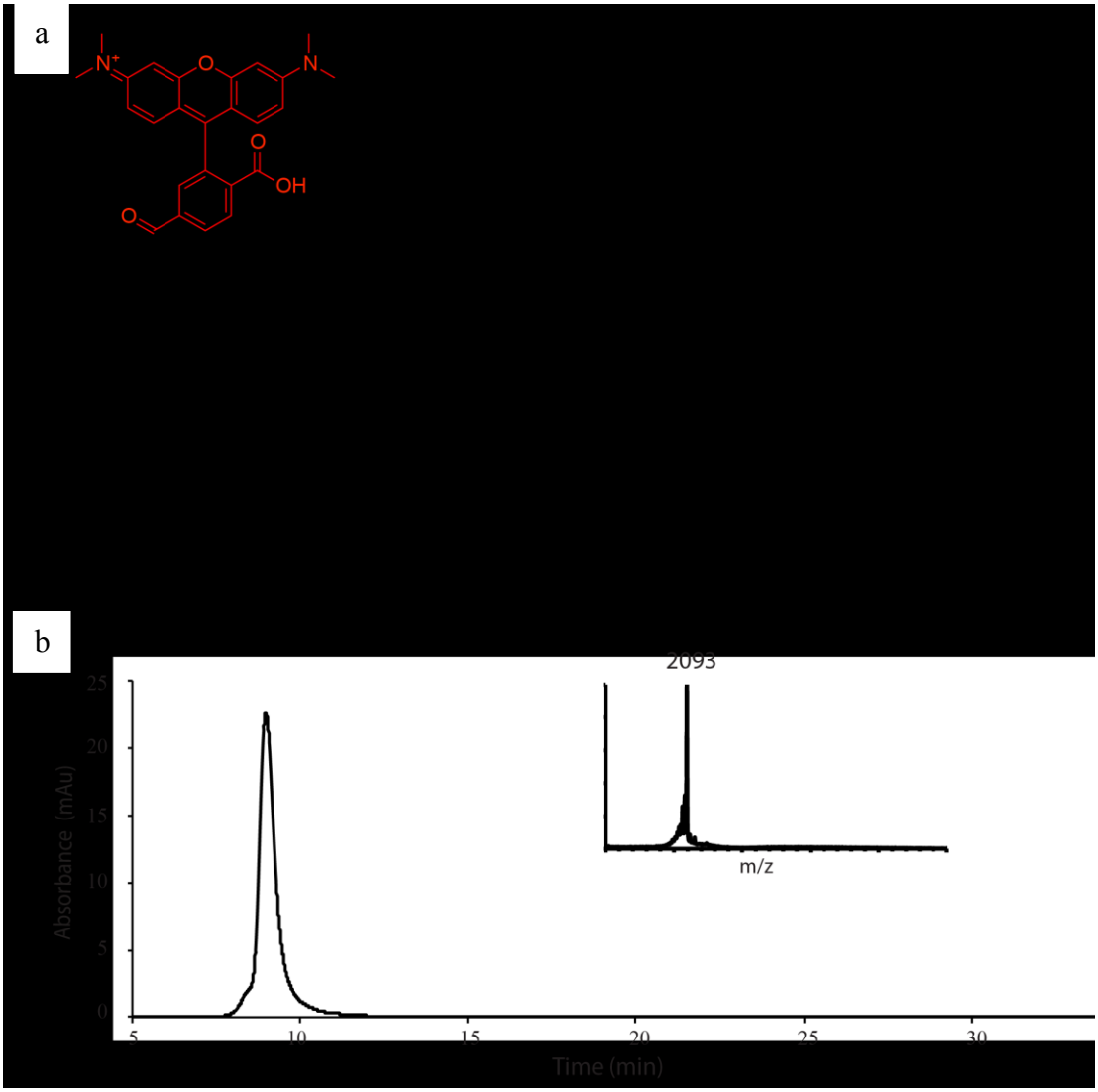

Figure 2-3 Characterization of acfTAT. (a) Chemical structure of acfTAT and its exact mass. The alkyl amide group on the peptide prevent dimerization in cells (arrow). (b) HPLC chromatogram of pure acfTAT and MALDI-TOF spectrum.

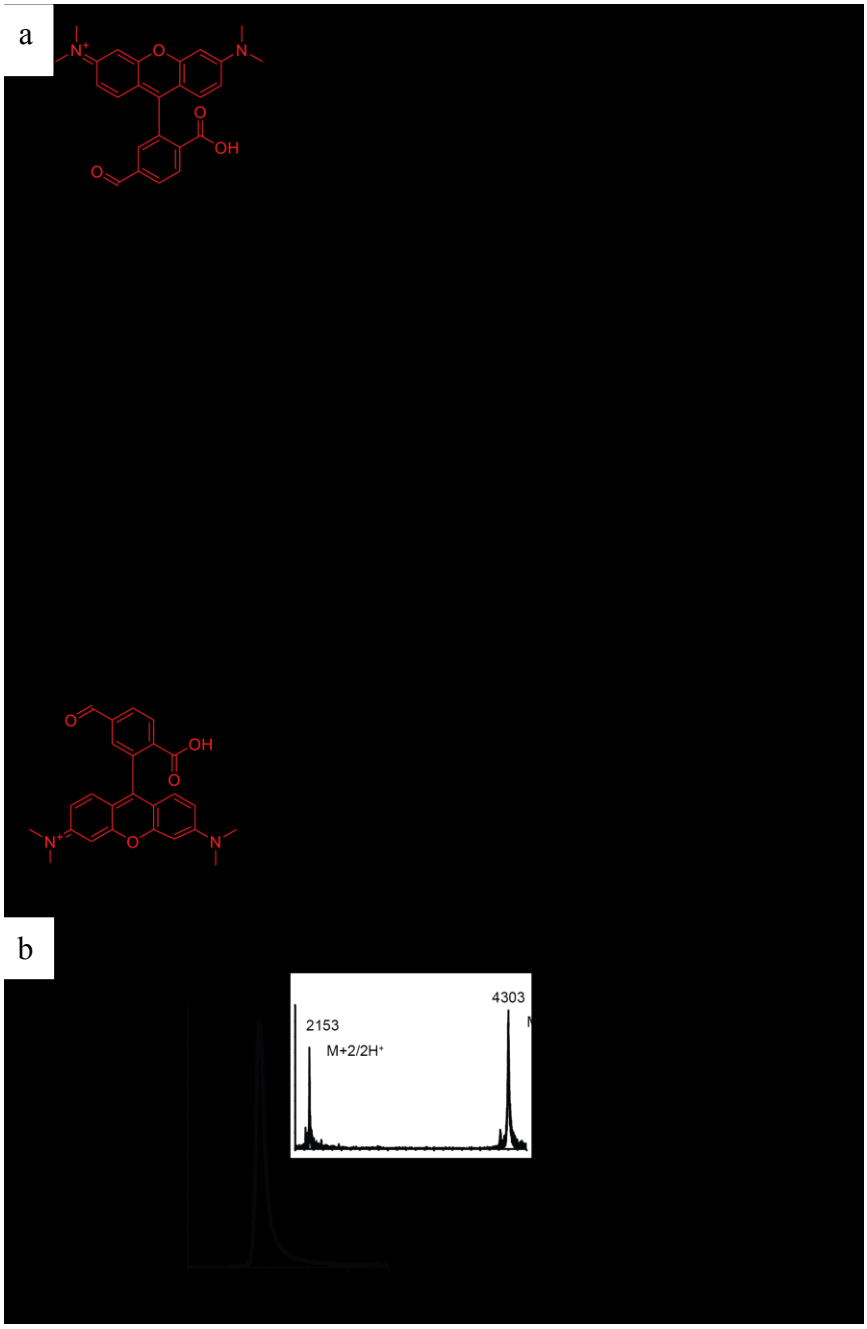

Figure 2-4 Characterization of nrfTAT. (a) Chemical structure of nrfTAT and its exact mass. (b) HPLC chromatogram of pure nrfTAT and MALDI-TOF spectrum. The 2153 m/z peak corresponds to doubly charged nrfTAT.

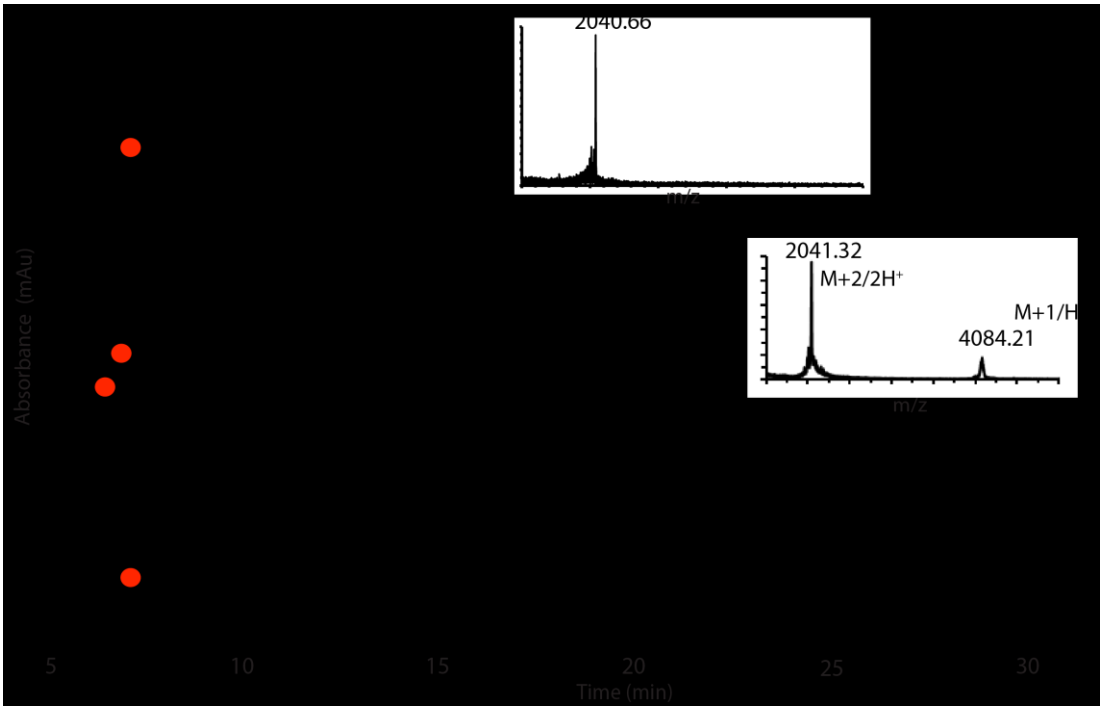

Figure 2-5 Characterization of dfTAT. HPLC analysis of reduction reaction of dfTAT after addition of the reducing agent tris(2-carboxyethyl)phosphine (TCEP). Pure dfTAT was mixed with a solution of TCEP (50 mM) in water and allowed to react for 15 min. The HPLC chromatogram shows a peak with rt = 14.3 min and is identical to the retention time of pure fTAT.

2.2.2 dfTAT penetrates the cytosol of live cells efficiently

I incubated fTAT, acfTAT, dfTAT and nrdfTAT for 1 h with HeLa cells, the mouse neuroblastoma cell line Neuro-2a and human primary dermal fibroblasts (HDFs). Internalization was first assessed by fluorescence microscopy. acfTAT (1–20 μM) localized in a punctate distribution consistent with accumulation of the peptide inside endosomes[72] (**Figure 2-6 (A)**). The fluorescence signal of dfTAT was also punctate below 2 μM but became distributed in the cytosolic space and nucleus of an increasing number of cells at higher concentrations (**Figure 2-6 (B) and 2-7**). The overall amount of dfTAT inside cells (in the cytosolic space and endosomes) also increased with the concentration of dfTAT administered extracellularly (**Figure 2-6 (C)**). I delivered dfTAT into the cytosolic space and nucleus of additional cell lines and primary intestinal porcine epithelial cells (**Figure 2-8**). In all cases, cells were not stained with SYTOX® Blue, indicating that their plasma membrane was not compromised and that the cells imaged were alive. Similarly to acfTAT, fTAT was localized inside endosomes at up to 10 μM. However, at 20 μM, many cells displayed cytosolic fluorescence, indicating that fTAT reproduced some of the activity of dfTAT by possibly dimerizing *in situ* (**Figure 2-9**). Finally, nrdfTAT displayed a cytosolic distribution similar to that obtained with dfTAT (**Figure 2-10**), indicating that the disulfide bond present in dfTAT was not required for cytosolic penetration.

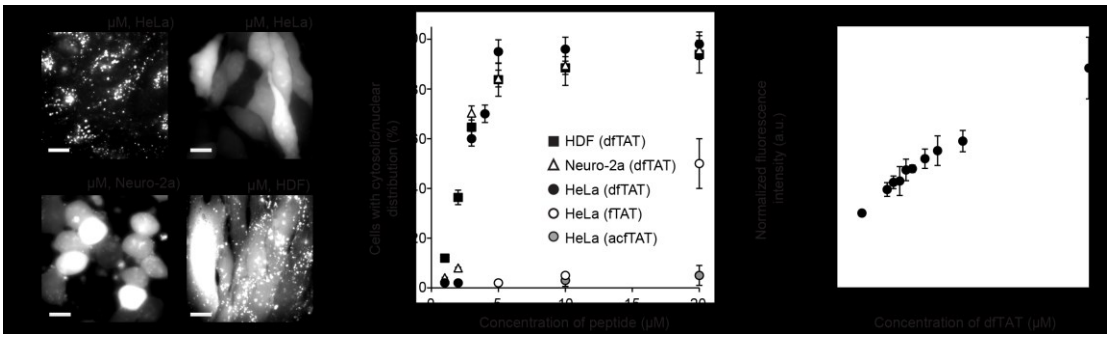

Figure 2-6 Cytosolic delivery of dfTAT in live cells is efficient. (a) Cellular localization of acfTAT and dfTAT assessed by fluorescence microscopy. Cells were incubated for 1 h with either acfTAT (20 μM) or dfTAT (5 μM), washed and imaged with a 100× objective. Monochrome images represent the emission of TMR at 560 nm. Scale bars, 10 μm. (b) Comparison of the cytosolic delivery efficiency of acfTAT, fTAT and dfTAT. Cells were incubated with acfTAT, fTAT or dfTAT (1–20 μM) for 1 h. The number of cells with detectable cytosolic and nuclear fluorescence distribution in microcopy images was counted and divided by the total number of cells present (1,000 cells per experiment). (c) dfTAT overall uptake in HeLa cells as a function of the concentration of dfTAT present in the incubation medium. Cells were incubated with dfTAT (1–10 μM) for 1 h, and relative uptake was assessed quantitatively by measuring the bulk fluorescence of cell lysates (300,000 cells per experiment). a.u., arbitrary units. The data in b and c represent the mean of triplicate experiments and the corresponding s.d.

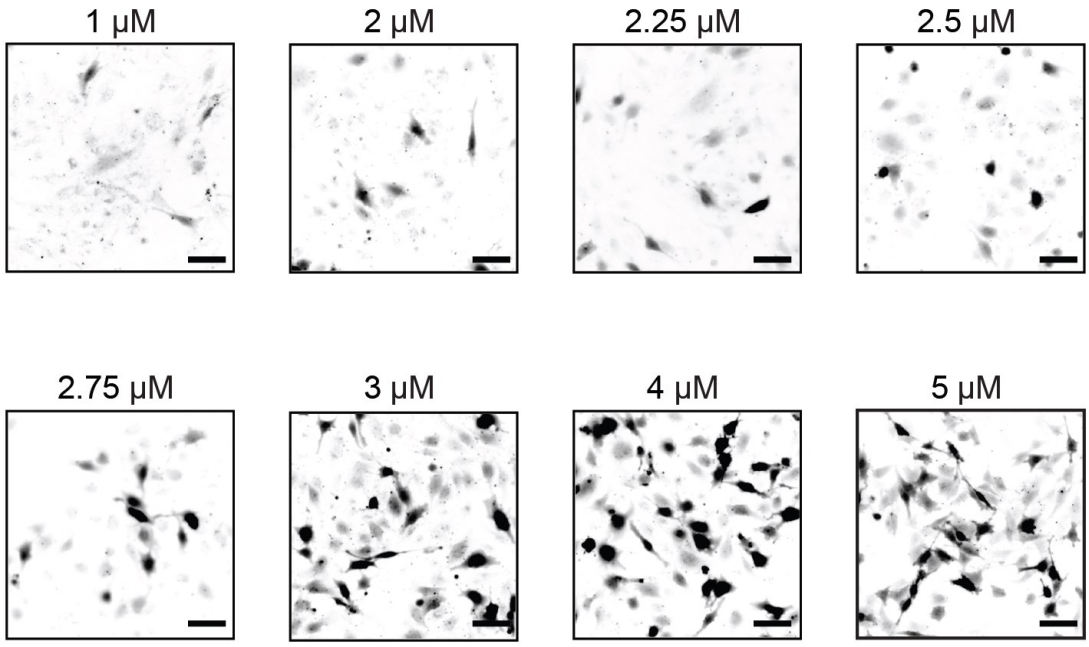

Figure 2-7 Cytosolic and nuclear fluorescence distribution of dfTAT is concentration dependent. HeLa cells were incubated with varying concentration of dfTAT (1, 2, 2.25, 2.5, 2.75, 3, 4, 5 µM). Cells were washed and imaged. Inverted monochrome images (20X objective) show a dramatic increase in the cytosolic delivery of dfTAT between 2-5 µM. Although not shown here, the number of cells in each image is approximately the same as determined by brightfield imaging. Cells that display a fluorescence punctate distribution are not clearly visible under these imaging conditions. Further analysis of these cells using 100X objective clearly show a fluorescence punctate distribution indicative of peptide trapped in endosomes. Scale bars: 50 µm

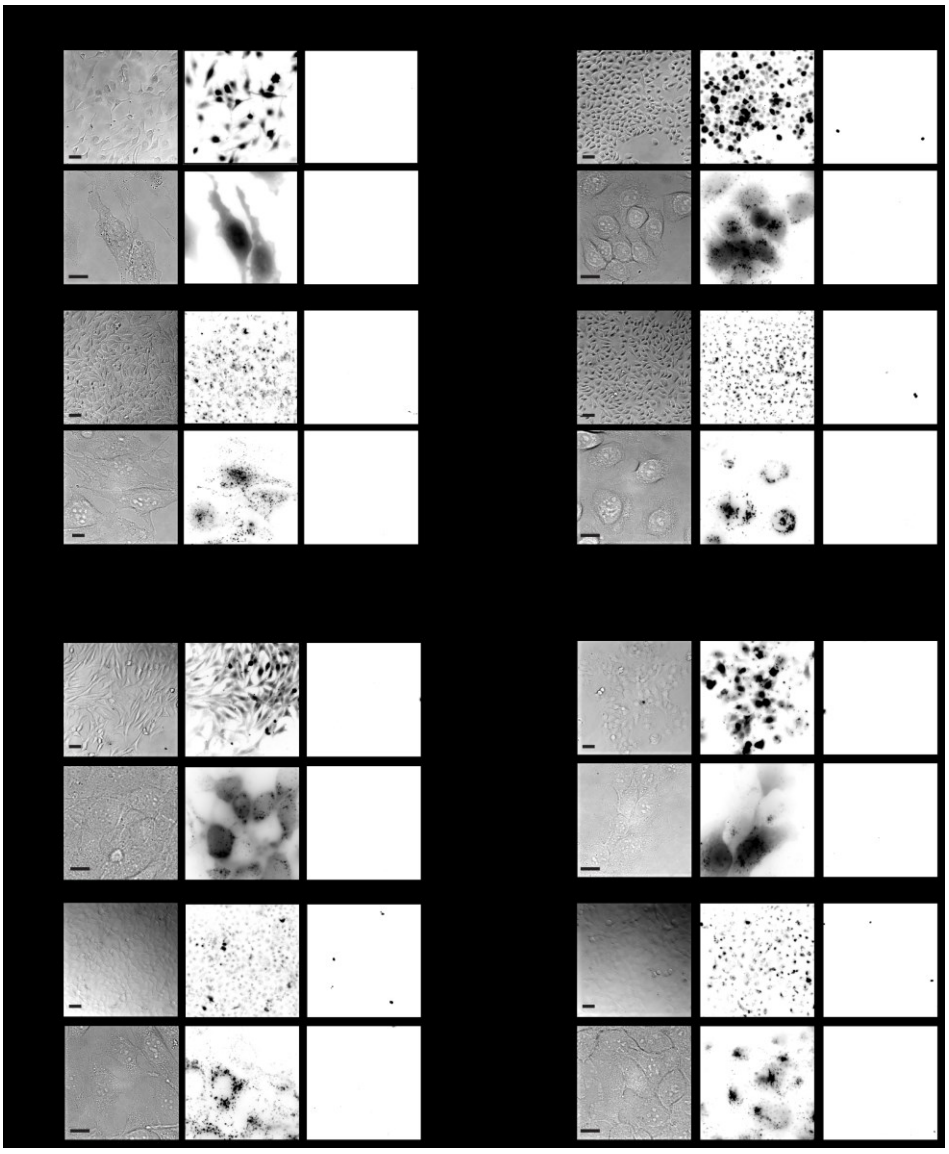

Figure 2-8 Delivery of dfTAT was achieved in multiple cell types. HeLa, COLO 316, NIH 3T3, HaCaT, Neuro-2a, MCH58, primary HDF and primary IPEC-1 cells were incubated with 5 μM dfTAT for 1 h, washed and imaged The fluorescence signal detected was in the cytosolic space and nucleus of cells (top panel 100X objective). After imaging cells were incubated in a humidified atmosphere containing 5 % CO_2 for 24 h, washed and imaged. (top panel: 20X objective, bottom panel: 100X objective) Cell morphology did not change after 24 h. Cell viability was assessed by exclusion of the cell-impermeable dye SYTOX® Blue after both 1 h and 24 h. The TMR fluorescence at the 24 h time point is different to that obtained at the 1 h time point presumably because of the intracellular degradation of the peptide. Scale bars: 20X objective, 50 μm; 100X objective, 10 μm.

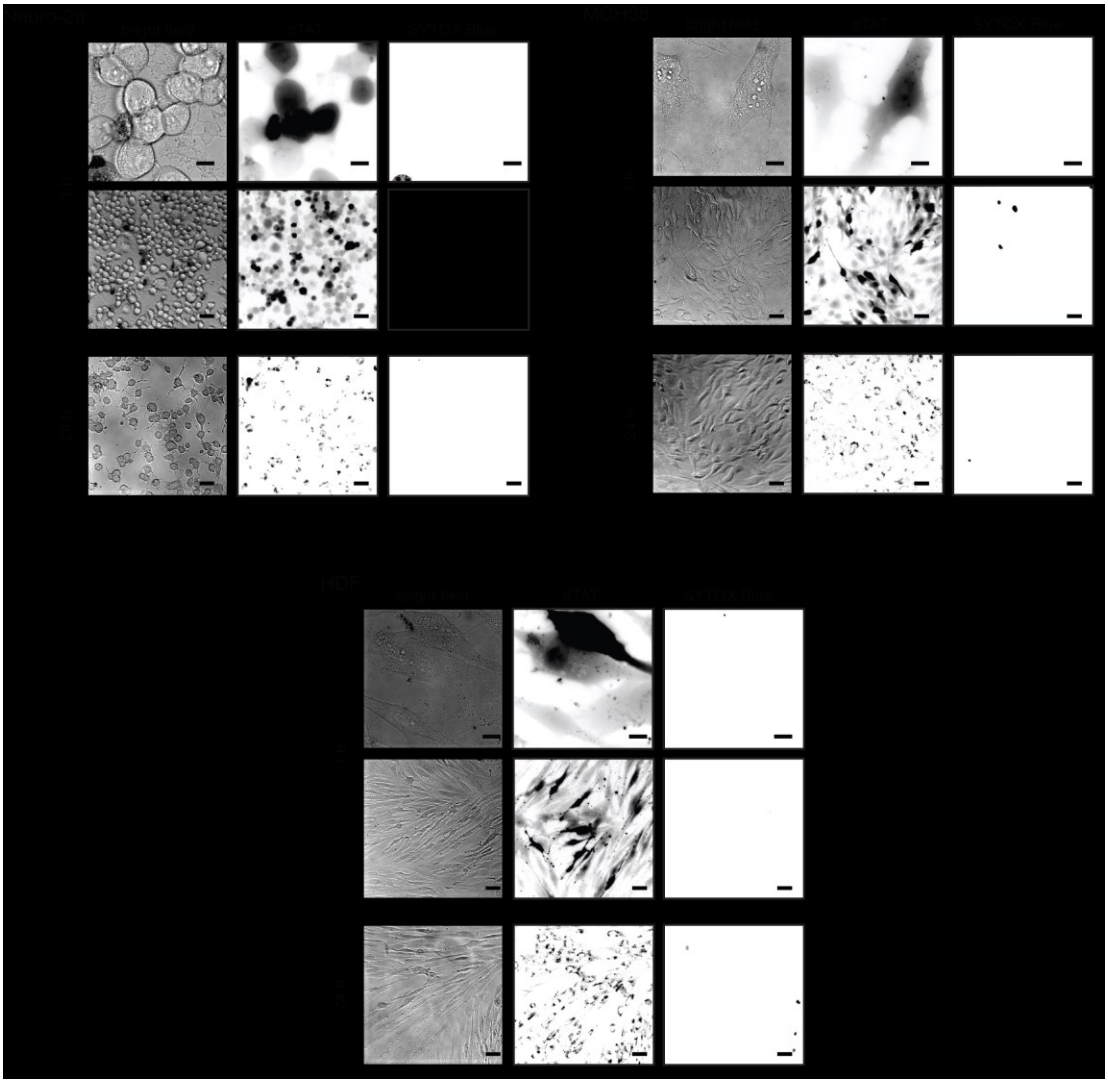

Figure 2-8 Continued.

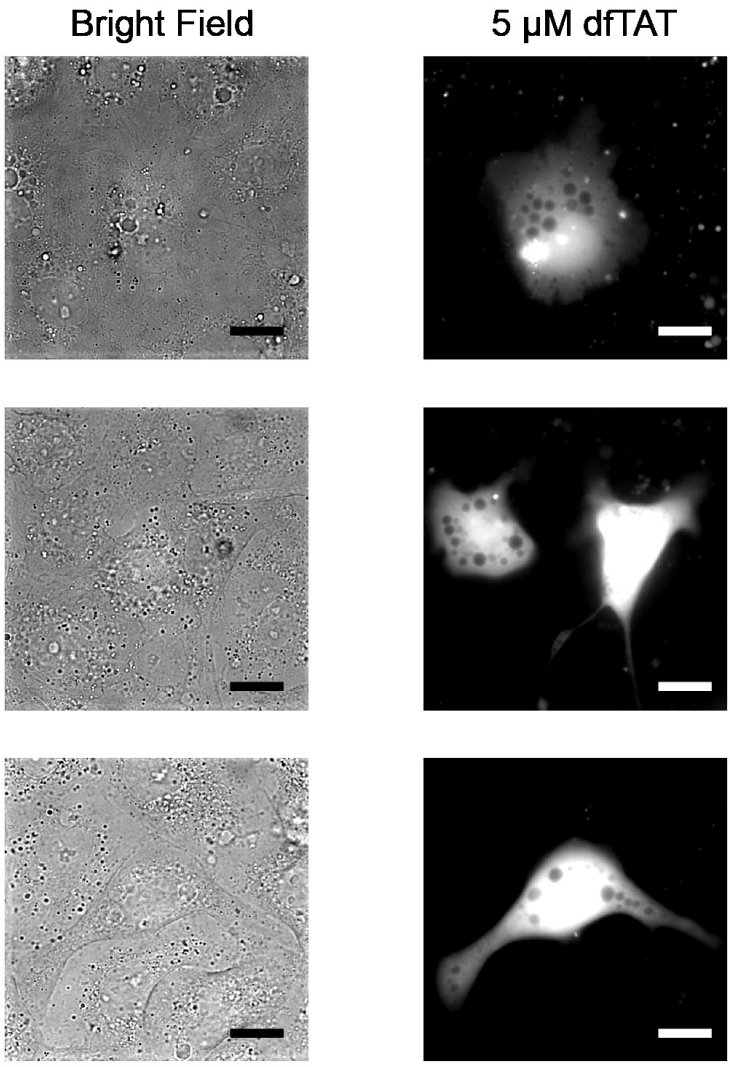

Figure 2-8 Continued.

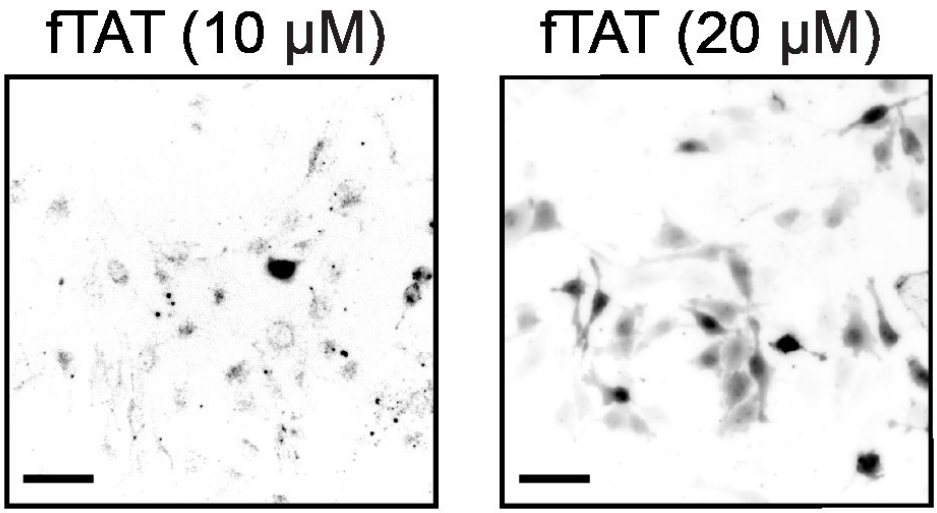

Figure 2-9 fTAT cellular localization after incubation with live cells depends on its concentration in the extracellular media. Inverted monochrome (black = fluorescence signal, white = no signal) fluorescence images of HeLa cells incubated with 10 or 20 µM of fTAT for 1 h. fTAT displays at fluorescence punctate distribution at 10 µM fTAT (left panel) while at 20 µM fTAT shows a significant increase in the population of cells displaying cytosolic and nuclear fluorescence distribution. Scale bars: 50 µm.

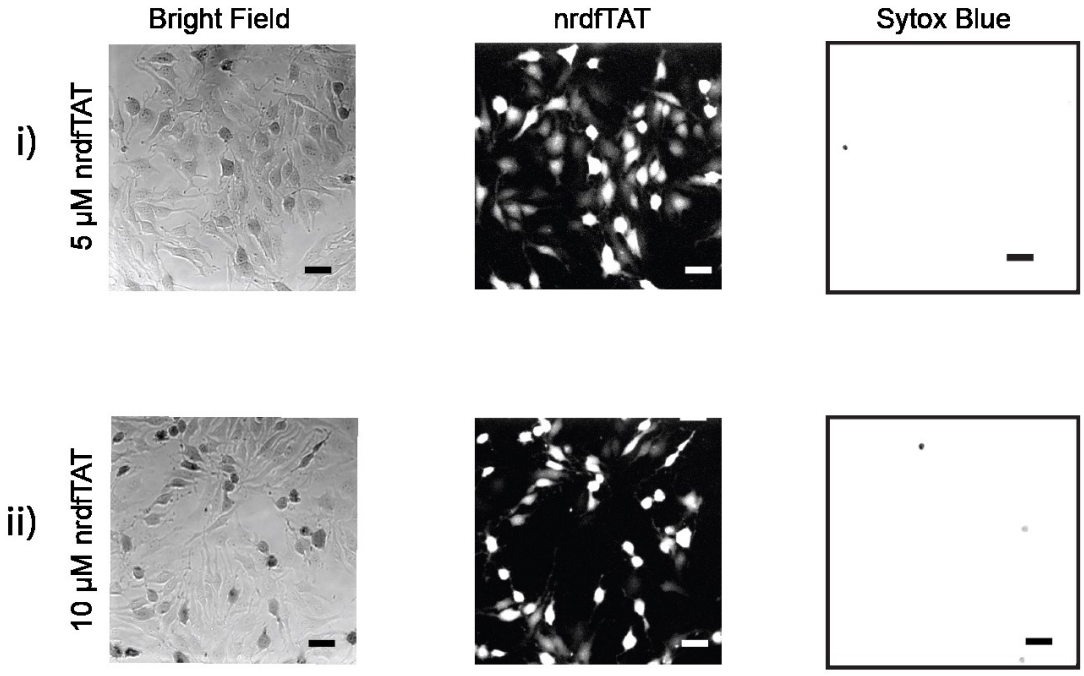

Figure 2-10 Delivery of nrdfTAT into live cells. Cells were incubated with nrdfTAT ((i) 2.5–5 µM and (ii) 5-10 µM*) for 1 h. Fluorescence images (monochrome (white = fluorescence signal, black = no signal) 20X image, center panel) show cytosolic delivery of nrdfTAT into HeLa cells at both concentrations. SYTOX® Blue (2 µM) was used as an indicator of cell death. Scale bars: 50 µm (inverted monochrome 20X image).

*The concentration of nrdfTAT was estimated by measuring the absorbance of TMR using a spectrophotometer, as described with other peptides. However, nrdfTAT has two TMR spaced by a 8.0 Å BMOE linker and such close proximity might affect the extinction coefficient of TMR. In order to take this effect into account, a concentration range for nrdfTAT was calculated based on the extinction coefficient of free TMR (91,500 mol-1cm-1) and that of dfTAT (45,500 mol-1cm-1) (dfTAT also has two TMR in close proximity).

2.2.3 dfTAT penetrates the cells in a two-step process

To test whether endosomal escape is involved in delivery of dfTAT, I assessed the effects of molecules that influence endocytosis[238-241]. Whereas filipin and chlorpromazine (inhibitors of caveolae- and clathrin-mediated endocytosis) had little effect, amiloride (inhibitor of macropinocytosis) and bafilomycin (vacuolar H^+-ATPase inhibitor) inhibited the delivery of dfTAT, suggesting that macropinocytosis and endosomal acidification are important for cytosolic penetration (**Figure 2-11**). To assess whether endosomal escape could be visualized, dfTAT was incubated with cells for 5 min to permit endocytic uptake; cells were washed and then imaged in a pulse-chase experiment. dfTAT was initially localized in a punctate distribution consistent with that of endosomes (100X objective, data not shown). Yet, an increasing number of cells displayed a cytosolic distribution at later time intervals. When imaged with a 20X objective, cells with a cytosolic distribution were brighter than cells with a punctate distribution (this is consistent with TMR being partially self-quenched when dfTAT is trapped inside endosomes; **Figure 2-12**), and this was used to quantify dfTAT's cytosolic penetration as a function of time. Consistent with the notion that dfTAT penetrates the cytosolic space after endocytic uptake, the percentage of cells with cytosolic fluorescence increased from 4.3 % to 76.9 % over a period of 40 min (**Figure 2-13**). To further test whether dfTAT escapes from endocytic organelles, I incubated cells first with that dfTAT penetrates the cytosolic space after endocytic uptake,

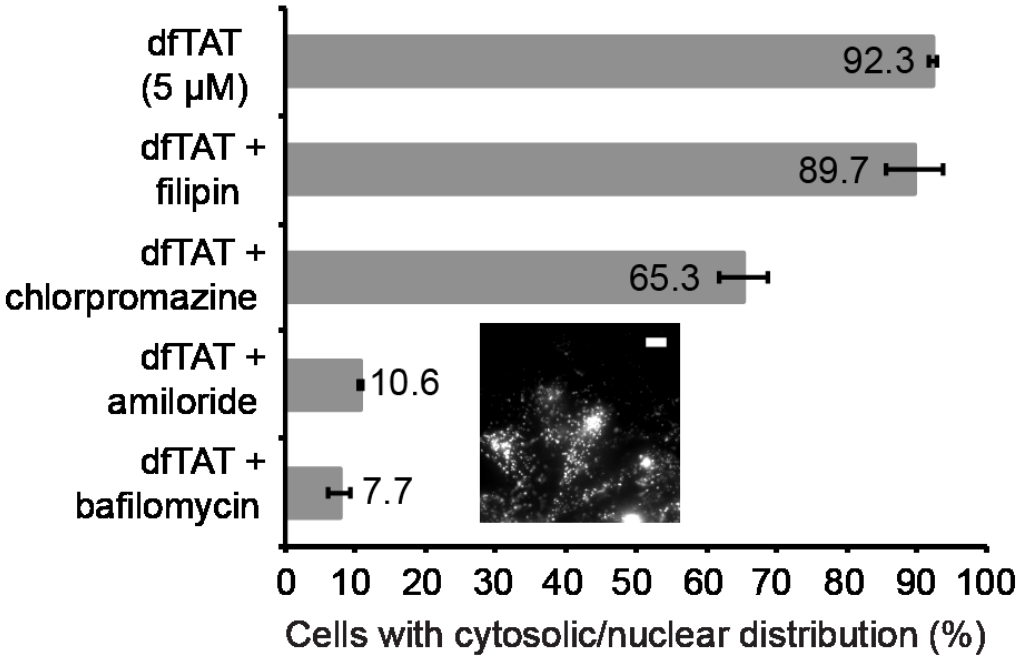

Figure 2-11 Effect of endocytosis inhibitors on the cellular distribution of dfTAT. HeLa cells were pretreated with each inhibitor for 20 min, washed and incubated with 5 µM dfTAT and inhibitor for 1 h. The percentage of cells displaying a cytosolic and nuclear fluorescence distribution was quantified as in Figure 2-6 (B). Inset, punctate distribution of dfTAT in the presence of bafilomycin (1,000 cells per experiment, experiments were performed in triplicates, mean ± s.d. represented). Scale bar: 10 µm.

Figure 2-12 Fluorescence emission spectra of dfTAT (5 µM) before and after reduction with the reducing agent TCEP (50 mM). The sample was excited at 556 nm and the emission was recorded between 570-750 nm. The emission spectra show that the fluorescence emission of dfTAT increases upon reduction of its disulfide bond. This is indicative of TMR self-quenching in the context of dfTAT. This evidence suggests that TMR fluorescence is quenched inside endosomes where, presumably, the peptide exists as a dimer. This behavior displayed by dfTAT allowed me to design the experiment performed in Figure 2-12.

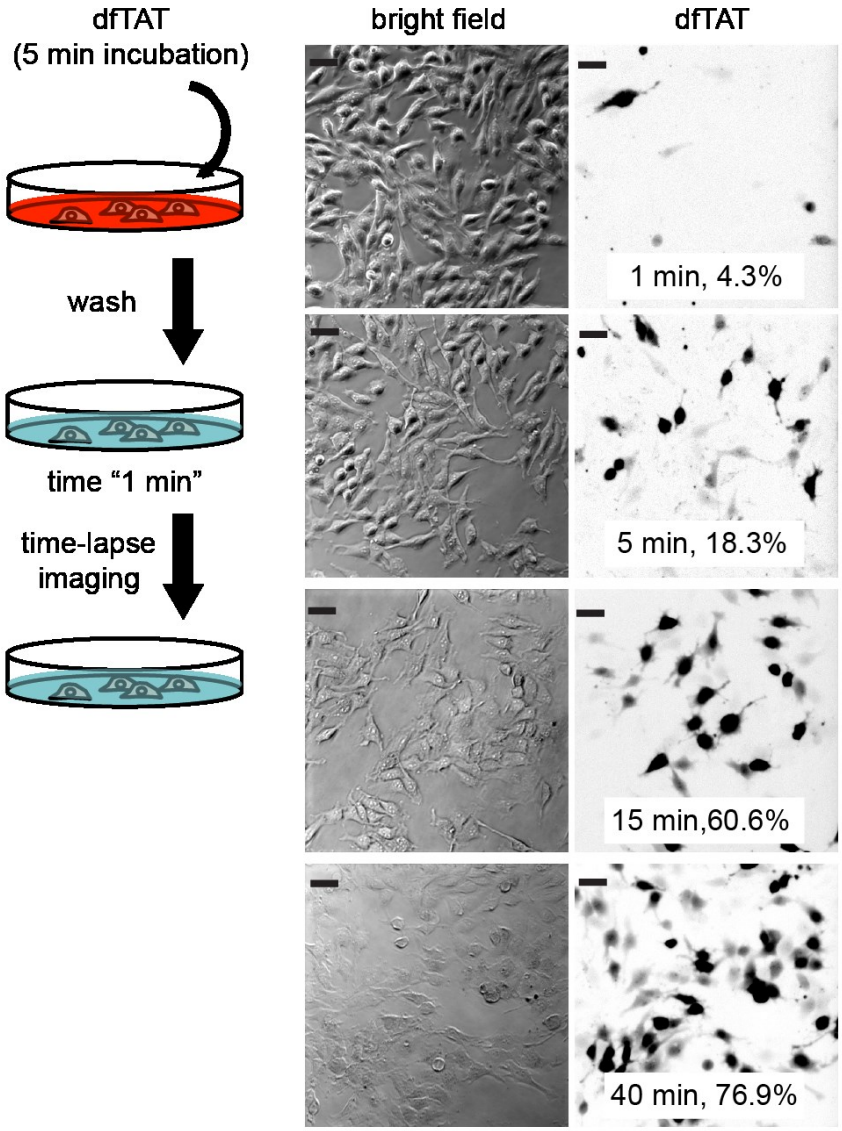

Figure 2-13 Pulse-chase experiment showing the progressive cytosolic penetration of dfTAT. HeLa cells were incubated with dfTAT (5 μM) for 5 min, washed and imaged with a 20X objective (TMR fluorescence images are represented as inverted monochrome) (a schematic of the protocol is shown on the left). The imaging intervals and corresponding percentages of cells with a cytosolic signal are represented. Scale bars: 50 μm.

the percentage of cells with cytosolic fluorescence increased from 4.3 % to 76.9 % over a period of 40 min (**Figure 2-13**). To further test whether dfTAT escapes from endocytic organelles, I incubated cells first with DEAC-K9, a fluorescent peptide that accumulates inside endosomes (**Figure 2-14**)[162]. After washing, cells were incubated with dfTAT. Although only a punctate distribution of fluorescence was observed with cells incubated with DEAC-K9 alone, subsequent addition of dfTAT led to a bafilomycin-dependent redistribution of the DEAC-K9 signal throughout the cytosolic space and nucleus (**Figure 2-15**). These data indicate that dfTAT accumulates inside endosomes already containing DEAC-K9 and that dfTAT endosomal escape is also accompanied by the leakage of luminal DEAC-K9.

2.2.4 dfTAT-mediated endosomal leakage is efficient

When endocytosed at similar levels, dfTAT escaped endosomes, whereas acfTAT did not, indicating that dfTAT is greatly more endosomolytic than acfTAT and is active inside endosomes as a dimer rather than as a reduced monomer (**Figure 2-16)**. However, the cytosolic fluorescence of dfTAT possibly obscures the signal that remains inside endosomes. Under such a scenario, dfTAT endosomal escape would appear more dramatic than it really is. To establish more precisely the efficiency with which dfTAT mediates endosomal leakage, I co-incubated dfTAT with SNAP-Surface, a cell-impermeable green fluorophore that can react with the SNAP protein fusion tag[242]. The experiment was performed in cells expressing a SNAP-H2B histone construct so that SNAP-Surface 488

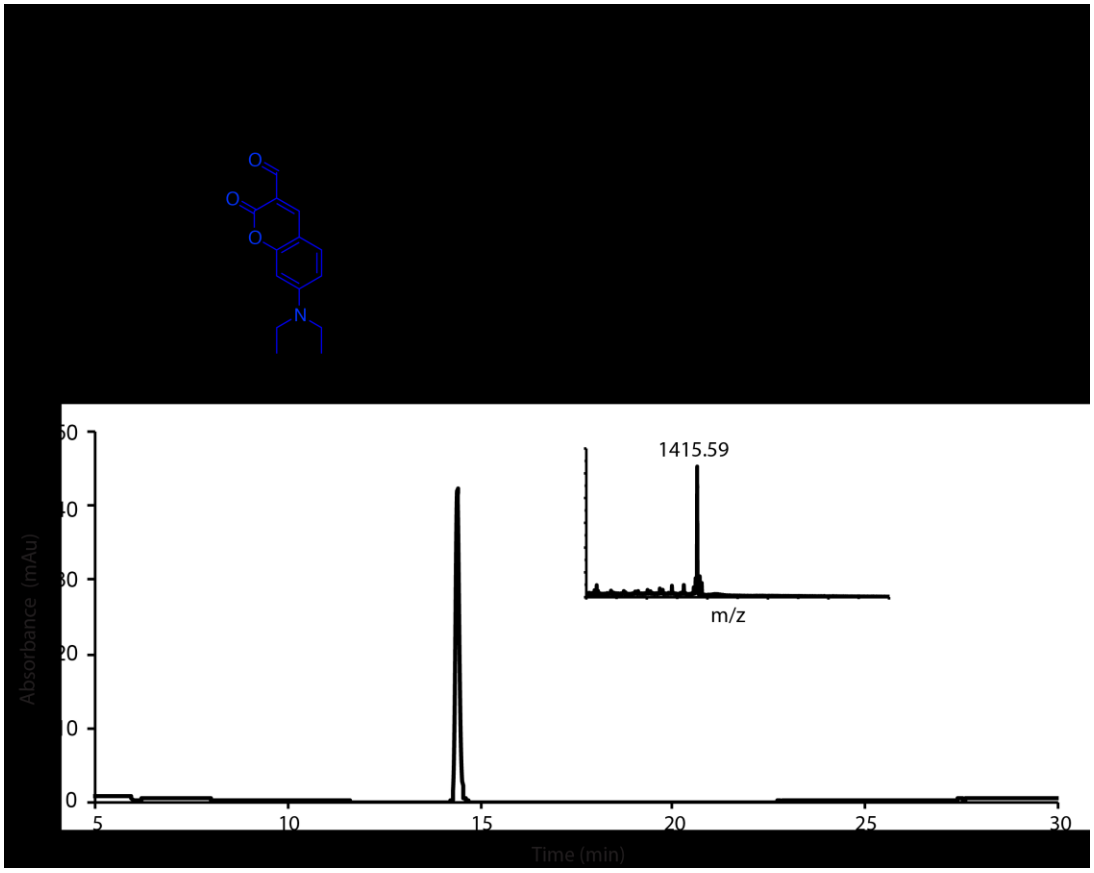

Figure 2-14 Structure and characterization of DEAC-K9. Structure and expected mass of DEAC-K9 (top). HPLC analysis and MALDI-TOF mass spectrum of pure DEAC-K9 (rt = 14.4 min) (expected mass: 1412.97, observed mass: 1415.59)

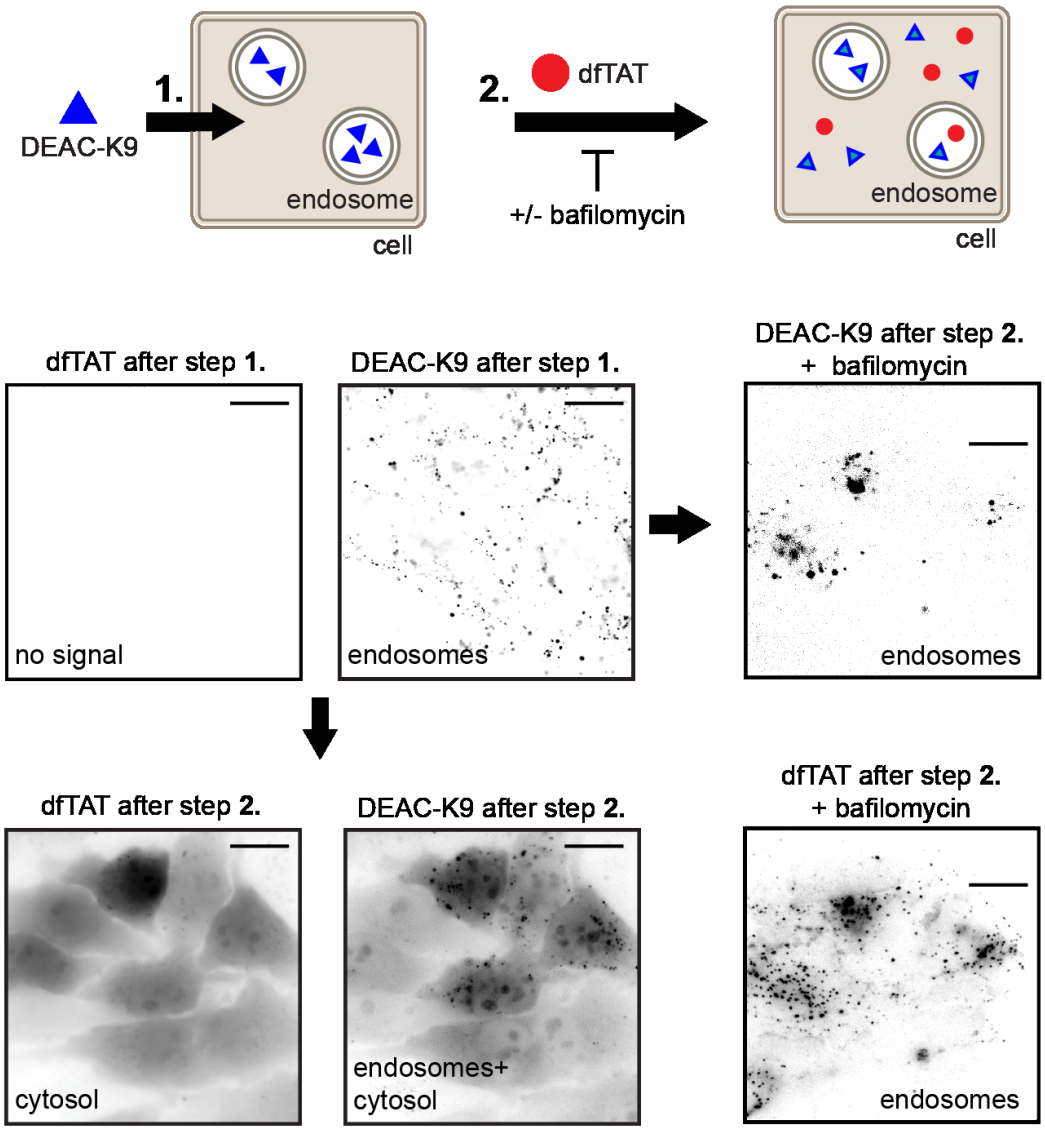

Figure 2-15 dfTAT causes the cytosolic release of molecules trapped inside endosomes. Microscopy images showing dfTAT-mediated release of molecules trapped inside endosomes; a schematic of the process is included (top). HeLa cells were incubated with 5 μM DEAC-K9 for 1 h and washed. Cells were subsequently incubated with 5 μM dfTAT for 1 h. Images are represented as inverted monochromes. Scale bars: 10 μm.

Figure 2-16 dfTAT displays a high endosomolytic activity when compared to acfTAT. HeLa cells were incubated with dfTAT (5 μM) for 5 min and acfTAT (50 μM) for 1 h. After 1h, the cells were washed with PBS/heparin, imaged and lysed. The lysis buffer used in this experiment contains 2 mM DTT. The bulk fluorescence of cell lysates on a 96-well plate was measured using a plate reader. The fluorescence of each sample was normalized to total protein content in the cell lysate, as determined by a Bradford protein assay. Similarly, the fluorescence of solutions of acfTAT at different concentrations (0.1, 0.5, 1, 5 and 10 μM) was measured using a plate reader. A calibration curve of the peptide fluorescence intensity v.s. peptide concentration was established. These data was used to estimate the average concentration of acfTAT and dfTAT inside cells. Data shows higher fluorescence intensity for acfTAT than dfTAT inside cells. These data suggests that dfTAT is a dimer inside endosomes and that this peptide is more endosomolytic than acfTAT (Model 1).

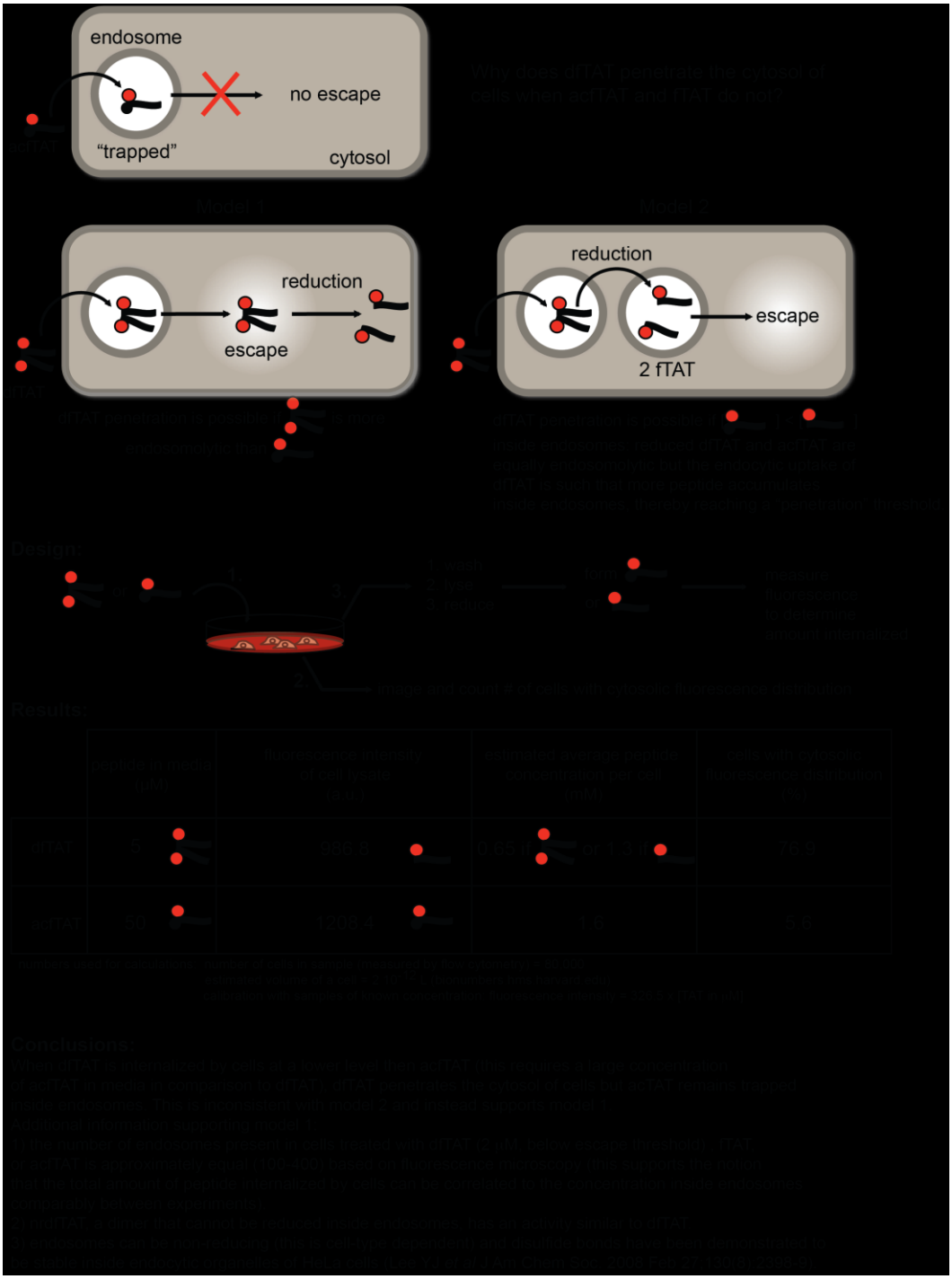

Figure 2-16 Continued.

would label the nucleus of cells upon delivery, deplete the cytosolic signal and reveal the amount of probe remaining trapped inside endosomes. Cells incubated with dfTAT and SNAP-Surface 488 displayed a nuclear staining (**Figure 2-17**), whereas cells incubated with SNAP-Surface 488 alone did not (**Figure 2-18**). Cells with a brightly labeled nucleus also contained only a few dim endosomes. Analysis of the fluorescence signal indicated that 50–90 % of the fluorophore escaped endosomes.

2.2.5 dfTAT-mediated delivery is not deleterious to cells

By inducing efficient endosomal leakage, dfTAT might negatively affect cell physiology. In addition, endosomal leakage has been previously observed in cells undergoing apoptosis[243]. Endosomal leakage could therefore be either a cause or a consequence of cell death. To address these issues, I treated HeLa, MCH58, HDF and Neuro-2a cells with dfTAT for 1 h and established viability 1 and 24 h after incubation using a SYTOX® Green exclusion assay (**Figure 2-19**). Viability was >95 % after treating cells with 5 μM dfTAT for 1 h—conditions required to achieve cytosolic distribution of dfTAT in >80 % of cells. Cell morphology was also unaffected by dfTAT incubation (**Figure 2-20**). Likewise, dfTAT incubation did not affect the proliferation rates of HDF, HeLa or Neuro-2a cells (**Figure 2-21**), and cells containing a cytosolic fluorescence signal indicative of efficient dfTAT endosomal escape were observed to divide normally by microscopy (**Figure 2-22**).

To characterize the physiological impact of dfTAT cytosolic penetration in greater detail, I performed transcriptome analysis on HDF cells incubated for 1 h in nrL-15

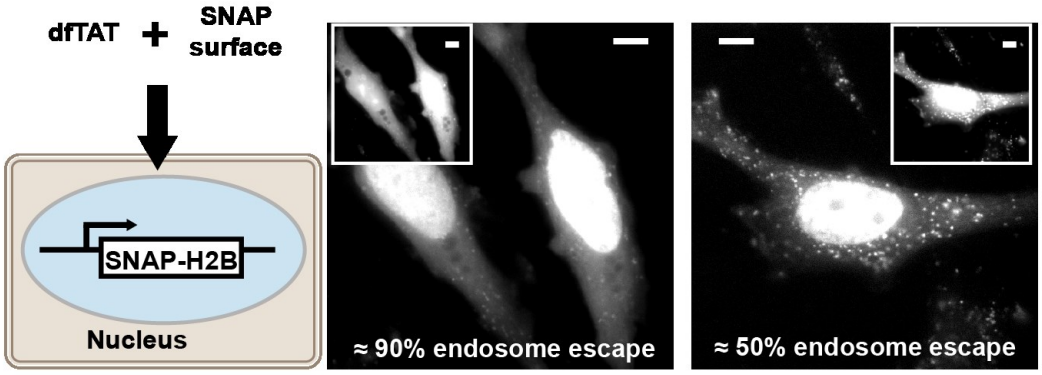

Figure 2-17 Endosomolytic efficiency of dfTAT. HeLa cells expressing SNAP-H2B were incubated with 5 μM dfTAT and 5 μM SNAP-Surface 488 (a schematic of the protocol followed is shown on the left). Representative fluorescence images (of 50 total) of SNAP-Surface are shown (dfTAT is in the inset). The SNAP-Surface 488 signal present in the nucleus is indicated as a percentage of the total signal. Scale bars: 10 μm.

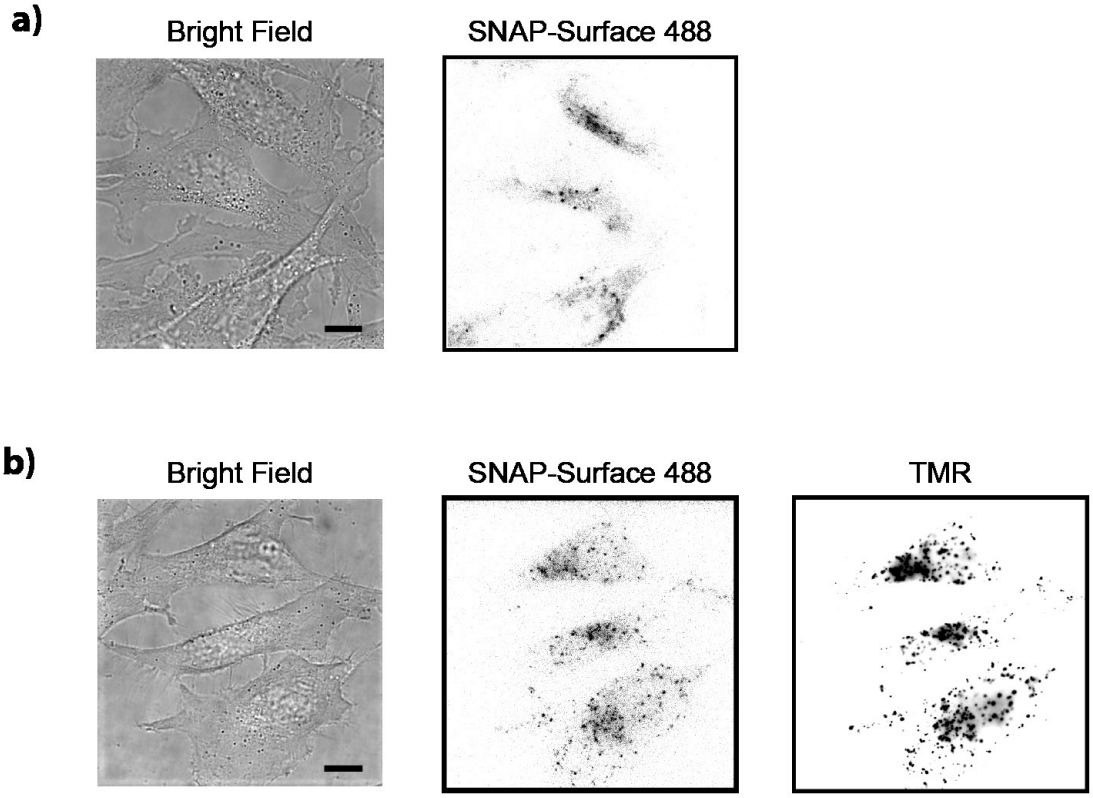

Figure 2-18 SNAP-Surface 488 enters cells via endocytosis and does not escape endosomes in the absence of dfTAT. (A) HeLa cells were incubated with 5 μM SNAP-Surface 488 for 1 h, washed and imaged. Inverted monochrome image shows a punctate distribution from SNAP-Surface 488 (right panel). (B) HeLa cells were incubated with 5 μM SNAP-Surface 488 and 2.5 μM dfTAT (a concentration in which dfTAT incubation does not result in significant cytosolic release) for 1 h, washed and imaged. Inverted monochrome images show SNAP-Surface 488 accumulation in endocytic organelles (punctate distribution) (right panel) and colocalization with TMR signal. Bright field images show HeLa cells morphology did not change after uptake of SNAP-Surface 488 and/or dfTAT (right panels). Scale bars: 10 μm.

Figure 2-19 dfTAT is not toxic to cells under conditions where efficient endosomal escape is achieved. (A) HeLa, MCH58, HDF and Neuro-2a cells were incubated with (1-50 μM) dfTAT for 1 h. Cell viability was assessed by a SYTOX® Green exclusion assay 1, 24, and 48 h (for HeLa) after incubation (1,000 cells/experiment, experiments in triplicates, average and standard deviations represented). (B) Histogram of flow cytometry data. HeLa cells were incubated with 5 μM dfTAT or no peptide (control) for 1h, washed and then incubated in SYTOX® Green (1 μM) for 15 min. Cells were then trypsinized for 5 min, resuspended in a total of 200 μl of nrL-15, and analyzed by flow cytometry (BD Accuri C6 Flow Cytometer). Histograms show that only 2 % and 7.5 % of cells are stained with the cell impermeable dye SYTOX® Green for untreated and treated cells, respectively.

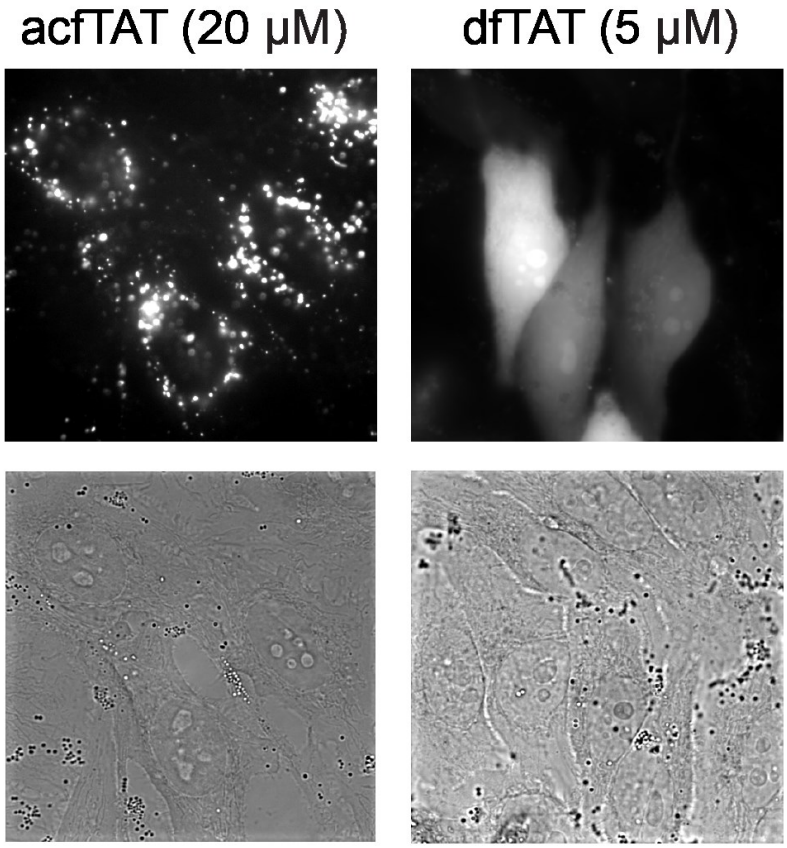

Figure 2-20 The cellular localization of acfTAT and dfTAT is different after incubation with live cells but cell morphology is not changed. Fluorescence (monochrome) and brightfield images (100X objective) of HeLa cells incubated with 20 μM acfTAT (left panel) and 5 μM dfTAT (right panel). The acfTAT peptide displays a fluorescence punctate distribution while dfTAT exhibits a cytosolic and nuclear fluorescence distribution. Brightfield images show no change in HeLa cell morphology upon peptide delivery.

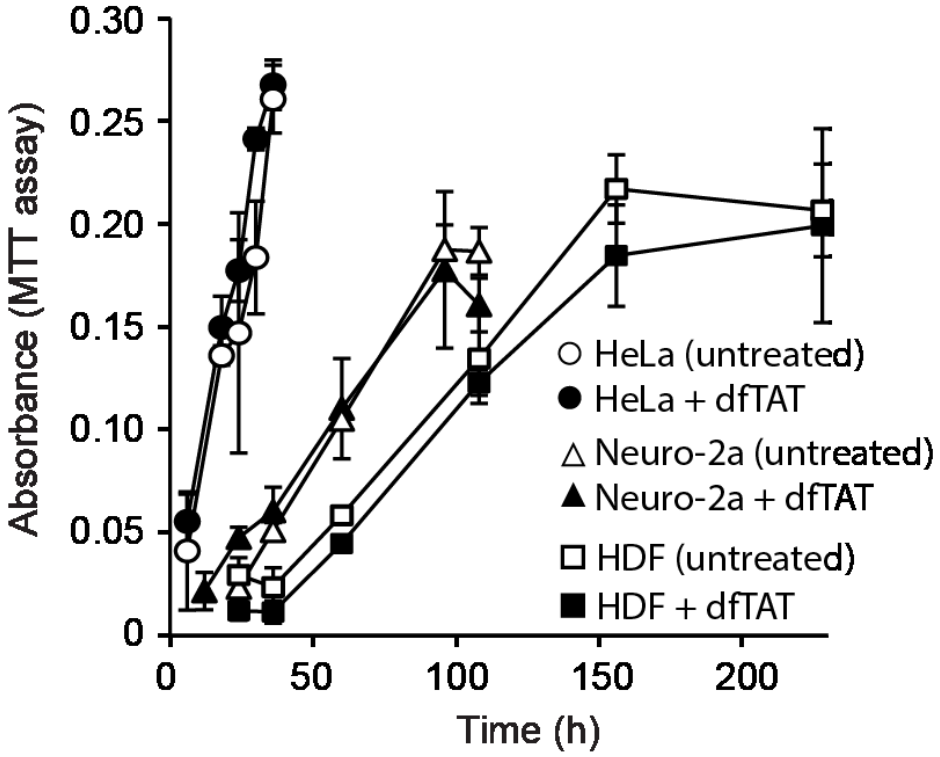

Figure 2-21 dfTAT-mediated delivery does not significantly affect cell proliferation. HeLa, Neuro-2a and HDF cells were incubated with 5 μM dfTAT for 1 h or left untreated. Proliferation was assessed using a MTT assay (150,000 cells/experiment, experiments in triplicates, mean and standard deviations represented).

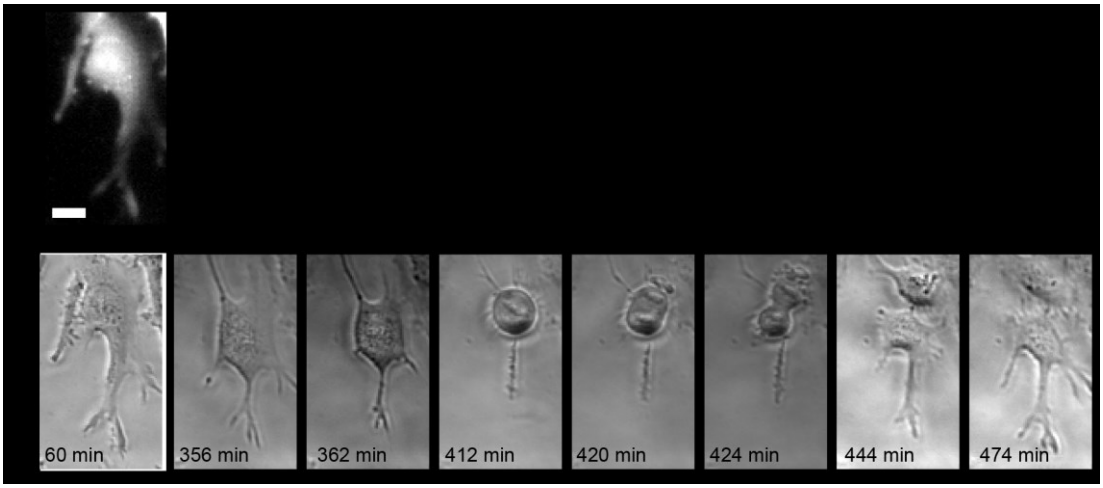

Figure 2-22 dfTAT-mediated delivery does not significantly affect cell division. Microscopy imaging showing that cells containing cytosolic dfTAT divide. HeLa cells were incubated with 5 μM dfTAT for 1 h, washed and imaged in a time-lapse experiment. Scale bars, 10 μm

medium with or without 5 μM dfTAT. Cells harvested immediately after dfTAT incubation showed 11 transcripts up- or downregulated more than twofold compared to those of untreated cells (twofold is used as a significance threshold; 47,321 total transcripts detected; **Figure 2-23**). Only two transcripts were dysregulated in cells incubated in DMEM for an additional 1 h and 24 h after treatment with dfTAT (**Figure 2-23 and 2-24**). Together, these results indicate that dfTAT has a minimal impact on mRNA expression and that cells recover rapidly from dfTAT-mediated endosomal leakage (corroborated by quantitative proteomic profile experiments; **Figure 2-25**).

If dfTAT perturbs many endosomes during a delivery step, I envisioned that endocytic trafficking might be a cellular process likely to be negatively affected following peptide incubation. In particular, I reasoned that dfTAT could cause endosomal leakage after an initial treatment but fail to be endocytosed or remain trapped inside damaged endocytic organelles after a second dfTAT incubation. I therefore tested the stepwise delivery of two different molecules (DEAC-K9 and SNAP-Surface 488). Cells were first incubated with dfTAT (5 μM) and DEAC-K9 (5 μM) for 1 h. As expected, this incubation resulted in the cytosolic distribution of both dfTAT and DEAC-K9 (data not shown). Twenty minutes later, cells were incubated with dfTAT (5 μM) and SNAP-Surface 488 (5 μM) for 1 h. Cells treated with dfTAT using this two-step protocol displayed cytosolic and nuclear fluorescence of both DEAC-K9 and SNAP-Surface 488 (**Figure 2-26**). Delivery of SNAP-Surface 488 did not occur in the absence of dfTAT (**Figure 2-18**) and was inhibited by bafilomycin, consistent with the notion that the second delivery step is also mediated by the endosomolytic activity of dfTAT. Moreover, the fluorescence of SNAP-

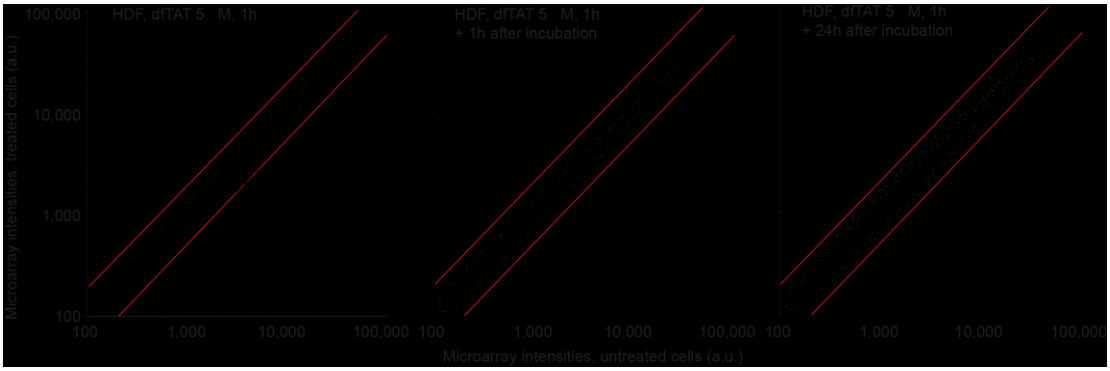

Figure 2-23 dfTAT-mediated delivery does not significantly affect transcription in primary cells. Whole-genome microarray analysis of HDF cells treated with dfTAT. HDF cells were treated with 5 μM dfTAT for 1 h and transcriptome analysis was performed immediately, 1 h, or 24 h after dfTAT treatment. The plot displays microarray intensity values of treated vs. untreated (same incubation steps but without peptide) samples. The red lines represent 2-fold intensity change cut-offs and transcripts up or down-regulated above these cut-offs are circled for clarity.

Figure 2-24 mRNA expression analysis in the presence of staurosporine. (a) In order to establish a positive control for the microarray analysis, staurosporin was used to induce apoptosis in HDF cells. Cells were treated with staurosporine (0.1 μM) for 1h and mRNA levels were analyzed as described in Figure 3. The identity of transcripts related to apoptosis that were up-regulated (highlighted in red) and down-regulated (highlighted in green) upon treatment with staurosporin are listed. Notably, a total of 1830 transcripts were found to be up-or down-regulated out of 47321 transcripts detected. (b) Analysis of the microarray intensities of untreated HDF cells vs. those of HDF cells treated with staurosporine (0.1 μM) for 1h. The red lines represent the 2-fold cut-offs. (c) Table listing the identity of transcripts that are up-regulated (highlighted in red) and down-regulated (highlighted in green) in HDF cells incubated with dfTAT (5 μM) and analyzed immediately after incubation (1h), or 1h (1h+1h) and 24 h (1h+24h) after incubation. The 11, 2, and 2 transcripts listed represent the total number of transcripts up or down-regulated in the 1h, 1h+1h, and 1h+24h samples, respectively.

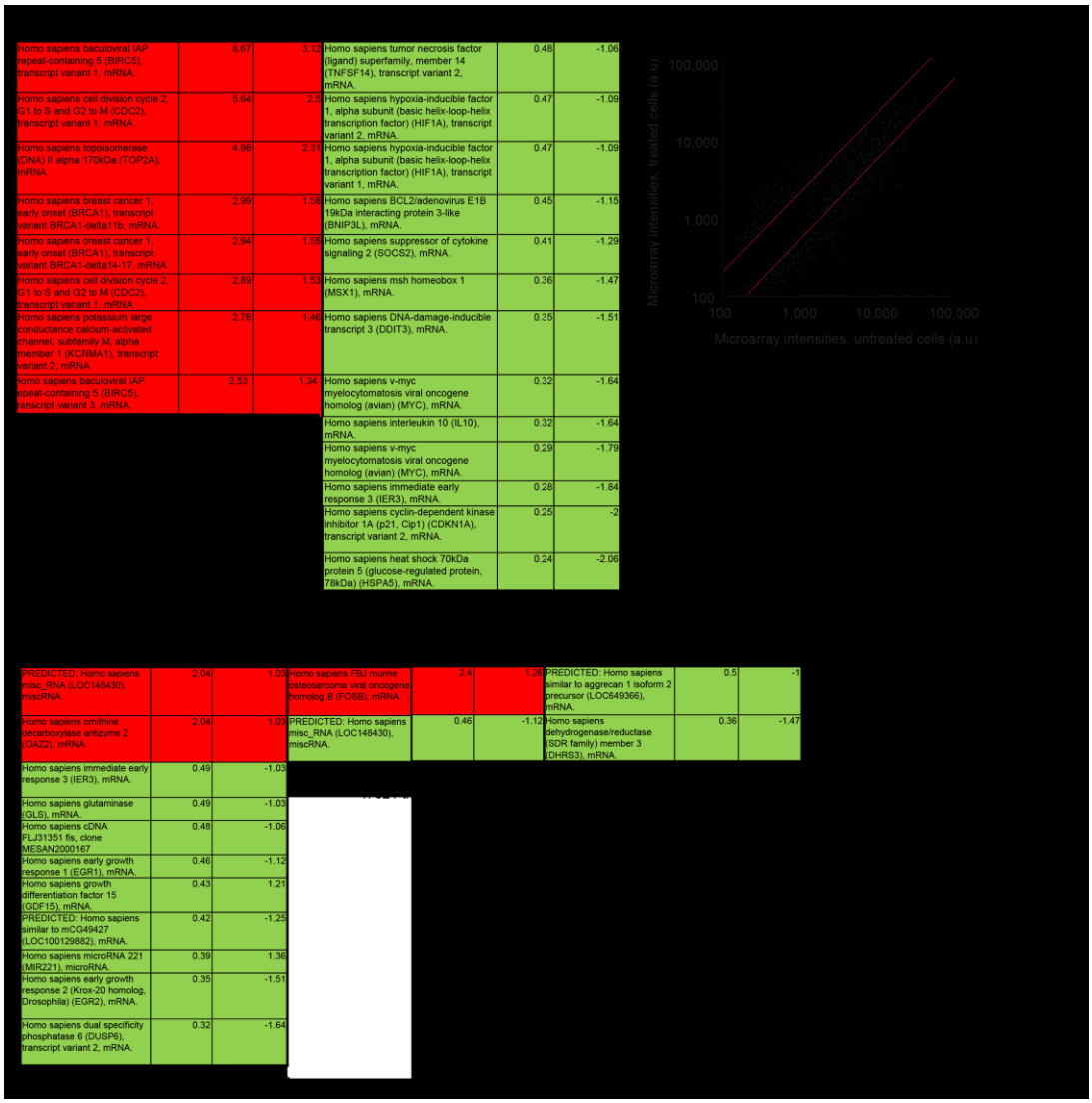

Figure 2-24 Continued.

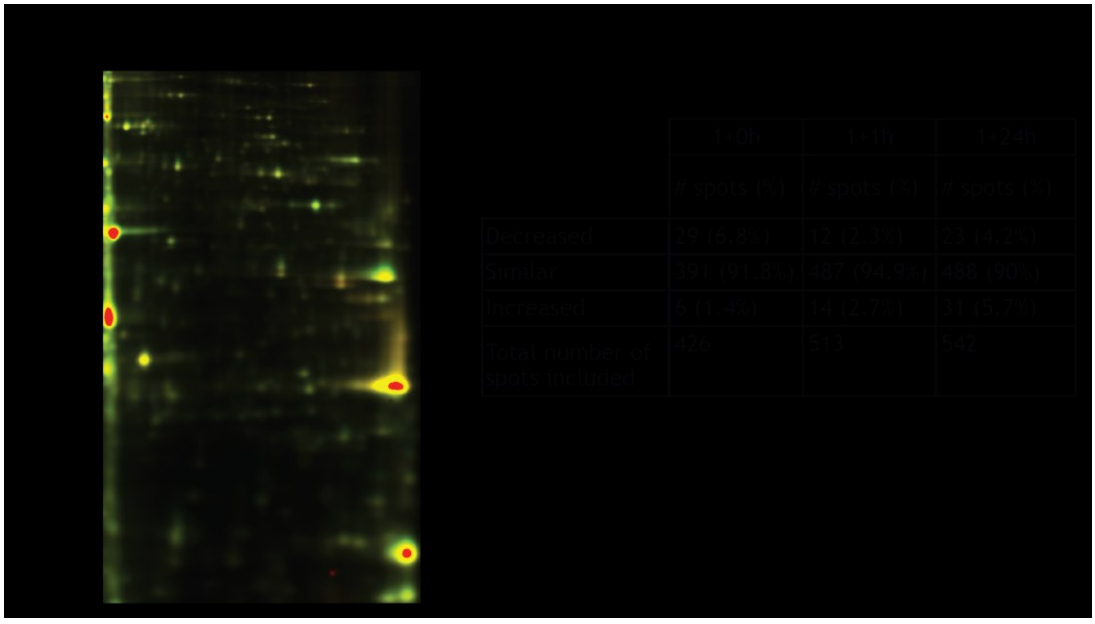

	1+0h	1+1h	1+24h
	# spots (%)	# spots (%)	# spots (%)
Decreased	29 (6.8%)	12 (2.3%)	23 (4.2%)
Similar	391 (91.8%)	487 (94.9%)	488 (90%)
Increased	6 (1.4%)	14 (2.7%)	31 (5.7%)
Total number of spots included	426	513	542

Figure 2-25 Differential in gel electrophoresis (DIGE) proteomic analysis of HDF cells treated with dfTAT (5 µM) for 1 h. (a) Representative green and red fluorescence overlay of 2D gel of cells treated with or without dfTAT for 1h and incubated in fresh media for an additional 1h (1+1h samples, treated sample is labeled with Cy3 and untreated with Cy5). Green and red were used as pseudo colors for Cy3 and Cy5 dyes, respectively, and a yellow color is indicative of equal fluorescence intensities. (b) Table summarizing analysis results obtained from the DIGE using the DeCyder v6.5 suite of software tools (GE Healthcare). Data was obtained using a 2 standard deviation model (95% confidence). Each pair (treated vs. untreated) were individually analyzed based on the normalized volume ratio of each individual protein spot from Cy3- or Cy5- labeled sample.

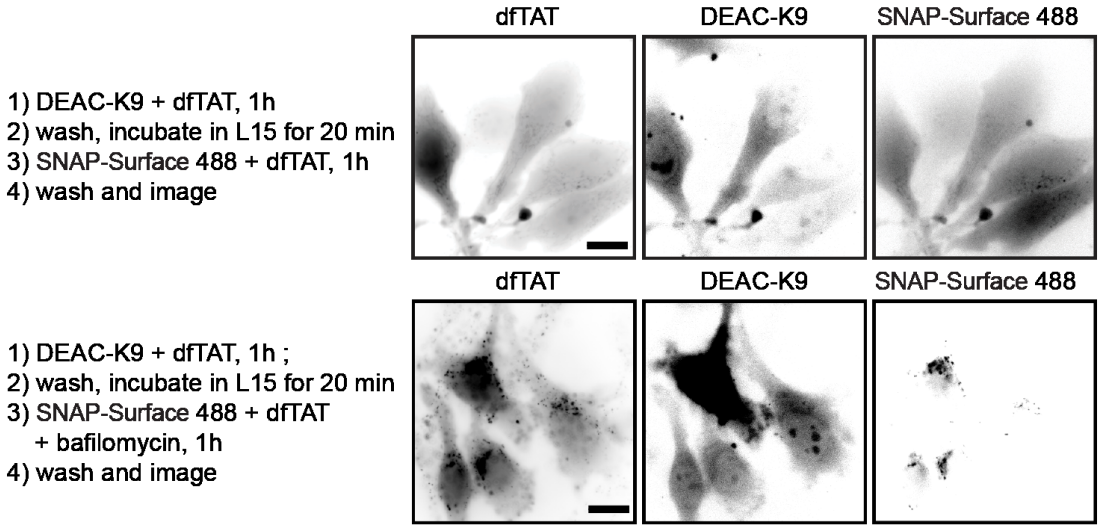

Figure 2-26 dfTAT-mediated delivery does not significantly affect endocytosis. Microscopy images showing that dfTAT-mediated endosomal escape can be repeated. HeLa cells were co-incubated with dfTAT (5 μM) and DEAC-K9 (5 μM) for 1 h (step1) (images not shown). After washing, dfTAT (5 μM) and SNAP-Surface 488 (5 μM) were co-incubated in the absence (top panel) or presence (bottom panel) of bafilomycin (200 nM) (step 3). Scale bars: 10 μm.

Surface 488 examined was comparable to that observed when SNAP-Surface 488 was delivered into untreated cells (one-step delivery) or simultaneously with DEAC-K9 (**Figure 2-27**). Together these results establish that dfTAT-mediated delivery can be repeated. This suggests that the endocytic route employed by dfTAT is not dramatically compromised after dfTAT-mediated endosomal leakage.

2.2.6 dfTAT delivers proteins by simple co-incubation

To determine whether dfTAT could deliver large proteins into the cytosol of cells, I chose EGFP (26 kDa) as a model cargo. Cells were incubated with EGFP and dfTAT for 1 h and examined by microscopy. EGFP was distributed into the cytosolic space and nucleus in more than 90 % of cells without observable toxicity (**Figure 2-28**). To estimate how much fluorescent and folded protein was delivered, cells were counted, harvested and lysed. The lysate was analyzed by PAGE, and the fluorescence of EGFP was quantified. On the basis of this analysis, approximately 34 μM and 23 μM of EGFP was present per HDF and Neuro-2a cell, respectively (**Figure 2-29**). As imaging confirmed that a large fraction of EGFP escaped endosomes (**Figure 2-28**), one can expect micromolar concentrations of proteins to be delivered in the cytosolic space of cells.

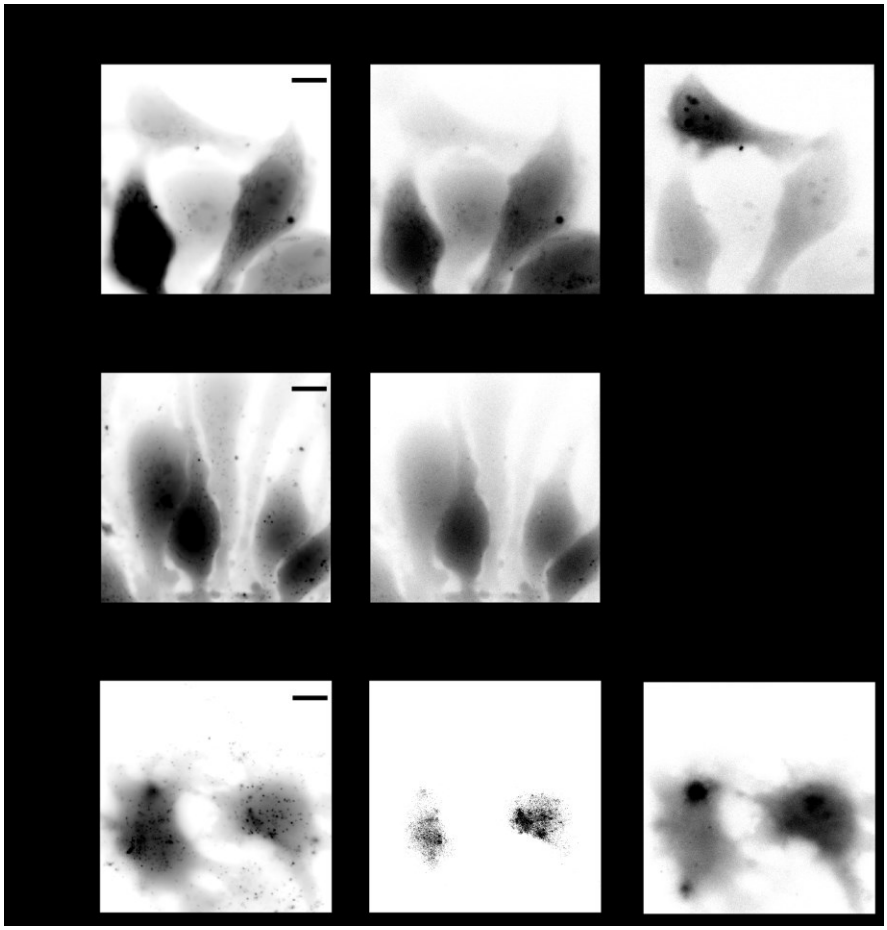

Figure 2-27 Simultaneous delivery of SNAP-Surface 488 and DEAC inside cells using a one step protocol. (a) HeLa cells were incubated with 5 µM dfTAT, 5 µM SNAP-Surface 488 and 5 µM DEAC-K9. Inverted monochrome images show cytosolic and nuclear fluorescence localization of dfTAT (red fluorescence), DEAC-K9 (blue fluorescence) and SNAP-Surface 488 (green fluorescence). Scale bars: 10 µm. (b) HeLa cells were incubated with 5 µM dfTAT and 5 µM SNAP-Surface 488. Inverted monochrome images show cytosolic and nuclear fluorescence localization of dfTAT and SNAP- Surface 488. Scale bars: 10 µm. (c) HeLa cells were first incubated with 5 µM dfTAT and 5 µM DEAC-K9 for 1 h. Cells were then washed, incubated with 5 µM SNAP-Surface 488 for 1 h and imaged. In one hand, inverted monochrome images show cytosolic and nuclear localization of TMR and DEAC but, in the other hand, SNAP-Surface 488 display a fluorescence punctate distribution. Scale bar: 10 µm.

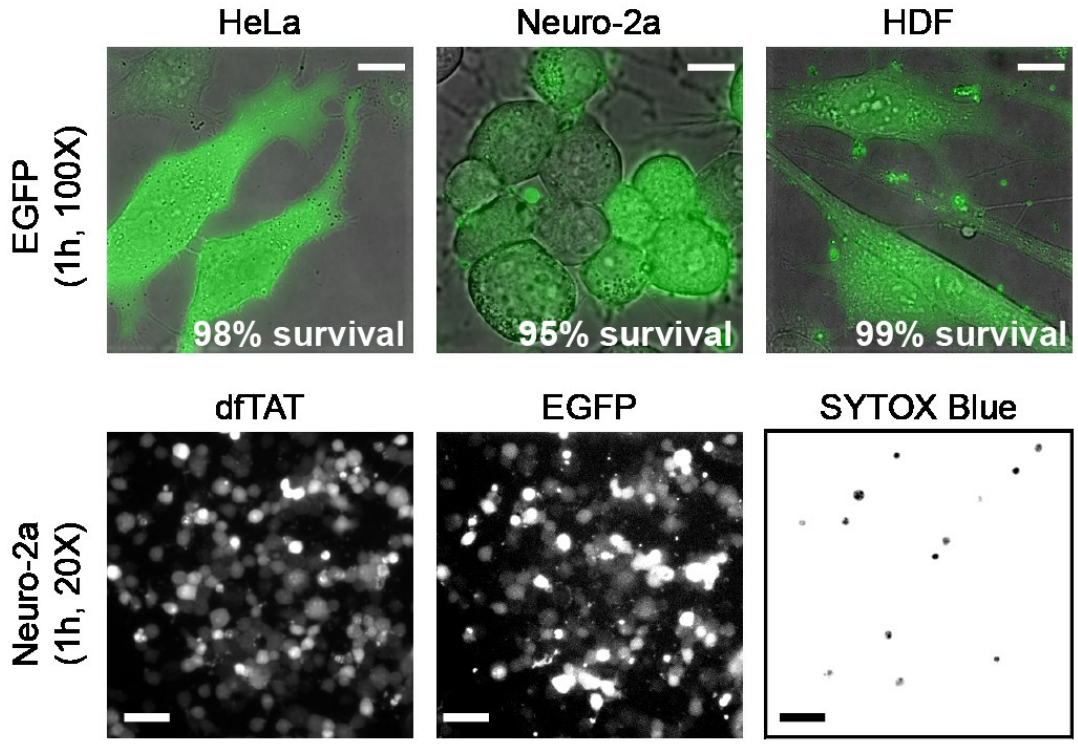

Figure 2-28 Delivery of intact and functional EGFP using co-incubation with dfTAT. Microscopy imaging showing that dfTAT delivers EGFP into the cytosol of live cells. HeLa, Neuro-2a and HDF cells were co-incubated with EGFP (10 μM) and dfTAT (5 μM) for 1 h. Scale bars: 100X objective, 10 μm; 20X objective, 100 μm.

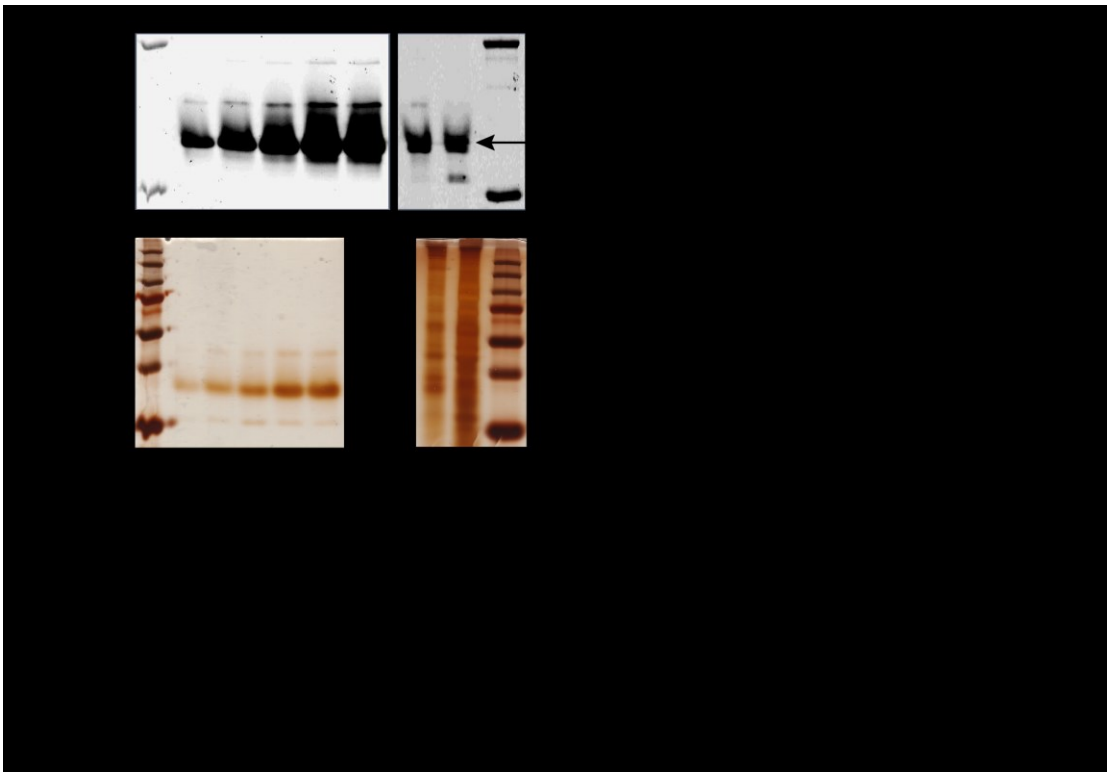

Figure 2-29 Quantitation of the concentration of EGFP delivered into the cytosol of HDF and Neuro-2a. HDF and Neuro-2a cells were co-incubated with dfTAT (5 μM) and EGFP (10 μM) for 1 h. After 1 h, cells were washed with PBS/heparin and lysed. The cell lysate was treated with nucleases and an aliquot of 27 μL was analyzed by PAGE (top right panel). Similarly, samples of known EGFP concentrations (determined by measuring absorbance at 488 nm and using an extinction coefficient of 55,000 mol-1cm-1) were analyzed by PAGE (top left panel). A fluorescence imager was used to measure the EGFP fluorescence intensity from the cell lysates and EGFP calibration samples. Silver staining was used to detect all proteins in the lysate. A calibration curve of EGFP fluorescence intensity vs. EGFP concentration was established and used to estimate the average concentration of EGFP in the cell lysates. The data obtained was used to calculate the concentration of EGFP per cell. Important numbers: Cell number on well: 79,600 (determined by flow cytometry); Cell volume: 2000 μm^3 (bionumbers.hms.harvard.edu.)

To determine whether dfTAT needs to interact with a particular protein in order to successfully deliver it, I characterized the binding of dfTAT to EGFP. No fluorescence resonance energy transfer (FRET) between dfTAT and EGFP could be detected under conditions used for cellular incubation assays (**Figure 2-30**). Similarly, no interaction between dfTAT and EGFP could be detected by native gel electrophoresis (**Figure 2-31**). In contrast, dfTAT and BSA were found to interact in this assay (presumably through electrostatic interactions). Interestingly, addition of BSA (or fetal bovine serum or heparin) to cell incubation medium reduced the cytosolic penetration of dfTAT in a concentration-dependent manner (**Figure 2-32**).

To further confirm that functional proteins can penetrate cells upon incubation with dfTAT, I tested delivery of Cre recombinase. In this assay, Cre induces recombination of a *loxP*-STOP-*loxP* sequence upstream of the EGFP-encoding gene of a reporter plasmid[244]. Therefore, cells transfected with the reporter plasmid express EGFP when Cre recombinase penetrates cells and excises the STOP signal sequence. Cells treated with TAT-Cre (1 μM) and dfTAT (5 μM) expressed EGFP (**Figure 2-33**), but the percentage of $EGFP^+$ cells was greater in the presence of dfTAT (47 %) than in the presence of fTAT or when TAT-Cre was incubated alone (<5 %).

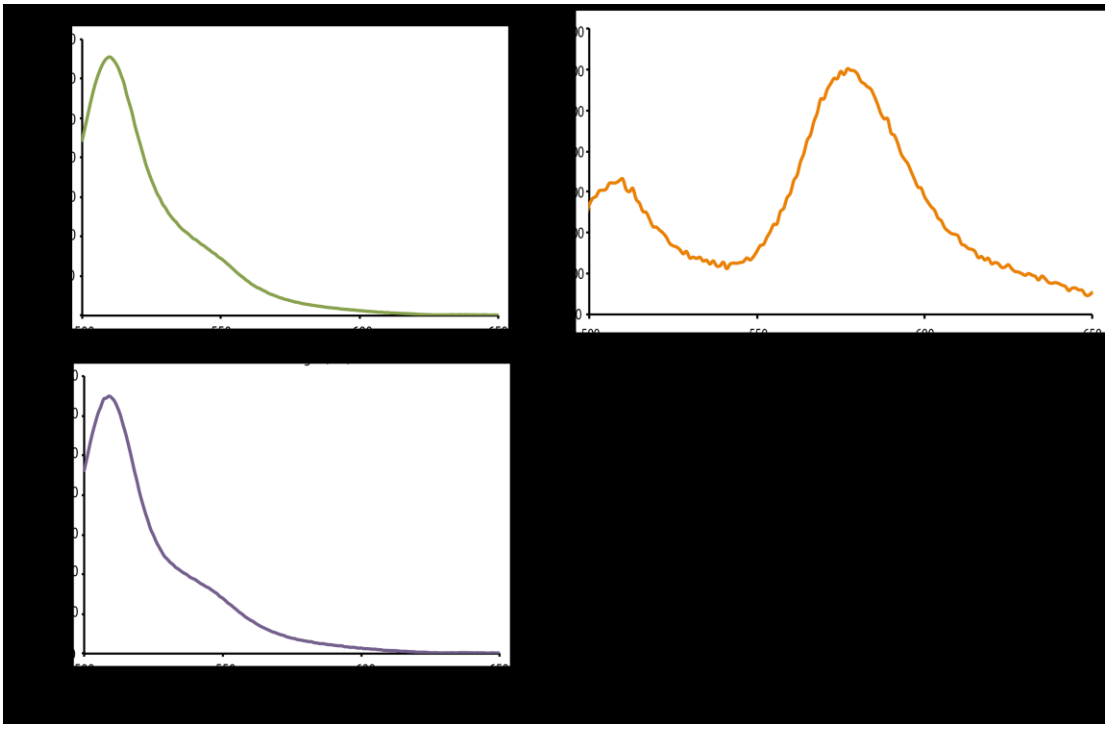

Figure 2-30 dfTAT and EGFP do not interact when co-incubated. (a) Fluorescence emission spectrum of EGFP (1 μM) (donor FRET pair) (EGFP, Ex/Em 488/508 nm) excited at 488 nm. The spectrum show an intense emission peak at around 510 nm and a small shoulder peak around 548 nm (b) Fluorescence emission spectrum of a solution of EGFP (1 μM) and dfTAT (5 μM) (acceptor FRET pair) (TMR, Ex/Em 556/580 nm) excited at 488 nm. The spectrum shows an intense emission peak at around 510 nm and a small shoulder peak around 548 nm. The contribution of TMR to the EGFP fluorescence spectrum (crossover fluorescence) was determined by measuring the fluorescence emission of a solution of dfTAT (5 μM) excited at 488 nm (not shown). The spectrum of the solution with EGFP and dfTAT is almost identical to the spectrum of EGFP alone (TMR fluorescence crossover signal was subtracted). (c) Fluorescence emission spectrum of ligated EGFP-CK(TMR). Using expressed protein ligation, EGFP was chemically ligated to CK(TMR) as described to produce EGFP-CK(TMR)7. EGFP-CK(TMR) was used a positive control for the FRET signal. Upon excitation at 488 nm, a dramatic increase in fluorescence between 560-630nm is observed (fluorescence max approximately 580 nm), indicative of a FRET signal due the close proximity between fluorophores. This increase in fluorescence intensity was not observed in the spectrum in part b) (indicative of no interactions between EGFP and dfTAT). Emission of all samples was scanned from 500 to 650 nm.

Figure 2-31 dfTAT and EGFP do not interact. (a) Native gel electrophoresis was used to determine binding interaction between dfTAT and EGFP. Samples were prepared by

incubating dfTAT (5 μM) with either EGFP (10 μM) or BSA (10 μM, protein with a pI = 4.7, used as a positive control) in nrL-15 for 30 min at 37 °C (pH 7.0, representing the pH of the extracellular milieu of the cell and pH 5.0 representing the lower pH that exists along the endocytic pathway). dfTAT alone, EGFP alone and BSA alone at the same concentration and pH were loaded on the same gel as controls. Fluorescence images of the gel were acquired using a Typhoon scanner. Green fluorescent bands corresponding to EGFP and a red fluorescence band correspond to dfTAT fluorescence. Red fluorescent bands corresponding to both dfTAT and BSA indicated binding between peptide and protein. In contrast, dfTAT fluorescence is not detected in bands corresponding to EGFP, indicating absence of binding. An image of the Commassie stained native gel is also shown (top left corner). (b) Coomassie staining, red fluorescence, and green fluorescence images of samples of dfTAT and EGFP at varying concentration and analyzed by native gel electrophoresis. Similar results were obtained with dmEGFP (EGFP not containing cysteine residues, data not shown).

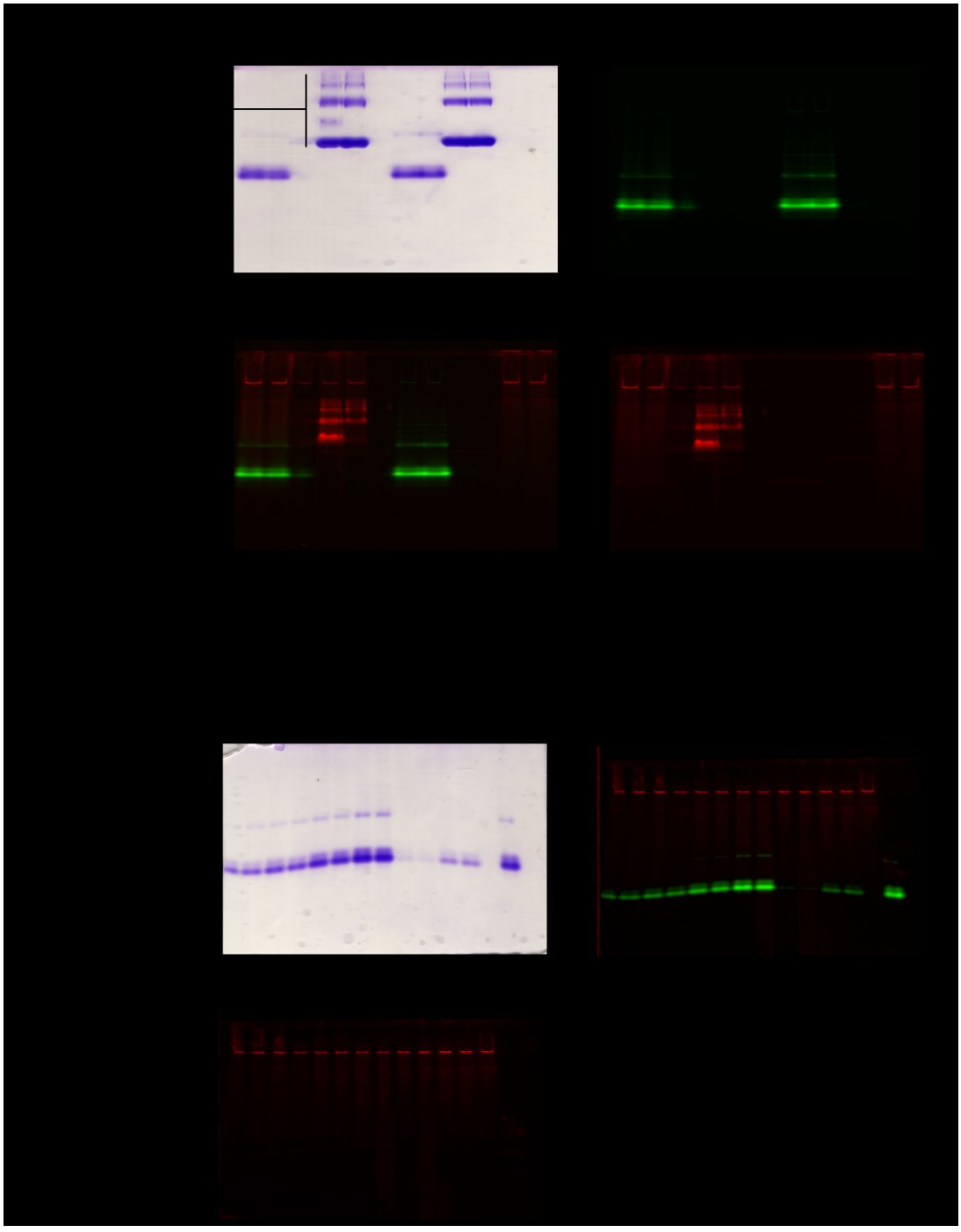

Figure 2-31 Continued.

Figure 2-32 Effect of BSA, heparin and FBS on dfTAT cell penetration. (a) Co-incubation of dfTAT with BSA results in a decrease in the percentage of cells displaying cytosolic release of dfTAT. HeLa cells were co-incubated with 5 μM dfTAT and 10 μM BSA for 1h. Cells show a punctate distribution of the peptide (monochrome 100X image) indicative of peptide being trapped in endocytic vesicles. In comparison, HeLa cells incubated with dfTAT (5 μM) alone show a homogenous cytosolic and nuclear distribution of peptide in a majority of cells. (b) Effect of FBS and heparin on dfTAT mediated cellular. HeLa cells were incubated with 5 μM dfTAT and heparin (1-100 μg/mL) or FBS (0.1-10%) for 1 h. Cells were washed and imaged. The % cells with cytosolic and nuclear distribution was calculated as described in Figure 1(b). Scale bars: 10 μm.

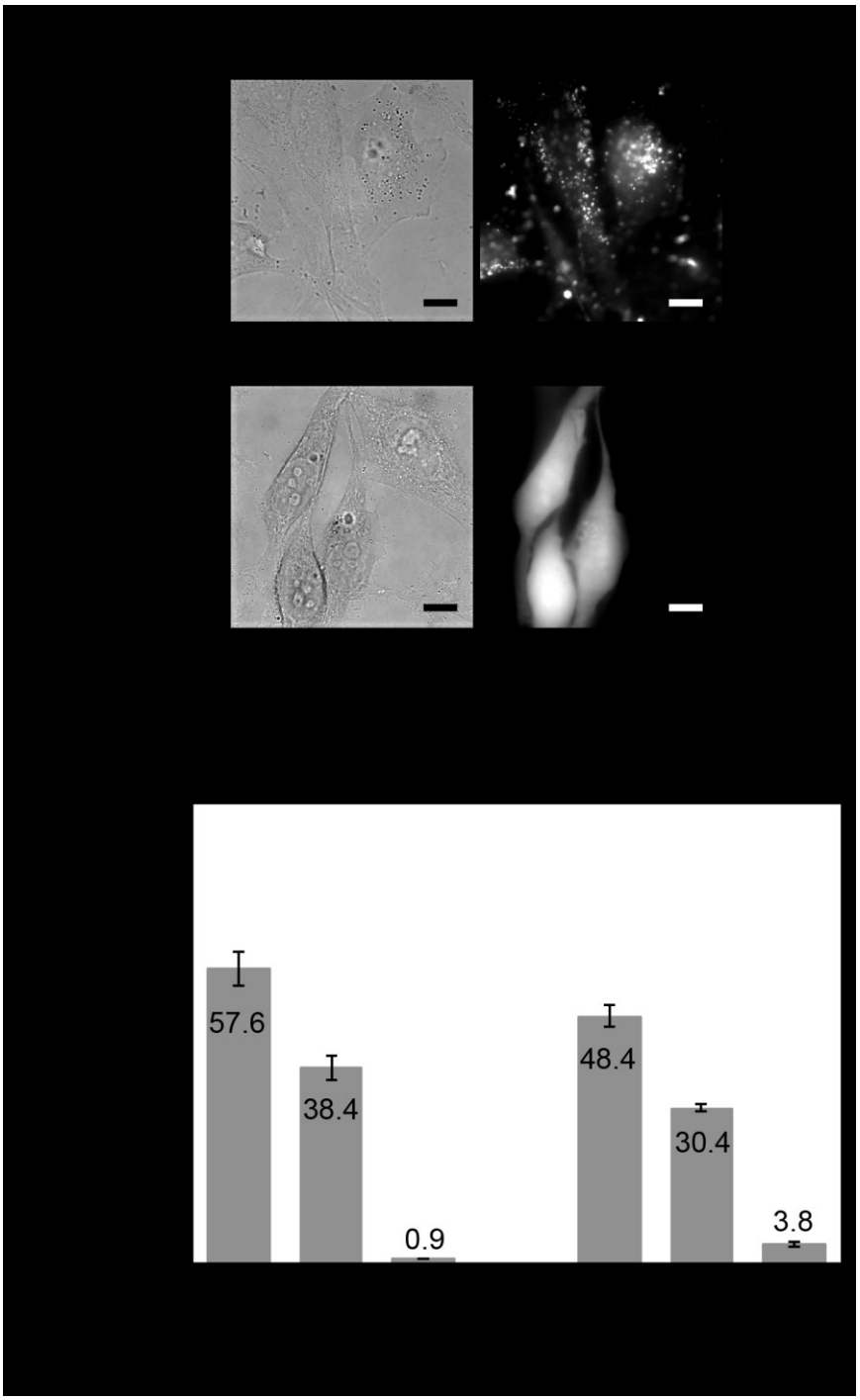

Figure 2-32 Continued.

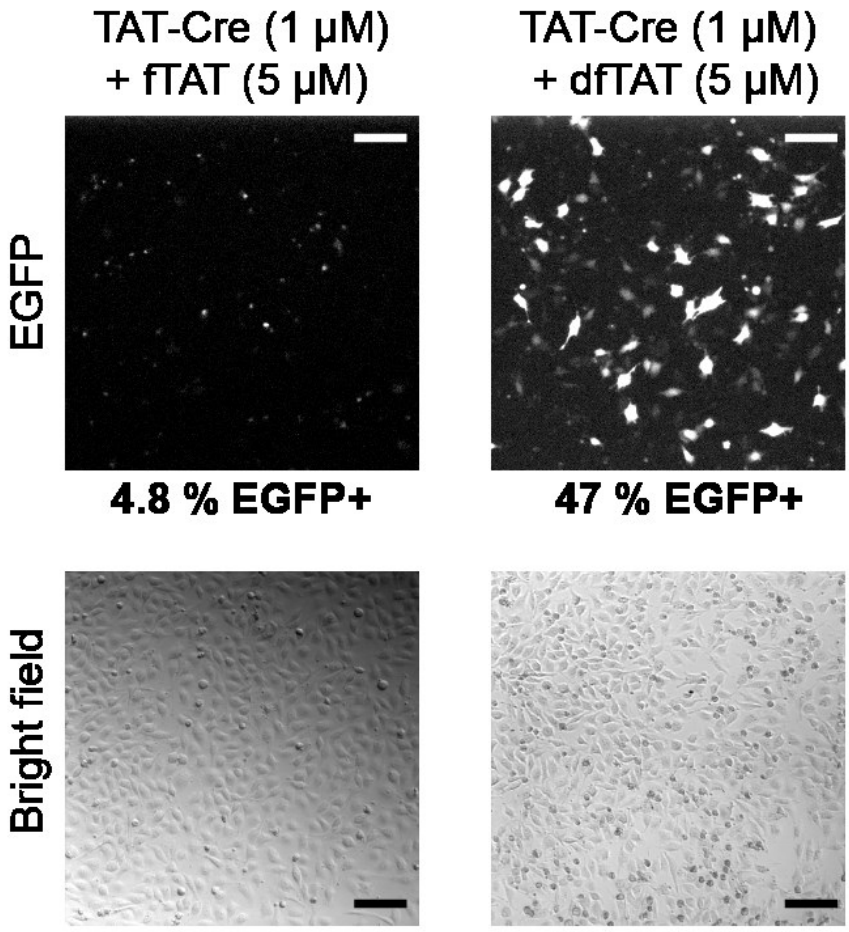

Figure 2-33 Delivery of intact and functional Cre-recombinase using co-incubation with dfTAT. Assay showing that dfTAT improves the delivery of TAT-Cre. HeLa cells transfected with a plasmid containing egfp upstream of a loxP-STOP-loxP sequence were incubated for 1 h with either fTAT (5 μM) or dfTAT (5 μM) in the presence of TAT-Cre (1 μM). $EGFP^+$ cells that result from successful TAT-Cre delivery were visualized and counted by microscopy (confirmed by flow cytometry). Scale bars: 100 μm.

I also delivered FITC–anti-ATP5A, a fluorescently-labeled antibody that recognizes the α-subunit of the mitochondrial ATP synthase. Cells treated with FITC–anti-ATP5A (20 μg/ml) and dfTAT (5 μM) contained green fluorescent tubular structures (**Figure 2-34**). Colocalization with the blue fluorescent mitochondrial marker pTagCFP-mito confirmed that these structures were mitochondria (**Figure 2-35 (A)**). Cells treated with FITC–anti-IgG, an antibody that does not target mitochondria, did not stain tubular structures (**Figure 2-35 (B)**). These experiments confirmed that dfTAT can deliver a functional antibody into live cells.

The transcription factor HOXB4 can penetrate cells, activate transcription and induce hematopoietic stem cell expansion, either by itself or when fused to $TAT^{245-247}$. I was therefore interested in determining whether dfTAT, by promoting cytosolic delivery, would enhance the transcriptional activity of this protein. NIH 3T3 cells were transfected with a vector containing the luciferase gene under a HOXB4-inducible promoter and with a β-galactosidase reporter as internal control. Cells were incubated with HOXB4 or TAT-HOXB4, in the absence or presence of dfTAT, for 1.5 h. I assessed the expression of luciferase by measuring the luminescence of cell lysates (normalized to β-galactosidase activity, luciferase induction represents a ratio of treated versus untreated cells). HOXB4 and TAT-HOXB4 (200 nM) alone induced a 2.2- and 5.0-fold increase in luciferase activity, respectively (**Figure 2-36**). In contrast, addition of dfTAT (3 μM) led to 53.1- and 307.4-fold luciferase induction, respectively. Neither dfTAT alone nor dfTAT incubated with TAT-mCherry led to the induction of luciferase, indicating that luciferase expression was dependent on the presence of HOXB4.

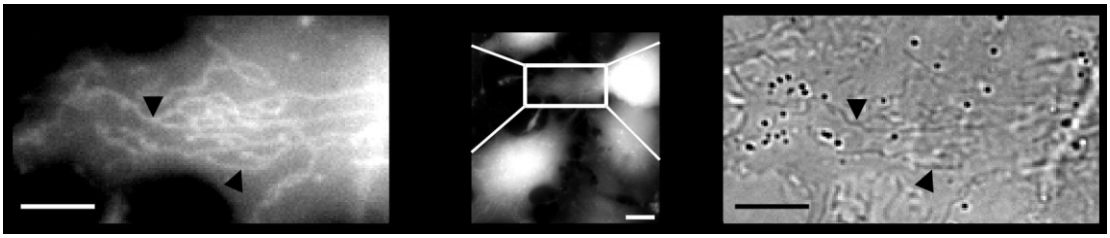

Figure 2-34 Delivery of an intact and functional antibody using co-incubation with dfTAT. Microscopy imaging showing that dfTAT mediates the delivery of an antibody. HeLa cells were co-incubated with FITC-anti-ATP5A (20 μg/mL) and dfTAT (5 μM) for 1 h. FITC-anti-ATP5A (green) is delivered in the cytosol of cells and stains tubular mitochondria (more clearly visible in zoomed-in image). Absence of SYTOX® Blue staining indicates that the cells imaged do not have a compromised plasma membrane. Black arrows point to tubular mitochondria. Scale bars: 100X objective, 10 μm; zoomed-in image, 2 μm.

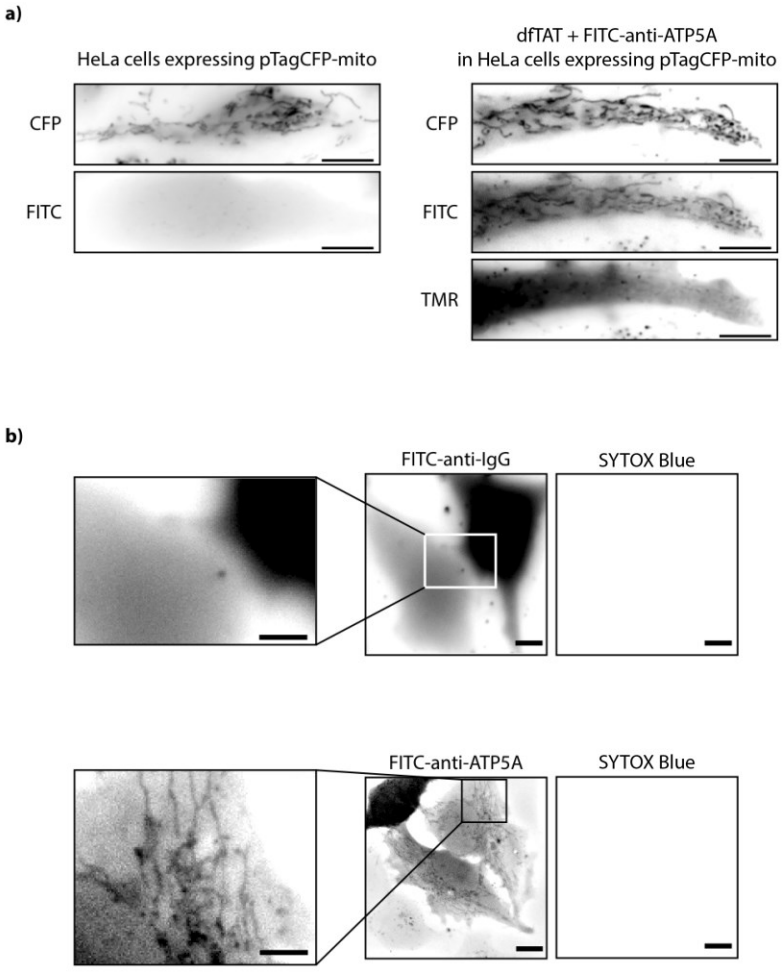

Figure 2-35 The FITC-anti-ATP5a antibody co-localizes with a fluorescently labeled mitochondrial protein expressed in live cells after dfTAT-mediated delivery. (a) Cells expressing TagCFP-mito (left) were imaged using the FITC and CFP filters. Tubular mitochondria were clearly observed only in the CFP channel. In a separate experiment, dfTAT (5 μM) and FITC-anti-ATP5A (20 μg/mL) were incubated for 1 h with cells expressing TagCFP-mito. The inverted monochrome images show co-localization of FITC-anti-ATP5A (FITC channel) and TagCFP-mito (CFP channel). Scale bars: 2 μm. (b) To confirm that the mitochondrial staining is specific to FITC-anti-ATP5A, an antibody without an intracellular epitope, FITC-anti-IgG, was delivered with dfTAT. FITC-anti-IgG (20 μg/mL) and dfTAT (5 μM) were incubated with cells for 1 h. Inverted monochrome images show a homogenous cytosolic fluorescence distribution (top). In contrast, cells that were incubated with FITC-anti-ATP5A show fluorescence in tubular structures (bottom). Scale bars: zoom-in image, 2 μm; 100X objective, 10 μm.

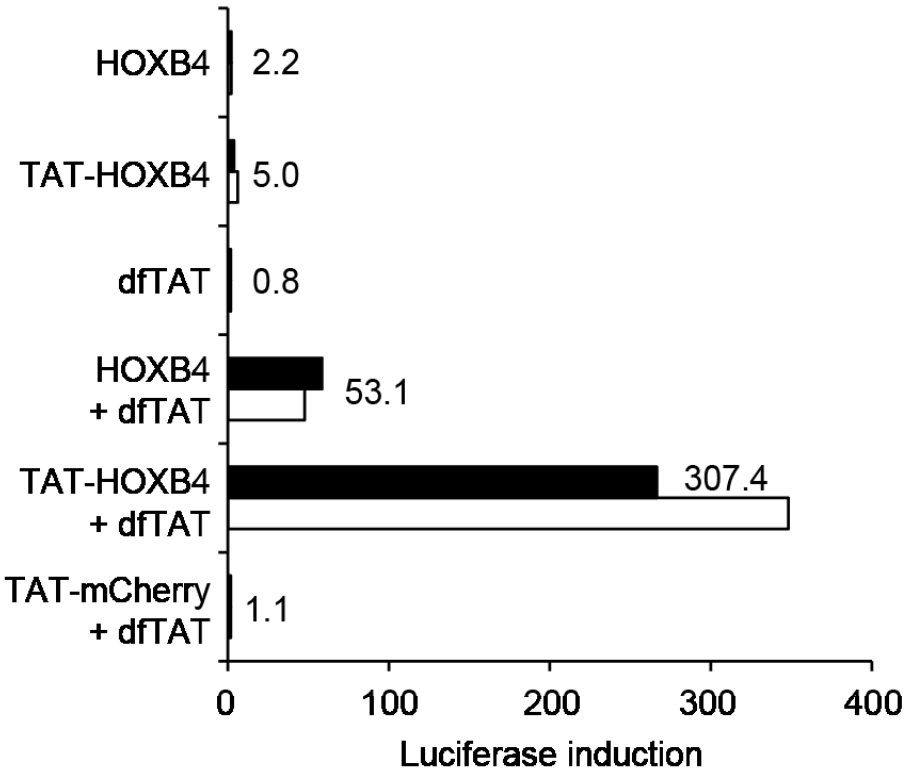

Figure 2-36 dfTAT mediated delivery of HoxB4 and TAT-HoxB4 improves the expression of a luciferase reporter. NIH 3T3 transfected with a HoxB4-dependent luciferase reporter were incubated for 1.5 h with either HoxB4 or TAT-HoxB4 (200 nM) in presence or absence of dfTAT (3 μM). TAT-mCherry (200 nM) and dfTAT (3 μM) serve as negative controls (400,000 cells/experiment, experiments in duplicate).

Although increasing the transcriptional output of HOXB4 is valuable, precisely controlling the level and activity of HOXB4 inside cells is important to achieve desirable biological outcomes[248]. Because dfTAT appears to act independently of the molecules used for co-incubation in my assays, I hypothesized that it might be possible to titrate the amount of protein that penetrates cells by varying the protein concentration in the medium while keeping dfTAT concentration constant. Under this scenario, the efficiency of endosomal escape should remain unaffected, but the amount of material released from endosomes should change. Initial experiments with DEAC-K9 showed that the amount of fluorescent peptide delivered inside cells could be titrated using this protocol (**Figure 2-37 and 2-38**). Consistent with these results, luciferase induction was proportional to the concentration of HOXB4 in the medium (**Figure 2-39**).

2.3 Discussion

By mediating endosomal leakage, dfTAT is remarkably efficient at delivering proteins and peptides into the cytosol of cells. Delivery is efficient because the amount of material that reaches the cytosol is substantial and the amount trapped inside endosomes is relatively low, and because cytosolic delivery occurs in most cells present in a sample. Endosomal escape appears to take place in most cells once dfTAT, which is intrinsically more endosomolytic than monomeric TAT, reaches a threshold concentration within endosomes. Future studies aimed at establishing the roles played by the two copies of the peptide TAT and of the fluorophore TMR, as well as their respective arrangement, should provide more molecular details about the activity of dfTAT. Establishing where dfTAT

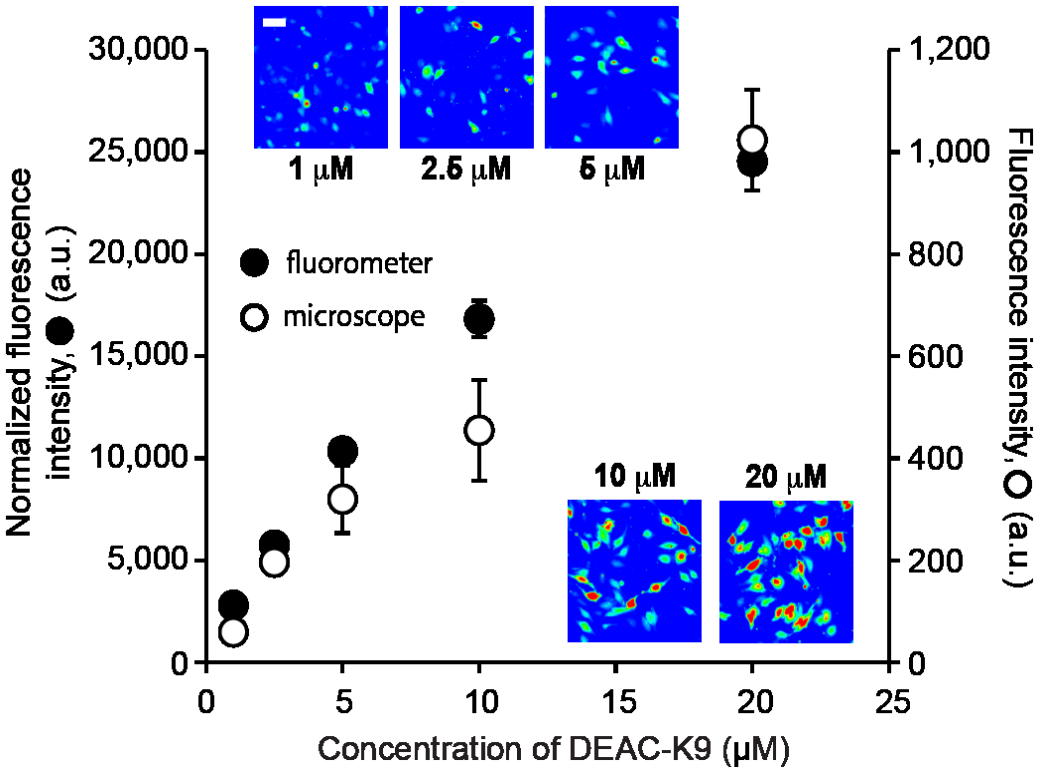

Figure 2-37 The amount of DEAC-K9 delivered in the cytosol and nucleus of live cells can be titrated. HeLa cells were incubated with dfTAT (5 μM) and increasing amounts of DEAC-K9 (1, 2.5, 5, 10, 20 μM). The fluorescence intensity of cells displaying cytosolic release was assessed by microscopy (representative 20X images are shown using a pseudocolored colorscale: blue=lowest intensity, red=highest intensity) and by measuring to the bulk fluorescence of cell lysates (microscope: 1,000 cells/experiment, fluorometer: 300,000 cells/experiment; experiments in triplicates, average and standard deviations represented). Scale bars: 10 μm

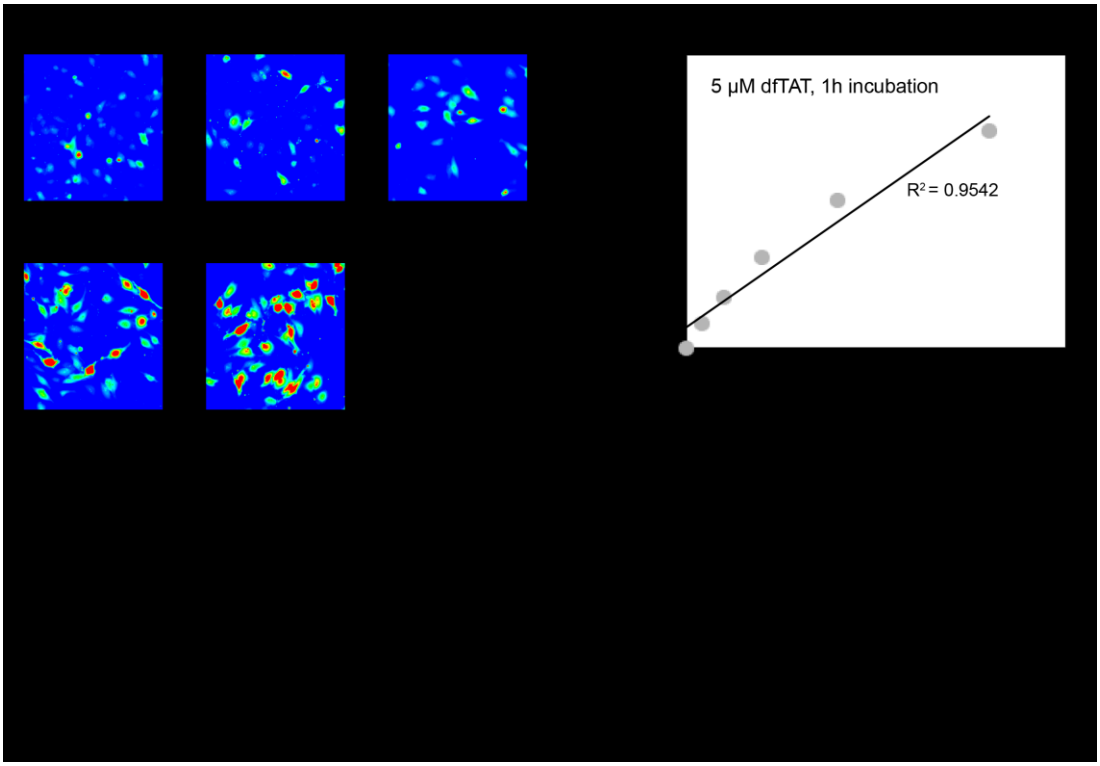

Figure 2-38 Determination of the amount of DEAC-K9 delivered into cells. HeLa cells were incubated with dfTAT (5 µM) and different concentrations of DEAC-K9 (1, 2.5, 5,10 and 20 µM) for 1 h. Cells were washed with PBS/heparin, imaged and lysed. The bulk fluorescence of cell lysates containing DEAC-K9 was measured using a fluorometer. Similarly, the fluorescence of solutions of DEAC-K9 at different concentrations (0.01. 0.1, 1, 10 and 100 µM) was measured using a fluorometer. A calibration curve of DEAC-K9 intensity vs. DEAC-K9 concentration was established. These data was used to estimate the average concentration of DEAC-K9 inside cells. Data shows a linear increase in the amount of DEAC-K9 delivered inside cells (top right panel). Consistent with these data, fluorescence images that show an increase in the fluorescence signal in the cytosol cells with increasing concentrations of DEAC-K9 incubated in the media (top left panel, and Figure 2-38).

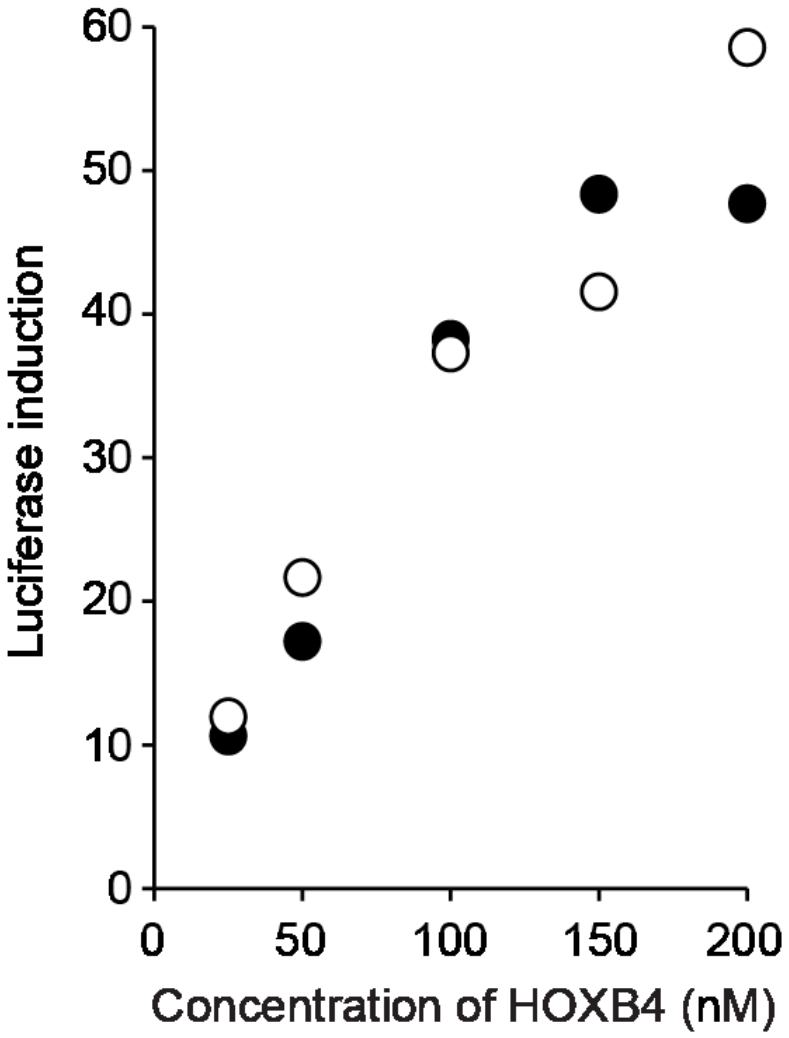

Figure 2-39 The induction of luciferase expression by dfTAT-medited delivery of HoxB4 into cells can be controlled. NIH 3T3 cells were co-incubated with HoxB4 (25-200 nM) and dfTAT (3 μM) and luciferase induction was measured as described in a (400,000 cells/experiment, experiments in duplicate).

escapes from the endocytic pathway should also provide valuable insights regarding its endosomolytic activity, which will be the focus of my next chapter. Notably, the membrane of endosomes can be lysed by fluorescently labeled cell-penetrating peptides upon light irradiation[162, 163]. dfTAT trapped inside endosomes (for example, after incubation at 2 μM) can indeed leak out of endosomes when TMR is continuously excited for several seconds (data not shown). Yet, all delivery experiments reported herein were performed in a dark room with a dim red light. The excitation of dfTAT, when required for fluorescence microscopy, was also minimized to less than 300 ms in all images shown. Overall, I conclude that the endosomal leakage mediated by dfTAT is light independent.

A remarkable aspect of dfTAT-mediated delivery is the minimal cellular responses associated with the efficient endosomal leakage observed. This is surprising because endosomal lysis can be extremely toxic by causing the rapid release of calcium into the cytosol of cells[249]. In addition, the leakage of endolysosomal proteases could contribute to toxicity[250-253]. Yet, I observed that cells were not only viable but also healthy. These results are presumably valid for only the one hour dfTAT incubation used in my assays. Continuous endosomal leakage induced by particulate wear debris induces inflammatory responses and apoptosis[254]. dfTAT could therefore promote similar effects if administered to cells for long incubation times. Notably, membrane repair mechanisms have also been shown to mask the effect of debris-induced endosomal leakage[254]. This, in turn, could also explain why dfTAT-mediated delivery is relatively innocuous under the conditions tested.

dfTAT delivers cell-impermeable molecules displaying diverse structures and properties. DEAC-K9, like dfTAT, is highly positively charged, and the isoelectric points

(pI) of Cre (9.4), and HOXB4 (9.8) are also not suggestive of favorable electrostatic interactions with dfTAT. EGFP, a protein with a lower pI (6.2), does not appreciably interact with dfTAT *in vitro*. It is therefore likely that dfTAT does not need to interact with a given protein outside the cell or within the lumen of endosomes to achieve cytosolic delivery of that protein. Instead, interactions that occur between dfTAT and a protein with low pI such as BSA are inhibitory. Similar inhibitory effects between arginine-rich cell-penetrating peptides and negatively charged species have been observed[74, 255].

The co-incubation protocol used herein allows several cargos to be delivered simultaneously. Alternatively, delivery can be performed in successive steps, without complex sample preparations and, as exemplified by the delivery of SNAP-Surface 488 or FITC–anti-ATP5A, is ideally suited for imaging applications. In addition, co-incubation provides the opportunity to titrate the extracellular concentration of target molecules independently of dfTAT. The amount of protein delivered to the cytosol and the biological output achieved can in turn be modulated. Although my approach is likely not optimal for *in vivo* delivery of biologics, it could offer several advantages over existing reagents for delivery to tissue cultures and the *ex vivo* manipulation of cells.

2.4 Materials and Methods

2.4.1 Peptide design, synthesis and purification

All peptides were synthesized in-house on the rink amide MBHA resin (Novabiochem) by solid-phase peptide synthesis (SPPS) using standard Fmoc protocols. Fmoc-Lys(Mtt)-OH, Fmoc-Lys(Boc)-OH, Fmoc-Gly-OH, Fmoc-Arg(Pbf)-OH, Fmoc-Gln(Trt)-OH and Fmoc-Cys(Trt)-OH (Novabiochem) were used to assemble the peptides. Reactions were carried out in a SPPS vessel at room temperature using a stream of dry N_2 to provide agitation. Fmoc deprotection was performed by addition of piperidine in dimethylformamide (DMF) (Fisher) (20 %, 10 mL) to the Fmoc-peptide resin (0.30 mmol). Deprotection reactions were carried out once for 5 min (1 × 5 min) and 1 × 15 min with a washing step in between reactions. Amino acid coupling reactions were carried out for 4 h with a mixture of Fmoc-amino acid (1.2 mmol), HBTU (Novabiochem) (0.44 g, 1.1 mmol) and di-isopropylethylamine (DIEA) (Sigma) (0.51 mL, 3.0 mmol) in DMF. Upon completion of the reactions, the resin was washed with DMF and dichloromethane (DCM) (Fisher). For DEAC-K9, the DEAC fluorophore (AnaSpec) was coupled to the N terminus of the peptide after coupling of the ninth Fmoc-Lys(Boc)-OH using a mixture of DEAC, HBTU and DIEA (4, 3.9 and 10 molar equivalents (eq) with respect to the peptide) in DMF. The reaction was carried out overnight using a stream of dry N_2 to provide agitation. For CK(ε-NH-TMR)TATG (fTAT), the Mtt protecting group at the ε-amino group of Lys on CK(ε-NH-Mtt)TATG was cleaved with 2 % trifluoroacetic acid (TFA) (Fisher) and 2 % tri-isopropylsilane (TIS) (Sigma) in DCM, and the resin was washed

with DCM and DMF. A mixture of TMR, HBTU and DIEA (4, 3.9 and 10 eq with respect to the peptide) in DMF was added to the resin, and the reaction was carried out overnight using dry N_2 to provide agitation. Following Fmoc-deprotection and peptide assembly, the resin was washed with DCM and dried *in vacuo*. The resin was then treated with TFA containing 2.5 % H_2O, 2.5 % TIS and 2.5 % ethanedithiol (EDT) (Sigma) for 3 h at room temperature to achieve global deprotection and cleavage from the resin. The crude peptide products were precipitated and washed with cold anhydrous Et_2O (Fisher). The precipitates were resuspended in water and lyophilized. The products obtained were then resuspended in 0.1 % aqueous TFA/acetonitrile. The peptides were analyzed and purified by reverse-phase HPLC. HPLC analysis was performed on a Hewlett-Packard 1200 series instrument and an analytical Vydac C18 column (5-μm particle size, 4 mm × 150 mm). The flow rate was 1 mL/min, and detection was at 214 nm and 550 nm. Semi-preparative HPLC was performed on a Vydac C18 10 × 250–mm column. The flow rate was 4 mL/min, and detection was at 214 nm and 550 nm. All runs used linear gradients of 0.1% aqueous TFA (solvent A) and 90% acetonitrile, 9.9 % water and 0.1% TFA (solvent B). The correct identity of the peptides was confirmed by MALDI-TOF performed with a Shimadzu/Kratos instrument (AXIMA-CFR). fTAT expected mass was 2,041.17; observed mass was 2,040.66. DEAC-K9 expected mass, 1,412.97; observed mass, 1,415.59.

2.4.2 Synthesis of acetamidated C(S-CH2CONH2)K(ε-NH-TMR)TATG (acfTAT)

C(S-CH_2CONH_2)K(ε-NH-TMR)TATG was formed after addition of iodoacetamide (Sigma) (0.275 mg, 1.49 μmol) to CK(ε-NH-TMR)TATG (148 μg, 0.074 μmol) in 25 mM HEPES, pH 7.5, under an atmosphere of N_2. The product was purified using analytical reverse-phase HPLC. Expected mass (MALDI-TOF), 2,098.19; observed mass, 2,096.31.

2.4.3 Generation of dfTAT by dimerization of CK(TMR)TATG (fTAT)

dfTAT was formed by dissolving (0.3 mg, 1.5×10^{-4} mmol) fTAT in aerated phosphate buffer saline (PBS), pH 7.4 (5 mL). Oxygen dissolved in the buffer acted to oxidize the thiol groups on the peptides and form a disulfide bond. The reaction was allowed to react overnight until completion (100 % yield according to HPLC analysis). The product was purified using analytical reverse-phase HPLC. Expected mass (MALDI-TOF), 4,080.34; observed mass, 4,084.21.

2.4.4 Generation of nrdfTAT using fTAT

Two fTAT peptides linked by the bis(maleimido)ethane (BMOE) (Pierce) linker (nrdfTAT) was formed by reacting pure fTAT (0.202 mg, 0.099 μmol) with BMOE (0.011 mg, 0.0496 μmol) for 3 h in PBS buffer, pH 7.2, under an atmosphere of N_2. The product was purified using analytical reverse-phase HPLC. Expected mass (MALDI-TOF), 4,313.39; observed mass, 4,303.

2.4.5 Cloning, overexpression and purification of TAT-Cre, TAT-mCherry, HOXB4 and TAT-HOXB4

The pTriEx-HTNC plasmid encoding His-tagged TAT-NLS-Cre (TAT-Cre) protein was purchased from Addgene. The TAT-Cre gene was then cloned into pTXB1 vector and transformed into *Escherichia coli* BL21 (DE3) cells (Agilent Technologies). The protein was expressed and purified as described[256]. Briefly, TAT-Cre was expressed with 1 mM IPTG at 37 °C for 3 h. TAT-Cre was then purified to homogeneity using a Ni-NTA resin (Qiagen) and cation-exchange chromatography (HiTrap SP HP) (GE Healthcare).

pTXB1-TAT-mCherry was obtained by inserting the TAT DNA sequence into the pTXB1-mCherry plasmid. The oligonucleotides with sequences 5′-TAT GGG TCG TAA AAA ACG TCG TCA GCG TCG TCG TGG TCA-3′ and 3′-ACC CAG CAT TTT TTG CAG CAG TCG CAG CAG CAC CAG TAT-5′ (Integrated DNA Technologies) coding for the TAT sequence, which contain NdeI sites, were annealed to generate dsDNA. The pTXB1-mCherry plasmid was cut with NdeI (New England Biolabs) and ligated with TAT dsDNA. The pTXB1-TAT-mCherry plasmid was transformed into BL21 (DE3) cells, and protein expression was induced with 1 mM IPTG at 16 °C for 24 h. Cells were harvested and resuspended in lysis buffer containing 20 mM Tris-Cl (pH 7.5) and 200 mM NaCl. After cell lysis by sonication and high-speed centrifugation at 15,000 r.p.m. (rotor radius: 23 cm) for 1 h, the soluble fraction was applied to chitin resin (New England Biolabs) pre-equilibrated with lysis buffer and incubated overnight at 4 °C (the protein contains a C-

terminal intein-chitin binding domain purification tag). The resin was washed with ten column volumes of lysis buffer. The protein was cleaved from the resin by incubating the beads with 1 column volume of cleavage buffer supplemented with 100 mM 2-mercaptoethanesulfonic acid and for 24 h at 4 °C. The protein was further purified using cation-exchange chromatography.

EGFP was cloned, expressed and purified as previously described[257]. The double-mutant EGFP (dmEGFP) was obtained by introducing the mutations (C49S, C71V) in the EGFP plasmid using site-directed mutagenesis. Because dmEGFP does not contain any Cys residue, this protein is unable to form a disulfide bond with fTAT. In all assays, results obtained with EGFP were similar to those obtained with dmEGFP. In the text, both EGFP and dmEGFP are therefore referred to as EGFP for simplicity.

The pTAT-HA-HOXB4 vector was generously provided by G. Sauvageau (Montreal University). His_6-HOXB4 was produced by cloning the *HOXB4* gene into pET-28a. Briefly, the *HOXB4* cDNA was first amplified from pTAT-HA-HOXB4 by using primers designed to introduce the NdeI and XhoI sites at the 5′ and 3′ ends, respectively (5′-GGC ATT CAT ATG GCT ATG AGT TCT TTT TTG ATC AAC TCA- 3′; 5′-GGT CAG TCT CGA GCT AGA GCG CGC GGG G-3′) (IDT). The PCR fragment was then inserted into the corresponding NdeI and XhoI sites of the 6xHis-tag vector, pET-28a. The fidelity of the reading frame was confirmed by sequencing. The procedure for the purification of both TAT-HOXB4 and HOXB4 is similar and has been previously described[247]. Briefly, BL21 (DE3) cells were transformed with either pTAT-HA-HOXB4 or pET28a-HOXB4 and induced at 37 °C for 5 h with 1 mM IPTG. The pelleted cells were

lysed by sonication in buffer A (8 M urea, 20 mM HEPES, 200 mM NaCl, pH 8.0). Lysates, which were obtained via high-speed centrifugation (14,000 r.p.m., 30 min at 22 °C), were then adjusted to 10 mM imidazole and incubated with Ni-NTA agarose beads for 60 min at room temperature. The nickel beads were then washed with buffer A containing 20 mM and 40 mM imidazole to eliminate the presence of any nonspecific products, and bound proteins were subsequently eluted with 100 mM and 250 mM imidazole in buffer A. Eluates from both concentrations of imidazole containing the proteins of interest (i.e., TAT-HOXB4 or HOXB4) were loaded on a HiTrap SP HP column at 4 °C in buffer B (4 M urea, 20 mM HEPES, 50 mM NaCl, pH 6.5) and eluted on the FPLC in a single-step at 4 °C with buffer C (20 mM HEPES, 1 M NaCl, pH 8.0). Both proteins were immediately desalted by diluting with 20 mM HEPES (pH 8.0) and concentrated using centrifugal filter units with 10K MWCO (EMD Millipore), divided into aliquots and flash frozen at –80 °C. Protein concentrations were determined using the Bradford protein assay (Bio-Rad).

2.4.6 Cell lines

HeLa (ATCC CCL-2), HaCat[258] (obtained from J. Massagué, Memorial Sloan-Kettering Cancer Center), NIH 3T3 (ATCC CRL-1658), COLO 316[259] (obtained from R. Burghardt, Texas A&M University), HDF (ATCC PCS-201-010), Neuro-2a (ATCC CCL-131) and MCH58[260] (obtained from E. Shoubridge, Montreal Neurological Institute and Hospital) were grown in Dulbecco's minimum essential medium (DMEM) (Fisher) supplemented with 10% fetal bovine serum (FBS) (Fisher) and 1× penicillin/streptomycin

(P/S) (Fisher) and kept at 37 °C in a humidified atmosphere containing 5 % CO_2. Intestinal porcine epithelial cells (IPEC-1, obtained from G. Wu, Texas A&M University) were cultured in growth medium containing DMEM, 10 % FBS, insulin (5 μg/mL; Sigma), hydrocortisone (1 μg/mL; Sigma), EGF (5 ng/mL; BD Biosciences) and 1× P/S and kept at 37 °C in a humidified atmosphere containing 5% CO_2[261]. Cultures were tested for *Mycoplasma* contamination using the PCR Mycoplasma Test Kit II (PromoKine). HeLa cells were profiled using STR, by ATCC before purchase, but other cell lines were not.

2.4.7 Delivery of peptides inside live cells

Cells were seeded in eight-well dishes so that the cells were 80–90 % confluent after 48 h. Each well was washed three times with PBS and Leibovitz's L-15 medium that did not contain the amino acid cysteine (nonreducing L-15, nrL-15). The medium (nrL-15) used for incubation lacks cysteine to avoid reduction of the disulfide bond of dfTAT. Cells were then incubated with different concentrations of the acfTAT, fTAT, dfTAT or nrdfTAT at 37 °C for 5–60 min. Cells were washed three times with PBS and nrL-15 and placed on an inverted epifluorescence microscope (Model IX81, Olympus) equipped with a heating stage maintained at 37 °C. Images were collected using a Rolera-MGI Plus back-illuminated electron-multiplying charge-coupled device (EMCCD) camera (Qimaging). Images were acquired using bright-field imaging and three standard fluorescence filter sets: CFP (excitation (Ex) = 436 ± 10 nm/emission (Em) = 480 ± 20 nm), RFP (Ex = 560 ± 20 nm/Em = 630 ± 35 nm) and FITC (Ex = 488 ± 10 nm/Em = 520 ± 20 nm). The

fluorescence intensities of different cells were measured with the SlideBook 4.2 software (Olympus), and the average fluorescence intensity was determined for each condition. Our laboratory has previously reported that cell-penetrating peptides labeled with fluorophores such as TMR can photosensitize membranes and cause endosomal leakage upon light irradiation[162, 163]. To minimize the role played by light irradiation in the activities reported herein, I performed all delivery experiments under conditions of minimal light irradiation (dark room with dim red light). When fluorescence imaging was required, probes (for example, SNAP-Surface 488 and EGFP) were imaged before dfTAT images were acquired. dfTAT was also excited for only a maximum of 300 ms. In contrast, the light dose required to observe light-induced endosomal leakage was typically 10- to 20-fold greater than that used for imaging. For experiments performed with Cre and HOXB4, cells were not imaged and not exposed to light during delivery (cells incubated with HOXB4 were never exposed to light, and cells incubated with Cre were imaged 12 h after incubation).

2.4.8 Delivery of peptides and proteins inside live cells by co-incubation with dfTAT

HeLa, HDF and Neuro-2a cells were seeded in eight-well dishes, grown and washed as described in the prior section. Cells were then co-incubated with 5 μM delivery peptide and with the cargo at the corresponding concentration for 1 h at 37 °C. Cells were washed three times with PBS and nrL-15 and placed on the microscope. Images were acquired as described before. For transfection and expression of SNAP-H2B and TagCFP-mito, plasmids were mixed with Lipofectamine 2000 reagent in opti-MEM medium and

incubated at room temperature for 30 min. The DNA complex was added to previously seeded HeLa cells (80 % confluent) on an eight-well dish, and cells were kept at 37 °C for 24 h. After 24 h, the wells were washed three times with PBS and nrL-15 before performing the delivery experiments using the SNAP-Surface 488, FITC goat anti-mouse IgG (Life Technologies, Cat. No. F2761) or mouse monoclonal FITC–anti-ATP5A (Abcam ab119688). The SNAP-Surface 488 fluorescence is known to be quenched (80 %) before reacting with the SNAP fusion tag[242]. Consequently, I considered the signal of SNAP-Surface 488 to be 80 % quenched when the molecule is trapped inside endosomes or distributed in the cytosol of cells, but fully fluorescent when localized in the nucleus of cells (where it reacts with SNAP-H2B). To estimate the amount of SNAP-Surface 488 that escapes from endosomes after dfTAT-mediated delivery, I analyzed the SNAP-Surface 488 fluorescence signal obtained after imaging using the SlideBook software. The total signal intensity of the cytoplasmic region was multiplied by 5 and compared to the total signal intensity of the nuclear region.

2.4.9 Quantitative determination of peptide and macromolecule uptake inside cells

HeLa cells were seeded in a 48-well dish, grown and washed as described above. For the peptide uptake experiment, each well was incubated for 1 h with varying concentration of acfTAT, fTAT or dfTAT (range: 5–25 μM peptide concentration). For the titration experiment, cells were incubated with dfTAT (5 μM) and varying concentration of DEAC-K9 (range: 1–20 μM) or EGFP (10 μM) for 1 h. Cells were then washed with PBS with heparin (1 mg/mL) and nrL-15 and imaged. To lyse cells, I

removed nrL-15 from the wells, and a total of 100 µl of lysis buffer (50 mM Tris, pH 7.5, 2 mM EDTA, 2 mM DTT, 0.1 % Triton X-100) were incubated with cells for 5 min (alternatively, cells were trypsinized and counted as described in the flow cytometry section). Cells were scraped off the dish, and the cell lysate was pipetted into a 1.5-mL microcentrifuge tube and centrifuged at 13,000 r.p.m. for 25 min (rotor radius: 8.4 cm). For uptake measurement, 70 µl of supernatant were collected and placed in a 96-well plate. The fluorescence emission intensity was measured using a plate reader equipped with a fluorescence module (Ex = 525 nm, Em = 580–640 nm) (GloMax-Multi+ Detection System, Promega). Alternatively, 80 µL of supernatant were diluted to a total volume of 100 µl, and the bulk fluorescence was measured using a SLM-8000C fluorometer (Ex = 435 nm, Em = 465–475 nm) (SLM Instruments). Fluorescence intensities were normalized to total protein concentration in each well (determined by Bradford protein assay, wherein 10 µl of each cell lysate is added to 200 µl of a 1× protein assay reagent and then incubated at room temperature for 30 min; absorbance at 600 nm is measured using the plate reader). To determine the amount of EGFP uptake, I mixed cell lysates (27 µl) with 3 µl of 5× SDS-PAGE loading buffer lacking DTT and analyzed them by SDS-PAGE (the sample was not boiled so as to avoid EGFP unfolding; SDS-PAGE does not unfold EGFP, as described in [262] ; DTT was not included to avoid cleavage of the disulfide bond that might form between fTAT and EGFP). Calibration curves were established for EGFP and DEAC-K9 by analyzing samples of known concentrations using SDS-PAGE gel and fluorescence, respectively. All experiments were performed in triplicate.

2.4.10 Quantitative analysis of TAT-HOXB4 and HOXB4 delivery with fTAT and dfTAT using a luciferase reporter

The murine fibroblast cell line (NIH 3T3, stably transfected with the E2A-PBX vector), the luciferase reporter vector, pML (5xHOX/PBX; contains a promoter with binding sites for HOXB4 and PBX) and the β-gal internal control vector used in the following studies were kindly provided by P. Zandstra (University of Toronto). The cells were initially cultured in 100-mm dishes at 37 °C with 5 % CO_2 in DMEM supplemented with 10% FBS. For experimental purposes, however, cells were seeded in 24-well plates at a density of 5×10^4–6×10^4 cells per well for 24 h. Subsequently, cells were cotransfected with 0.8 μg/ml of pML (5xHOX/PBX) and of the β-gal internal control vector using Lipofectamine 2000. Twelve hours post transfection, cells were washed and incubated with TAT-HOXB4 or HOXB4 (both at 200 nM, unless, otherwise noted; see below) with or without fTAT or dfTAT in nrL-15 for 90 min. Some cells were also incubated with TAT-mCherry (200 nM) with and without the peptides. After incubation, all cells were washed with PBS and lysed according to the manufacturer's protocol for the reporter lysis buffer (RLB) (Promega). For titration experiments, the same protocol was followed, with the exception that HOXB4 concentrations were varied (25, 50, 100, 150 and 200 nM). In order to quantitate the luciferase reporter activity, I added 100 μl of luciferase assay reagent (Promega) to 20 μl of cell lysate and bioluminescence was immediately measured using a SpectraMaxL luminometer (Molecular Devices). For the purposes of measuring transfection efficiency, 180 μl of β-gal assay buffer were mixed with 20 μl of cell lysate in a 96-well plate and incubated at 37 °C for 30 min. The β-gal assay buffer is composed of 75 % 0.1 M sodium phosphate, pH 7.5, 24 % *o*-nitrophenyl

β-D-galactopyranoside (ONPG made at a concentration of 4 mg/mL in 0.1 M sodium phosphate) (Sigma) and 1% 100-fold solution (10 % 1 M magnesium chloride solution, 32 % β-mercaptoethanol and 58 % distilled water). Absorbance was then measured at 450 nm using the plate reader. As the absorption spectrum of the chromophore (TMR) conjugated to the peptide used in this study overlaps with that of β-gal, 20 µl of cell lysate containing the peptide were also diluted with 180 µl of the lysis buffer, and absorbance values obtained at 450 nm were subtracted from those of the β-gal. The luciferase activity of all samples was determined as a ratio of the luciferase activity to the β-gal activity, and the fold-increase in luciferase activity was established by normalizing the luciferase activity of each sample to that of cells, which were transfected but had no protein delivered.

2.4.11 Cell viability assays

In order to determine cells that had compromised plasma membranes, I treated cells with SYTOX® green (SYTOX® blue in some cases) and Hoechst (Invitrogen). SYTOX® dyes are cell impermeable and stain the DNA of cells with compromised plasma membranes. The Hoechst dye is cell permeable and stains the DNA of all cells. Images were acquired using the green and blue filter. The green and blue images were used to count cells with a blue- or green-stained nucleus. ImageJ was used to count the dead (green) and total cells (blue). Cytotoxicity was determined from the ratio of SYTOX® green–positive cells/total number of cells. An MTT (3-(4,5-dimethylthiazol-2-yl)-2,5-diphenyltetrazolium bromide) assay was performed to determine the effect of the peptide

on cell proliferation. Cells were seeded in a six-well dish, grown and washed as described above. One well from the dish was incubated with 5 μM dfTAT at 37 °C for 1 h. A second well was left untreated and served as control. Cells were washed three times with PBS and nrL-15. Cells were trypsinized and seeded into 96-well dishes containing 200 μl of DMEM. The cells were then allowed to attach to the bottom of the dish for 12 h. The MTT assay was then performed at specific time points to measure cell proliferation. The DMEM was removed and replaced with 100 μl of nrL-15, and 10 μl of a 12 mM MTT stock solution were added to the wells. The 96-well dish was incubated at 37 °C for 4 h. After the incubation, 100 μl of a 10 mM SDS-HCl solution were added to each well. The solution was mixed thoroughly by pipetting up and down and was incubated for 13 h. After the incubation each sample was mixed, and the absorbance at 600 nm was measured. Controls included a negative control where 10 μl MTT was added to 100 μl of nrL-15 alone (no cells). A second control consisted of cells treated with the delivery peptide but to which no MTT was added to subtract the contribution of TMR from the measured absorbance. The absorbance of the negative control was subtracted from all samples. The final time point measurement for each cell type corresponded to 100 % cell confluency.

2.4.12 Whole-genome microarray analysis

HDF cells were cultured in 24-well dishes and incubated with nrL-15 (untreated cells), nrL-15 supplemented with dfTAT (5 μM, treated cells) or nrL-15 supplemented with staurosporine (0.1 μM) for 1 h. Cells were trypsinized immediately after washing with PBS or nrL-15 (1-h time point). Alternatively, cells were trypsinized after 1 h (1 h +

1 h) or 24 h (1 h + 24 h) incubation in 10 % FBS/DMEM. Cells were removed from each well by gentle pipetting and spun down at 12,000 r.p.m. for 4 min at 4 °C. The cell pellets were preserved in 1 mL Trizol (Ambion, Life Technologies) and shipped frozen to the UT Southwestern microarray facility, where total RNA was extracted and analyzed on an Illumina Human HT-12 v4 sequencer using reported protocols (https://microarray.swmed.edu/protocols/protocol/illumina-gene-expression-probe-labeling).

2.4.13 Differential in gel electrophoresis (DIGE) proteomic analysis

HDF cells were treated with or without dfTAT as described in the whole-genome microarray analysis assay. A volume of 150 µl of lysis buffer (10 mM Tris, pH 7.5, 1 % CHAPS and 1× protease inhibitor cocktail) was added to each well. After 5 min, the solution was transferred to an Eppendorf tube, and 20 µl of nuclease cocktail were added to the cell lysates and incubated on ice for 30 min. The lysate was spun down at 13,000 r.p.m. for 10 min at 4 °C. The supernatant was saved, and an aliquot was used in Bio-Rad protein assay for quantification of total protein in the cell lysates. Methanol-chloroform precipitation was performed on the remaining sample[263]. All DIGE experiments were performed with pH 3–10 NL gradients. Each sample (~50 µg of protein) was resuspended in 30 µl of labeling buffer (7 M urea, 2 M thiourea, 4 % CHAPS, 30 mM Tris, 5 mM magnesium acetate). All samples were individually labeled with Cy3 or Cy5 (GE Healthcare) for 30 min on ice and in the dark (200 pmol), after which the reaction was quenched by the addition of 10 mM lysine for 10 min followed by the addition of an equal

volume of 2× rehydration buffer (7 M urea, 2 M thiourea, 4 % CHAPS, 4 mg/mL DTT). The combined samples were brought up to 250 µl with 1× rehydration buffer (7 M urea, 2 M thiourea, 4 % CHAPS, 2 mg/mL DTT, 0.5 % IPG buffer, pH 3–10). All strips were subjected to isoelectric focusing for 25,000 V h, according to manufacturers' recommendations. DIGE-associated instrumentation was manufactured by GE Healthcare. Electrophoresis instrumentation was from Hoefer. Cy2/3/5-specific 16-bit data files were acquired at 100-µm resolution separately by dye-specific excitation and emission wavelengths using a Typhoon Trio Variable Mode Imager in a manner that greater than 90% of the proteins were in the linear range of detection.

2.4.14 Determination of dfTAT and EGFP interaction by FRET

Fluorescence emission spectra were obtained using an SLM-8000C fluorometer upgraded with the Phoenix package (ISS) and Vinci v.1.6 PC software (ISS). The experiments were conducted using a quartz cuvette at room temperature. The samples were excited at 488 nm (slit width = 1 mm), and the fluorescence emission was scanned from 500 to 650 nm (slit width = 1 mm). All samples (1 µM EGFP or dmEGFP and 5 µM dfTAT) were prepared using nrL-15. A 12% native gel was run using Tris-glycine running buffer at 100 mV for 2 h. Samples containing dfTAT (5 or 10 µM) were co-incubated with either varying concentration of dmEGFP (10–20 µM) or BSA (10 µM) in nrL-15 (pH 5.0 and 7.0) for 30 min at 37 °C before gel loading. Fluorescence images of dfTAT and EGFP bands on the gel were detected using a fluorescence scanner (Typhoon, GE Healthcare).

(dfTAT fluorescence detection: Ex, 568 nm; Em, 620 nm. EGFP fluorescence detection: Ex, 488 nm; Em, 525 nm.) Gels were then stained with Coomassie blue.

3. AN L- TO D- AMINO ACID CONVERSION IN AN ENDOSOMOLYTIC ANALOG OF THE CELL-PENETRATING PEPTIDE TAT INFLUENCES PROTEOLYTIC STABILITY, ENDOCYTIC UPTAKE, AND ENDOSOMAL ESCAPE[264]

3.1 Introduction

In this chapter, I use dimeric fluorescence TAT developed in the previous chapter as a model CPP to explore the broader consequences of L- to D-stereochemical conversion. In particular, I determine the impact of chirality on endosomal escape during the cell penetration process and how an unnatural D-CPP affects cell physiology once inside a cell. I hypothesize that inversion of stereochemistry of dfTAT, allows for protection against degradation from endocytic proteases, and therefore promotes enhanced endosomal escape activity. In this work, I show that the inversion of chirality provides protease-resistance without altering the overall mode of cellular entry, a process involving endocytic uptake followed by endosomal escape and cytosolic entry. However, while inversion of chirality reduces endocytic uptake, the D-peptide (D-dfTAT), once in the endosome, is significantly more prone to escape than its L counterpart. Moreover, the D-peptide is retained in the cytosol of cells for several days while the L-peptide is degraded within hours. Notably, while the L-peptide is relatively innocuous to cells, the D-peptide

---

exerts a prolonged anti-proliferative activity. Together, my results establish connections between chirality, protease- resistance, cellular penetration, and intracellular activity that may be useful for the development of future delivery agents with improved properties.

3.2 **Results**

Cell-penetrating peptides (CPPs) have become important tools for the delivery of macromolecular cargoes inside cells [17, 265, 266]. These delivery agents show promise in therapeutic applications and are useful reagents for cell biology assays [23, 247, 267]. For instance, CPPs (TAT, Penetratin, etc.) are currently tested in several pre-clinical and clinical trials [71, 268]. However, CPPs exposed to cells or serum are rapidly degraded and this can consequently render these compounds less effective *in vivo* or *in vitro* [269-273]. To protect CPPs from degradation, a common strategy has been to employ D-amino acids instead of their L-amino acid counterparts. D-peptides are protease resistant and this approach has been applied to CPPs such as TAT, R9, penetratin, hLF, pVEC, and Sweet Arrow Peptide [270, 274-277]. In addition, the extended *in vivo* half-lives of D-peptides over L-peptides have contributed to the successful development of D-polyarginine CPPs as cancer contrast agents [74, 278]. How inversion of chirality impacts the multifaceted functions of CPPs, however, remains unclear.

Several reports have indicated that cellular uptake of CPPs is independent of peptide backbone chirality [276, 279]. Uptake of the CPPs studied was thought to involve direct plasma membrane translocation. This is because uptake persisted at 4 °C, a condition that typically abolishes endocytosis [276]. In many cases, however, the penetration

of CPPs into cells involves different routes of cellular entry [280]. Instead of crossing the plasma membrane directly, certain CPPs are first internalized by endocytosis and accumulate inside endosomes. In a second step, CPPs escape from endosomes to penetrate the cytosolic space [110, 233]. The effect of chirality on endocytosis has been reported for the CPPs R9, penetratin, and hLF. Preferential uptake of L-CPPs over D-CPPs was observed, suggesting that chirality is important for the interactions between these compounds and cell surface partners that induce endocytosis [281]. Together, these studies reveal conflicting results that highlight how L- to D-amino acid conversion may lead to CPP-dependent results.

To date, several questions related to the effect of chirality on CPPs' activities remain unanswered. In particular, how chirality impacts endosomal escape during the cell penetration process and how an unnatural D-CPP affects cell physiology once inside a cell are still unclear [282]. The issue of endosomal escape is important because this step is critical for the successful delivery of molecules of interest into a cell [230]. Similarly, the issue concerning the physiological impact of cell penetration is of significance when one considers, for instance, using cellular delivery protocols as a tool for cell biology and therapeutic applications (i.e. most applications would benefit from delivery protocols that only minimally disrupt cells).

In this report, I address these questions by using dfTAT (dimeric fluorescent TAT) as a model CPP. dfTAT is a disulfide bonded dimer of the prototypical CPP TAT. dfTAT is capable of escaping from endosomes with extremely high efficiency [157]. For instance, while TAT escapes endosomes with an estimated efficiency of less than 1% (i.e. 1% of

peptide present in a cell reaches the cytosol while 99% remains trapped inside endosomes), the endosomal escape efficiency of dfTAT exceeds 90% [134, 157, 244]. Mechanistically, cytosolic penetration of dfTAT involves egress from late endosomes (it does not involve escape from other endocytic organelles or direct plasma membrane translocation) [283]. This egress appears to be mediated by the leaky fusion of late endosomal membranes and involves interactions between the positively-charged CPP and the anionic lipid bis(monoacyl)glycerophosphate (BMP)[283]. From a delivery point of view, the mode of cell penetration by dfTAT is useful because macromolecules, endocytosed along with dfTAT after co-incubation with cells, can also be released into the cytosol of cells (i.e. by leaking out of late endosomes along with the endosomolytic CPP). This approach has been used to deliver an enzyme, a transcription factor, peptides, and cell-impermeable small molecules with high efficiencies[157]. Importantly, the leakage induced by dfTAT appears to be relatively innocuous to cells as dfTAT-mediated delivery does not lead to changes in cellular proliferation or transcriptional responses. dfTAT therefore represents a CPP with desirable properties and with an activity sufficiently high to enable mechanistic studies.

Herein, I investigate the cell penetration of a D-amino acid analog of dfTAT to establish the impact of chirality on cytosolic access. I establish that a L- to D-amino acid substitution, by inhibiting peptide degradation from endocytic proteases, promotes enhanced endosomal escape activity. I also establish that the D-CPP, after successful cytosolic entry, gives rise to perturbations in proliferation and transcription more severe than L-CPP. This can be attributed to the prolonged intracellular retention of the D-

peptide. For the first time, I therefore report on an anti-proliferative effect of a D-CPP and reveal additional advantages and disadvantages inherent to conferring protease-resistance to an endosomolytic agent. I envision these findings are relevant to other cell-permeable molecules (e.g. stapled peptides, peptoids, CPPs, etc.), in particular those that, like dfTAT, have high arginine residue content.

3.2.1 Generation of D-dfTAT: a protease resistance cell-penetrating peptide

dfTAT (i.e. L-dfTAT) and D-dfTAT were prepared by synthesis of the peptide CK(TMR)RKKRRQRRRG or ck(TMR)rkkrrqrrrG, respectively, on solid-phase followed by disulfide bond formation of the cysteine residue in solution (**Figure 3-1, Figure 3-2; Figure 3-3**). TMR is the red fluorophore carboxytetramethylrhodamine and is conjugated to the ε-NH_2 of the lysine side chain.

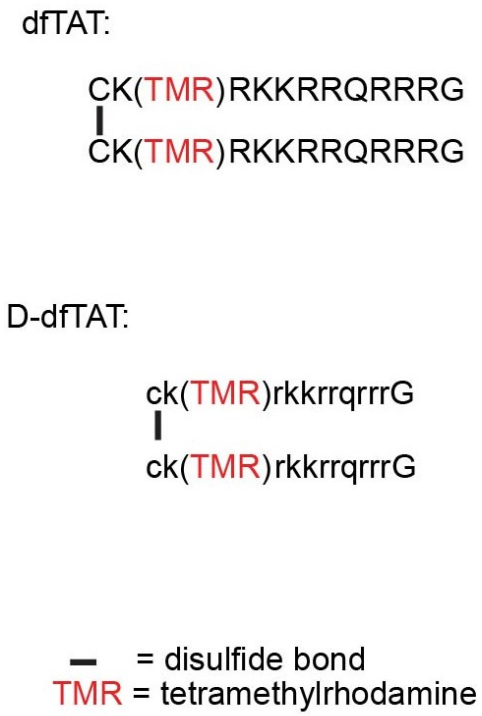

Figure 3-1 Schematic representation of the amino acid sequence of dfTAT (top) and D-dfTAT (bottom).

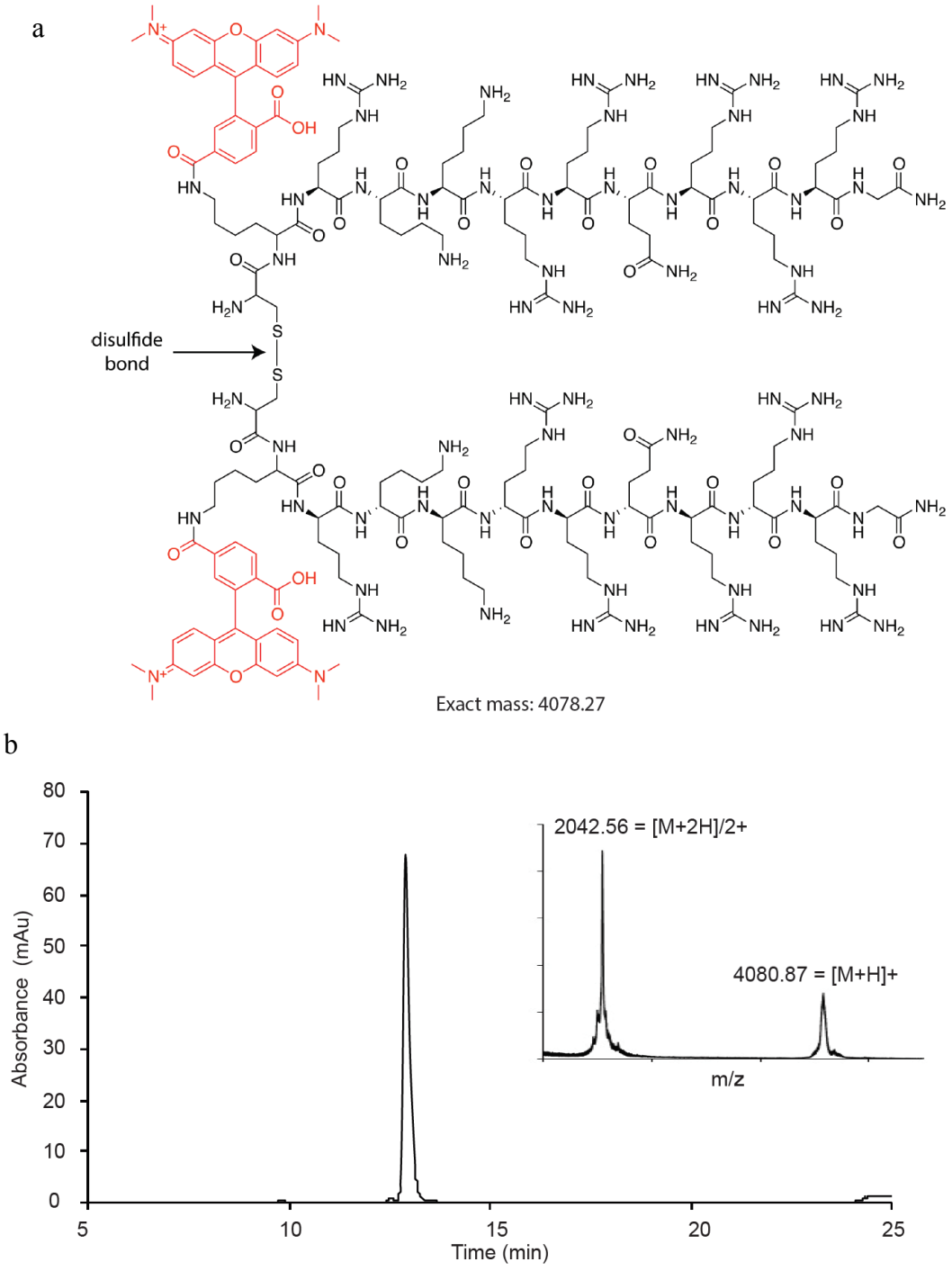

Figure 3-2 Characterization of dfTAT. a) HPLC and b) MALDI-TOF MS spectrum of dfTAT (retention time, rt=12.94 min). Mass Spectrum of dfTAT: observed [M+H]+ = 4080.87, [M+2H]/2+ = 2042.56 predicted Exact Mass (M) = 4078.27 Da.

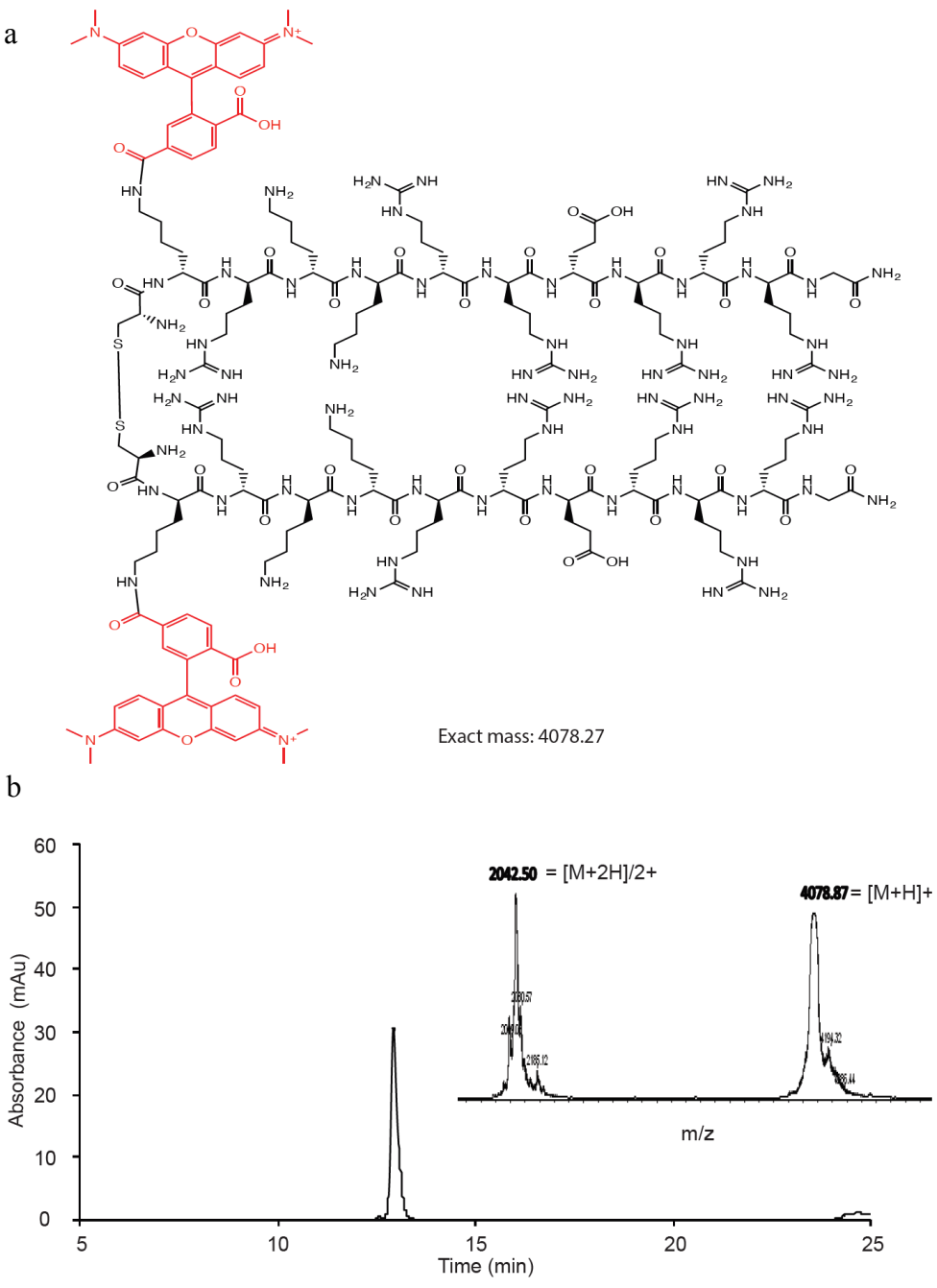

Figure 3-3 Characterization of D-dfTAT. a) HPLC and b) MALDI-TOF MS spectrum of D-dfTAT (rt=12.91 min). Mass Spectrum of D-dfTAT: observed [M+H]+= 4078.87, [M+2H]/2+= 2042.50 predicted M = 4078.27 Da

3.2.2 D-dfTAT is protease resistant and capable of penetrating cells

To confirm that the incorporation of D-amino acids confers protease resistance to D-dfTAT, the peptide was exposed to trypsin *in vitro*. Consistent with the high Arg and Lys content of the TAT sequence, the parent compound dfTAT was degraded by trypsin within minutes as evidenced by HPLC analysis (**Figure 3-4**). In contrast, D-dfTAT remained intact for the duration of the experiment (48h).To determine whether the cell penetration activity of dfTAT is retained after a L-to D-amino acid substitution, HeLa and human dermal fibroblast (HDF) cells were incubated with 1 or 5 μM dfTAT or D-dfTAT for 1h and examined by fluorescence microscopy. At 1 μM, both peptides show a punctate distribution indicative of endosomal entrapment (as previously reported for dfTAT). In contrast, at 5 μM peptide incubation, cells displayed a diffuse cytoplasmic fluorescent signal accompanied with a nucleolar staining observable immediately after incubation (**Figure 3-5**). These fluorescence staining are consistent with successful entry of each peptide into the cell's cytosolic space as cytosolic entry presumably precedes targeting to nucleoli[16, 157, 284]. In addition, the fluorescence signal of D-dfTAT was low in the nucleus (apart from the nucleoli), and a sharp contrast was observed with the cytoplasmic/nucleolar signal. The fluorescence staining of cells was monitored for 24 h to establish how the fluorescence signal of each peptide changes overtime (**Figure 3-6**). The nucleolar staining of dfTAT disappeared within 2 hours. The diffuse signal of dfTAT also progressively disappeared overtime and was replaced by a punctate distribution in less than 24h (**Figure 3-6**). In contrast, the fluorescence signal of D-dfTAT remained

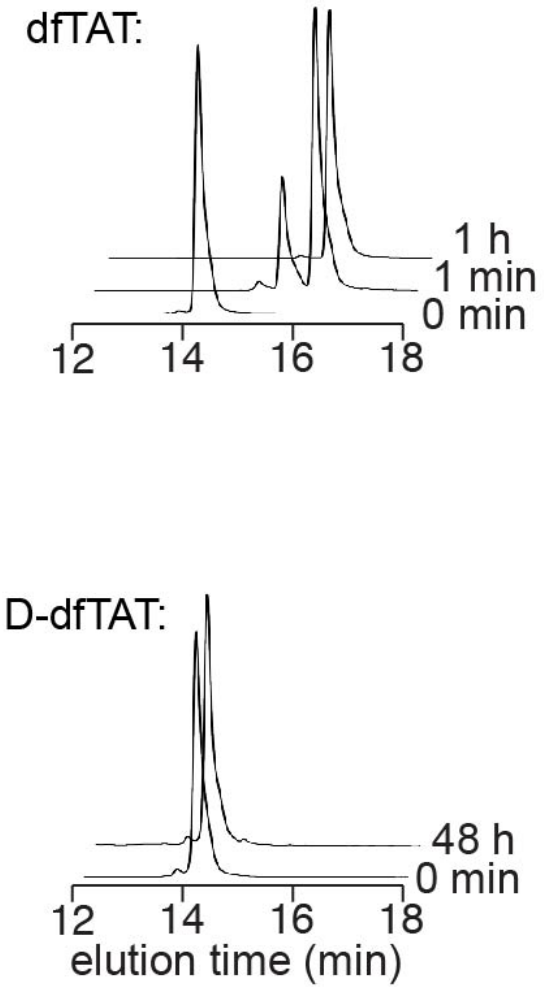

Figure 3-4 HPLC analysis of dfTAT and D-dfTAT before and after treatment with trypsin. The peptides (10 μM) were each analyzed before (0 min time point) and after incubation with trypsin (0.025%) for the indicated times. Reactions were quenched at different time intervals with 0.01% TFA in water (1 min, 1 h and 48 min). Peaks are detected by monitoring the absorbance of the TMR chromophore at 550.8 nm.

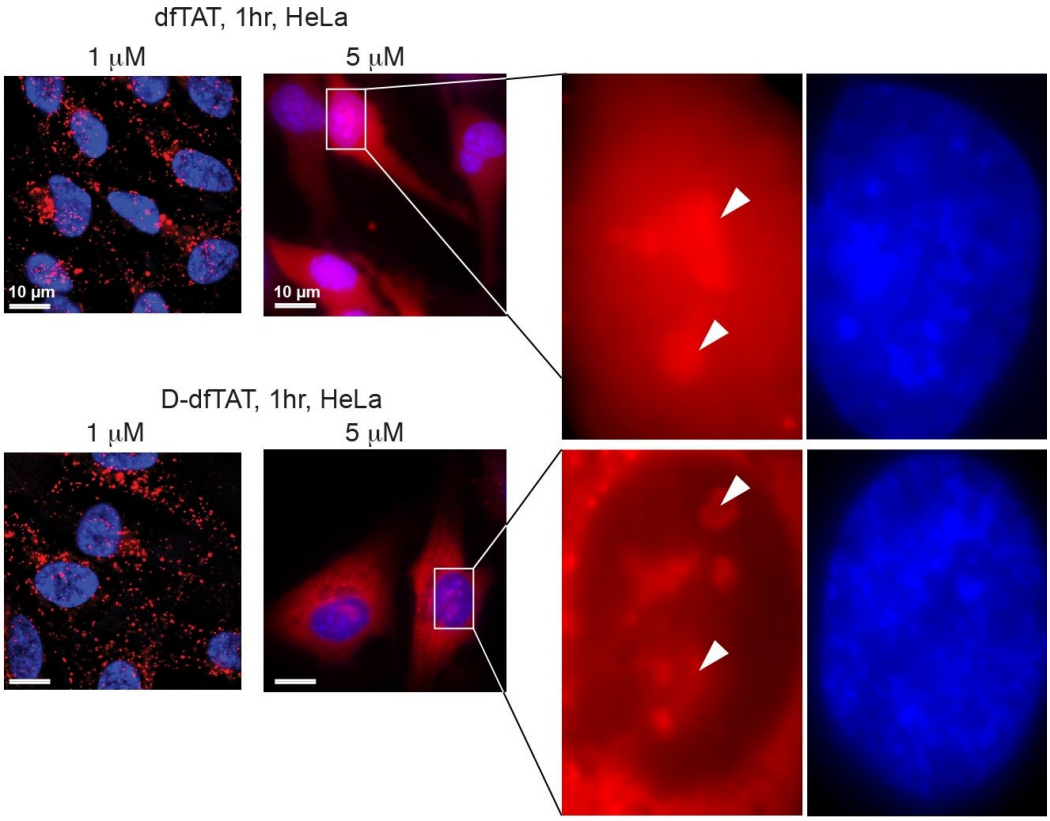

Figure 3-5 Cellular distribution of dfTAT and D-dfTAT after 1 hr incubation. HeLa cells were incubated with dfTAT or D-dfTAT at 1 or 5 μM for 1 h, washed and then stained with the cell permeable Hoechst nuclear stain (1μg/mL). Live cells were imaged with a 100X objective. Fluorescence images are overlays of the TMR emission at 560 nm (pseudocolored red) and Hoechst emission at 460 nm (pseudocolored blue). Insets to the left show a zoom in into the nucleolar staining of each peptide (white arrowheads). Scale bars, 10 μm.

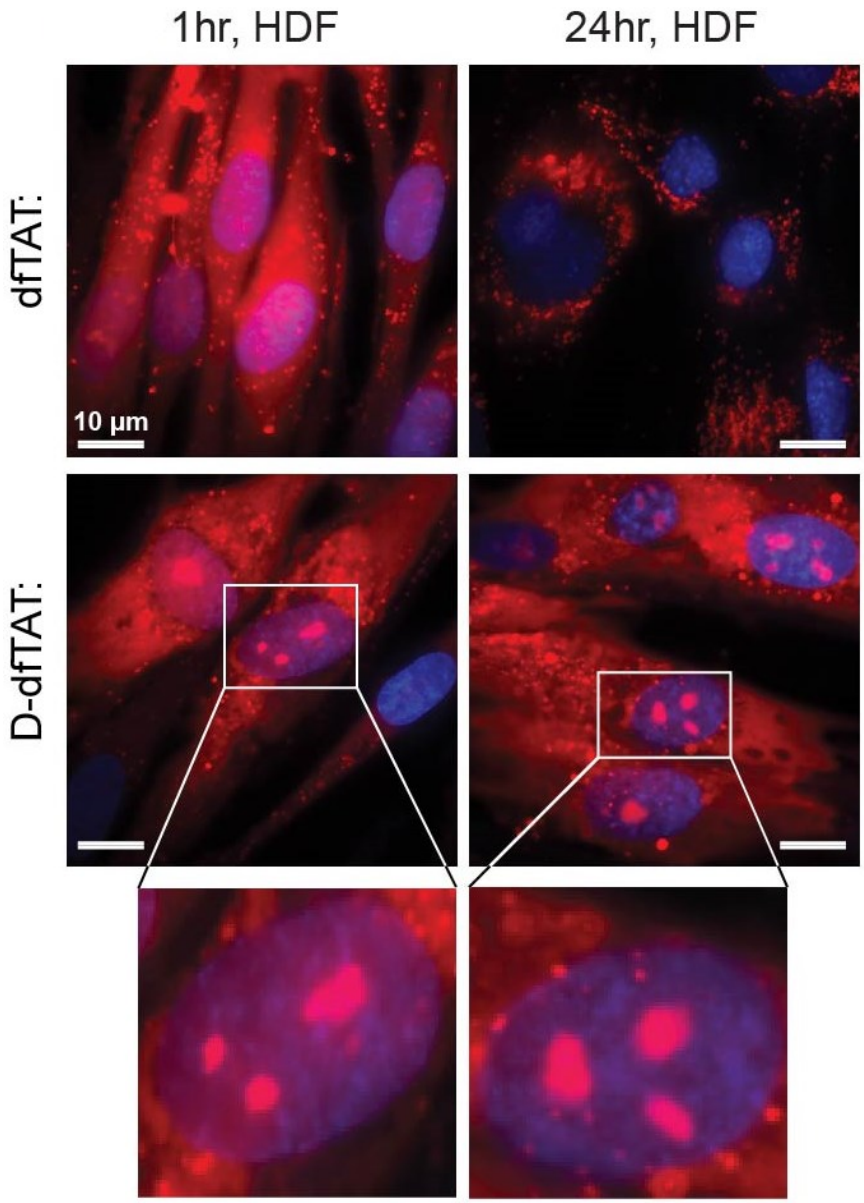

Figure 3-6 Cellular distribution of dfTAT and D-dfTAT immediately after delivery and after 24h. HDF cells were incubated with dfTAT or D-dfTAT at 5 µM for 1 h and washed. Cells were imaged with a 100X objective either immediately after treatment or after an additional 24 h incubation. Fluorescence images are overlays of the TMR emission at 560 nm (pseudocolored red) and Hoechst emission at 460 nm (DNA stain added during imaging, pseudocolored blue). Scale bars, 10 µm.

unchanged and a strong nucleolar staining was retained throughout the duration of the experiment (**Figure 3-6**).

To assess the stability of each peptide *in cellulo*, an analysis of cellular extracts was performed using gel electrophoresis. A high percentage acrylamide gel was used to separate the full-length peptides from smaller degradation fragments (the peptides are reduced with DTT to simplify the analysis; consequently the monomeric peptides fTAT and D-fTAT are detected in this assay). The fluorescence signal of TMR, a moiety presumably not readily degradable by cells, was used to detect all the species generated upon cellular exposure. Cells were incubated with dfTAT or D-dfTAT (5 μM) for 1 h, washed, and incubated with fresh media (media not containing peptide) for up to 24h. Incubation medium and cell lysates were extracted at various time points. The samples recovered from the medium immediately after incubation of cells with dfTAT and D-dfTAT display a single species comparable in size to that of the pure control peptide fTAT (reduced dfTAT) (**Figure 3-7**). The cell lysates obtained from cells incubated with D-dfTAT show a similar band, independent of incubation time. In contrast, the lysate of cells incubated with dfTAT for 1 h show a band corresponding to fTAT and a smear corresponding to smaller degradation species. Analysis of the band intensities by densitometry shows that approximately 25% of the peptide is intact while 75% is degraded. This ratio remains relatively unchanged after an additional 1 and 3 hours of incubation in fresh media. However, the band corresponding to fTAT is not present anymore at the 24 h time point. Overall, these data indicate that dfTAT is rapidly degraded during incubation with cells and during the delivery process. The degradation of dfTAT

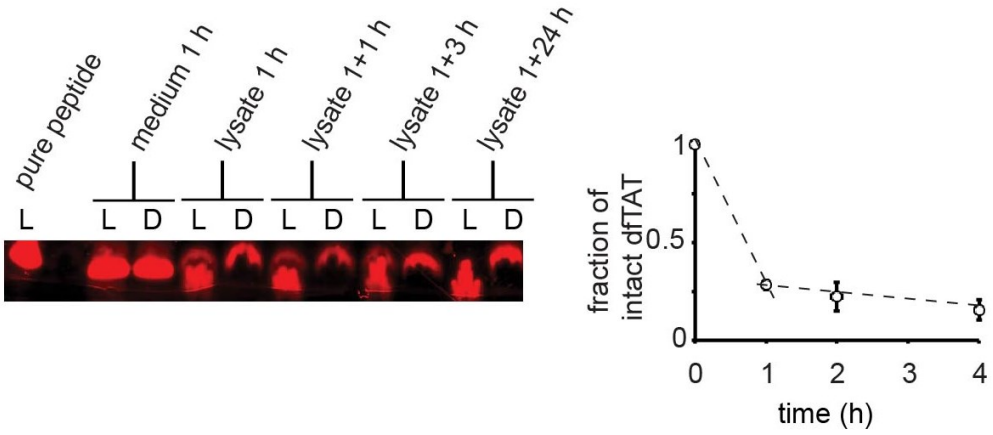

Figure 3-7 Analysis of peptide degradation by Tris-Tricine gel electrophoresis of cell lysates. HeLa cells were incubated with 5 μM dfTAT or D-dfTAT for 1 h and lysed either immediately (1 h), or at 1 h, 3 h or 24 h after peptide incubation. Cells lysates were analyzed by electrophoresis along with an aliquot of the peptide solution incubated with cells (medium 1 h) and with a sample of pure peptide. The gel was imaged on a fluorescence scanner. The fluorescent bands were quantified by densitometry to generate the graph presented. The data reported represent the average and corresponding standard deviations of biological triplicates.

continues after cellular penetration, however on a slower time scale. In contrast, D-dfTAT resists degradation throughout the duration of the experiment.

3.2.3 Both dfTAT and D-dfTAT deliver macromolecules inside cells and access the cytosol of cells by using a similar endocytic route

The utility of dfTAT is based on the fact that this reagent renders endosomes leaky and that, consequently, it can mediate the efficient cytosolic delivery of macromolecules into live cells by a simple co-incubation protocol[157]. To determine whether D-dfTAT displays a similar activity, a Cre recombinase delivery assay was performed. In this assay, successful nuclear delivery of Cre recombinase (38 kDa) results in the expression of an EGFP reporter. I used TAT-Cre, a Cre recombinase fused to the protein transduction domain (PTD) TAT. TAT-Cre has previously been shown to enter cells and I therefore used this reagent to assess how dfTAT-mediated delivery compares to the commonly used PTD approach [285]. As shown in **Figure 3-8**, incubation of cells with TAT-Cre led to expression of EGFP in approximately 10 % of the cell population. In contrast, addition of 5 μM of dfTAT or D-dfTAT peptide during incubation led to more than 70% of cells positive for EGFP expression. Similar results were obtained for co-incubation of cells with dfTAT and D-dfTAT with the DEAC-k5 peptide (Figure A-1). These data suggest that both dfTAT and D-dfTAT are capable of delivering a macromolecule inside the cytosol and nucleus of live cells at a level superior to that observed with a PTD fusion alone.

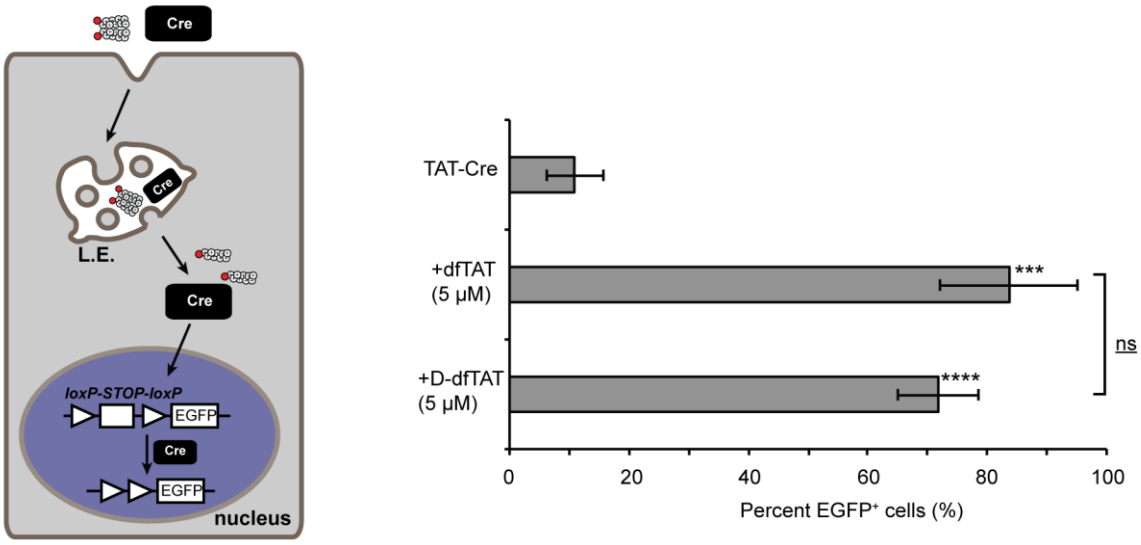

Figure 3-8 dfTAT and D-dfTAT deliver Cre recombinase into live cells. HeLa cells were transfected with a plasmid containing EGFP upstream of a loxP-STOP-loxP sequence. The cells were then co-incubated with dfTAT or D-dfTAT (5 μM) and 4 μM Cre recombinase. Cells positive for EGFP expression were counted 24 h after the protein delivery treatment.*** represents P≤0.001 and **** represents P≤0.0001 compared to control (TAT-Cre). Bracket indicates comparison of P-values obtained using t-test analysis of dfTAT and D-dfTAT treatments (ns = P>0.05)

dfTAT penetrates the cytosol of cells by escaping from late endosomes via interactions with the lipid BMP [283] .To examine whether D-dfTAT follows the same route for cellular entry, D-dfTAT was incubated with cells transfected with a dominant-negative Rab7 (DN-Rab7), a construct known to block endocytic trafficking between early and late endosomes [286, 287]. The effect of Rab7 and DN-Rab7 on peptide endocytic uptake was established by measuring the overall fluorescence of cell lysates. The cytosolic penetration activity of D-dfTAT was established by counting the number of cells displaying a distinct nucleolar staining by the peptide. Notably, this assay does not directly measure how much peptide remains trapped inside endosomes versus how much escapes endosomes. Instead, it is a binary assay that establishes whether or not endosomal leakage is achieved above a detection threshold determined by the fluorescence microscopy set-up. As previously observed with dfTAT the overall endocytic uptake of D-dfTAT was not significantly altered by overexpression of the Rab7 constructs, indicating that DN-Rab7 does not prevent D-dfTAT from accumulating inside endosomes. However, DN-Rab7 inhibited cytosolic penetration of D-dfTAT while wild-type did not (**Figure 3-9**). These results indicate that DN-Rab7 blocks the endosomal escape of D-dfTAT and that, consequently, D-dfTAT escapes from endocytic organelles that are downstream of early endosomes in the endocytic pathway. In addition, to further test the involvement of endocytic trafficking in cell penetration, cells were pre-incubated with anti-BMP (50 μg/ml), an antibody previously shown to block membrane fusion within late endosomes [128, 288, 289]. As in the case of DN-Rab-7, the cell penetration of dfTAT and D-dfTAT was inhibited by this treatment to a similar extent (**Figure 3-10**). Overall, these data support the model that both

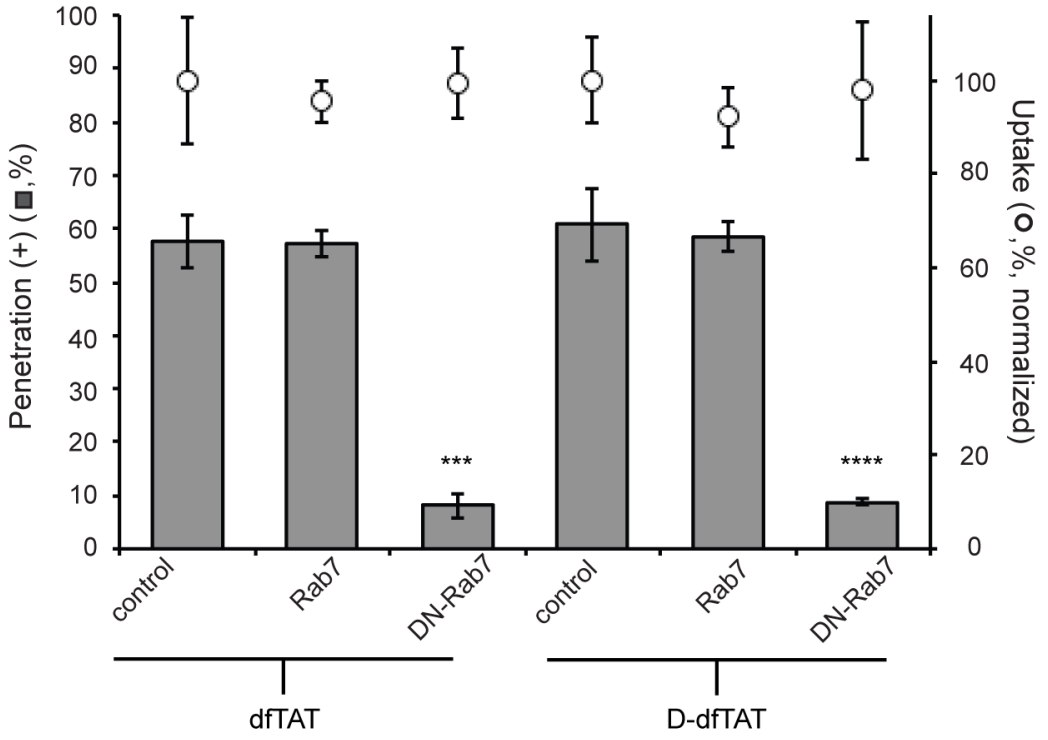

Figure 3-9 Cytosolic penetration of D-dfTAT is blocked by expression of dominant-negative Rab7. HeLa cells were transfected with Rab7 or dominant negative Rab7 (DN-Rab7). dfTAT or D-dfTAT (3 μM) was then incubated with cells for 1 h and cell penetration was quantified. The total fluorescence of cell lysates was also measured to assess the impact of each treatment on peptide endocytic uptake. The uptake for cells transfected with Rab7 or DN-Rab7 was normalized to the uptake of cells treated with dfTAT or D-dfTAT respectively. *** represents $P \leq 0.001$ and **** represents $P \leq 0.0001$ compared to control.

Figure 3-10 D-dfTAT major route of cellular entry is via endocytosis followed by endosomal escape in a manner similar to dfTAT. a) Cytosolic penetration of D-dfTAT is blocked by the anti-BMP antibody. HeLa cells were pre-incubated with anti-BMP mAb or the control anti-IgG mAb for 30 min. dfTAT or D-dfTAT (3 μM) was then incubated with cells for 1 h and cell penetration was quantified. The total fluorescence of cell lysates was also measured to assess the impact of each treatment on peptide endocytic uptake. b) Given the possibility of a secondary mode of penetration in a minority of cells (<5%, as described in Figure 2), the uptake data presented in Figure 4 may include endocytosis-dependent and endocytosis-independent uptake. In order to address how much signal may be contributed by endocytosis-independent cytosolic entry, the fluorescence intensity of cells positive for peptide penetration in the presence of DN-Rab7 was estimated (these are the cells in which uptake cannot be fully accounted for by endocytosis). HeLa cells were transfected with Rab7 or dominant negative Rab7 (DN-Rab7). Cells were then incubated with D-dfTAT at 3 μM. Images are pseudocolored based on the fluorescence intensity of D-dfTAT in the cells (Scale bars, 100 μm). These representative data confirm that the number of cells positive for peptide penetration decreases when DN-Rab7 is expressed (as shown in Figure 2b). However, the overall fluorescence intensity of the few cells positive for peptide penetration in the presence of DN-Rab7 is equivalent (as shown by the pseudocolored scale) to the fluorescence intensity of cells positive for peptide penetration in the presence of wild type Rab7 (as exemplified with cells highlighted with a white box; this observation was made in 10 images taken of the DN-Rab7 condition, the fluorescence intensity of 30 cells surveyed). Therefore, I estimate that endocytosis-independent uptake, if present in 5% of cells, may contribute 5% or less of the total signal reported.

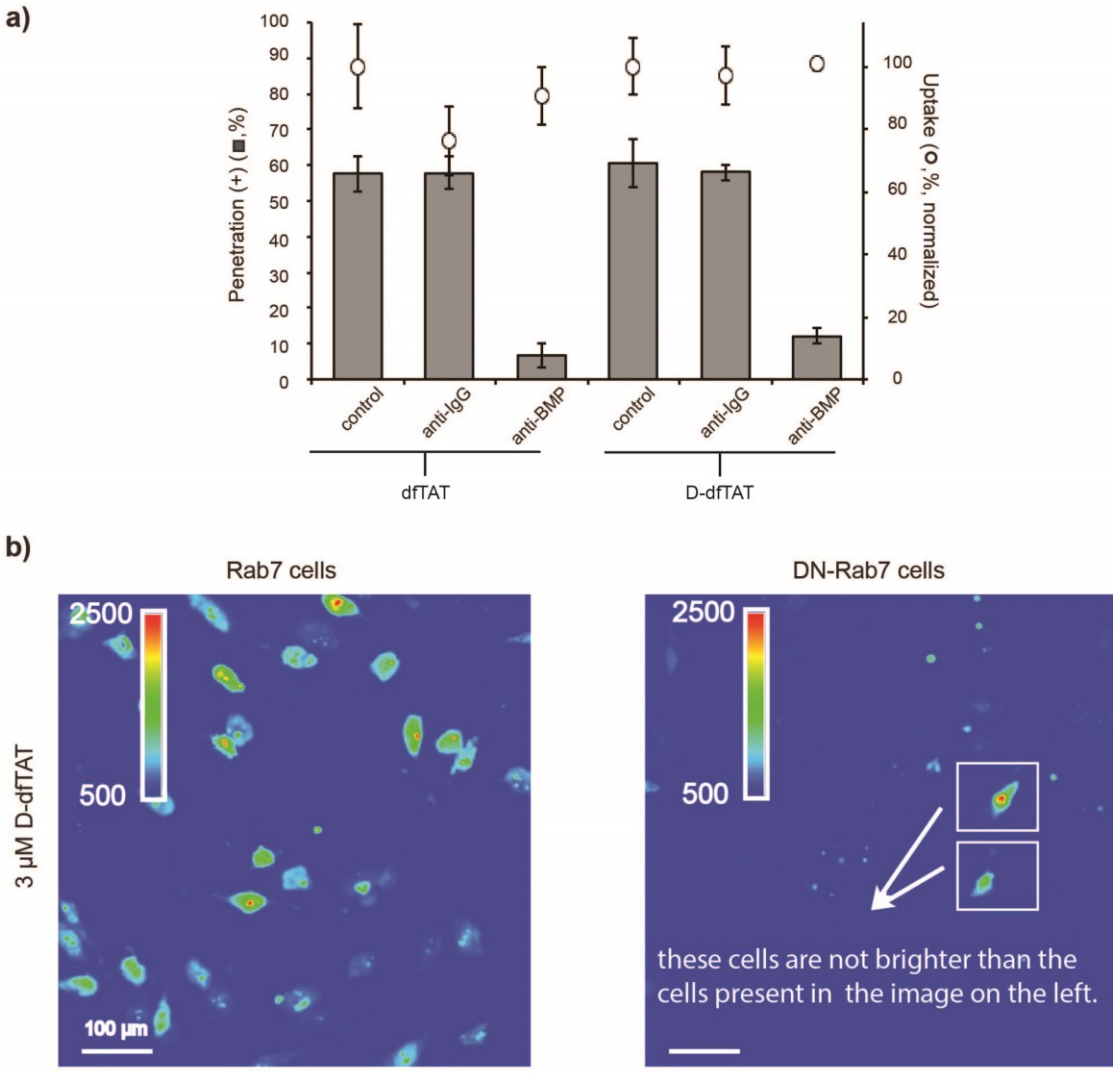

Figure 3-10 Continued.

dfTAT and D-dfTAT reach the cytosol by an endocytic route in a majority of cells. It is important to note that penetration persisted in approximately 5% of cells in the presence of DN-Rab7 or anti-BMP. On one hand, it is possible that the inhibitors did not work effectively in these cells (i.e. maybe because of low expression, degradation, etc…). On the other hand, these results may suggest that a secondary route of entry (e.g direct plasma membrane translocation) is also plausible, albeit much less predominant than endosomal escape.

In principle, the previous results indicate that the peptide escapes from either late endosomes or lysosomes is possible [290]. In the case of dfTAT, I have previously ruled out the involvement of lysosomes by establishing that dfTAT does not release material loaded inside lysosomes [283] . Yet, D-dfTAT might differ significantly from dfTAT in this instance. In particular, one can envision how dfTAT might be rendered inactive inside lysosomes because it is extensively degraded. In contrast, by being protease-resistant, D-dfTAT could remain membrane-disrupting in this milieu. To test this idea, the endosomes of HeLa cells were preloaded with DEAC-k5, a fluorescent and protease-resistant polylysine peptide (**Figure 3-11**). As shown in exp 1 of **Figure 3-12**, endosomes loaded with DEAC-k5 are observed by fluorescence microscopy as puncta inside cells (endosomal entrapment is confirmed by co-localization with lysotracker). Cells were then washed and treated with D-dfTAT immediately (**Figure 3-12**, exp 2) or 2 hours (**Figure 3-12**, exp 3) after DEAC-k5 incubation. The additional incubation time in the latter experiment was used to allow lysosomal accumulation of DEAC-k5. Microscopy images show that D-dfTAT is able to redistribute the fluorescence of DEAC-k5 inside cells after

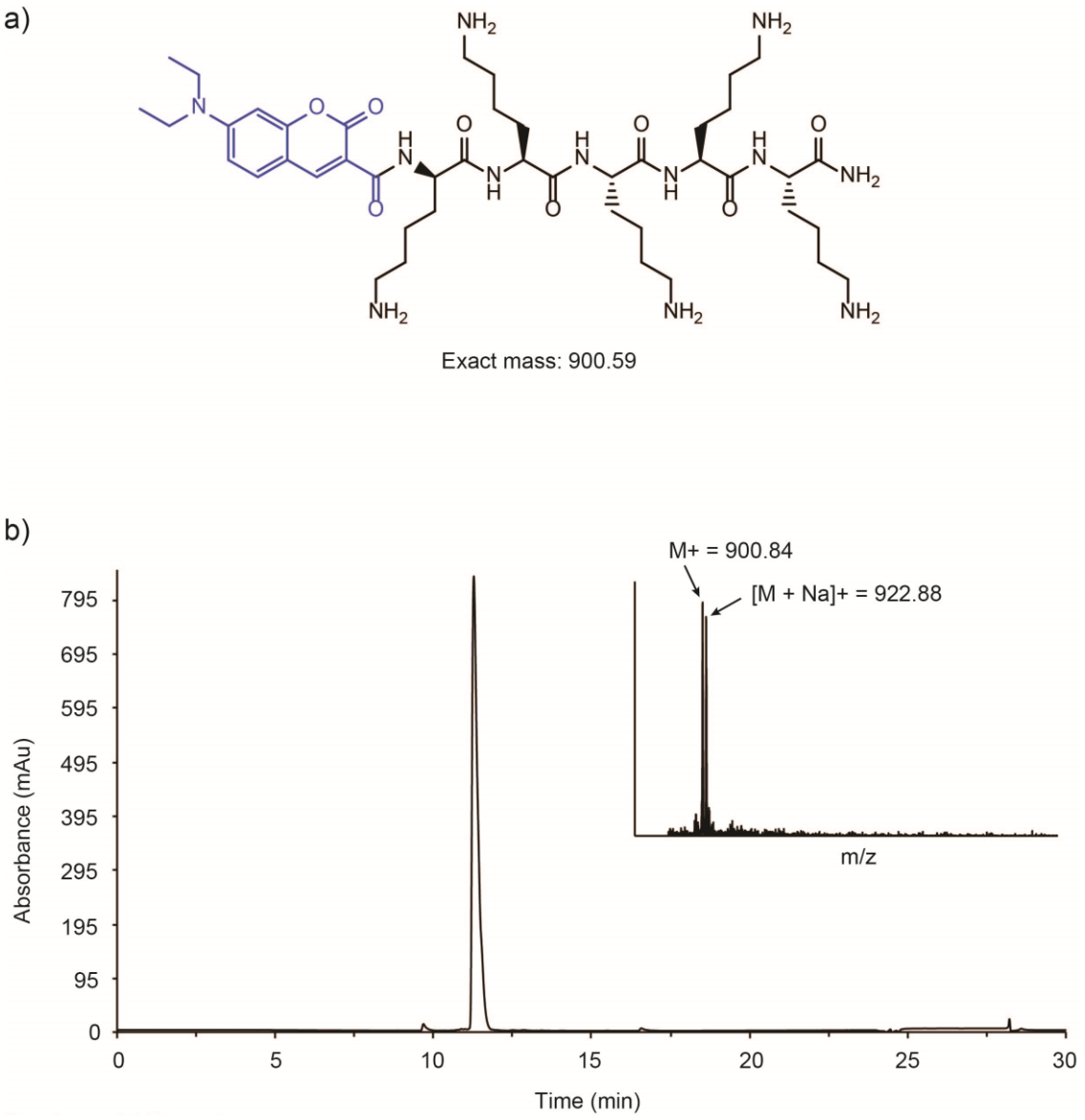

Figure 3-11 Characterization of DEAC-k5. a) Structure and expected mass of DEAC-k5. b) The HPLC spectrum of DEAC-k5 (rt= 11.8 min) and the MALDI-TOF mass spectrum are shown. Observed mass are $[M]^{+}$= 900.84 and $[M+Na]^{+}$ = 922.88, predicted mass of 900.59 Da.

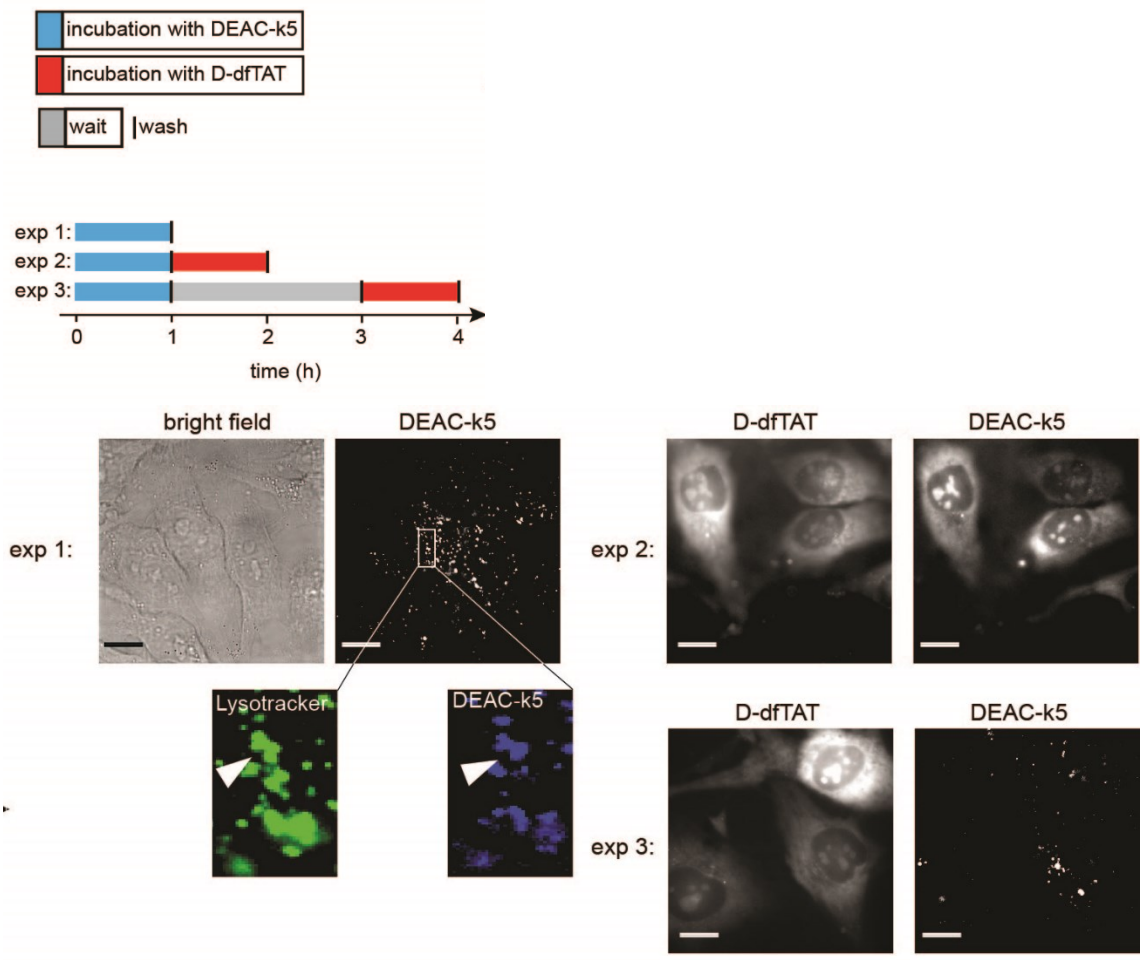

Figure 3-12 D-dfTAT causes the release of a peptide preloaded into endosomes but not that of peptide preloaded into lysosomes. In experiment 1, cells were incubated with DEAC-k5 (20 µM) for 1h and washed. Cells were then incubated with lysotracker during imaging to establish the accumulation of DEAC-k5 inside endosomes. In experiment 2, cells were incubated with DEAC-k5 (20 µM) for 1 h, washed and then incubated with D-dfTAT (5 µM) for 1 h. Experiment 3 was performed as experiment 2 with the exception of a 2 h waiting time between incubation with DEAC-k5 and D-dfTAT. Fluorescence images represented are either monochromatic or pseudocolored green for lysotracker and blue for DEAC-k5. Scale bars, 10 µm.

immediate incubation (like D-dfTAT, DEAC-k5 stains nucleoli because it is positively charged and presumably binds nucleolar nucleic acids). This is presumably because D-dfTAT is capable of causing the leakage of late endosomes that still contain DEAC-k5.In contrast, D-dfTAT was not able to cause cytosolic release of DEAC-k5 in exp 3. In particular, D-dfTAT still displayed a nuclear/cytosolic distribution but the DEAC-k5 fluorescent distribution remained punctate (exp3 in **Figure 3-12**). This in turn suggests that D-dfTAT, like dfTAT, does not cause the release into the cytosol of material that has accumulated inside lysosomes. Overall, these data also indicate that dfTAT and D-dfTAT use an identical route of cellular entry involving late endosomes. To further confirm that the membrane of these organelles is the site of peptide penetration, the activity of dfTAT and D-dfTAT towards liposomes mimicking late endosomes (i.e. BMP, PC, PE, cholesterol) was assessed *in vitro*. In particular, both peptides were capable of inducing liposome leakage with equivalent efficiencies (**Figure 3-13**). Furthermore, the affinity of the peptides to BMP containing liposomes were similar (Figure A-2). In addition, dfTAT and D-dfTAT are partitioned into hexane by the presence of BMP to a similar extent (Figure A-2). This establishes that the chirality of the peptide is not an important determinant in its interaction with lipids found in late endosomes.

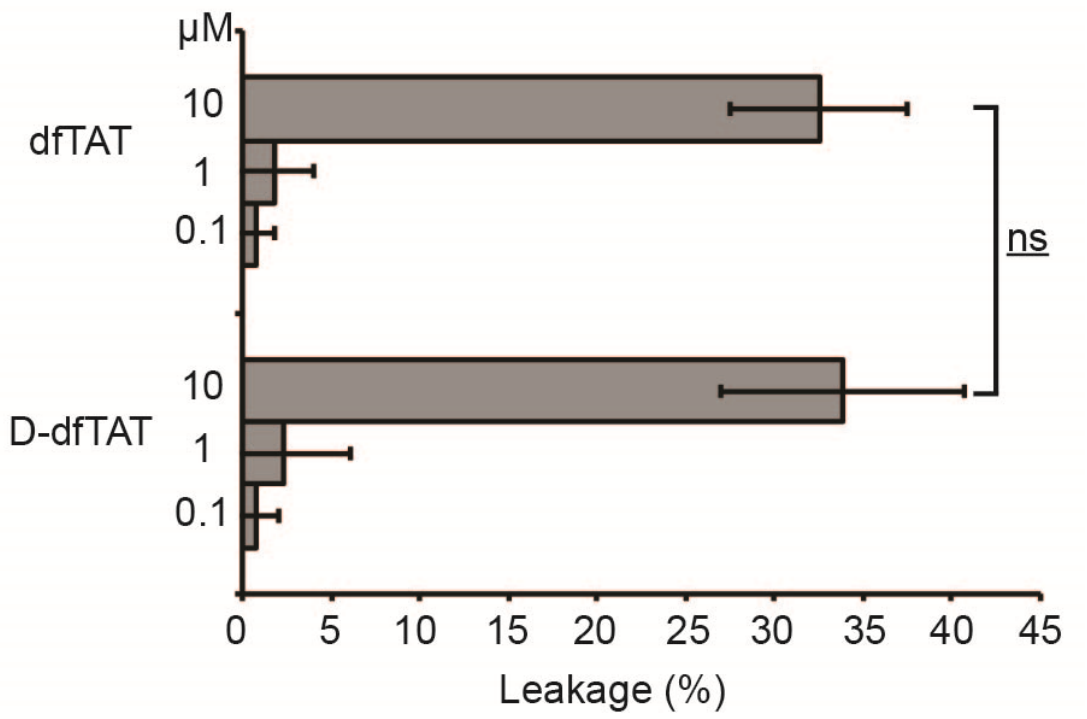

Figure 3-13 D-dfTAT causes leakage of liposomes with a lipid composition mimicking that of late endosomes. Liposomes loaded with calcein (500 μM) were incubated with dfTAT or D-dfTAT (0.1, 1 or 10 μM). The fluorescence signal of free calcein was quantified after peptide treatment. ns represents $P > 0.05$.

3.2.4 L- to D- substitution negatively impacts endocytosis but favors endosomal escape

The previous experiments indicate that dfTAT and D-dfTAT share similar cell penetration properties, at least qualitatively. In order to establish whether the two peptides differ in their respective efficiencies quantitatively, the penetration activity of each compound was determined as a function of peptide concentration. First, cells were incubated with increasing concentrations of each peptide. Cells were then examined by fluorescence microscopy. Cells displaying a distinctive nucleolar staining are counted as positive for penetration (the cells counted are also negative for SYTOX Blue staining, indicating that their plasma membrane is not compromised and that these cells are not dead). At any given concentration of peptide in the incubation media, the number of cells positive for penetration was similar between the two peptides (with the exception of 10 μM, where D-dfTAT is more active than dfTAT) (**Figure 3-14**). Cells negative for cell penetration typically display a punctate distribution consistent with endosomal entrapment of the peptide and weak endosomal escape [291]. This assay is however only binary in nature and only reveals whether penetration is achieved above a detection threshold dictated by the fluorescence microscope. To quantify the activity of each peptide in greater detail, overall peptide uptake was also measured (**Figure 3-15**).

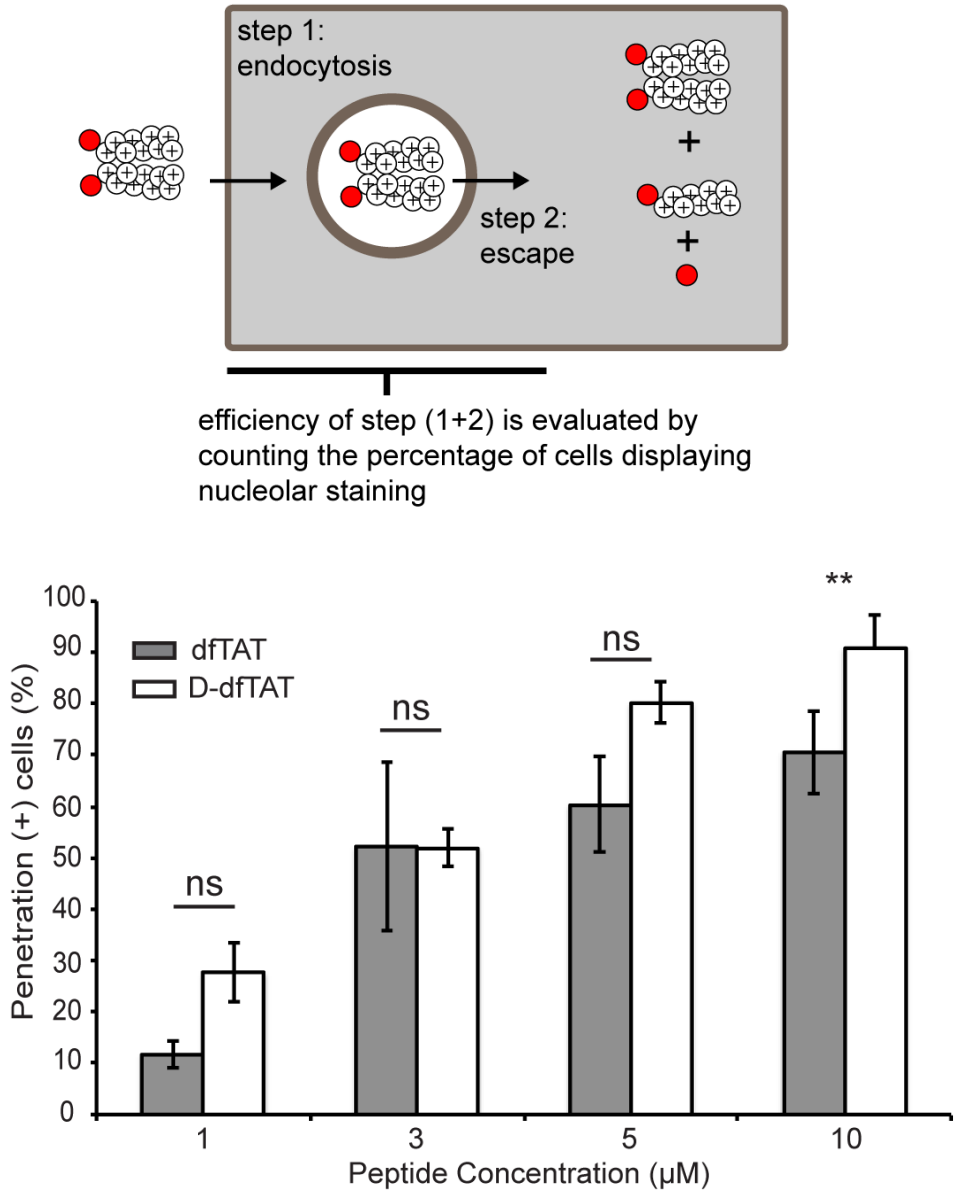

Figure 3-14 Evaluation of the cytosolic delivery efficiency of dfTAT and D-dfTAT as a function of peptide concentration in incubation media. HeLa cells were incubated with peptides (1-10 μM) for 1 h. The percentage of cells detected as positive for penetration was established by microscopy (ns represents P >0.05, ** = P≤0.01).

Figure 3-15 Quantification of whole cell uptake by dfTAT and D-dfTAT as a function of the peptide concentration in incubation media. HeLa cells were incubated with peptides (1-10 μM). The overall amount of peptide internalized by cells (endosomal + cytosolic) was assessed by measuring the bulk fluorescence of cell lysates. The illustration summarizes the protocol used for this assay.

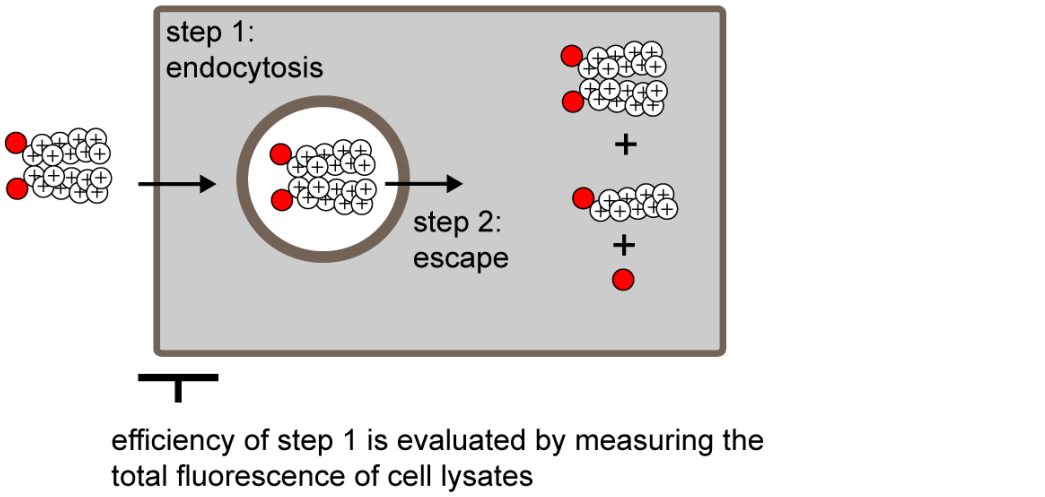

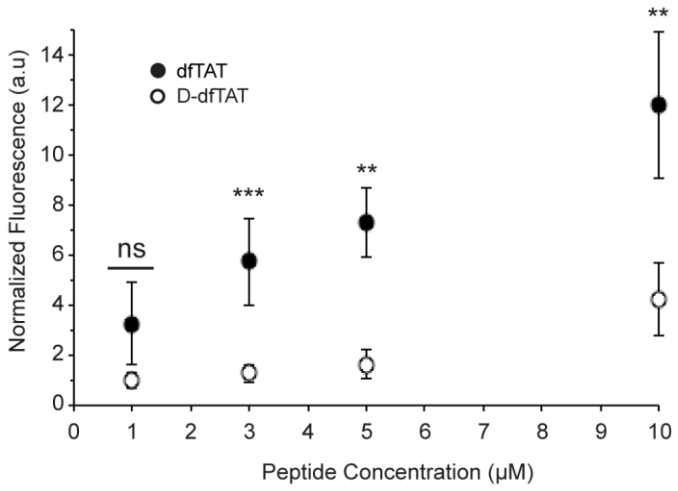

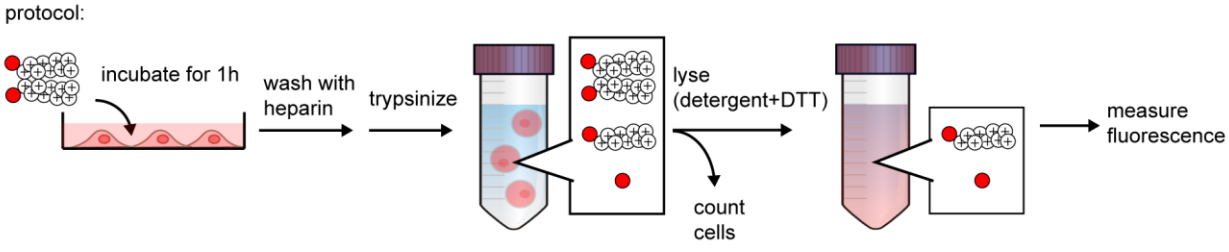

Figure 3-15 Continued.

This was performed by measuring the bulk fluorescence emission of cell lysates. This assay was chosen because the fluorescence of the dimeric CPPs is partially quenched in comparison to that of their monomeric counterparts (**Figure 3-16**). In addition, one may expect that once inside cells, the CPP might give rise to multiple species, including the intact dimer, the reduced monomer, and degradation fragments. Consequently, cell lysis enabled us to chemically reduce the pool of dimeric CPPs present in cells so as to generate unquenched species that can be better quantified (**Figure 3-16**). This analysis shows that the overall cellular fluorescence is 3 to 4 fold higher for cells treated with dfTAT than for cells treated with D-dfTAT (**Figure 3-15**; preferential uptake of the L-CPP over the D-CPP were corroborated by flow cytometry and fluorescence microscopy, although these assays suffer from the possible caveat of partial fluorescence quenching described above, **Figure 3-17**). Control experiments indicated that none of the fluorescence detected was associated with extracellular membrane binding (**Figure 3-18**). Notably, it is conceivable that there would be less D-dfTAT inside cells than dfTAT if the export of the peptides from inside to outside of cells was greater for the D-CPP than for the L-CPP. To test this possibility, cells were treated with both CPPs for 1 h and washed using protocols that remove extracellular peptides (**Figure 3-18**). The media of cells incubated for up to 6 hours were then collected and the presence of the TMR signal was subsequently detected by fluorescence spectroscopy (**Figure 3-19**). Based on this assay, significantly more fluorescent species are released into the medium after delivery with dfTAT than after delivery with D-dfTAT (where no to little fluorescence is detected). Therefore, preferential export of D-dfTAT does not account for the differences observed in

Figure 3-16 The fluorescence emission of dfTAT and D-dfTAT increases upon reduction of the disulfide bond. a) HPLC analysis of purified dfTAT and D-dfTAT in absence and presence of the reducing agent tris(2-carboxyethyl)phosphine (TCEP). Pure dfTAT and D-dfTAT was mixed with a solution of TCEP (50 mM) in water and allowed to react for 15 min. The HPLC chromatogram show a peak with rt = 12.9 min for both dfTAT and D-dfTAT and rt= 9.7 min for the reduced peptides. b) Bar graph of the fluorescence emission of dfTAT and D-dfTAT (1.25 μM) in the absence and presence of the reducing agent TCEP (50 mM). The samples were excited at 556 nm and the emission was scanned between 560-760nm. c) Quantification of the uptake fluorescence intensity, with or without DTT, in cells treated with dfTAT and D-dfTAT. HeLa cells were incubated with 5 μM dfTAT or D-dfTAT. Cells were then trypsinized and lysed in presence or absences of DTT (2mM). The overall amount of peptide internalized by cells (endosomal + cytosolic) was assessed by measuring the bulk fluorescence of cell lysates.

Together, these results indicate that the fluorescence of dfTAT and D-dfTAT is partially quenched when the peptides are in their dimeric form. As indicated in the main text, we therefore concluded that the reduction of cell lysates was necessary to obtain quantitative data of peptide uptake into cells. However, the contribution of the dimer fluorescence is relatively small (see -/+ DTT comparison), indicating that the peptides are presumably already reduced after entry into the cytosolic space (this is consistent with the observation that disulfide bonds are reduced in a matter of second by once inside cell [134].

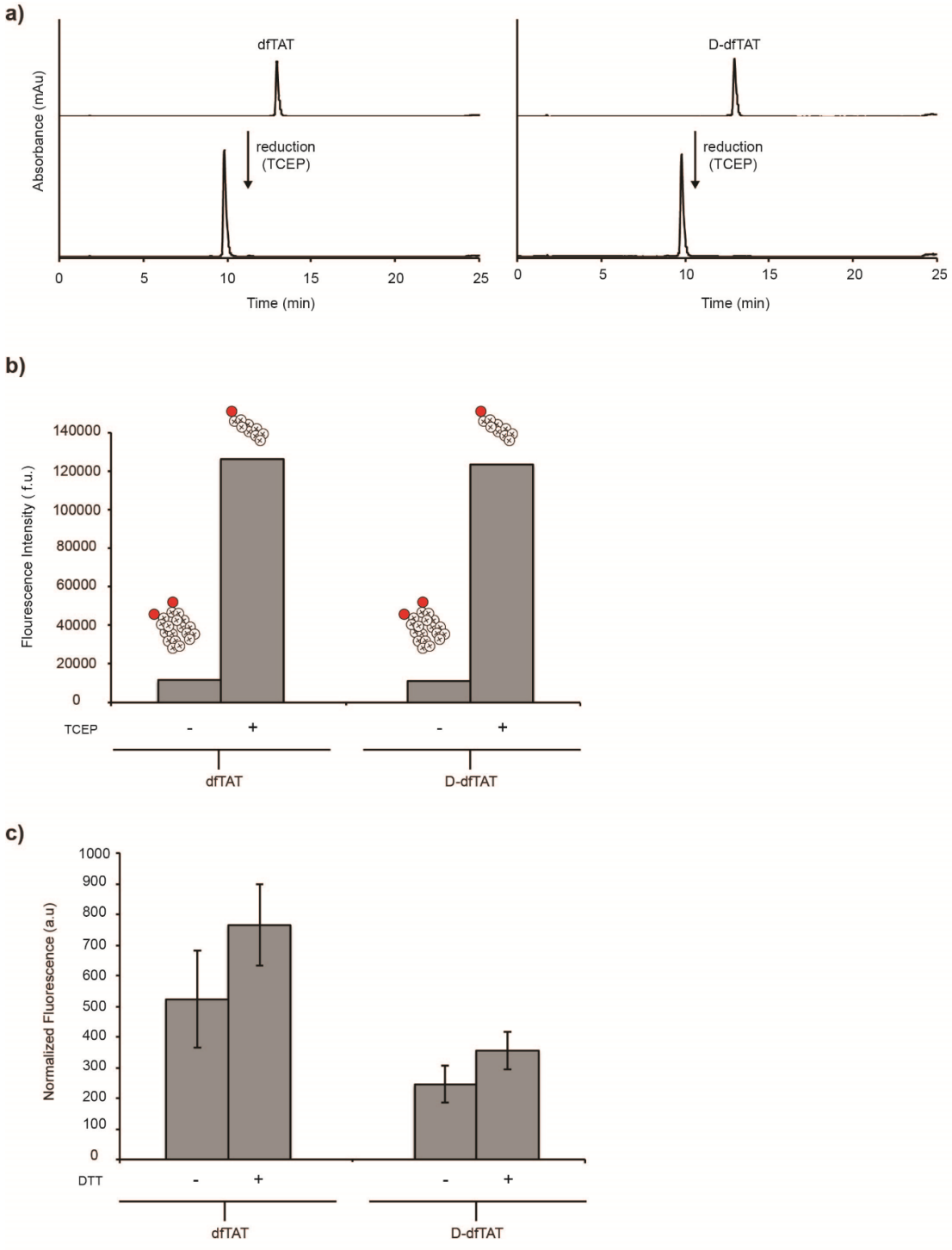

Figure 3-16 Continued.

Figure 3-17 Comparison of the cellular uptake of dfTAT and D-dfTAT. a) The overall amount of peptide internalized by cells (endosomal + cytosolic) was measured using flow cytometry. HeLa cells were incubated with dfTAT or D-dfTAT at different concentrations (1-10 μM). Cells were then analyzed and fluorescence intensity was quantified as a function of concentration. b) The overall amount of peptide internalized by cells was quantified using fluorescence microscopy. HeLa cells were incubated with dfTAT or D-dfTAT at 5 μM. Images are pseudocolored based on the fluorescence intensity of dfTAT and D-dfTAT in the cells. Scale bars, 100 μm.

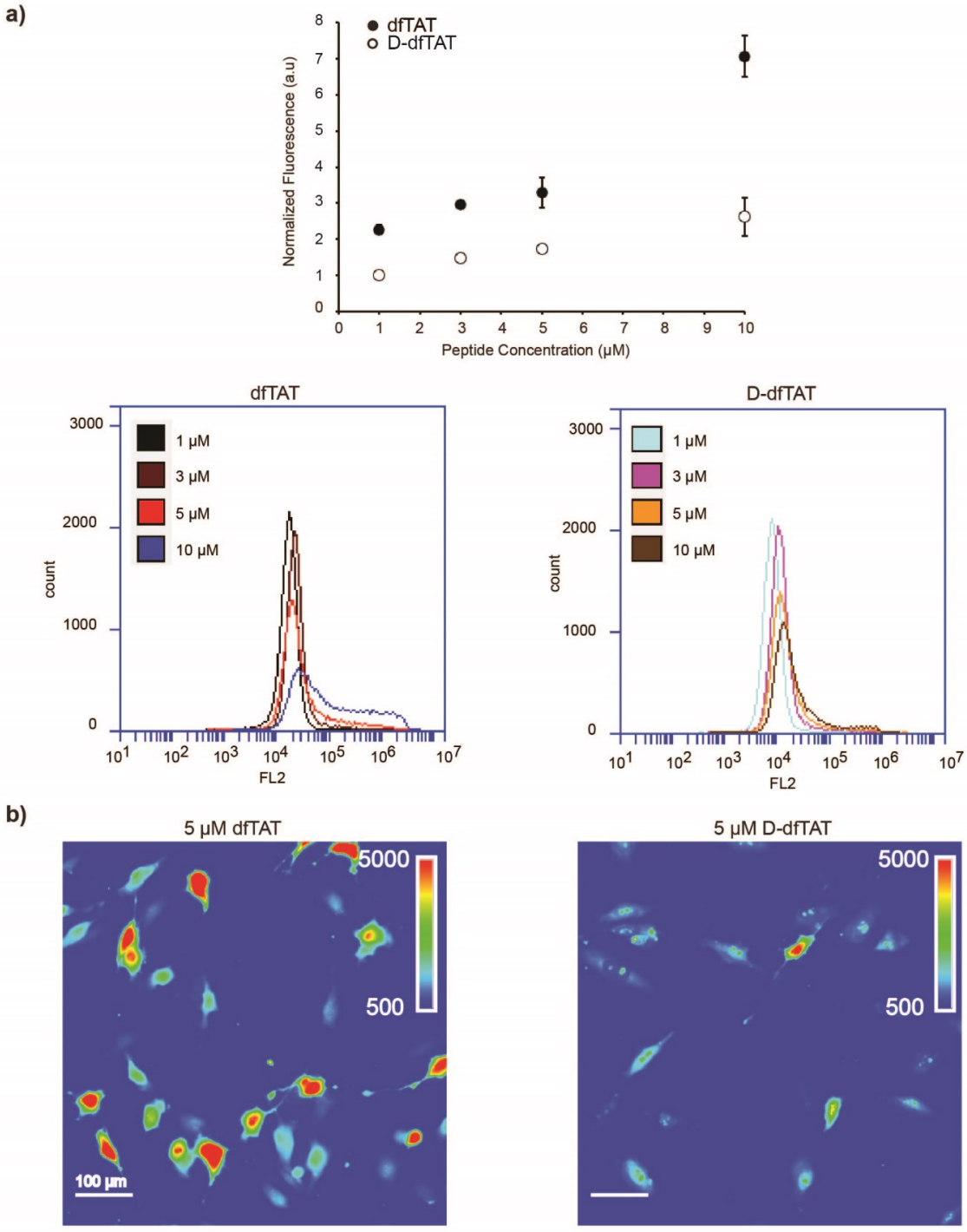

Figure 3-17 Continued.

Figure 3-18 The uptake fluorescence intensity of dfTAT and D-dfTAT is not a consequence of extracellular membrane binding. Cells were treated with dfTAT and D-dfTAT at 5 μM for 1 h. The cells were then washed using three separate protocols that insure removal of peptide bound extracellularly. For all protocols, cells were first washed three times with L-15 supplemented with heparan (1 mg/mL) and once with nrL-15. Sample 1: control cells were then trypsinized and resuspended in nrL-15 for flow cytometry. For sample 2: The cells were then washed again three times with L-15 supplemented with heparan (1 mg/mL) and once with nrL-15. For sample 3: The cells were then trypsinized and resuspended in nrL-15 and centrifuged. The supernatant was removed and the cell pellet was trypsinized (50 μL) and resuspended once again in nrL-15 for flow cytometry analysis. The bar graph shows the average mean fluorescence intensity values from the flow cytometry (each condition was performed in triplicate). An example of the flow cytometry histogram for each condition is shown below the bar graph.

Because the cell fluorescence is independent of the various treatments used, I conclude that portion of extracellular peptide that could potentially contribute to signal is negligible.

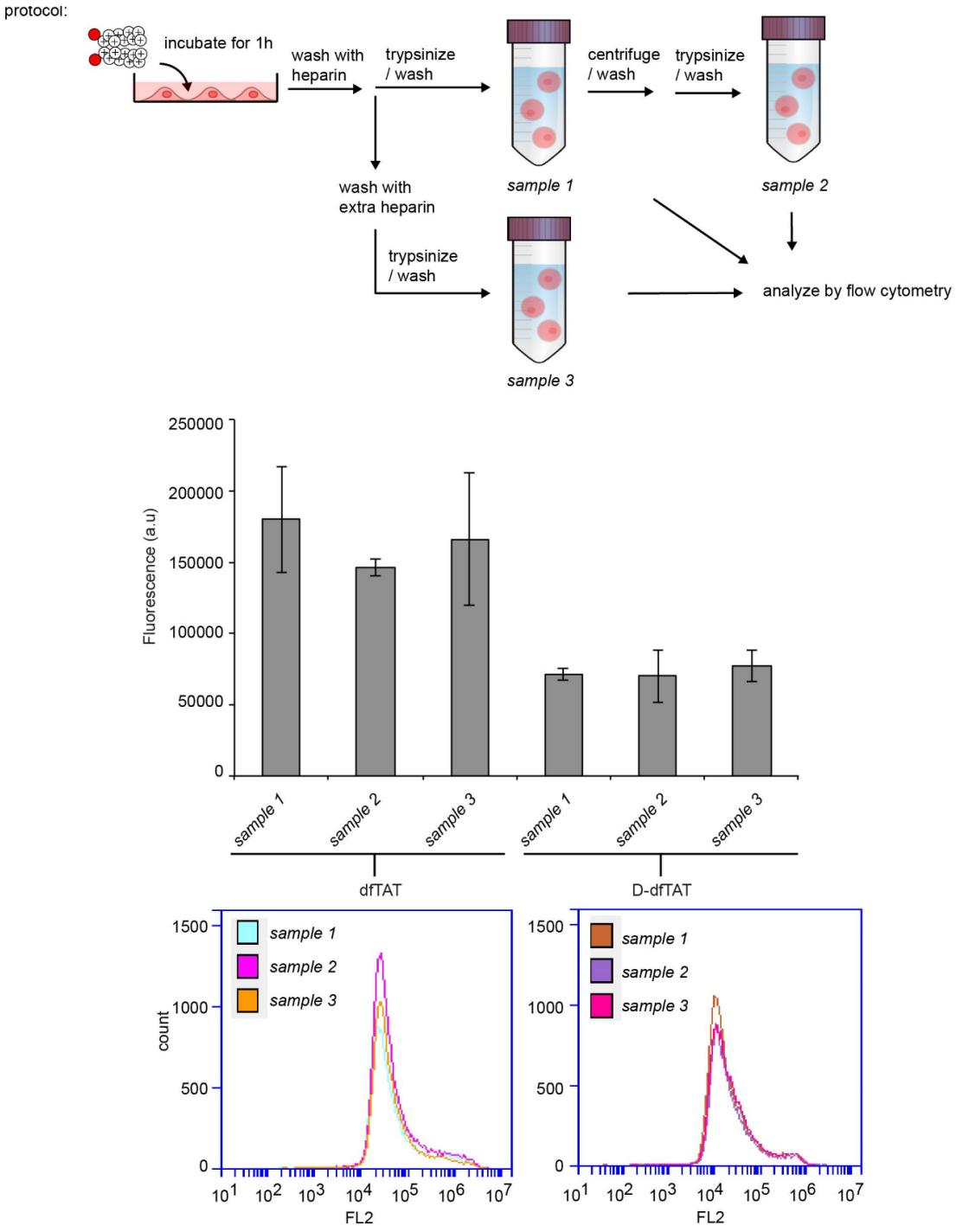

Figure 3-18 Continued.

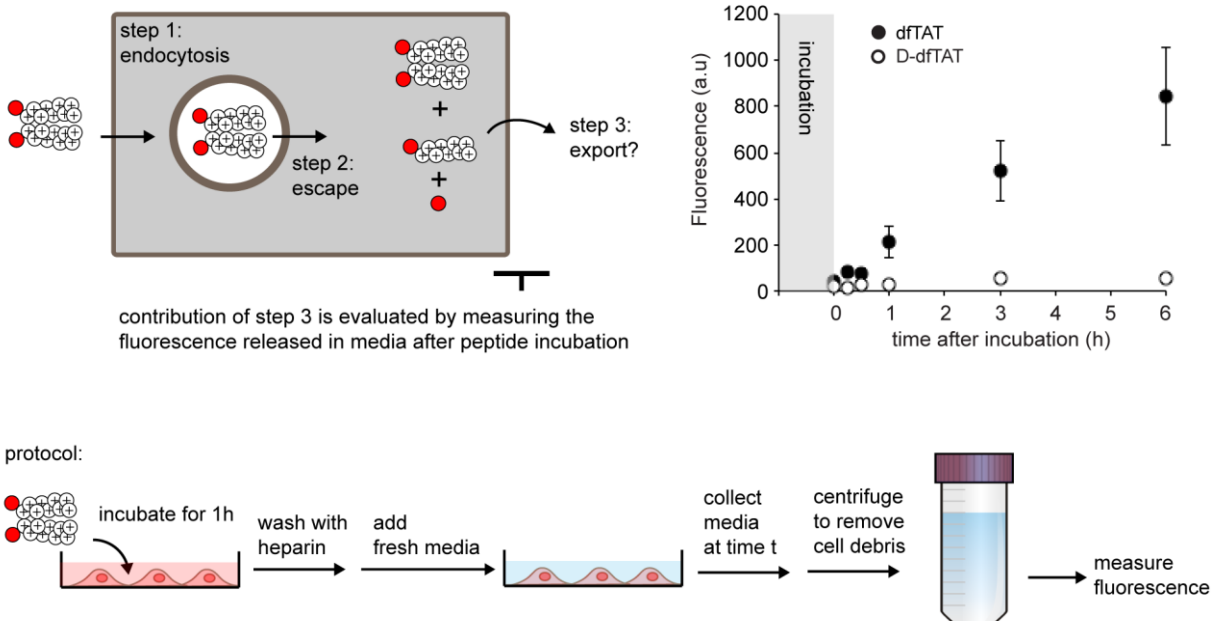

Figure 3-19 Determination of the contribution of peptide export after dfTAT or D-dfTAT treatment. HeLa cells were incubated with 5 µM dfTAT or D-dfTAT for 1h. The cells were washed and the media in all wells was replaced. The media for each time point condition was removed at the indicated times (0, 0.25, 0.5, 1, 3, and 6 hours post incubation). The fluorescence intensity of the media collected form treated cells was measured and normalized to the media obtained from untreated cells. All the data reported in this figure represent the average and corresponding standard deviations of biological triplicates.

Figure 3-15. Overall, considering that intracellular fluorescence signals detected in Figure 3-15 are proportional to initial endocytic uptake (i.e. step 1 in Figure 3-14), these results indicate that an L to D conversion reduces endocytosis of the CPP.

Given that D-dfTAT is endocytosed less efficiently than dfTAT and yet leads to equivalent numbers of cells positive for penetration, the previous data indicated that D-dfTAT might be able to escape from endosomes at lower concentrations than dfTAT. Using microscopy analysis of cells treated with lysotracker green, a fluorescent markers of late endosomes and lysosomes, I found that the number of endosomes present in cells treated with dfTAT is similar to that present in cells treated with D-dfTAT (**Figure 3-20**). I therefore reasoned that the overall uptake measured in Figure 3b is proportional to the concentration of peptide present inside endosomes prior to endosomal escape. To estimate the relative endosomal escape efficiency of each peptide, the penetration activities of D-dfTAT and dfTAT were therefore plotted as a function of overall uptake (**Figure 3-21**). These data show that the ability of D-dfTAT to escape from the endocytic pathway increases dramatically within a narrow range of intracellular concentrations. In contrast, dfTAT achieves similar cell penetration activities but requires a larger intracellular concentration to do so. Notably, the plot of dfTAT appears to plateau at high levels of peptide uptake, indicating that significant increases in intracellular concentration only lead to minor improvements in penetration. Moreover, under low intracellular uptake conditions, the percentage of penetration positive cells for dfTAT is approximately 7 fold less than in the case of D-dfTAT (e.g. uptake of ~3). Overall, these data indicate that D-dfTAT is capable of escaping endosomes more effectively than dfTAT (for a discussion

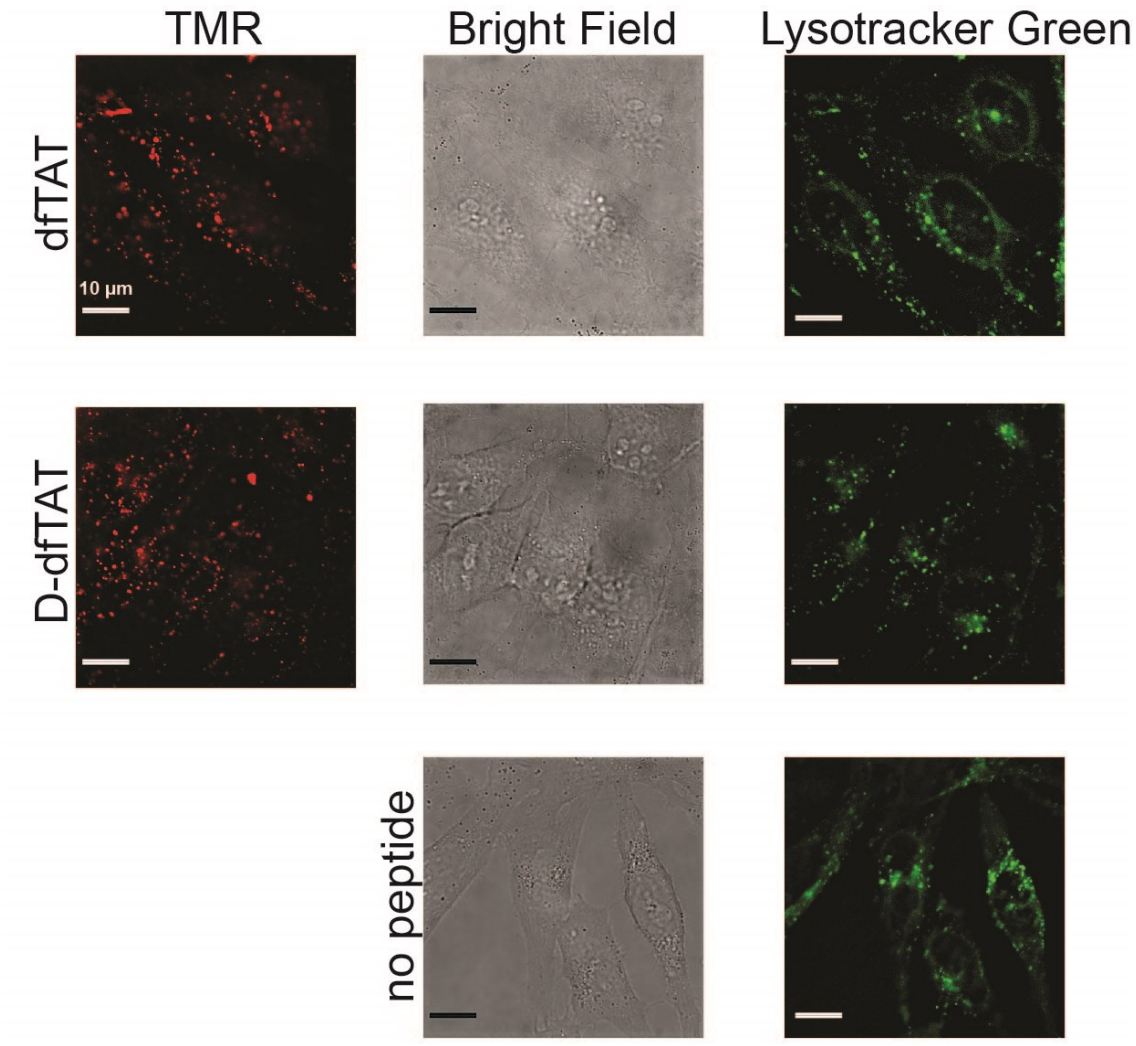

Figure 3-20 The number of endosomes present in cells treated with dfTAT is similar to that present in cells treated with D-dfTAT. HeLa cells were treated with 2 µM dfTAT or D-dfTAT respectively for 1h. Cells were then washed and incubated with 500 nM lysotracker green for 10 min. The fluorescent images show a punctate distribution for both the peptide and lysotracker green. Scale bar, 10 µm.

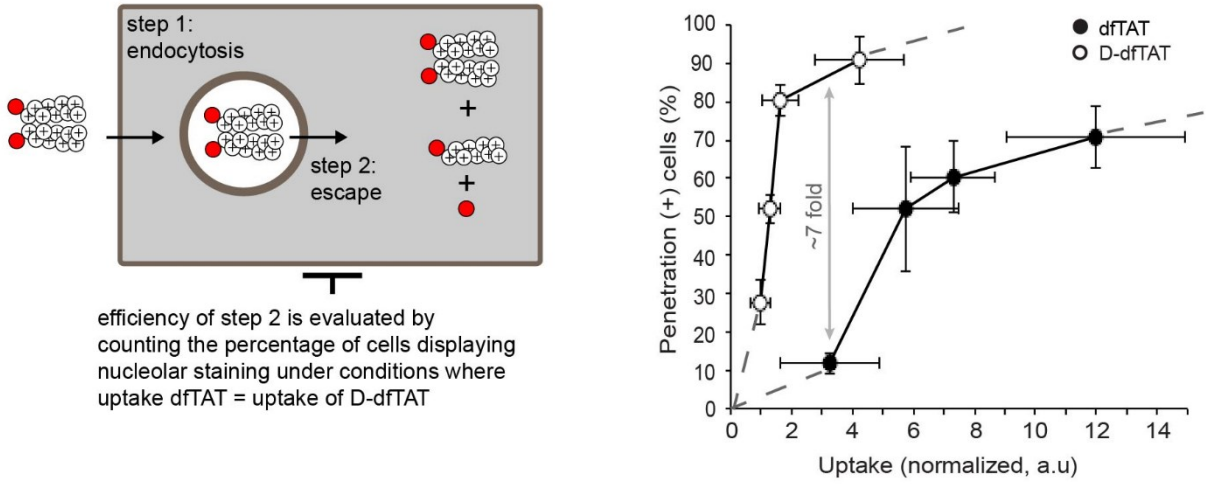

Figure 3-21 Evaluation of the endosomal escape activity of dfTAT and D-dfTAT as a function of the total amount of peptide internalized by cells (rationale highlighted in scheme). The data represented combines the peptide penetration and uptake measured in Figure 3-14 and 3-15.

on the possible yet small contribution of peptide uptake by an endocytosis-independent process, please see **Figure 3-10**).

In order to assess whether the differences in endosomal activity detected between the two peptides might arise from the partial endosomal proteolytic degradation of dfTAT, cell penetration activities were quantified in the presence of protease inhibitors. First, HeLa cells were pre-incubated with the cysteine-protease inhibitor E-64D and the cysteine, serine and threonine proteases inhibitor leupeptin [292, 293]. To establish whether this cocktail may protect the peptide from degradation prior to endosomal escape, cells were treated with 5 μM dfTAT for only 10 min and lysed immediately. This condition allows for peptide accumulation in the endocytic pathway (i.e. cells display a punctate peptide distribution under this condition) without providing sufficient time for endosomal escape. The cell lysates were analyzed by gel electrophoresis and densitometry analysis was performed on bands representing intact and degraded peptide fractions. As shown in **Figure 3-22**, a 20% increase in the amount of intact peptide was achieved in the presence of inhibitors. While these results do not pinpoint the site of action of the inhibitors within the cell (e.g. plasma membrane vs endocytic organelles), they nonetheless indicated that an increase of the amount of intact peptide present within endosomes could be achieved. This inhibitor cocktail was then used to determine whether protection against endosomal proteolytic degradation could impact the cell penetration activity of dfTAT. HDF cells were pre-treated with E-64D and leupeptin and then treated with D-dfTAT and dfTAT (2 μM) for 1h. The percentage of cells positive for penetration was then measured (**Figure 3-23**). The penetration activity of D-dfTAT was not impacted by the presence of

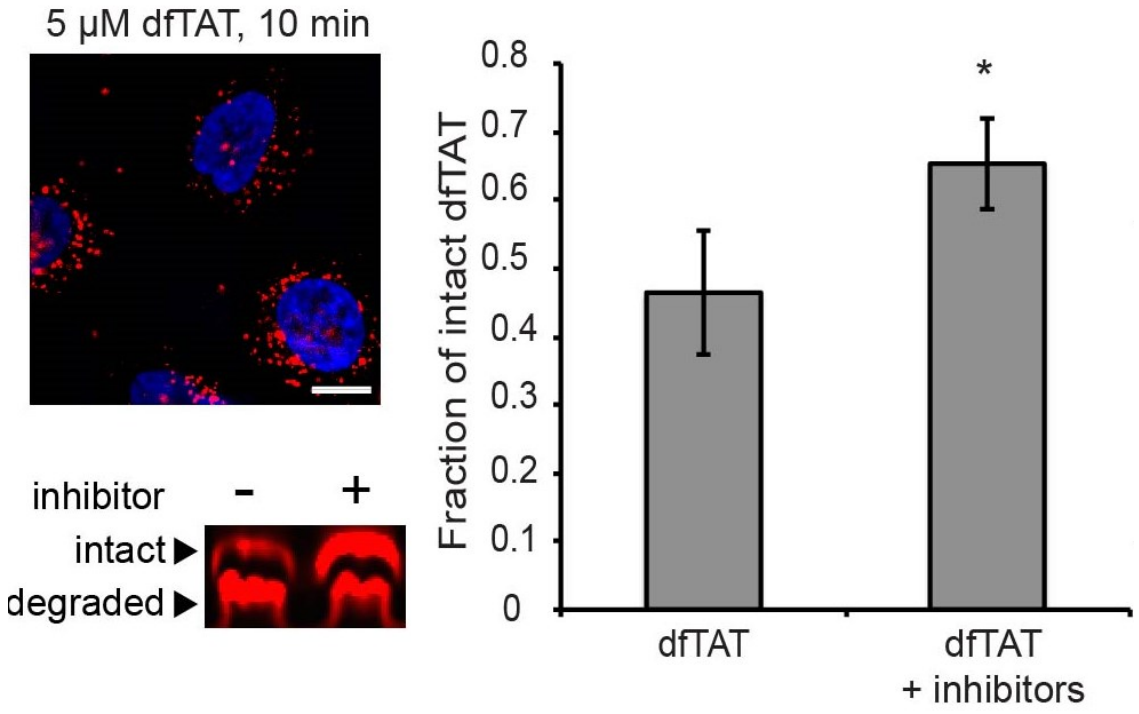

Figure 3-22 A protease inhibitor cocktail protects dfTAT from proteolytic degradation prior to cytosol delivery. HeLa cells were pre-incubated (40 min) with E-64D (40 µM) and leupeptin (28 µM). Cells were then treated with dfTAT (5µM) in presence of E-64D for 10 min. Cells lysates were analyzed by gel electrophoresis. Bands corresponding to intact and degraded peptide, detected using a fluorescence scanner, were quantified by densitometry to generate the bar graph presented. The data reported represent the average and corresponding standard deviations of biological triplicates. P-values are obtained using t-test analysis (*= P ≤0.01) between dfTAT with or without inhibitors.

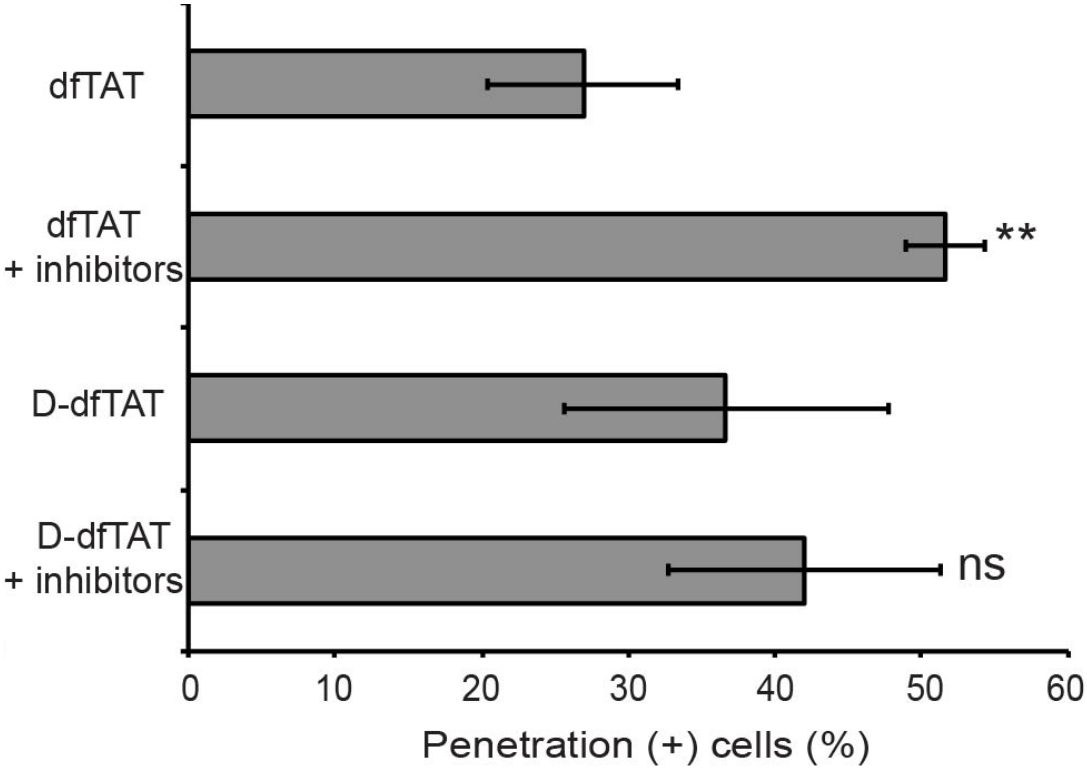

Figure 3-23 A protease inhibitor cocktail increases the penetration activity of dfTAT but not of D-dfTAT. HDF cells were pre-incubated (40 min) with the protease inhibitor cocktail (40 μM E-64D and 28 μM leupeptin). The cells were then treated with dfTAT or D-dfTAT (2μM) in presence of E-64D for 1h. The percentage of cells detected as positive for penetration was established by microscopy.

inhibitors, indicating that these compounds do not indirectly affect endocytosis and endosomal escape. In contrast, the activity of dfTAT was significantly increased by the inhibitor cocktail (approximately 2-fold increase at 2 μM). These data therefore suggest that proteolytic degradation along the trafficking pathway of the peptide might reduce its overall penetration activity.

3.2.5 Endosomal scape is not toxic to cells, but intracellular retention of D-dfTAT inhibits cells proliferation and impacts transcription

The viability of cells, determined using a SYTOX BLUE exclusion assay, was 95% and 98% after treatment with dfTAT and D-dfTAT (5 μM), respectively. dfTAT did not impact the proliferation of HDF or MCH58 cells. Likewise, D-dfTAT was innocuous to HDF and HeLa. However, the proliferation of MCH58 cells was blocked by this peptide (**Figure 3-24**; **Figure 3-25; Figure A-4**). Consistent with these results, bright field images of MCH58 cells treated with D-dfTAT for 1 h show no appreciable change in confluency over a period of 48 h (**Figure 3-26**). In order to gain a more detailed insight into how cells respond to each peptide, a microarray analysis was performed. I have previously reported that, despite causing extensive leakage of endocytic organelles, dfTAT does not dramatically impact the transcriptional program of cells treated with the peptide for one hour (analysis was performed one hour after incubation) [157]. Herein, I repeated this analysis 24 h after incubation to compare the effects of dfTAT and D-dfTAT. This choice was made based on the fact that dfTAT is completely degraded inside cells at this time

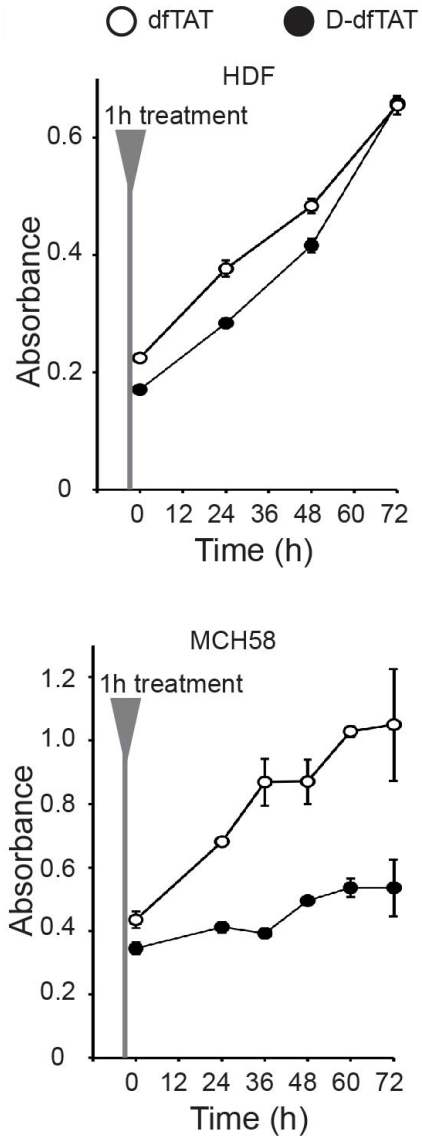

Figure 3-24 D-dfTAT impacts cellular proliferation more dramatically than dfTAT after cytosolic delivery. Proliferation assays. HDF and MCH58 cells were incubated with 5 μM dfTAT or D-dfTAT for 1h. Cells were then incubated in growth media (DMEM/10%FBS) and cellular proliferation was monitored over a period of 72 h using a MTT assay. Experiments were performed in triplicates with average and standard deviation indicated.

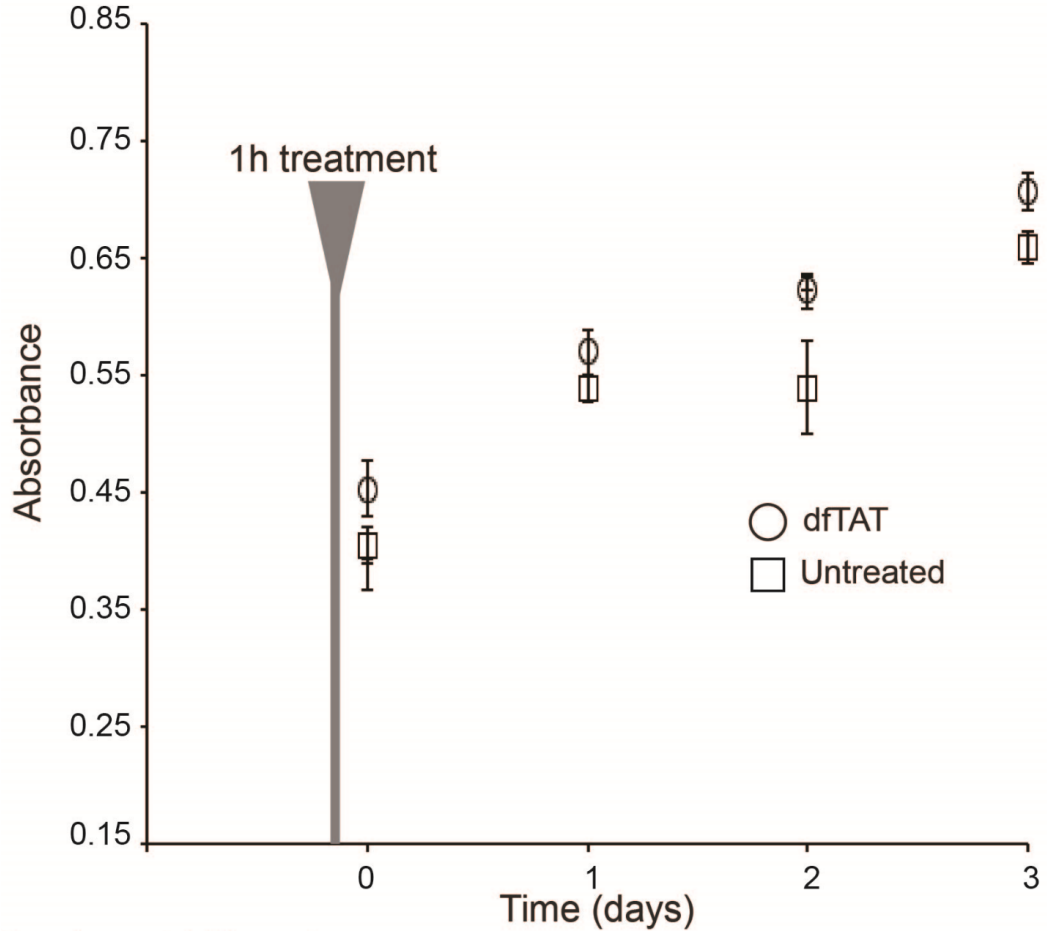

Figure 3-25 Proliferation assay. dfTAT treated HDF cells proliferate at a similar rate to untreated cells. HDF cells were incubated with 5 μM dfTAT or D-dfTAT in nrL-15 for 1h. Cells were then incubated in growth media (DMEM/10%FBS) and cellular proliferation was monitored over a period of 72h using a MTT assay. Experiments were done in triplicates with average and standard deviation indicated.

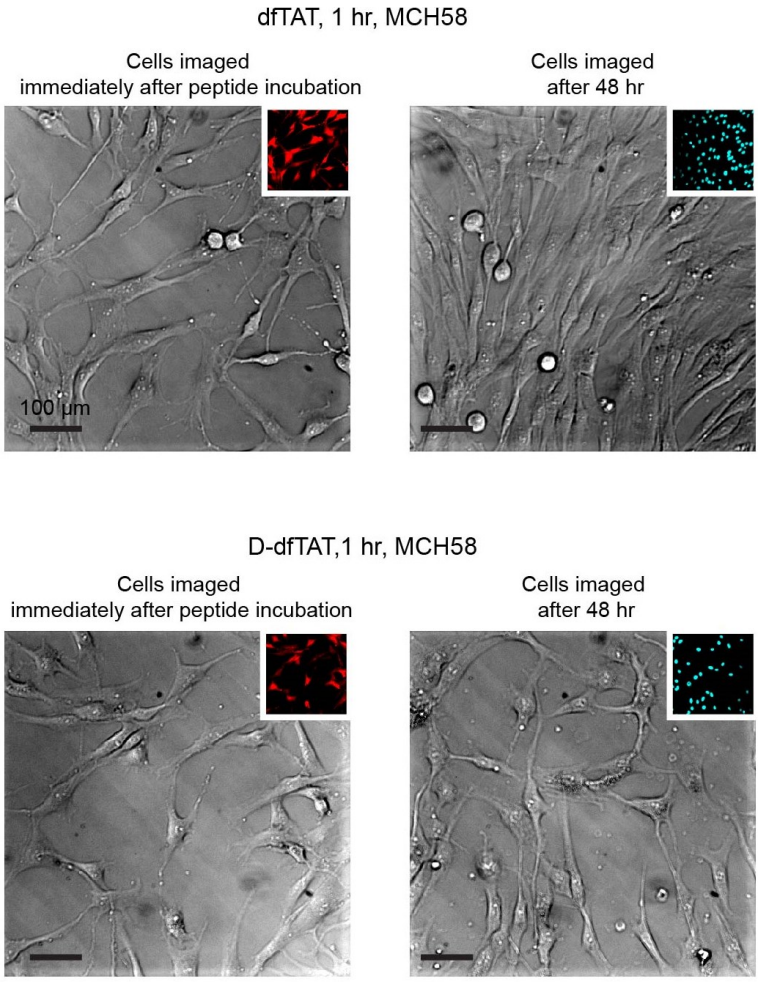

Figure 3-26 The effect of dfTAT and D-dfTAT treatment on cell growth was monitored by microscopy. MCH58 cells were grown to 50-60% confluency and incubated with 5 µM dfTAT or D-dfTAT for 1h. Cells were washed and imaged. The cells were then incubated in growth media (DMEM/10%FBS) and imaged again at 48 h. Bright field images of live cells taken immediately after incubation and after 48 h are shown using a 20X objective. Insets show fluorescence images of dfTAT and D-dfTAT treatment pseudocolored in red (emission 560 nm) and Hoechst emission pseudocolored in cyan (emission 480 nm). Scale bars, 100 µm.

point while D-dfTAT remains intact (**Figure 3-7**). Cells were images before mRNA extraction to insure efficient dfTAT or D-dfTAT delivery (Figure A-5). As previously observed, HDF cells treated with dfTAT were virtually identical to untreated cells (1/47000 transcript being overexpressed over a 2-fold threshold). MCH58 cells were slightly more perturbed with a total of 20 transcripts dysregulated. In contrast, D-dfTAT caused the dysregulation of 215 and 551 transcripts in HDF and MCH58 cells, respectively (**Figure 3-27**). These data establish that the transcriptional response induced by D-dfTAT is cell-dependent, yet consistently more severe than in the case of dfTAT. Notably, the level of transcriptional dysregulation induced by D-dfTAT also correlates with the effect of the peptide on proliferation (dysregulation of pro-apoptotic, as well as pro-survival genes, is identified in the microarray data; a list is provided in **Table 3-1**).

3.3 Discussion

dfTAT is a multitasking molecule utilizing the endocytic pathway to access the cytosolic space of cells (**Figure 3-28**) [157]. On the cell surface, it interacts with cell components that facilitates endocytic uptake. In the lumen of late endosomes, it interacts with BMP to induce membrane leakage [283] . Upon cytosolic access, dfTAT is reduced to monomeric fTAT. fTAT then accumulates at nucleoli. Throughout this pathway, dfTAT is presumably subjected to proteolysis. The results clearly establish that substituting L-amino acids for their D- isomers protects the peptide from degradation. In particular, based on intracellular peptide distribution and gel analysis, D-dfTAT is stable for a minimum of 24 h after cell penetration. In contrast, dfTAT is already partially degraded after 1 h

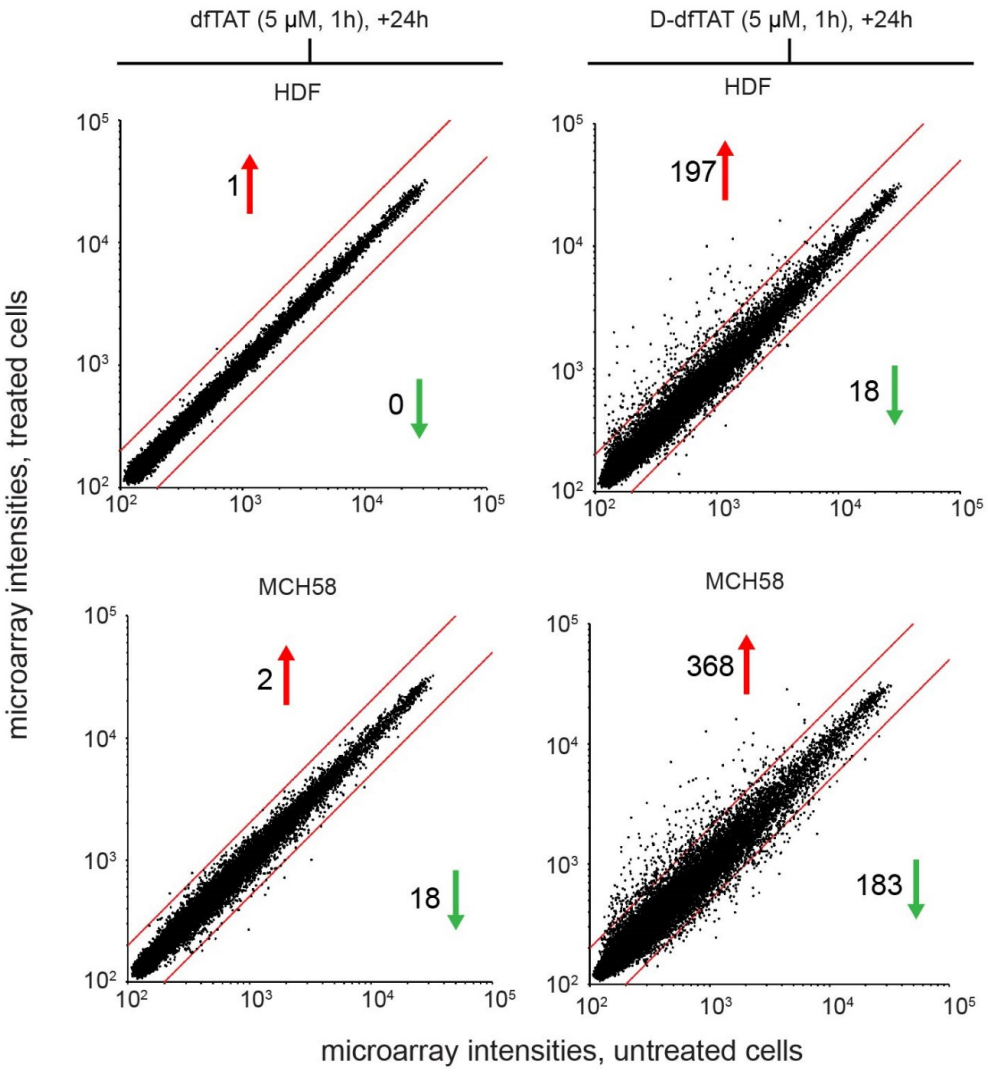

Figure 3-27 RNA-seq analysis of HDF and MCH58 cells treated with D-dfTAT or dfTAT (5µM) in L-15 for 1 h. Untreated cells were incubated without peptide in L-15 for 1 h. After 24 h in growth media (DMEM/10%FBS), cells were pelleted for total RNA extraction. The scatter plots shown display the microarray intensity values of 47,000 transcripts in treated cells (dfTAT or D-dfTAT, Y-axis) vs. untreated cells (x-axis). Analyses were performed in duplicate from two independent cell cultures. Both sets of microarray analyses yielded similar results. A representative set of results is shown (both sets are deposited in GEO accession bank). The red lines indicate the 2-fold intensity thresholds. The number of genes up and down-regulated beyond these thresholds are indicated with a red or green arrow respectively.

Table 3-1 Table showing the list of names of gene transcripts related to cell death and proliferation that are affected after treatment with D-dfTAT. The upward red arrow indicates an up regulation compared to control while the downward green arrow indicates a down regulation using a two-fold threshold. Data were analyzed through the use of QIAGEN's Ingenuity ® Pathway Analysis (IPA®, QIAGEN Redwood City, www.qiage.com/ingenuity).

MCH58 Cells : D-dfTAT treated* in comparision to untreated cells

List of transcripts associated with cell death:

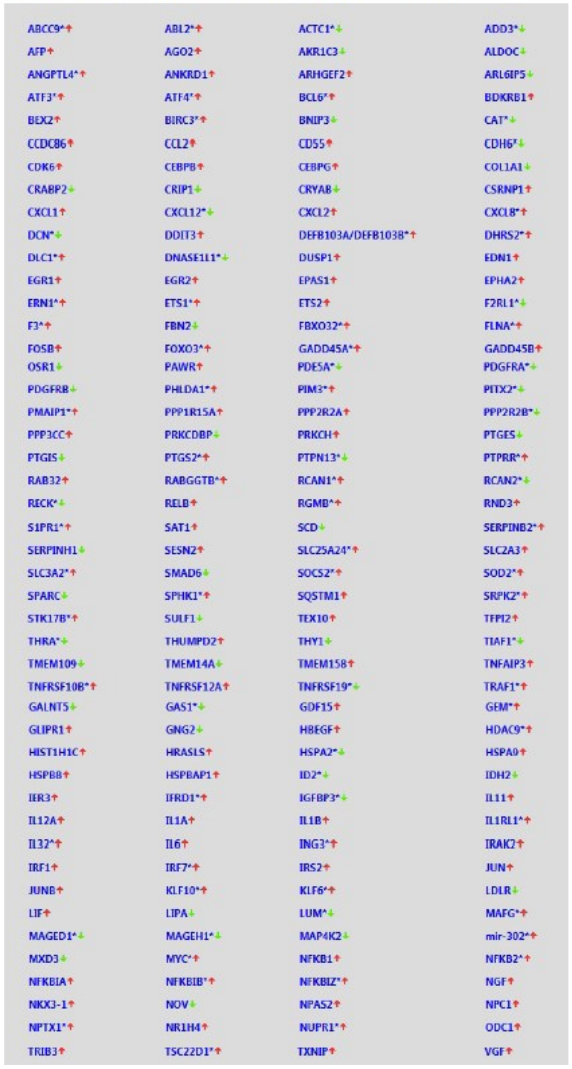

List of transcripts associated with proliferation:

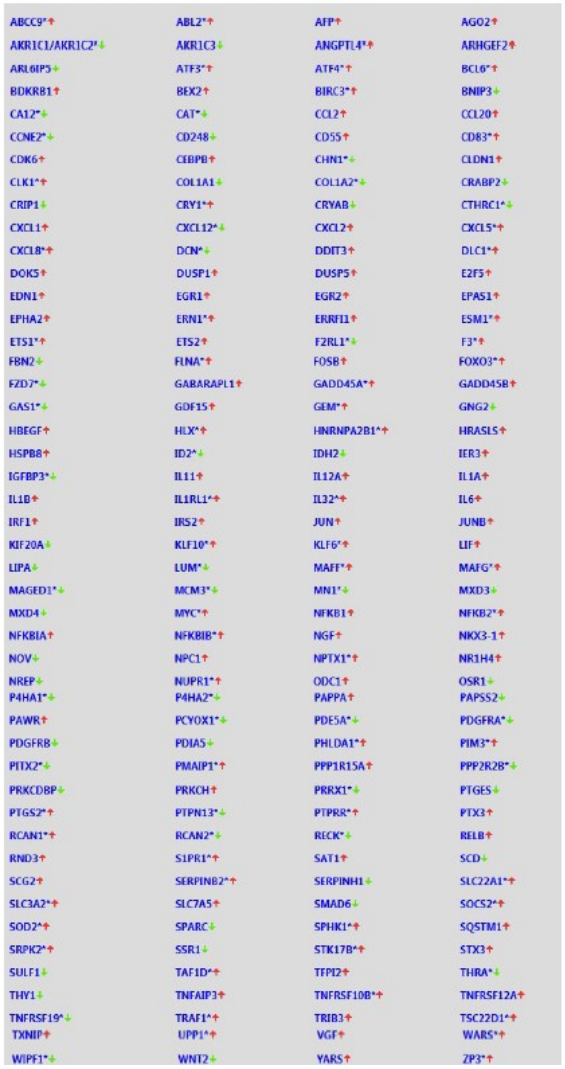

Table 3-1 Continued.

incubation and fully degraded at 24 h. The degradation observed at 1 h is presumably a combination of proteolysis within the lumen of endosomes and cytosolic proteolysis after entry into cells.

While inversion of chirality protects the delivery peptide from protease degradation, a change in stereochemistry should also impact the interaction of this compound with other chiral molecules[281]. My assays suggest that an inversion of chirality does not impact the overall mechanism of cell penetration. Like dfTAT, D-dfTAT enters cells by endocytosis followed by escape from late endosomes via interactions with BMP. At first glance, both peptides also appear to enter cells with relatively equal efficiencies. Overall, this suggests that chirality in not a critical aspect of the interaction between the CPP and molecules involved in its intracellular transport. Yet, upon closer examination, the results reveal that the individual steps of endocytosis and endosomal escape are impacted in opposite ways by chirality; endocytosis is reduced while endosomal escape is increased (**Figure 3-28**). Based on my results, the reduction in endocytosis could not be explained by a preference in D-dfTAT export during incubation. The export of D- dfTAT was significantly lower than dfTAT during the time course of the experiment, presumably due to stability and retention of D-dfTAT at the nucleoli.

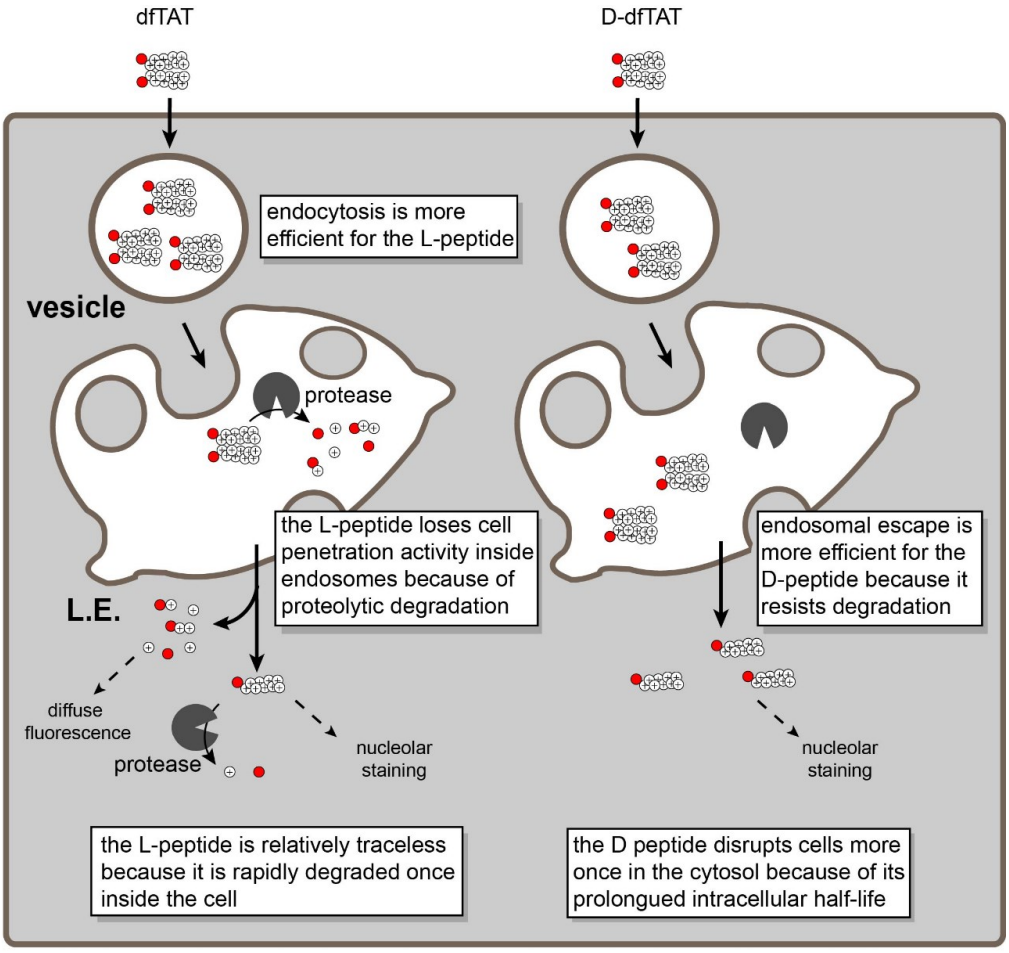

Figure 3-28 Schematic representation modeling the similarities and differences observed in the cellular penetration of dfTAT and D-dfTAT. dfTAT is internalized by endocytosis at a higher level than D-dfTAT. Along the endocytic pathway, dfTAT is partially degraded by proteolytic enzymes while D-dfTAT is not. Upon reaching the late endosome both dfTAT and D-dfTAT induce the leakage of BMP-containing membranes. Due to proteolytic degradation, the endosomal escape efficiency of dfTAT is, however, diminished compared to D-dfTAT. Upon escaping from late endosomes, D-dfTAT and intact dfTAT are represented as being reduced to their monomer counterparts in the cytosol (e.g. by action of glutathione). The peptide then diffuses into the cytosolic space and accumulate at nucleoli. The degradation products of dfTAT contribute to a diffuse cytosolic fluorescent distribution. D-dfTAT remains intact inside cells for several days and impacts the physiology of cells negatively. In contrast, cytosolic enzymes degrade dfTAT in a matter of hours. This in turn leads to a dramatically diminished physiological impact.

D-dfTAT is significantly less prone to internalization by endocytosis than dfTAT. The parent compound TAT is known to interact with negatively-charged heparan sulfate proteoglycans on the cell surface [104, 294]. The role played by these interactions with respect to endocytosis remains, however, unclear: proteoglycans might act as docking sites for the peptide and might or might not be directly involved in inducing endocytosis. In *in vitro* binding assays, Brock and co-workers have found no differences in the binding of L-CPPs or D-CPPs to heparan sulfate [281]. Yet, they have also reported a decrease in endocytic uptake by D-CPPs (CPPs tested were r9, D-penetratin, and D-hLF) when compared to their L counterpart. Overall, these data suggest that interactions with chiral species other than heparan sulfate might play an important role in endocytosis. The identities of these chiral species, however, have yet to be established.

Given that dfTAT and D-dfTAT differ in the extent to which they accumulate into endocytic organelles, comparing these peptides with respect to the subsequent step of endosomal escape is challenging. Nonetheless, to address this issue, I compared the propensity of the peptides to reach the cytosol of cells under conditions where the same amount of peptide is endocytosed (rather than conditions where incubation is performed at the same concentration). Based on this analysis, D-dfTAT induces endosomal leakage at a luminal concentration significantly lower than that required for dfTAT. Yet, dfTAT reaches the cytosol of cells in a degraded form. In addition, protease-inhibitors increase the endosomal escape activity of dfTAT, Finally, dfTAT and D-dfTAT have similar membrane leakage-inducing activities *in vitro*. Overall, my interpretation is therefore that dfTAT is not necessarily less capable of inducing endosomal leakage per se, but that

instead it is degraded by proteases while trafficking within the endocytic pathway. As a result, the amount of membrane-active dfTAT present inside endosomes represents only a portion of what is measured in the fluorescence measurements (intact dfTAT might represent approximately ~25% of total signal based on Figure 1c). Overall, D-dfTAT therefore appears to gain activity simply because, unaffected by proteolysis, it can accumulate inside late endosomes at concentrations higher than dfTAT.

I have previously shown that dfTAT is not toxic to cells[157] .This is confirmed in this report as dfTAT does not significantly impact the proliferation of two cell lines. Cells treated with dfTAT are also virtually indistinguishable on a transcriptional level from untreated cells at 24 h. Overall, this indicates that dfTAT-mediated endosomal leakage is well tolerated by cells. This is in sharp contrast to D-dfTAT, which has a deleterious impact on both proliferation and transcription. Based on the notion that both dfTAT and D-dfTAT share a similar mechanism of cell penetration, I interpret the impact of D-dfTAT on cellular proliferation not to be associated with the delivery process per se but that it is instead a result of interactions with cytosolic and nucleolar partners that take place post-delivery. In particular, one can speculate that the positively charged peptide interacts with negatively charged nucleic acid in the nucleoli and disrupts ribosome-associated processes. While dfTAT could potentially have similar interactions and lead to similar deleterious effects, this peptide is degraded rapidly and its effects are minimized. In contrast, the protease-resistant D-dfTAT remains intact in the cytosol and nucleoli of cells for a prolonged time and cellular responses become detectable.

Overall, my data reveal several insights relevant to the design of future cell-permeable peptide-based agents (e.g. stapled peptides, retro-inverso peptides, peptoids, CPPs, etc.). One is that conferring protease resistance to a CPP helps promote its activity inside endosomes. This is important as such approach might help generate agents that are cell-permeable at sub-micromolar concentrations and, thereby, more relevant to in vivo applications. Additionally, I infer that proteolytic degradation inside the endocytic pathway acts as a major determinant of peptide activity. For instance, one can envision how certain CPPs might appear relatively ineffective at escaping endosomes not because of low membrane-permeation activity per se, but rather because of a high propensity to be degraded and inactivated in this environment. Furthermore, for the first time, I establish that protease-resistance has a significant impact on the cytosolic activity of CPPs. In particular, our results highlight that a protease-resistant CPP can reside in the cytoplasm and nucleus of cells for an extended period of time and consequently induce numerous cellular responses. This is problematic for in vitro applications that aim at delivering bioactive cargos to probe or manipulate biological processes (ideally, cells should not be perturbed by the delivery agent itself if one is to investigate the intracellular effects of a cargo). In addition, one can speculate that this could be equally problematic for in vivo applications given that extended cellular retention of a delivery agent often leads to off-target effects [267]. When considering these issues, it is apparent that the strategy of all-L to all-D residue conversion is not an ideal strategy to improve CPP properties. However, my results now point toward the idea of conferring protease-resistance to endosomolytic agents in an environment dependent manner. In particular, I envision that delivery agents

that are protease resistant inside endosomes but degradable in the cytosol should provide clear improvements. Therefore, establishing the feasibility of such strategy will be the focus of future studies.

3.4 Materials and Methods

3.4.1 Peptide design, synthesis, and purification

All peptides were synthesized on the rink amide MBHA resin (Novabiochem, San Diego, CA) by solid phase peptide synthesis (SPPS). Fmoc-Lys(Mtt)-OH, Fmoc-Lys(Boc)-OH, Fmoc-D-Lys(Boc)-OH, Fmoc-D-Lys(Dde)-OH, Fmoc-Gly-OH, Fmoc-Arg(Pbf)-OH, Fmoc-D-Arg(Pbf)-OH, Fmoc-Gln(Trt)-OH, Fmoc-D-Gln(Trt)-OH, Fmoc-Cys(Trt)-OH (Novabiochem) were used to assemble the peptides using standard Fmoc protocols. Boc-D-Cys(Trt)-OH (Novabiochem) was added to the N-terminus of D-fTAT (single chain monomeric peptide) and the Boc protecting group was removed upon TFA cleavage. All reactions were performed at room temperature in a SPPS vessel. Reactions were agitated using a stream of dry N_2. For each amino acid coupling the reaction was agitated for 4 h with a mixture of Fmoc-amino acid (1.6 mmol), HBTU (Novabiochem) (1.5 mmol) and di-isopropylethylamine (DIEA) (sigma) (4.0 mmol) in dimethylformamide (DMF) (Fisher). After addition of each amino acid, Fmoc deprotection was performed by addition of 20% piperidine in DMF. The reaction was carried out twice: 1x 5 min followed by 1x 15 min with a DMF washing step between reactions. Upon completion of the linear chain assembly, the peptidyl-resin was washed

with DMF and dichloromethane (DCM) (Fisher). DEAC-k5 was synthesized by coupling five Fmoc-D-Lys(Boc)-OH. The DEAC (Anaspec) fluorophore was conjugated to the N-terminus of the peptide by reaction of DEAC, HBTU and DIEA (4, 3.9 and 10 eq.) in DMF overnight. CK(ε-NH-TMR)TATG (L-fTAT) was synthesized as described earlier[157]. Briefly, MTT protecting group was removed using 1% trifluoroacetic acid (TFA) (Fisher) and 2% triisopropylsilane (TIS) (Sigma) in DCM. The peptidyl-resin was washed with both DMF and DCM between each reaction. For ck(ε-NH-Dde)rkkrrqrrrG (D-TAT), the Dde protecting group was removed using 2% Hydrazine (sigma) in DMF. The peptidyl resin for both peptides was then reacted with a mixture of TMR, HBTU and DIEA (4, 3.9 and 10 eq.) and agitated overnight. For L-fTAT, the resin was washed and Fmoc-deprotection was performed to remove the N-terminal Fmoc moiety. For D-fTAT and L-fTAT, the peptide (and remaining protecting groups) were then cleaved from the resin by treatment with 92.5% TFA, 2.5% H_2O, 2.5% TIS and 2.5% ethanedithiol (EDT) (Sigma) for 3h at room temperature. The crude peptide was precipitated in cold anhydrous ether (Fisher). The precipitate was resuspended in water and lyophilized. The lyophilized product was dissolved in 0.1%TFA/water. The peptides were analyzed and purified by reverse-phase HPLC. HPLC analysis was performed on a Hewlett-Packard 1200 series instrument and an analytical Vydac C18 column (5 μm, 4 x 150 mm). The flow rate was 1 mL/min, and detection was at 214 nm and 550 nm. Semi-preparative HPLC was performed on a Vydac C18 10 x 250 mm column. The flow rate was 4 mL/min, and detection was at 214 nm and 550 nm. All runs used linear gradients of 0.1% aqueous TFA (solvent A) and 90% acetonitrile, 9.9% water, and 0.1% TFA (solvent B). The correct

identity of the peptides was confirmed by MALDI-TOF performed with a Shimadzu/Kratos instrument (AXIMA- CFR, Shimadzu, Kyoto). fTAT, expected mass: 2041.17, observed mass: 2040.66. DEAC-k5, expected mass: 900.59, observed mass: 900.84

3.4.2 Generation of D-dfTAT by dimerization of D-dfTAT

fTAT or D-fTAT (0.3 mg, 1.5 x 10^{-4} mmol) were dissolved in 5 mL of aerated phosphate buffer saline (PBS) at pH 7.4. The reaction was agitated on a nutator overnight (100% yield based on HPLC analysis). dfTAT and D-dfTAT were purified using analytical reverse-phase HPLC. Expected mass (MALDI-TOF): 4078.27, observed mass dfTAT and D-dfTAT were 4080.87 and 4078.87 respectively.

3.4.3 Cell culture and transfection

HeLa (ATCC CCL-2), MCH58 and HDF(ATCC PCS-201-010) cells were grown in Dulbecco's Minimum Essential Media (DMEM, Fisher) supplemented with 10% fetal bovine serum (FBS) (Fisher) and 1X penicillin/streptomycin (P/S) (Fisher) and incubated at 37 °C in a humidified atmosphere containing 5% CO_2.

For transfection experiments, rab7 (GFP-rab7 WT, Addgene plasmid # 12605) and DN-rab7 (GFP-rab7 DN, Addgene plasmid # 12660) were a gift from Richard Pagano. For transfection of the TAT-Cre experiment, *loxp-stop-loxp*-EGFP (pPCALNL-GFP, Addgene plasmid # 13770) and gWiz GFP (ALDEVRON LOT# 35237) were purchased.

Each plasmid (250 ng) was mixed with Lipofectamine 2000 (1 μL) in opti-MEM medium and allowed to incubate for 10 min at room temperature. The DNA/lipofectamine complex was then incubated for 18h at 37°C with HeLa cells seeded in an eight-well dish.

3.4.4 dfTAT and D-dfTAT degradation

An *in vitro* proteolysis assay was performed by addition of 1 μL of 0.5% trypsin to 19 μL of either dfTAT or D-dfTAT (10 μM) and incubated at room temperature. Reactions were quenched at specific time points by addition of 80 μL of 0.1% TFA in water. The samples were analyzed on a reverse phase HPLC using a 15-40% gradient (0.1% TFA/90% Acetonitrile).

For the *in cellulo* assay, HeLa cells were seeded in a 24 well dish and allowed to grow to 90% confluency. The wells were washed three times with PBS and once with Leibovitz's L-15 medium that does not contain the amino acid cysteine (non reducing L-15, nrL-15). nrL-15 is used for incubation since it lacks cysteine and avoids the reduction of the disulfide bond of dfTAT. Cells were then incubated with dfTAT or D-dfTAT (5μM) for 1 h. The cells were washed three times with PBS, lysed at different time point as indicated in the text using a lysis buffer (50 mM Tris, pH7.5, 2 mM EDTA, 2mM DTT, 0.1% Triton X-100 and protein inhibitor cocktail; 75 μL per well). The samples were then treated with DNAse (3 μL, Genesse) for 15 min on ice. The samples were centrifuged at 4°C, 13,000 RPM for 20 min. The supernatant (cell lysate) (39 μL) was added 6 μL of loading dye. The samples were boiled for 10 min at 100°C. The samples were run on a

16.5%Tris-Tricine gel (Bio Rad, Cat# 3450063) using a running buffer composed of 100 mM Tris, 100 mM Tricine, 0.1% SDS pH 8.3.

3.4.5 Delivery of peptides and proteins into live cells

HeLa, HDF and MCH58 cells were seeded in an 8-well dish. The cells were grown to 80-90% confluency in a 37°C humidified atmosphere containing 5% CO_2. The wells were washed three times with PBS and once with nrL-15. Cells were incubated with dfTAT or D-dfTAT (5 μM) at 37°C for 1 h (unless otherwise specified). The cells were then washed three times with L-15 supplemented with heparin (1 mg/mL) once with nrL-15. Cells were treated with the cell impermeable nuclear stain SYTOX® BLUE or SYTOX ® GREEN to identify cells with a compromised plasma membrane (i.e. dead cells). Alternatively, cells were incubated with cell permeable Hoechst for nuclear staining. Cells were imaged using an inverted epifluorescence microscope (Model IX81, Olympus, Center Valley, PA) equipped with a heating stage maintained at 37 °C. Images were collected using a Rolera-MGI Plus back-illuminated EMCCD camera (Qimaging, Surrey, BC, Canada). Images were acquired using bright field imaging and three standard fluorescence filter sets: CFP (Ex = 436 ± 10 nm / Em= 480 ± 20 nm), RFP (Ex = 560 ± 20 nm / Em= 630 ± 35 nm). For viewing and processing individual fluorescent images, the SlideBook 4.2 software (Olympus, Center Valley, PA) was used. Cells that displayed a cytosolic and nucleolar peptide staining were considered positive for cytosolic penetration (penetration(+)).The percentage of penetration (+) cells was calculated by dividing the

number of cells that displaying a fluorescent nuclear staining (20X images) by the total number of cells present (acquired using bright field imaging). Cells negative for cytosolic penetration typically display a punctate distribution consistent with endosomal entrapment of the peptides. Cells with plasma membrane compromised stained by SYTOX dyes were considered dead and excluded from the analysis. For each experiment, an average of three 20X pictures were taken, representing 300-400 cells. The reproducibility of all the experiments was assessed by performing experiments with independent batches of cell cultures on three different days (i.e. biological triplicates).

To monitor the intracellular localization of dfTAT and D-dfTAT after cell delivery (1 h incubation), cells were washed and incubated in fresh growth media (DMEM/10% FBS). The dish was placed at 37 °C in a humidified atmosphere containing 5% CO_2. Cells were imaged after 24 and 48h.

For delivery of TAT-Cre, HeLa cells were co-transfected with pCALNL-GFP andgWiz-GFP (control plasmid for transfection efficiency) for 18h. Cells were then washed and co-incubated with dfTAT or D-dfTAT and TAT-Cre (4 μM) for 1 h. The cells were washed again and the media was re-placed with fresh DMEM. The cells were placed back in the incubator for 24h. The cells were then imaged as described above. To quantify the results, $EGFP^+$ cells were counted and divided by the total number of cells that were transfected (control cells that were transfected with gWiz GFP (250 ng)) in each 20X image.

To investigate the process of cellular entry, HeLa cells were incubated in L-15 with DEAC-k5 (20 μM) for 1 h. Cells were then washed three times with PBS and

incubated either immediately or after 2h in nrL-15 with D-dfTAT (5 μM) or without peptide (control cells) for 1h. The cells were then washed three times with L-15 supplemented with heparin (1 mg/mL). Alternatively, the incubation steps were inverted. HeLa cells were first incubated with D-dfTAT for 1h and then washed as described above. Cells were then incubated in nrL-15 for 20 min. The cells were then incubated with DEAC-k5 (20 μM in L-15) for 1 h. Cells were washed and imaged as described earlier.

To establish the involvement of BMP *in cellulo*, HeLa cells were incubated with 50μg/ml anti-BMP mAb (mouse, Z-PLBPA) or anti-IgG mAb (mouse, ab99763) in L-15 for 30 min at 37°C. Cells were washed and incubated with D-dfTAT (3 μM). Cells were then imaged as previously described.

To assess whether endosomal proteolytic degradation could play a role in the difference in cell penetration activity observed between dfTAT and D-dfTAT, protease inhibitor were used. In particular, HDF cells were pre-incubated with the 40 μM E-64D (sigma) and 28 μM leupeptin (sigma) in nrL-15 for 40 min. The treatment was removed and the cells were incubated with D-dfTAT or dfTAT (2 μM) in the presence of 40 μM E-64D. The cells were then washed and imaged as described above. For determination of the amount of intact peptide remaining prior to cytosolic access, HeLa cells were pre-incubated with the 40 μM E-64D (sigma) and 28 μM leupeptin (sigma) in nrL-15 for 40 min. The treatment was removed and the cells were incubated with dfTAT (5 μM) in the presence of 40 μM E-64D for 10 min. The control cells were treated with dfTAT (5 μM) for 10 min in absence of inhibitors. The cells were then washed, lysed and processed as described above for preparation to run on a 16.5% Tricine gel (Bio Rad, Cat# 3450063).

3.4.6 Quantitative determination of peptide uptake

HeLa cells were seeded in a 48-well dish and grown to 80% confluency. Cells were treated with dfTAT and D-dfTAT for 1h at various concentrations (range: 1-10 μM). Total peptide uptake was measured in two ways: Fluorescence measurements of a cell lysate assay or flow cytometry. For whole cell lysate analysis, cells were washed with heparin (1mg/mL) and then trypsinized (50 μL) for 3 min. Cells were resuspended in nrL-15 (350 μL) and centrifuged at 4°C, 2,500 rpm for 10 min. The supernatant was removed and the cell pellet was resuspended in nrL-15 (50 μL). An aliquot of the resuspended cells (3 μL) was removed and used through flow cytometry to normalize for total number of cells per sample. The remaining resuspended cells were lysed by addition of 50 μL of a lysis buffer (components: 50mM Tris, pH7.5, 2 mM EDTA, 4mM DTT, 20% Triton X-100 and protein inhibitor cocktail) and vortexing. For the whole cells lysates in the absence of DTT, the lysis buffer prepared and used lacked DTT (components: 50mM Tris, pH7.5, 2 mM EDTA, 20% Triton X-100 and protein inhibitor cocktail). The samples were vortexed and a volume of 80 μL of supernatant for each condition was placed in a 96 well plate. The fluorescence emission intensity was measured using a plate reader equipped with a fluorescence module (Ex=525, Em=580-640 nm) (GloMax®-Multi+ Detection System, Promega, Fitchburg, WI). To normalize the aliquot of cells (3 μL) was resuspended in nrL-15 (97 μL) and the total amount of cells per samples was determined using flow cytometry.

For fluorescence measurement using the flow cytometer, cells were trypsinized and resuspended in nrL-15 medium. Cells were analyzed using a BD Accuri C6 flow

cytometer equipped with the FL2 filter (Ex = 488 nm/Em = 533 ± 30 nm). All data was acquired at flow rate of 66 μL/min with detection of a minimum of 40,000 events. The geometric mean of the FL2 signal for each experiment was determined using the Flowjo software. The data reported represent the average and corresponding standard deviations of three independent experiments for each peptide concentration.

For export measurements, HeLa cells were seeded in a 48-well dish and grown to 80% confluency. Cells were treated with dfTAT and D-dfTAT at 5 μM for 1 h. Cells were washed according to protocol and the medium was replaced with fresh new media (200 μL, DMEM+FBS+P/S). The extracellular media from separate wells was removed at specific time points. The media was centrifuged at 8,000 rpm for 8 min. The media samples from each time point were aliquoted into a 96 well plate. The fluorescence intensity was measured as mentioned above using a plate reader. The data was normalized by comparison to the fluorescence of the extracellular media of the untreated cells.

To determine whether the peptide remained bound to the cell surface after the initial wash, HeLa cells were seeded in a 48-well dish and grown to 80% confluency. Cells were treated with dfTAT and D-dfTAT at 5 μM for 1 h. The cells were then washed in three different ways. For all conditions, cells were first washed three times with L-15 supplemented with heparin (1 mg/mL) and once with nrL-15. Sample 1: control cells were then trypsinized and resuspended in nrL-15 for flow cytometry. For sample 2: The cells were then washed again three times with nrL-15 supplemented with heparin (1 mg/mL) and once with nrL-15. For sample 3: The cells were then trypsinized and resuspended in nrL-15 and centrifuged at 4°C, 2,500 rpm for 10 min. The supernatant was removed and

the cell pellet was trypsinized (50 µL) for 3min. The trypsinized cells were then resuspended in nrL-15 for flow cytometry analysis.

3.4.7 Liposome Preparation and leakage assays

Lipids used in the experiments consisted of: 1,2-dioleoyl-s-glycero-3-phosphocholine (DOPC), 1,2-dioleoyl-sn-glycero-3-phosphoethanolamine (DOPE), sn-(3-oleoyl-2-hydroxy)-glycerol-1-phospho-sn-1'-(3'-oleoyl-2'-hydroxy-glycerol) (BMP), cholesterol (chol) (Avanti Polar Lipids). Liposomes were prepared by first transferring various volumes of lipids dissolved in chloroform (stock solutions of know concentrations) into scintillation vials. For liposomes mimicking the intraluminal late endosomes vesicles (L.E.) the molar ratios of lipids consisted of 77:19:4 BMP:PC:PE. For liposomes mimicking the plasma membrane, the lipid mixture was 65:15:20 PC:PE:Chol. The lipid film was prepared by removing the chloroform from the lipid mixture using a stream of N_2 and then placing the vial in a desiccator for 24h. A buffer containing 100 mM NaCl, 10 mM NaH_2PO_4 pH7.4, and 60 mM calcein was added to the lipids film for hydration. The lipids were then mixed vigorously and swelled for 1 h at 42°C under N_2 to obtain multilamellar vesicles (MLVs). For production of unilamellar vesicles (LUVs), the MLVS were extruded (20 passes) through a 100 nm pore size polycarbonate membrane (Whatman) using a Mini-Extruder (Avanti Polar Lipids). Dynamic light scattering was used to determine the average diameter size distribution of the liposomes using a Zeta Sizer (Malvern instrument). The liposomes were purified by gel filtration using a Sephadex G-50 (GE Healthcare) column (2.5 x 17.5 cm) to separate the liposomes from

free calcein. The eluate was collected in a 96 well plate and the plate was read using a Promega GloMax-Multi plate reader (Promega) at 450 nm and 750 nm corresponding to the wavelength of detection for calcein and liposome respectively.

Purified calcein-loaded LUVs were mixed with D-dfTAT or dfTAT at different ratios for 1 h at room temperature in 100 mM NaCl, 10 mM NaH_2PO_4 pH5.5. Samples were centrifuged for 1 min at 4,000 rpm. To measure the amount of leaked calcein and separate soluble liposomes from released calcein, the supernatants were purified using an illustra NAP-10 Sephadex G-25 column (GE Healthcare) (the elution volumes of liposomes and free calcein were determined independently with pure samples). Fractions were collected in a 96-well plate and the fluorescence of calcein was measured using a Promega GloMax-Multi plate reader (Ex 490nm, Em 520-560nm). The percent leakage was calculated using the following equation:

$$\%\ \text{Leakage} = 100 \times \frac{\mathrm{Fl_t} - \mathrm{Fl_0}}{\mathrm{Fl_{max}} - \mathrm{Fl_0}}$$

where Fl_t is the free calcein fluorescence intensity of a sample at a specific peptide:lipid ratio measured after 1 h, Fl_0 is the free calcein fluorescence intensity of a untreated sample and Fl_{max} is the free calcein fluorescence intensity of a sample after treatment with 0.2 % Triton X-100.

3.4.8 Cell proliferation assays

A MTT assay was performed to compare the effect of dfTAT to D-dfTAT on the proliferation rate of MCH58 and HDF. Cells were seeded and grown in a 6-well dish and

treated as described earlier. Each well was incubated with either 5 μM dfTAT or D-dfTAT at 37 °C for 1 h. Cells were washed, trypsinized and seeded into 96-well dishes containing 100 μL of DMEM/10%FBS. The cells were then allowed to adhere to the bottom of the dish for 12 h. The DMEM was removed, replaced with 100 μL of fresh DMEM/10%FBS and 10 μL of a 12 mM MTT stock solution was added to the wells. The 96-well dish was incubated at 37 °C for 4 h, followed by addition of 100 μL of SDS-HCl (10 mM). The cells were then allowed to incubate with this solution for 12 h. After the incubation each sample was mixed and the absorbance at 560 nm was measured. Controls included a negative control where 10 μL MTT was added to 100 μL of DMEM alone (no cells). A second control consisted of cells treated with the delivery peptide but to which no MTT was added to subtract the contribution of TMR from the measured absorbance. The absorbance of the negative control was subtracted from all samples. Assays were performed at multiple time points to obtain a cellular proliferation curve.

3.4.9 Whole genome microarray analysis

MCH58 and HDF cells were seeded in 24-well dishes and incubated with dfTAT or D-dfTAT (5μM) or nrL-15 (untreated cells), for 1h. Cells were then washed and the media was replaced by DMEM. The cells were then placed back into the 37°C humidified atmosphere containing 5% CO2 incubator for 24 h. After 24hr, the cells were then trypsinized after washing with PBS or nrL-15 (1h + 24h time point). Cells were pipetted into an eppendorf tube and spun down at 12k RPM for 4 min at 4°C. The cell pellets were preserved in 1 mL TRIzol (Ambion®, Life Technology) and shipped frozen to the

UTsouthwestern microarray facility for total RNA extraction and analysis using Illumina Human HT-12 v4 sequencer. The protocol is described in this link (https://microarray.swmed.edu/protocols/protocol/illumina-gene-expression-probe-labeling/). Data sets are deposited in GEO accession bank, GSE90575.

4. THE ENDOSOMAL ESCAPE PROPERTY OF POSITIVELY CHARGED CELL-PENETRATING PEPTIDES IS DEPENDENT ON THE NUMBER OF ARGININE RESIDUES PRESENT IN THE SEQUENCE

4.1 **Introduction**

The chemical properties that confer dfTAT its endosomolytic activity and that distinguish it from its far less active monomeric counterpart are currently not understood. Understanding the features that provide high cell-penetration activity to dfTAT may therefore guide the development of analogs possessing better performance and consequently that are more therapeutically relevant. In addition, cell-penetration rules learned with this lead compound may also be applicable to other delivery systems that utilize the endocytic pathway as a route of cellular entry, including liposomes and nanoparticles. In this chapter, I aim to establish the role associated with the peptide sequence of dfTAT on cellular delivery. Previous reports have attributed the internalization activity of TAT predominantly to its arginine-residues[32-34]. However, given the low efficiency of this CPP, most studies have measured endocytic uptake without quantifying the process of endosomal escape directly. In contrast, the unusually high endosomolytic activity of dfTAT allowed me to characterize the residues important for this activity. I hypothesize that the endosomolytic activity of dfTAT is dependent on the arginine content and specifically the number of arginine residues present.

In this work, I show that the polyarginine peptides can recapitulate the observed endosomolytic activity of dfTAT; while a polylysine construct cannot. Interestingly, a

minimum number of 12 arginines is required to achieve cytosolic penetration, however peptides containing less arginines remained entrapped in endocytic vesicles. Furthermore, I show that the difference in cellular penetration is not due to a decrease in amount of peptide internalized. Using *in vitro* assays, I demonstrate that while all polyarginine peptides are able to bind to late endosomal liposomes to the same extent, the membrane leakage observed increases as a function of arginine content. Together, my results provide insights into the molecular parameters required for efficient cellular penetration of arginine-rich CPPs, information that is important to consider when generating new delivery agents.

4.2 Results

4.2.1 Generation of dfR_n and dfK_n reagents

Polyarginine or polylysine analogs of dfTAT were synthesized. In particular, given that dfTAT contains 16 basic residues, dfR8 (16 arginine residues) and dfK8 (16 lysine residues) were produced to evaluate the importance of charge (**Figure 4-1**). Additionally, a series of dfRn peptides, where n= 4,5,6 or 7, were synthesized to determine the minimum number of arginine residues required to recapitulate the endosomolytic activity of dfTAT.

4.2.2 The positive charge in dfTAT is necessary but not sufficient for its cell penetration activity

dfTAT induces leakage from late endosomes by interacting with the lipid BMP[283]. dfTAT is cationic while BMP is anionic, suggesting that electrostatic interactions may be important for activity. To establish whether charge alone is a determining factor for endosomal escape, polyarginine or polylysine analogs of dfTAT were synthesized. In particular, given that dfTAT contains 16 basic residues, dfR8 (16 arginine residues) and dfK8 (16 lysine residues) were first produced (**Figure 4-1**). Cells were incubated with each peptide for 1h and the cellular penetration of each compound was assessed by live cell fluorescence microscopy. The measurements are based on the fact that, when endosomal escape fails, a distinct punctate fluorescence can be observed[103, 295, 296].

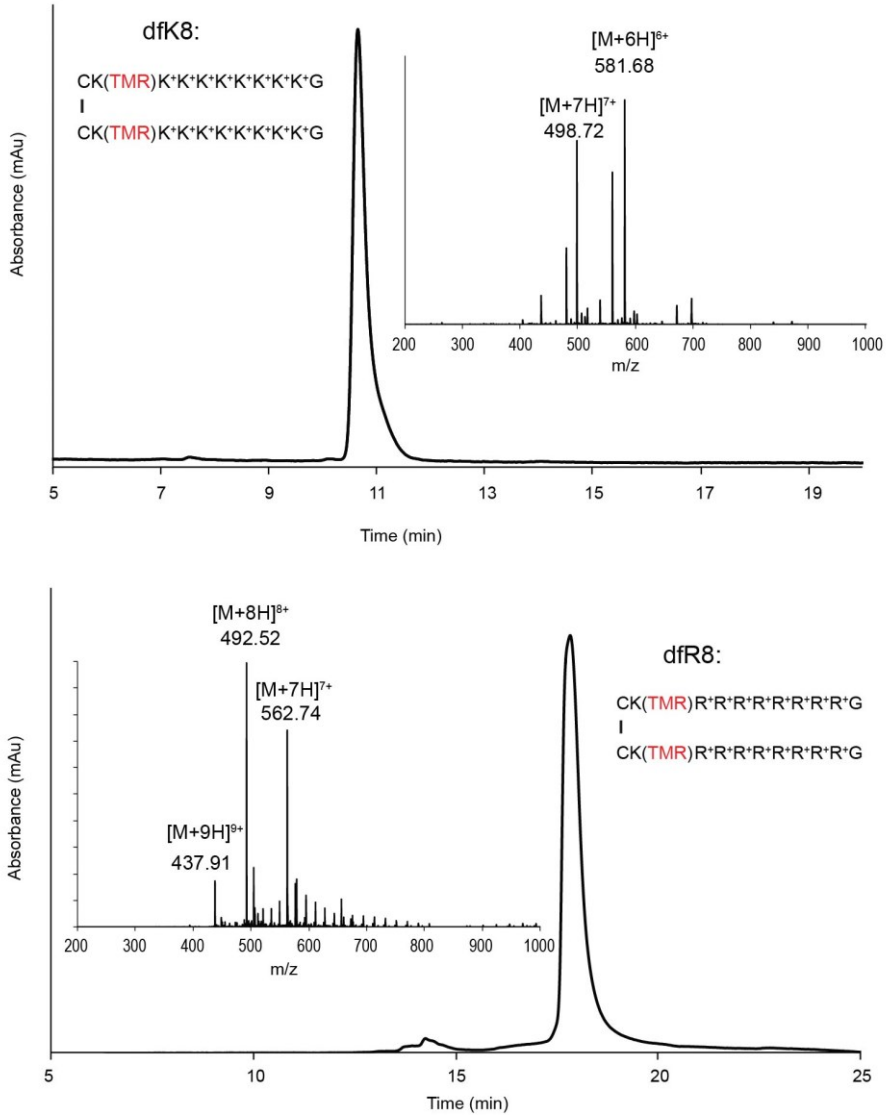

Figure 4-1 HPLC and ESI MS spectrum of dfK8 and dfRn series. The expected and observed masses for the corresponding peptides can be found in the material and methods section.

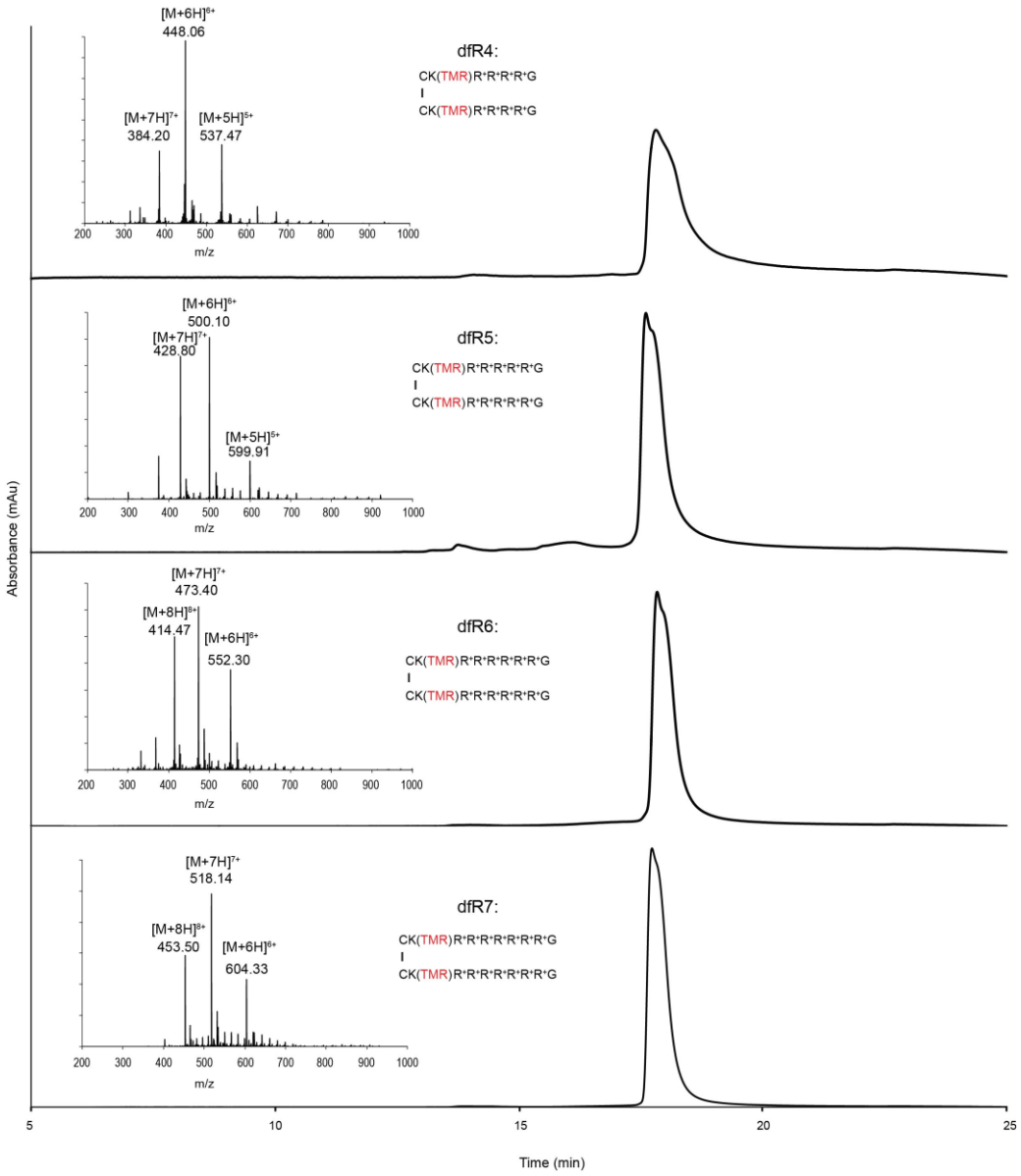

Figure 4-1 continued.

This is a result of endosomal entrapment of the fluorescent peptides. In contrast, upon endosomal escape, a diffuse cytosolic fluorescence can be detected[157, 194]. Moreover, because polycationic peptides tend to accumulate at nucleoli upon cytosolic entry, nucleolar staining can also be observed[16, 284]. While the cytosolic signal is admittedly unreliable because of possible out-of-focus contributions, the nucleolar signal is useful because it validates that the compounds have indeed penetrated cells. Therefore, I use a binary assay in which cells are counted as either positive or negative for nucleolar staining. When compared to dfTAT, dfK8 showed no cell penetration activity (**Figure 4-2**). More precisely, dfK8 appears trapped in the endocytic pathway at all concentrations tested (**Figure 4-2**). In contrast, dfR8 appears to be more active than dfTAT. dfR8 displays an increased number of penetration positive cells at 3 and 5 μM when compared to both dfTAT and dfK8. Notably, the level of endocytic uptake of dfK8 was also lower than both dfTAT and dfR8 at all concentrations tested (**Figure 4-3**)**.** To insure that peptide penetration was not associated with cellular toxicity, I conducted a Sytox ® Blue exclusion assay. To my surprise, cell treatment with dfR8 at 5 and 10 μM resulted in 13% and 47% decrease in cell viability respectively (**Figure 4-4**). The cytotoxic effect of dfR8 treatment could be attributed to the increased number of arginine and not the charge since both dfK8 and dfTAT showed no cellular toxicity at all concentrations tested.

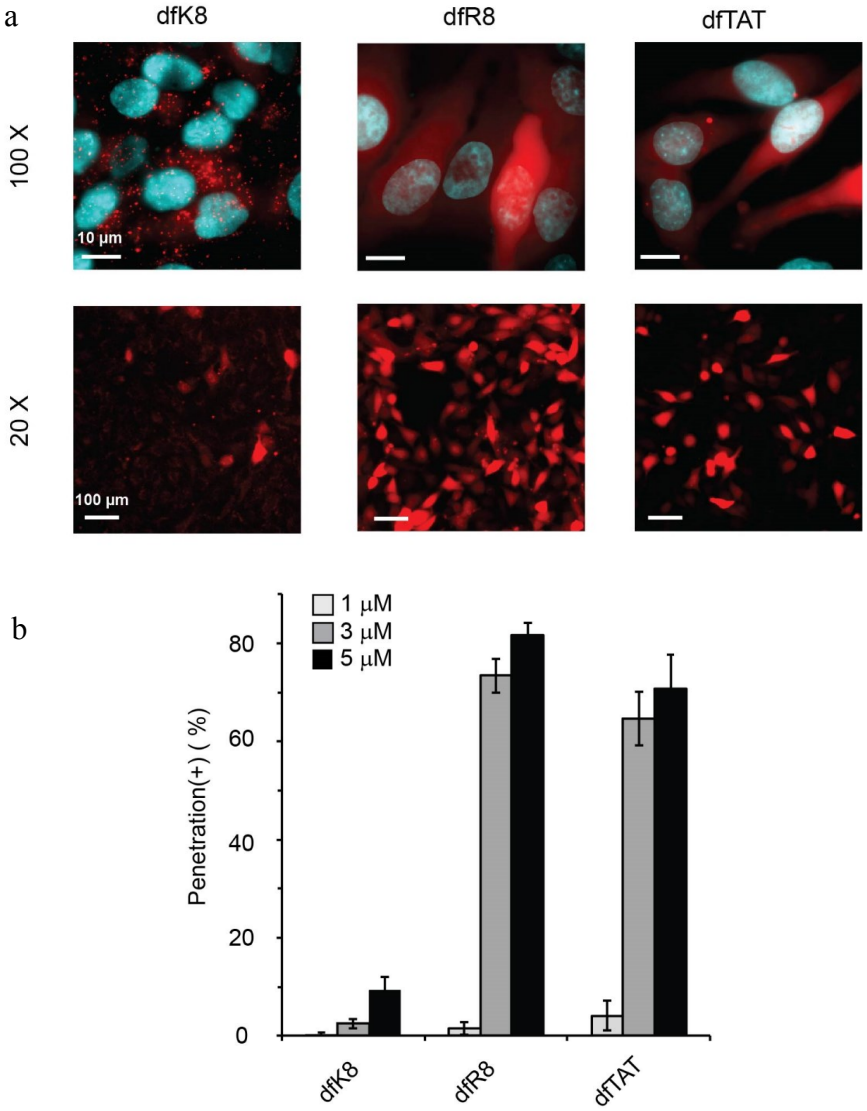

Figure 4-2 Comparison of cellular distribution of the peptides after 1 h incubation. a) HeLa cells were incubated with dfTAT, dfR8 and dfK8 at 5 µM for 1 h, washed and then stained with the cell permeable Hoechst nuclear stain (1µg/mL). Live cells were imaged with a 20X and 100X objective. Fluorescence images are overlays of the TMR emission at 560 nm (pseudocolored red) and Hoechst emission at 460 nm (pseudocolored blue). Scale bars, 10 and 100 µm for 100X and 20X respectively. b) Evaluation of the cytosolic penetration efficiency of dfTAT, dfR8 and dfK8 as a function of peptide concentration present in the incubation media. HeLa cells were incubated with peptides (1-5 µM) for 1 h. The percentage of cells detected as positive for penetration was established by microscopy.

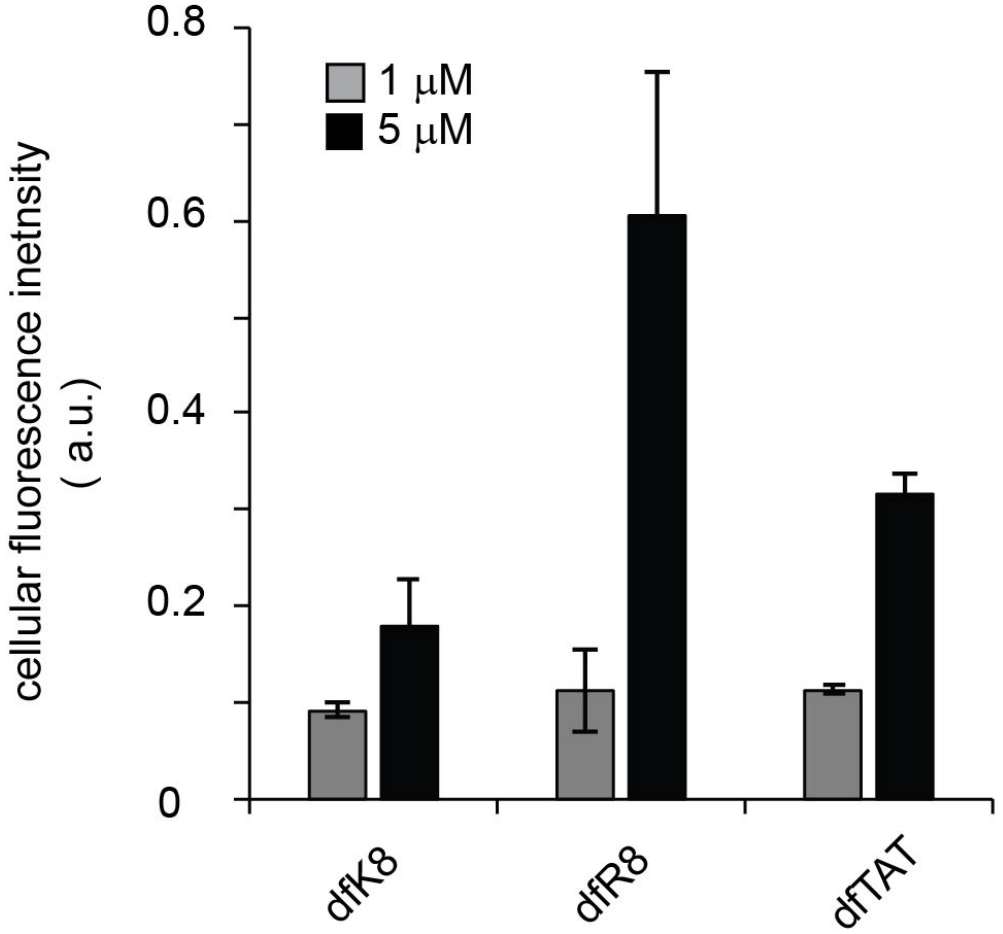

Figure 4-3 Quantification of total cellular uptake by dfTAT, dfR8 and dfK8 as a function of the peptide concentration in incubation media. HeLa cells were incubated with peptides (1 and 5 μM) as in figure 4-2). The overall amount of peptide internalized by cells (endosomal + cytosolic) was assessed by measuring the bulk fluorescence of cell lysates.

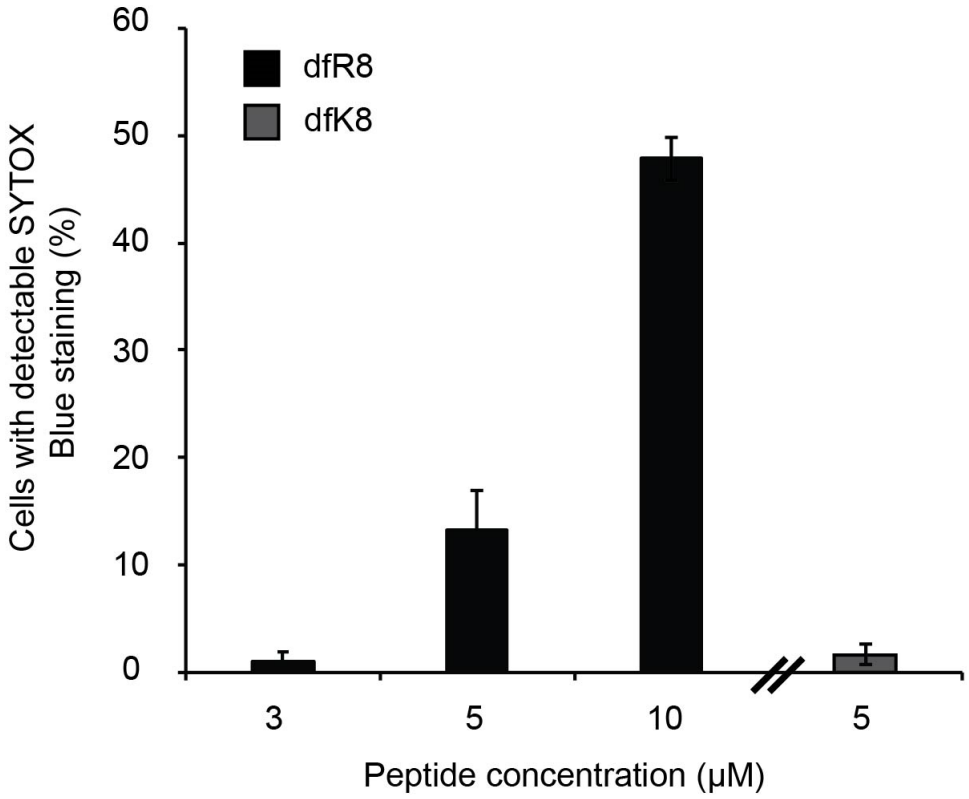

Figure 4-4 dfR8 is cytotoxic at high peptide concentrations. HeLa cells were incubated with dfR8 or dfK8 for 1h at specified peptide concentrations. Cell viability was assessed by a SYTOX Blue exclusion assay immediately after the incubation.

4.2.3 A peptide with the same number of arginine's found in dfTAT mimics its endosomolytic activity

Although dfR8 recapitulated the endosomolytic activity displayed by dfTAT, it did however exhibit increased cytotoxicity. I decided to test how the number of arginine residues present impacts cell penetration. To test this, a series of dfRn peptides, where n= 4, 5, 6 or 7 were synthesized. The peptide dfR4, the smallest compounds of the series, displays no detectable cell penetration, regardless of the concentration tested (from 1 to 5 μM). Instead, the peptide appears to exclusively accumulate inside endosomes, as indicated by co-localization with Lysotracker Green (**Figure 4-5 and Figure 4-6**). The activity of dfR5 was similarly poor. In contrast, dfR6, dfR7, and dfR8 displayed a robust cytosolic penetration, comparable to that of dfTAT at all concentrations tested (**Figure 4-5 and Figure 4-7**). While the cytosolic penetration assay establishes whether a peptide can reach the cytosolic and nucleolar space (above the detection threshold of the imaging set-up), it does not address how much peptide enters cells. To test how the dfRn peptides compare to dfTAT in that regard, the total fluorescence of cells incubated with 5 μM of each reagent was measured. In particular, to avoid artifacts that could arise from the peptides having different fluorescence intensities depending on whether they localize in endosomes or in the cytoplasm, cell lysates were analyzed (the fluorescence intensities measured are normalized to the number of cells present in the incubation dish)[157]. As shown in **Figure 4-8**, the overall cellular uptake increases with the number of arginine residues, with dfR8 showing almost 3 fold more peptide inside cells than dfR4. Overall,

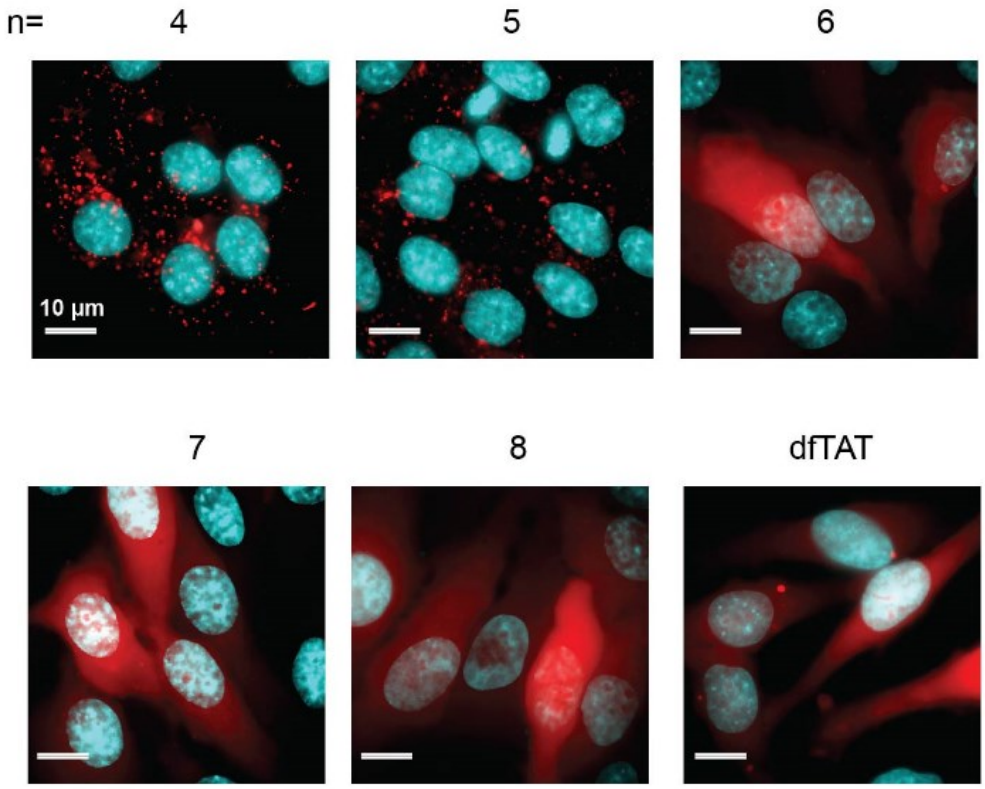

Figure 4-5 Comparison of cellular distribution of the polyarginine peptides after 1 h incubation. HeLa cells were incubated with dfTAT, dfRn constructs (n= 4, 5, 6, 7 or 8) at 5 µM for 1 h, washed and then stained with the cell permeable Hoechst nuclear stain (1µg/mL). Live cells were imaged with a 100X objective. Fluorescence images are overlays of the TMR emission at 560 nm (pseudocolored red), Hoechst emission at 460 nm (pseudocolored cyan). Scale bars, 10 µm.

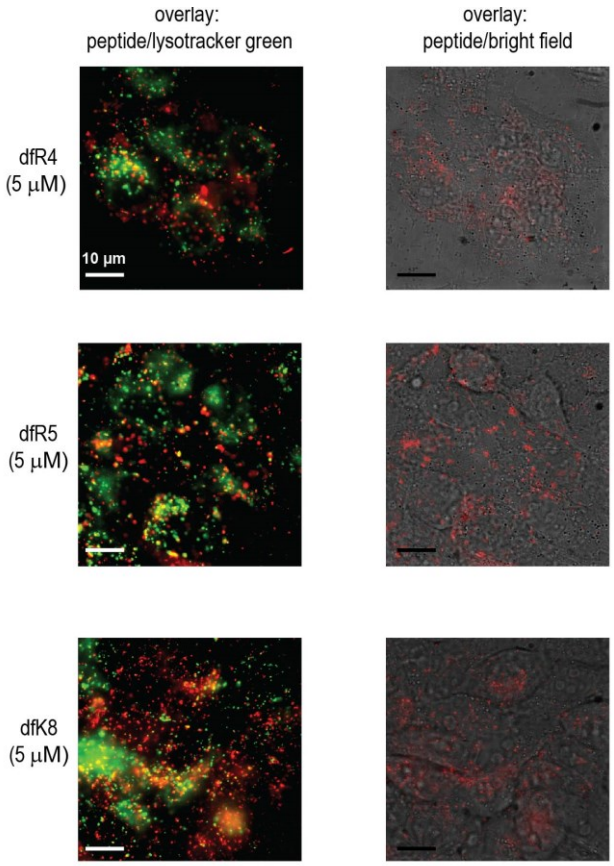

Mander's overlap coefficients (M)	M1	M2
dfR4	0.7099	0.5789
dfR5	0.7991	0.5906
dfK8	0.7117	0.9115

Figure 4-6 dfR4, dfR5 and dfK8 co-localize with LysoTracker green, a marker of acidified endocytic organelles. HeLa cells were incubated with the specified peptides at 5 μM for 1 h. The cells were washed and then incubated with lysotracker green and imaged. Images are overlays of either peptide/ lysotracker (pseudocolor: red for peptide and green for lysotracker) or peptide/ bright field. Mander's overlap coefficients were determined using Image J software. M1 is a ratio of the sum of the red pixels (peptide) where the green pixel (lysotracker) is above 0 (true signal) divided by the total red pixels. M2 is a ratio of the sum of the green pixel where the red pixel is above zero (true signal) divided by the total green pixels.

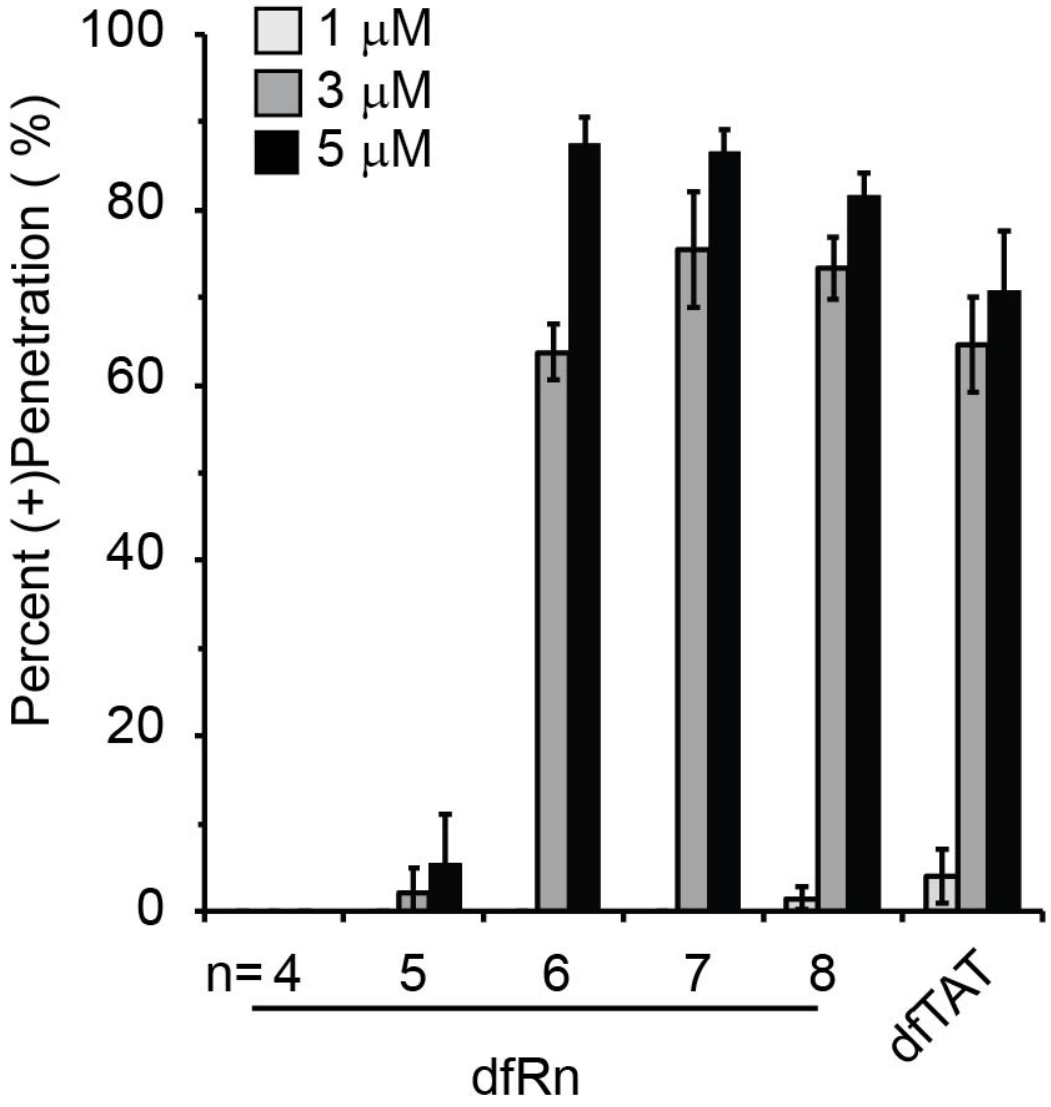

Figure 4-7 Quantitative determination of the cytosolic delivery efficiency of dfRn constructs in comparison to dfTAT as a function of peptide concentration present in the incubation media. HeLa cells were incubated with peptides (1, 3 and 5 μM) for 1 h. The percentage of cells detected as positive for penetration was established by microscopy.

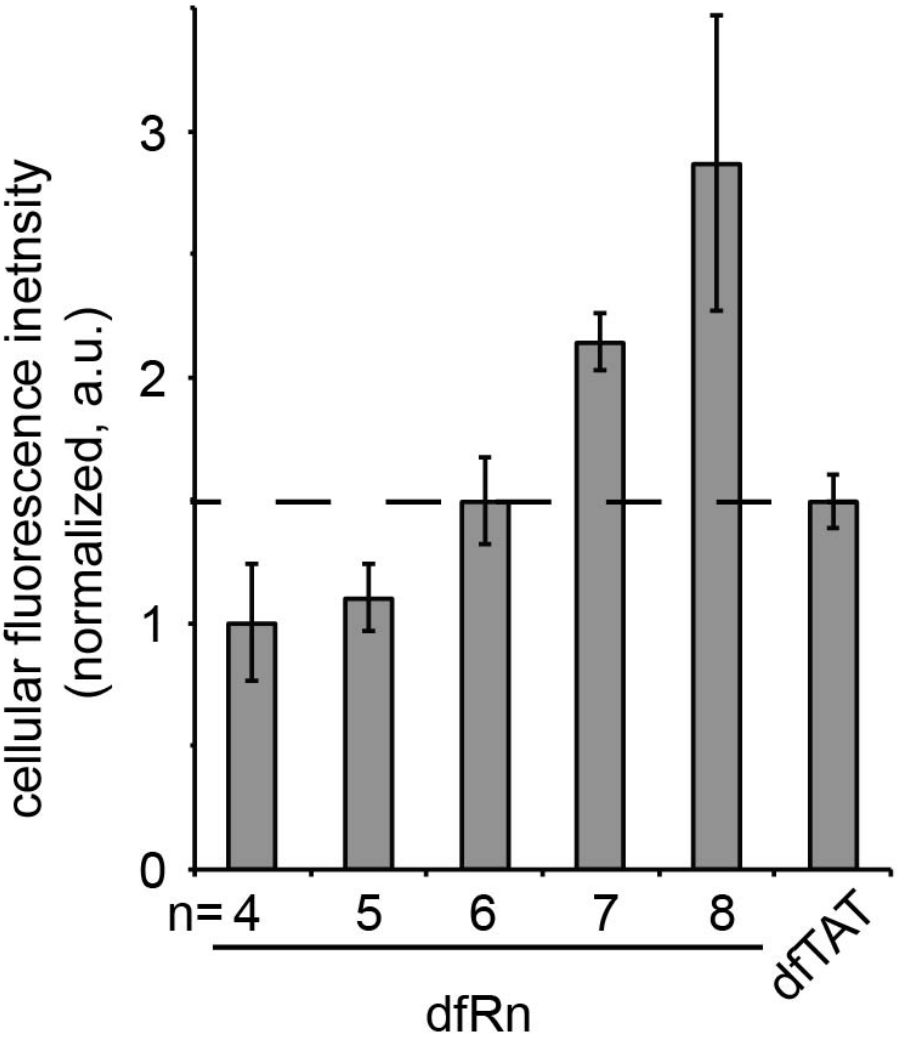

Figure 4-8 Comparison of the total cellular uptake of peptide as a function of the number of arginine. HeLa cells were incubated with peptides (5 μM). The overall amount of peptide internalized by cells (endosomal + cytosolic) was assessed by measuring the bulk fluorescence of cell lysates. All fluorescence measurements were normalized to the lowest averaged fluorescence measurements obtained (ie. dfRn where n=4).

these results suggest a threshold behavior where 12 arginine residues is a cutoff required for cytosolic access. Notably, dfTAT also contains 12 arginine residues.

4.2.4 Differences in endocytic uptake are not solely responsible for differences in cell penetration

The cytosolic penetration of dfR6, dfR7 and dfR8 is endocytosis dependent (**Figure 4-9**). Consistent with the mechanistic studies performed with dfTAT, this suggests that cytosolic penetration involves endocytic uptake followed by endosomal escape. Conceptually, the peptides dfR4 and dfR5, which stay trapped inside endosomes, could therefore fail to reach the cytosolic space because their uptake is poor and does not permit sufficient accumulation of peptide inside endosomes for escape. To test this idea, I looked for peptide incubation concentrations that would lead to similar uptake for dfR4, dfR5, and dfR6. I found that cell incubation with 20 μM dfR4 and 10 μM dfR5 yielded a peptide uptake comparable to that of 5 μM dfR6, as measured by the total fluorescence of cell lysates (**Figure 4-10**). Yet, under these conditions, dfR4 remained unable to reach the cytosol and deliver cargo into cells (**Figure 4-10**). dfR5, although slightly more active, was also unable to reproduce the activity of dfR6. Together, these results suggested that differences in how much peptide is endocytosed by cells cannot account for the differences in cytosolic penetration observed between dfR4/5 and dfR6/7/8.

Figure 4-9 dfR6, dfR7 and dfR8 penetrate the cytosol by escaping from the endocytic pathway. a) Pulse-chase assay showing the progressive cytosolic penetration of the peptides. HeLa cells were incubated with either dfR6 (5 μM), dfR7 (3 μM) or dfR8 (3 μM) for 5 min. The cells were washed and imaged with a 20X objective. The number of cells that were positive for penetration were counted at the specified time interval after delivery. b) dfR6 and dfR8 can release a peptide that is preloaded into endosomes. In experiment 1 (exp 1), cells were incubated with DEAC-k5 (20 μM) and then imaged. In exp 2, cells were incubated with DEAC-k5 for 1 h, washed and then incubated for 1 h with either dfR6 or dfR8 (5 μM). Cells were then imaged using a 100X objective. Fluorescence images represented are pseudocolored cyan for DEAC-k5 and red for TMR. Scale bars, 10 μm.

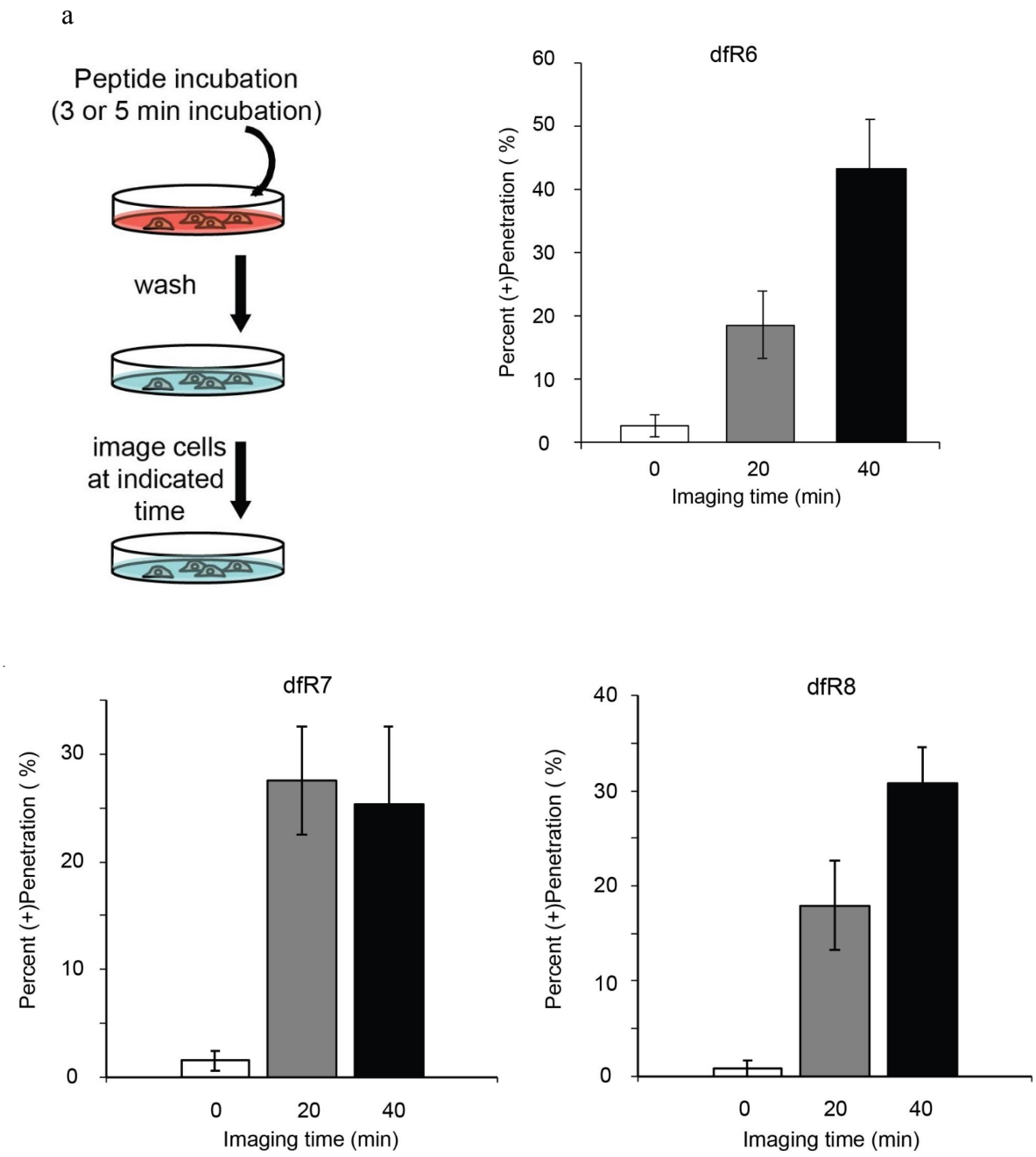

Figure 4-9 Continued.

b

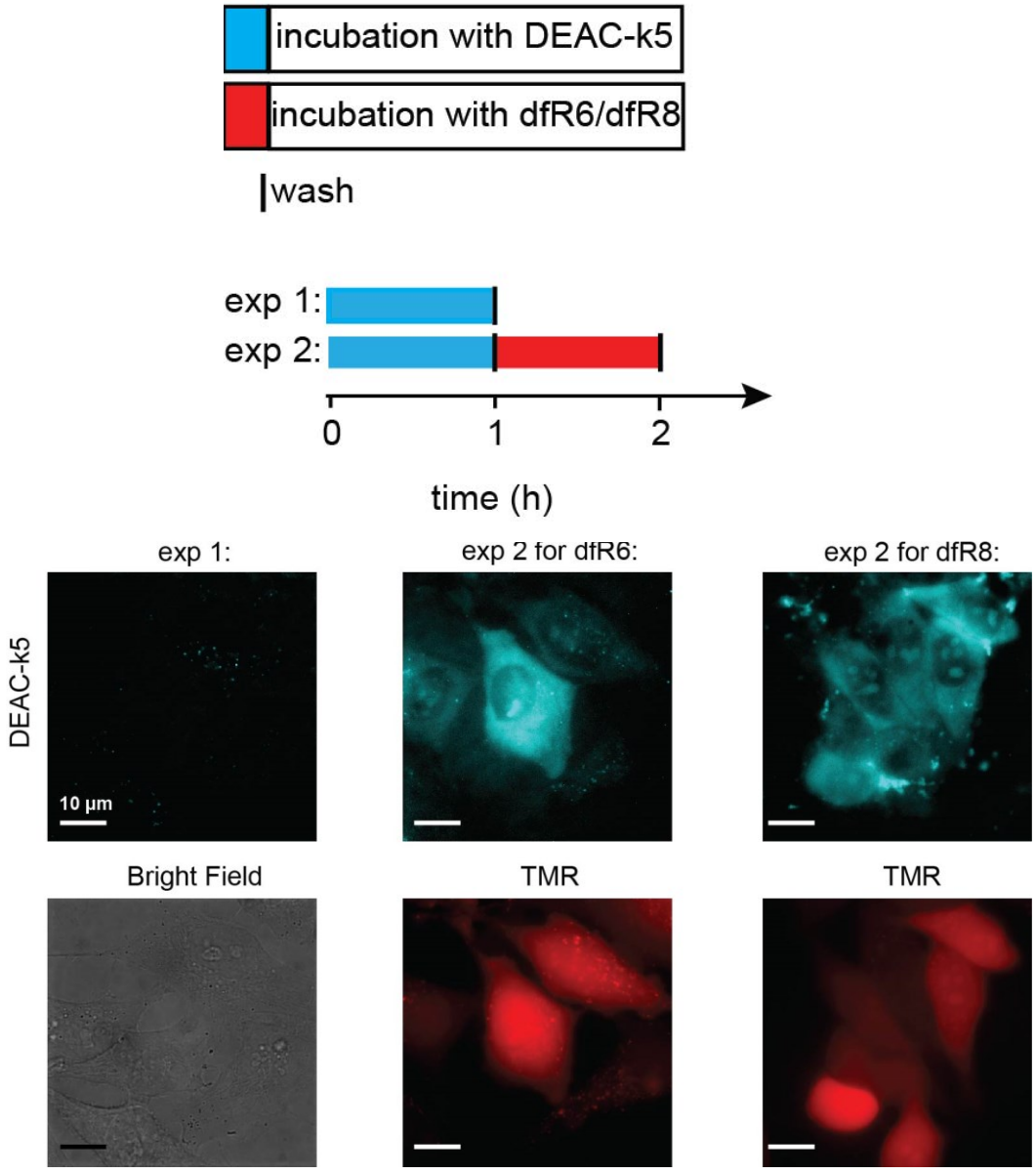

Figure 4-9 Continued.

Figure 4-10 The endocytic uptake does account for the difference observed in the endosomolytic activity of polyarginine peptide. a) Evaluation of the total cellular uptake of dfR4, dfR5 and dfR6. HeLa cells were incubated with either 20 μM dfR4, 10 μM dfR5 or 5 μM dfR6. The overall amount of peptide internalized by cells was assessed by measuring the bulk fluorescence of cell lysates. All fluorescence measurements were normalized to the lowest averaged fluorescence measurements obtained (ie. dfRn where n=4). b) Determination of the cytosolic delivery efficiency of peptides. HeLa cells were incubated with peptides dfR4, dfR5 and dfR6 as described in part a. The percentage of cells detected as positive for penetration was established by microscopy. c) dfRn constructs with the number of arginine less than 12 ($n<6$) cannot deliver cargo to the cytosolic space of cells. HeLa cells were incubated with either 20 μM of dfR4 or 5 μM dfR6 in the presence of 10 μM of DEAC-k5. Cells were washed and imaged with a 20X objective. Fluorescence images of the TMR emission at 560 nm (pseudocolored red) and CFP emission at 436 nm (pseudocolored cyan). Scale bars, 100 μm.

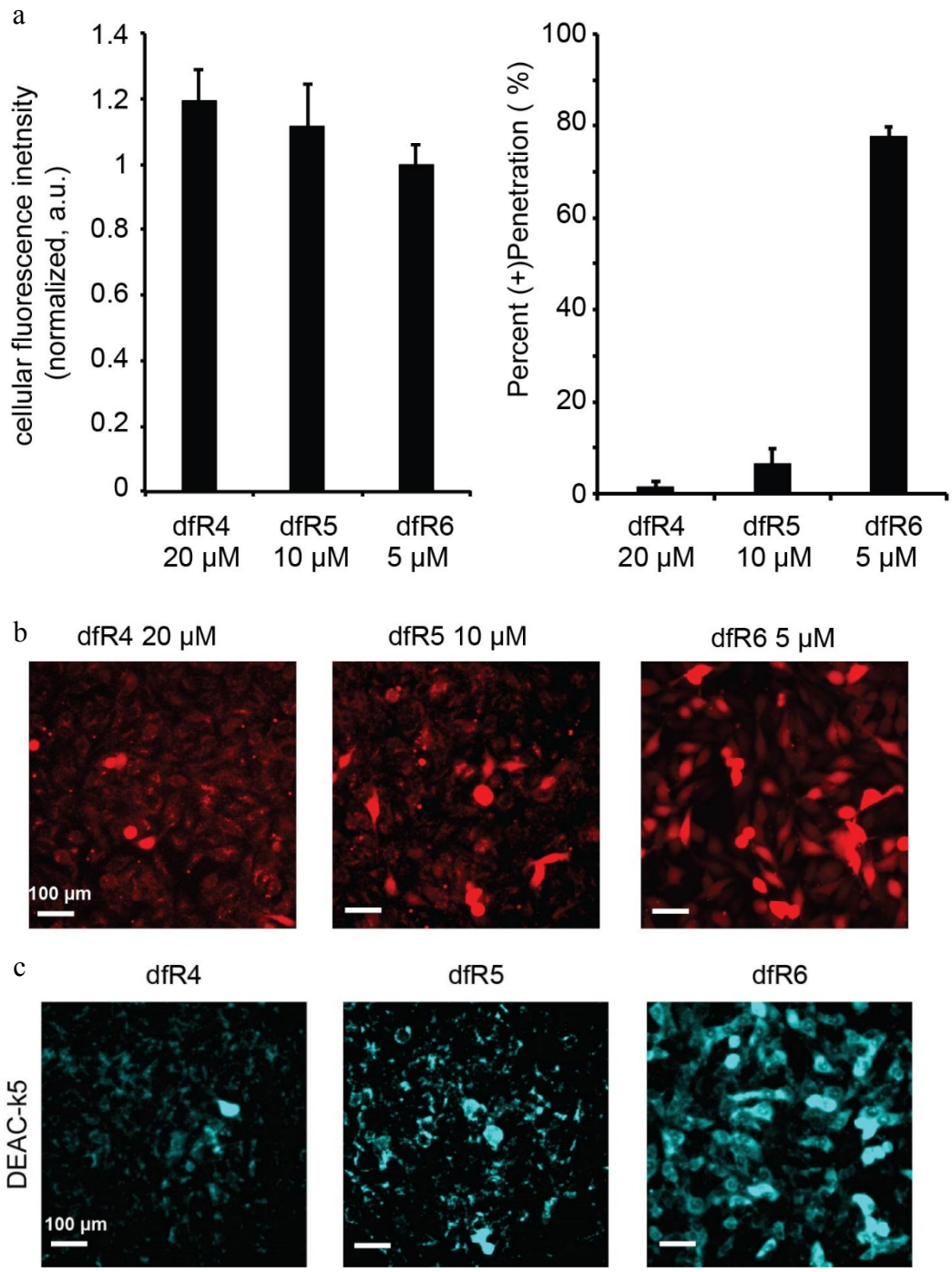

Figure 4-10 Continued.

4.2.5 A non-linear response for cell penetration of polyarginine peptides can be explained by the ability of the peptides to induce leakage of late endosomal compartments

In order to compare the membrane disruption activity of the dfRn compounds, liposomes with a lipid composition mimicking the lipid bilayers of the plasma membrane and late endosomes were prepared. The liposomes were prepared with PC:PE:chol (65:15:20) to model the plasma membrane and early endosomes (PM/E.E. LUVs) and with BMP:PC:PE (77:19:4) to model late endosomes (L.E. LUVs)[128, 288, 289]. Calcein was encapsulated inside the liposomes and peptide-induced liposome disruption was quantified by measuring calcein leakage. When incubated with PM/E.E. LUVs, the peptides dfTAT and dfRn did not cause significant leakage. However, when incubated with L.E. LUVs, dfRn peptide induced leakage in a manner linearly proportional to arginine content (R^2=0.99) (**Figure 4-11**). Notably, the activity of dfTAT was similar to that of dfR6 and dfR7, indicating again that the membrane disruption activity of dfTAT is mainly mediated by its arginine residues.

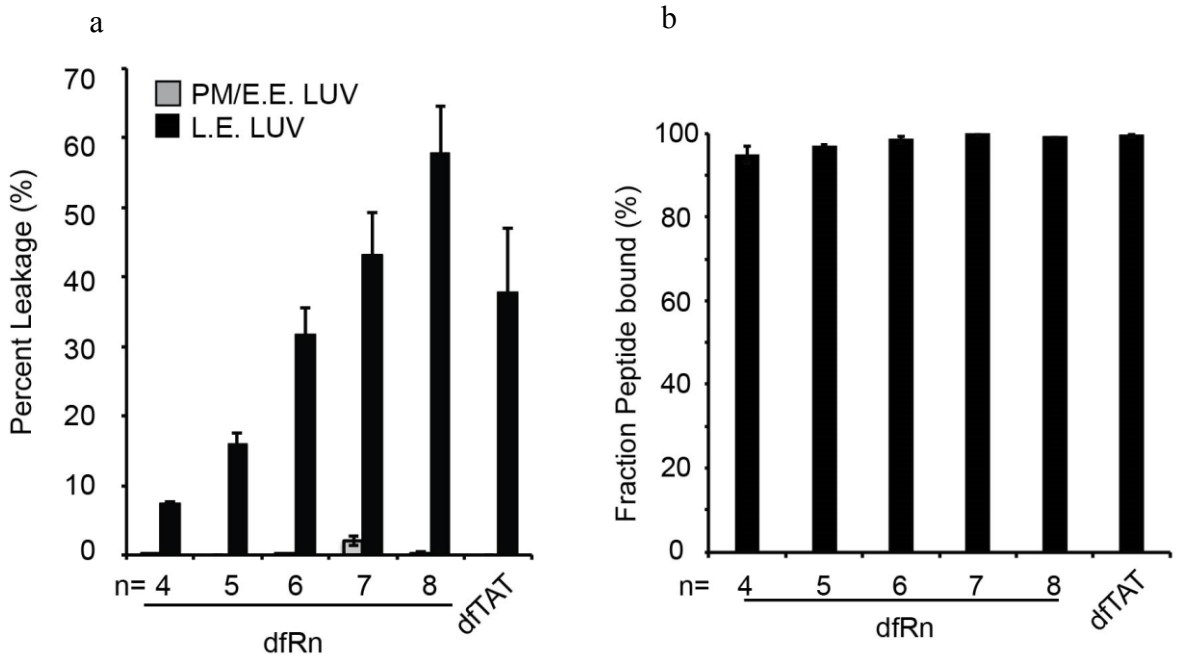

Figure 4-11 The in vitro leakageactivity of dfRn increases as a function of n. a) Comparison of liposomal leakage activity caused by dfRn constructs and dfTAT. L.E or PM mimicking liposomes (500 μM) loaded with calcein were incubated with peptides at 10 μM. The fluorescence signal of free calcein was quantified after peptide treatment. b) Determination of the affinity of dfRn and dfTAT to PM and LE LUVs. L.E or PM mimicking liposomes (500 μM) were incubated with peptides at 10 μM. The samples were spun down at 13,000 RPM and the fluorescence signal in the supernatant corresponding to the unbound peptide was quantified.

4.3 Discussion

My results indicate that the arginine residues of dfTAT account for its endocytic uptake and for its endosomal escape activity. In particular, the activities of dfTAT and dfR6 are very comparable. This would therefore suggest that the residues other than arginine, namely 4 lysine residues and 2 glutamine residues, are not contributing significantly to the cytosolic penetration of dfTAT. The data also indicate that a content of 12 arginine residues is an approximate threshold necessary for high endosomal escape efficiency. Below this threshold, the peptides tested are mostly inactive and trapped inside endosomes. In contrast, above this threshold, a clear increase in cytosolic egress is achieved. However, this was also associated with an increase in cellular toxicity at higher concentrations. Interestingly, both the endocytic uptake and the leakage activity of the dfRn peptides are proportional to the number of arginine residues present (n × 2). It is therefore likely that, in the case of shorter peptide such as dfR4 and dfR5, a relatively lower endocytic uptake and a weaker membrane disrupting activity lead to conditions under which there is simply not enough peptide inside endosomes to cause any detectable endosomal leakage. It should be noted however that the peptides tested can be partially degraded during their transit in endocytic organelles[264]. In principle, differences in their propensity for proteolysis could therefore also contribute to the non-linear cytosolic release response observed.

If dfTAT can be simplified to dfR6, why not simply use R12, a peptide with similar arginine content but with a linear structure? Interestingly, fluorescently labeled R12 CPPs have already been reported to penetrate cells[73, 297, 298]. However, these peptides seem to

enter cells by a mechanism that involves direct translocation at the plasma membrane. In our laboratory, this is a process that we have also detected and attributed in part to the membrane oxidation of cells grown under 20% oxygen (e.g. ambient air)[297]. Overall, it would appear that CPPs with different structures but with similar arginine content take different routes into the cells. Investigating how this is possible may in turn reveal how to favor specific delivery pathways. Notably, it is worth noticing that dfR6 differs form a linear R12 peptide in several ways. First, a disulfide bond separates two R6 peptides. In the context of dfTAT, I have already established that a non-reducible linker could replace this disulfide bond without causing a loss of activity, indicating that the presence of disulfide group is not necessary per se[157]. However, it is possible that the presence of a spacer between two R6 sequences is somehow making the peptide behave differently than a peptide with 12 contiguous arginine residues. Consistent with this idea, Schepartz and co-workers have reported that arginine topology played a determining role in the intracellular trafficking of minimally cationic proteins, including their endosomal escape[136]. Alternatively, it is important to note that dfR6 contains two tetramethylrhodamine moieties while the R12 previously studied were labeled with only a single copy of this fluorophore. It is therefore possible that the addition of an extra fluorophore contributes to changing how the peptides interact with cells. Overall, further structure-activity relationship studies are required to provide a more detailed molecular understanding of the parameters that dictate the behavior of these CPPs.

4.4 Material and Methods

4.4.1 Peptide design, synthesis, and purification

All peptides were synthesized on the rink amide MBHA resin (Novabiochem, San Diego, CA) by solid phase peptide synthesis (SPPS). Fmoc-Lys(Mtt)-OH, Fmoc-Lys(Boc)-OH, Fmoc-Gly-OH, Fmoc-Arg(Pbf)-OH, Fmoc-Gln(Trt)-OH, Fmoc-Cys(tbuthio)-OH (Novabiochem) were used to assemble the peptides using standard Fmoc protocols. All reactions were performed at room temperature in a SPPS vessel. Reactions were agitated using a stream of dry N_2. For each amino acid coupling, the reaction was agitated for 4 h with a mixture of Fmoc-amino acid (1.6 mmol), HBTU (Novabiochem) (1.5 mmol) and di-isopropylethylamine (DIEA) (sigma) (4.0 mmol) in dimethylformamide (DMF) (Fisher). Fmoc deprotection was performed by addition of 20% piperidine in DMF. The reaction was carried out twice: 1x 5 min followed by 1x 15 min with a DMF washing step between reactions. After generation of the linear peptidyl chain, the peptidyl-resin was washed with DMF, followed by dichloromethane (DCM) (Fisher) for storage. DEAC-k5 (D-amino acid) was synthesized by coupling five Fmoc-D-Lys(Boc)-OH. The DEAC (Anaspec) fluorophore was conjugated to the N-terminus of the peptide by reaction of DEAC, HBTU and DIEA (4, 3.9 and 10 eq.) in DMF overnight. CK(ε-NH-TMR)RnG peptides (n=4, 5, 6, 7 or 8) where generated similar to work described earlier for CK(ε-NH-TMR)TATG (L-fTAT)[157]. Briefly, the MTT group found on C(tbuthio)K(ε-NH-MTT)RnG was removed using 1% trifluoroacetic acid (TFA) (Fisher) and 2% triisopropylsilane (TIS) (Sigma) in DCM. The peptidyl-resin was washed

with both DMF and DCM between each reaction. The peptidyl-resin was then reacted with a mixture of TMR, HBTU and DIEA (4, 3.9 and 10 eq.) and allowed to react overnight. The peptidyl-resin was washed and Fmoc deprotection was performed to remove the N-terminal Fmoc moiety. To remove the tbuthio protecting group on the side chain of cysteine, the peptidyl-resin was then incubated in presence of tributylphosphine (PBU_3) (180 µL PBU_3, 500 µL DMF and DCM and 50 µL H_2O; 3 times the volume is used for a full cleavage resign>100 mg). The peptides with the remaining protecting groups were cleaved from the resin by treatment with 92.5% TFA, 2.5% H_2O, 2.5% TIS and 2.5% ethanedithiol (EDT) (Sigma) for 3h at room temperature. The crude peptides were precipitated in cold anhydrous ether (Fisher). The precipitates were resuspended in 0.1%TFA/water and lyophilized. The lyophilized product was dissolved in 0.1%TFA/water. The peptides were analyzed and purified by reverse-phase HPLC. HPLC analysis was performed on a Hewlett-Packard 1200 series instrument and an analytical Vydac C18 column (5 µm, 4 x 150 mm). The flow rate was 2 mL/min, and detection was at 214 nm and 550 nm. Semi-preparative HPLC was performed on a Vydac C18 10 x 250 mm column. The flow rate was 4 mL/min, and detection was at 214 nm and 550 nm. All runs used linear gradients of 0.1% aqueous TFA (solvent A) and 90% acetonitrile, 9.9% water, and 0.1% TFA (solvent B). The correct identity of the peptides was confirmed by electrospray ionization mass spectrometry (ESI) performed with an exactive plus orbitrap mass spectrometer instrument (Thermo Fisher Scientific).

4.4.2 Generation of dfR_n and dfK_n peptides by dimerization reactions

fRn (where n=4, 5, 6,7 or 8), fK8 and fTAT (0.3 mg, 1.5 x 10^{-4} mmol) was each dissolved in 5 mL of aerated phosphate buffer saline (PBS) at pH 7.4. The reaction was left to incubate overnight (100% yield based on HPLC analysis). dfRn (where n=4, 5, 6,7 or 8), dfK8 and dfTAT were purified using reverse-phase HPLC. Expected masses were: dfTAT: 4078.27, dfR4: 2683.48, dfR5: 2995.7, dfR6: 3307.92, dfR7: 3620.14, dfR8: 3932.36, dfK8: 3484.25. The calculated observed masses based on ESI were dfTAT: 4076.24, dfR4: 2682.36, dfR5: 2994.6, dfR6: 3306.8, dfR7: 3619.28, dfR8: 3932.16, dfK8: 3484.08.

4.4.3 Cell culture

HeLa cells (ATCC CCL-2) were grown in Dulbecco's Minimum Essential Media (DMEM, Fisher) supplemented with 10% fetal bovine serum (FBS) (Fisher) and 1X penicillin/streptomycin (P/S) (Fisher) and incubated in a humidified atmosphere containing 5% CO_2 at 37 °C.

4.4.4 Delivery of peptides into live cells

HeLa cells were seeded in an 8-well dish or a 48-well dish and were grown to 80-90% confluency in a 37°C humidified atmosphere containing 5% CO_2. The cells were washed three times with PBS and once with nrL-15. Cells were incubated with each peptide (dfRn, dfKn or dfTAT) at 37°C for 1 h (unless otherwise specified). This was

followed by washing the cells three times with L-15 supplemented with heparin (1 mg/mL) and an extra nrL-15 wash. Cells were treated with the cell impermeable nuclear stain SYTOX® BLUE or SYTOX ® GREEN to take into account cells that had a damaged plasma membrane (i.e. dead cells). Alternatively, the cell permeable Hoechst was used for nuclear staining. Cells were imaged using an inverted epifluorescence microscope (Model IX81, Olympus, Center Valley, PA) equipped with a heating stage maintained at 37 °C. Images were collected using a Rolera-MGI Plus back-illuminated EMCCD camera (Qimaging, Surrey, BC, Canada). Images were acquired using bright field imaging and three standard fluorescence filter sets: CFP (Ex = 436 ± 10 nm / Em= 480 ± 20 nm), RFP (Ex = 560 ± 20 nm / Em= 630 ± 35 nm), FITC (Ex = 488 ± 10 nm / Em= 520 ± 20 nm). For viewing and processing individual fluorescent images, the SlideBook 4.2 software (Olympus, Center Valley, PA) was used. Cells that displayed a cytosolic and nucleolar peptide staining were considered positive for cytosolic penetration (penetration(+)).The percentage of penetration (+) cells was calculated by dividing the number of cells that displaying a fluorescent nuclear staining (20X images) by the total number of cells present (acquired using bright field imaging). Cells that displayed a punctate distribution consistent with endosomal entrapment of the peptides, were considered negative for penetration and were not counted. Cells stained by SYTOX dyes were considered dead and were excluded from the analysis. For all quantitative experiments performed, an average of at least three 20X pictures were taken, representing 300-400 cells. The reproducibility of all the experiments was assessed by performing experiments with independent batches of cell cultures on three different days (i.e. biological triplicates).

4.4.5 Determination of mechanism of cellular entry

To investigate the process of cellular entry, HeLa cells were incubated in L-15 with DEAC-k5 (20 μM) for 1 h. Cells were then washed three times with PBS and then incubated with dfRn peptide (5 μM) or in nrL-15 (control cells) for 1h. Cells were washed and imaged as described earlier.

4.4.6 Quantitative determination of peptide uptake

HeLa cells were seeded in a 48-well dish and grown to 80% confluency. Cells were treated with peptides for 1h at various concentrations (range: 1-10 μM). The total amount of peptide uptake was measured by a whole cell lysate analysis. Cells were washed with heparin (1mg/mL) and then trypsinized (50 μL) for 3 min. Cells were resuspended in nrL-15 (350 μL) and centrifuged at 4°C, 2,500 rpm for 10 min. The supernatant was discarded and the cell pellet was resuspended in nrL-15 (50 μL). An aliquot from the resuspended cells (3 μL) was removed to determine the total number of cells per sample by analysis using flow cytommetry. The remainder of resuspended cells were lysed by addition of 50 μL of a lysis buffer (components: 50mM Tris, pH7.5, 2 mM EDTA, 4mM DTT, 20% Triton X-100 and protein inhibitor cocktail) and 3 min of vortexing. A volume of 70 μL of the lysed cells for each condition was placed in a 96 well plate. The fluorescence emission intensity was measured using a plate reader equipped with a fluorescence module (Ex=525, Em=580-640 nm) (GloMax®-Multi+ Detection System, Promega, Fitchburg,

WI). To normalize the aliquot of cells (3 µL) was resuspended in nrL-15 (197 µL) and the total amount of cells per samples was determined using flow cytometry.

4.4.7 Liposome Preparation

The lipids used in the experiments consisted of: 1,2-dioleoyl-s-glycero-3-phosphocholine (DOPC), 1,2-dioleoyl-sn-glycero-3-phosphoethanolamine (DOPE), sn-(3-oleoyl-2-hydroxy)-glycerol-1-phospho-sn-1'-(3'-oleoyl-2'-hydroxy-glycerol) (BMP), cholesterol (chol) (Avanti Polar Lipids). Liposomes were prepared by first transferring various volumes of lipids dissolved in chloroform (stock solutions of known concentrations) into scintillation vials. For liposomes mimicking the intraluminal late endosomes vesicles (L.E.) the molar ratios of lipids consisted of 77:19:4 BMP:PC:PE. For liposomes mimicking the plasma membrane, the lipid mixture was 65:15:20 PC:PE:Chol. The lipid film was prepared by removing the chloroform from the lipid mixture using a stream of N_2 and then placing the vial in a desiccator for 24h. A buffer containing 100 mM NaCl, 10 mM NaH_2PO_4 pH7.4, with or without 60 mM calcein was added to the lipids film for hydration. The lipids were then mixed vigorously and swelled for 1 h at 42°C under N_2 to obtain multilamellar vesicles (MLVs). For production of unilamellar vesicles (LUVs), the MLVS were extruded (20 passes) through a 100 nm pore size polycarbonate membrane (Whatman) using a Mini-Extruder (Avanti Polar Lipids). Dynamic light scattering was used to determine the average diameter size distribution of the liposomes using a Zeta Sizer (Malvern instrument). The liposomes were purified by

gel filtration using a Sephadex G-50 (GE Healthcare) column (2.5 x 17.5 cm) to separate the liposomes from free calcein. The eluate was collected in a 96 well plate and the plate was read using a Promega GloMax-Multi plate reader (Promega) at 450 nm and 750 nm corresponding to the wavelength of detection for calcein and liposome respectively.

4.4.8 Liposome leakage assays

Purified calcein-loaded LUVs were mixed with different peptides at a 1:50 peptide: lipid ratio for 1 h at room temperature in 100 mM NaCl, 10 mM NaH_2PO_4 pH5.5. Samples were centrifuged for 1 min at 4,000 rpm. To measure the amount of leaked calcein and separate soluble liposomes from released calcein, the supernatants were purified using an illustra NAP-10 Sephadex G-25 column (GE Healthcare) (the elution volumes of liposomes and free calcein were determined independently with pure samples). Fractions were collected in a 96-well plate and the fluorescence of calcein was measured using a Promega GloMax-Multi plate reader (Ex 490nm, Em 520-560nm). The percent leakage was calculated using the following equation:

$$\% \text{ Leakage} = 100 \times \frac{\mathrm{Fl_t} - \mathrm{Fl_0}}{\mathrm{Fl_{max}} - \mathrm{Fl_0}}$$

where Fl_t is the free calcein fluorescence intensity of a sample at a specific peptide:lipid ratio measured after 1 h, Fl_0 is the free calcein fluorescence intensity of a untreated sample and Fl_{max} is the free calcein fluorescence intensity of a sample after treatment with 0.2 % Triton X-100.

4.4.9 Liposome binding assays

To determine the difference in the binding affinity of peptides to LUVs of different lipid compositions. The LUVs were incubated for 1 h with either peptide at the same peptide to lipid ratio as the leakage assay (1:50) using the buffer composition of 100 mM NaCl, 10 mM NaH_2PO_4 pH 5.5. Samples were centrifuged at 13,000 rpm for 3 min. The supernatant was removed to measure the amount of unbound peptide (using the fluorescence emission of TMR). To insure that quenching due to the proximity of the TMR fluorophore in the dfTAT constructs would not affect my results, the supernatant was reduced with TCEP (50 mM). The TMR fluorescence was measured using the red channel (Ex= 525nm, Em=580-640 nm) of a Promega GloMax-Multi plate reader (Promega). The amount of peptide bound to the MLVs was determined according to the following equation:

$$P_b = P_{tot} - P$$

Where P_{total} is the amount of peptide from the supernatant in the absence of MLVs, P is the fraction of unbound peptide at a particular lipid concentration and P_b is the fraction of bound peptide at a particular lipid concentration.

5. SUMMARY AND CONCLUSIONS

dfTAT: a highly efficient cellular delivery agent

Over two decades of research in the field of macromolecular delivery have been dedicated to enhancing the endosomal escape property of CPPs. Various approaches to improving this activity have been proposed; however, to date the efficiency remains sub-optimal. Multivalency is one methodology that has been suggested. Multivalent compounds are generated by attaching multiple copies of their functional unit to a single scaffold. It has been suggested that this results in a higher local concentration of the active peptide/protein at the membrane. In this research, I used this approach to generate a dimeric version of the TAT peptide called dfTAT (dimeric fluorescent TAT) and established that it has an unprecedented level of endosomolytic activity. I show that dfTAT was able to penetrate the cytosolic space of cells more efficiently than its monomeric counterpart, TAT. Interestingly, the monomeric TAT could not recapitulate dfTAT's activity, even when the same amount of peptide was present inside the endocytic vesicles. This work, therefore, confirms the important role that multivalency plays in cellular penetration. The viability, proliferation and gene expression data show that the high endosomal disruption generated by dfTAT is well tolerated by the cells, as no negative impact was observed. This result was unexpected, since the efficient disruption of endosomes could result in the release of proteases, toxic enzymes and calcium ions into the cytosolic space of cells. It is possible that this observation is a result of the slow kinetics of the peptide release, allowing for ample of time for the cells to recuperate and

repair the disrupted membrane. Both the high endosomal escape efficiency and low toxicity, make dfTAT an ideal delivery agent, unique from what has been previously reported. I show that dfTAT can be used to efficiently deliver a variety of macromolecules inside cells. Some examples include: the biologically active enzyme TAT-Cre, the mitochondrial targeting antibody anti-ATP5a, and the transcription factor HOXB4, the latter which is important for hematopoietic stem cell expansion. I also demonstrated that the amount of HOXB4 delivered could be tightly controlled by modulating the amount of protein that was administered extracellularly. This is important for many therapeutic applications, since opposing effects have been observed by altering the dose of the molecule administered. Furthermore, multiple molecules could be administered either simultaneously or sequentially. The latter suggests that while dfTAT disrupts endocytic vesicles, it does not negatively impact this pathway. Overall, the properties mentioned make dfTAT a unique delivery agent, and unveiling the structural characteristics required for this highly efficient endosomolysis is important for developing new and improved delivery agents.

Impact of chirality and protease-resistance on endosomal escape

While multivalency was shown to clearly impact the endosomal escape efficiency of CPPs, I sought further insights into additional parameters that could influence CPP activity. In particular, I wanted to determine how CPP chirality and proteolytic degradation impacted its cell penetration property. The latter, in particular, is important many CPPs show promise as delivery tools, however upon exposure to cells or serum, CPPs are rapidly degraded. This innate property renders CPP activity less effective. One

way to overcome degradation is by substituting L-amino acids for D-amino acids. In doing so, the change in chirality results in a proteolytically stable CPP. How chirality impacts the endosomal escape property of CPPs however is not clear. This is in part due to the fact that most studied CPPs remain extremely inefficient at escaping these vesicles. Therefore, I used dfTAT as the proto-type and standard for a highly efficient endosomal reagent. I generated a reagent, D-dfTAT or D-amino acid dfTAT, which combines the parameters of inversing chirality and increasing protease resistance. I then determined that dfTAT was degraded in an hour, upon incubation with cells. However, D-dfTAT remained stable over all time points tested (over 48 h). Also, I showed that D-dfTAT, in a fashion similar to dfTAT, is capable of penetrating cells via the same endocytic route. However, by measuring the total fluorescence of a cell lysate, I determined that dfTAT was endocytosed three to four- fold higher than D-dfTAT. Conversely, under conditions in which the same amount of each peptide was found in the endosomes, D-dfTAT was more efficient at escaping the late endosome than dfTAT.

Interestingly, these findings shed light on the dependency of peptide internalization based upon peptide chirality. Conversely, *in vitro* assays using late endosomal liposomes showed no changes in lipid binding or calcein leakage between both peptides. These assays suggest that the interaction of the peptide with BMP in LE is independent of the peptide's chirality. Furthermore, my results indicate that supplementing cells with endocytic protease inhibitors increased the endosomal escape efficiency of dfTAT. Therefore, the reduced dfTAT activity observed could in part be due to the extensive degradation it experiences along the endocytic pathway. Therefore, D-

dfTAT portrays an overall enhanced endosomal escape property, which is ideal for both *in cellulo* and *in vivo* experiments. However, by performing viability and proliferation assays, I have shown that MCH58 cells treated with D-dfTAT proliferate at a slower rate than untreated or dfTAT- treated cells. Interestingly, this was not observed in HDF cells, which could be explained by a difference in the amount of peptide internalized. In order to gain detailed insights into how cells respond to the peptides, I performed a microarray analysis. Using dfTAT, I had previously shown that neither the peptide treatment nor the endosomal leakage had a negative impact on cellular proliferation. Interestingly, the D-dfTAT treatment resulted in the dysregulation of 215 and 551 genes in the HDF and MCH58 cells, respectively. Since both D-dfTAT and dfTAT penetrate the cells via the same mechanism, I attributed this difference in behavior to be attributed to the retention of D-dfTAT in the cells. This retention could result in D-dfTAT interaction with many of the cytosolic and nucleolar proteins necessary for cellular homeostasis. It is known that TAT localizes in the nucleolus due to its high positive charge. In fact, fluorescent images of cells treated with D-dfTAT show a clear nucleolar staining that persists over 48 h. This indicates that D-dfTAT could in particular be interacting with nucleic acids in this compartment, and thus be disrupting important processes. While dfTAT could have similar interactions, the peptide is rapidly degraded and therefore its effects on the cells are minimized. These results highlight that while increasing peptide stability is important to improving CPP activity, this might come at the costs of negatively impacting cellular physiology. This issue is particularly important when considering the use of CPPs for *in vivo* applications.

The role of cationic residues in endosomal escape

The importance of the arginine residues for cellular internalization in cationic-based CPPs has been established by many pioneers in the field; however, it remains to be determined whether this extends to endosomal escape. As mentioned above, this is due to the inefficient endosomal escape property of most well-studied CPPs. Therefore, I again used dfTAT as a prototype for highly endosomoloytic CPPs in an effort to answer this question. dfTAT also shares some similarities with other molecules that display enhanced endosomal escape activities. For instance, recent reports have suggested that proteins with a very high density of positive charges can escape from endosomes. This is for instance the case for supercharged GFP (scGFP), a GFP variant engineered with 36 surface exposed cationic residues (+1.3/kDa)[299]. It is also the case for viral capsid proteins that naturally display charge density as high as +2/kDa and that can either directly participate in the viral entry into host cells or that can be used to deliver exogenous cargos[300]. Notably, dfTAT, has a charge density of +4.4/kDa, may also be considered a "supercharged" species.

My work shows that the polylysine construct, dfK8, while containing the same number of positive charges as dfTAT (the monomer TAT has 6 Arg and 2 Lys, a total of 8 positive side chain charges, and therefore the dfTAT dimer would have 16 side chain positive charges), was unable to escape the endocytic pathway at any concentration tested. Conversely, dfR8 (also containing 16 side chain positive charges) recapitulated and surpassed the observed penetration activity of dfTAT. This suggests that the positive charge is not sufficient for the endosomal escape of CPPs. It appears that endosomal escape is dependent on the presence of arginine residues. This can be explained by the

bidentate nature of the arginine residue, in comparison to the monodentate lysine. For example, arginine could engage in a higher level of interaction with BMP in the late endosome, due to its ability to form two hydrogen bonds with the phosphate polar head group. However, I also observed that dfR8 was associated with cytotoxicity at higher concentrations. Interestingly, dfR8 and dfTAT contain the same number of positive charges, however differ in arginine content (dfTAT:12 Arg, dfR8: 16 Arg). It is currently unclear why dfR8 is more toxic than dfTAT and whether dfR8 expresses this deleterious effect from the outside or inside of cells or both. Similar toxicity was also observed with the dfR7 peptide. Future work will also be required to fundamentally understand why the presence of the extra arginine's result in a more toxic peptide. However, I reasoned that since dfR8 had a similar penetration activity as dfTAT, it is possible that by decreasing the amount of arginine, I could find an active compound that was not cytotoxic. In fact, dfR6 (12 Arg per dimer), a peptide containing the same total number of arginines as dfTAT, was able to recapitulate its penetration activity and shows similar extremely low cytotoxicity. Interestingly, peptides with an arginine content less than 12 (per dimer) such as dfR4 (8 arginines) and dfR5 (10 arginines) remain entrapped in the endocytic pathway at any concentration tested. Furthermore, both the endocytic uptake and the endosomal release activity of the dfRn peptides was proportional to the number of arginine residues present in the peptide. This suggested that the peptide constructs such as dfR4 and dfR5 (total arginine content less than 12) has a lower endocytic uptake and a weaker membrane disrupting activity which ultimately results in not enough peptide present in the endosome for sufficient endosomal leakage. Interestingly, even at concentration inside the

endosomes in which dfR4 and dfR5 were higher than dfR6, dfR4 and dfR5 still remained entrapped endosomes while dfR6 escapes and reaches the cytosolic space. This data showed that peptides with less than 12 arginines are weak at disrupting membranes and it endosomal escape is not simply dependent on the concentration of peptide present. The number of arginine residues per peptide play an important role in the endosomal escape activity. The *in cellulo* assays were also complemented with an *in vitro* liposome leakage assay. My results show that the leakage of these liposomes is dependent on the peptides total arginine content. This indicates that there is a minimum amount of arginine required in the peptide to interact with BMP and result in leakage.

Current model for dfTAT mechanism and implications

Taken together, my work suggests that chirality plays an important role in cell surface internalization. However, my data also demonstrates that the exact peptide sequence is not necessary. For example, dfTAT is comprised of six noncontiguous arginines per monomer (12 per dimer) and dfR6 contains the same number of arginines in a contiguous stretch, are internalized with the same efficiency. At first glance, this data might seem contradictory. In particular one might ask how the interaction of the peptide could depend on chirality but not on the specific peptide sequence. The uptake of CPPs has been reported to involve interactions with HSPGs on the cell surface. However, it has been reported that the interaction of the CPP with heparan sulfate (HS) is independent of chirality[199]. Therefore, I hypothesize that in addition to HS, there are co-attachment factors or receptor proteins that may mediate the internalization of cationic CPPs inside cells. In particular, the interaction with these receptors would be dependent on stereochemistry.

This suggests that dfTAT's cellular entry occurs via two mutually inclusive pathways: chirality dependent and independent. In support of this hypothesis, Futaki and colleagues used a photo- crosslinking approach to demonstrate that the CPPs R8 and R12 interact with Syndecan-4 and CXCR4 receptors, respectively[105, 301]. These receptors have also been shown to trigger endocytosis. Hence, I concluded that D-dfTAT triggers endocytosis via its interaction with HS. However, it cannot interact with the chiral-dependent protein receptors involved in endocytosis. This decreases the total amount of D-dfTAT entering cells to a greater extent than does dfTAT, since one pathway is essentially shut down. To understand how the receptor is sequence independent, I hypothesized that the peptides would adopt a secondary structure that exposes the minimum recognition motif required for the peptide to activate the receptor for endocytosis. The minimum number of arginines that would be required for binding would be arginine number two through six on each monomer of dfTAT (TAT=$R_1XXR_2R_3XR_4R_5R_6$). This would suggest that in dfR6, the third arginine in each monomer would not be involved in this interaction (R_6=$R_1R_2R_3R_4R_5R_6$). This $R_2R_3XR_4R_5R_6$ construct would be the minimum motif per monomer required for activation of the protein receptor. Furthermore, dfR7 and dfR8 result in enhanced internalization because the extra arginines provide surplus electrostatic interactions in addition to the minimum required sequence. This results in a higher affinity of dfR7/8 to the protein receptor. Future structural analysis of the peptide constructs with membranes would be required to test this hypothesis.

After internalization, dfTAT is initially entrapped inside endocytic vesicles. dfTAT travels along the endocytic pathway and reaches the late endosome. Experiments

have shown that dfTAT escapes from the late endosome by interaction with BMP. By altering dfTAT's chirality using D-amino acid (Chapter 3), I was able to show that the interaction of dfTAT with BMP is independent of chirality. Both dfTAT and D-dfTAT bind and cause the leakage of liposomes containing high BMP content to a similar extent. Therefore, this interaction BMP/dfTAT interaction would presumably be an electrostatic interaction of the phosphate backbone with the positively charged arginine residues. My work also highlights the importance of the 12 total arginines found in dfTAT, which are necessary for its endosomolytic activity. Furthermore, my data shows that dfTAT is degraded by proteases along the endocytic pathway that ultimately diminish its endosomolytic activity. dfTAT is also degraded in the cytosolic space of cells. It is currently unknown which proteases or pathways are occurring in the cells that result in the degradation of dfTAT. Identification of these process will be important as they can be modulated to enhance dfTAT's *in cellulo* activity. However, it is important to note that the susceptibility of dfTAT to degradation could be an important and ideal feature. My work shows that cells treated with dfTAT shows no observable impact on the cell's physiology or transcriptional regulation. On the contrary, the non-degradable version D-dfTAT shows a dramatic negative impact on the cells growth and transcriptome levels. Future work will be necessary to identify peptides that are proteolytically resistant inside endosomes (which results in increased endosomolysis), however are readily degraded in the cytosolic space.

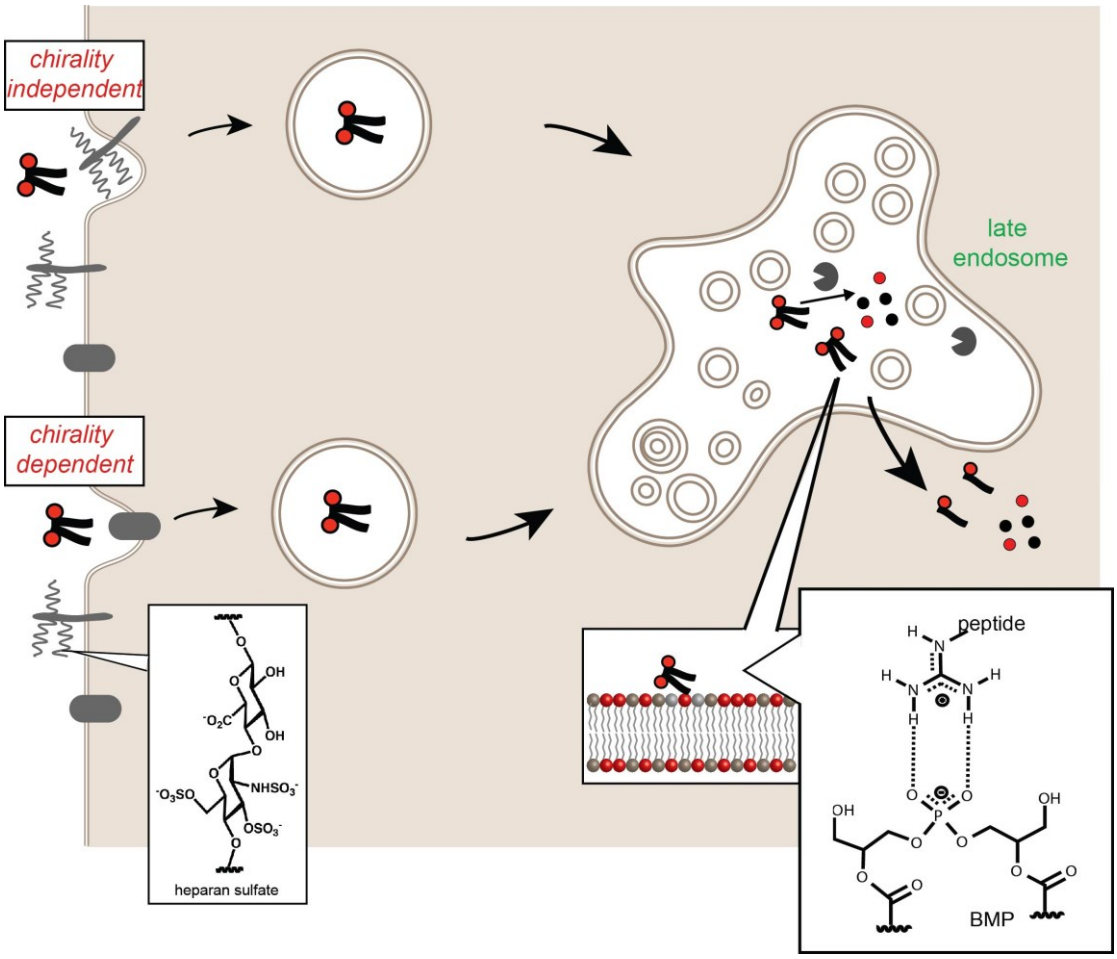

Figure 5-1 Model of dfTAT entry and escape from the endocytic pathway. dfTAT enters cells via two simultaneous pathways: Chirality independent and Chirality dependent. In the first pathway, dfTAT interacts electrostatically with the sulfates and carboxylates on Heparan sulfate present on the cell surface. In the chirality dependent pathway, it is possible that open interaction with the membrane a conformational change in dfTAT allows for a chirality dependent interaction with proteins found on the cell surface. In both scenarios, an induction of endocytosis occurs, in which dfTAT is initially entrapped inside endocytic vesicles until reaching the late endosomes. dfTAT escapes from the late endosome via electrostratic interaction with BMP and this interaction is independent of peptide chirality. Furthermore, due to proteases found along the endocytic pathway dfTAT is degraded inside endosomes and is further degraded in the cytosolic space. The intracellular degradation of this peptide is important as it results in a peptide that shows no observed impact on the cell's physiology.

Future work

As described above, experiments designed to determine the structure of dfTAT and the identification of its cell-surface membrane interacting partners are necessary to gain further insight into the mechanism of dfTAT's cellular penetration. In addition, studies are necessary to further elucidate the structural characteristics that are important for dfTAT's activity.

The work detailed in this thesis is part of a broader project that aims at establishing the structure-activity relationships that will reveal the molecular properties required for efficient endosomal escape. This is work that I have started as part of my thesis project however additional work is still required. The original working hypothesis for dfTAT was that multivalency (the number of peptide copies greater than one), high arginine-content, close proximity between each CPP copy, and presence of hydrophobic moieties contribute to it's high endosomolytic activity. While I have shown in this thesis that in fact multivalency and high arginine content play a role, other parameters remain to be identified. To test this hypothesis, a focused library of peptides based on the dfTAT prototype will need to be synthesized in which each parameter is varied. The peptides will then be characterized based on their cellular penetration properties. This will ultimately lead to a deeper understanding of the molecular features that are important to achieve efficient escape from endosomes. This knowledge is critical because it will lay a solid foundation for the rationale design of delivery agents with improved therapeutic value.

Future work is necessary to test 1) the effect of the fluorophore on dfTAT's activity 2) the effect of the disulfide bond linker between the two TAT copies 3) the effect of the position of the fluorophore and linker with respect to one another.

1) The effect of the TMR fluorophore

Fluorophore substitution

dfTAT contains two tetramethylrodamine fluorophores each conjugated to the side chain of a lysine amino acid (see table below). The TMR fluorophore was initially conjugated to the TAT peptide as a means to visualize the peptide inside cells using fluorescence microscopy. One hypothesis is that TMR plays an important role in the endosomolytic activity of dfTAT. To test this hypothesis, replacing the TMR fluorophore and conjugating other known fluorophores (Eg. Fluorescein (FL) and 7-Diethylaminocoumarin-3-carboxylic acid (DEAC)) in place of it could allow one to determine the importance of the fluorophore. In addition to giving insight into the role of TMR in dfTAT's activity, this study will be extremely valuable as it could provide a variety of fluorescently labeled, highly endosomolytic CPPs with different fluorescence emission wavelengths. This is important for delivery of probes that could be labeled with fluorophores that emit at a wavelength similar to TMR. Establishing whether TMR could be replaced with other fluorophore could increase the applications of this delivery methodology.

Replace the fluorophore for hydrophobic amino acids

TMR is composed of multiple aromatic rings in its structure, it is possible that the hydrophobicity of this molecule could play a role in dfTAT's endosomolytic activity. To test this hypothesis, the TMR fluorophore in dfTAT could be replaced with aromatic amino acids (Phe, Tyr, Trp). These residues are ideal because of the presence of the aromatic ring and their hydrophobic nature. Furthermore, these are naturally occurring amino acid which make them non-traceable and more attractive as therapeutic tools.

2) The effect of the linker

It has been postulated that multimerization of CPPs might increase membrane activity by an avidity effect. Attaching several copies of TAT in close proximity could indeed create a high local concentration of peptide at the sites where it interacts with the membrane. However, how proximity between peptides affects activity is not understood. To address this issue, Bis-maleimide (BM) linkers (Pierce) of various length can be used to connect two CK(TMR)TAT (BMOE, BMDB, BMB, BMH contain 2,4,5,6 methylenes, respectively; BM(PEG)2 and BM(PEG)3 contain 2- and 3-unit polyethylene glycol spacers). One possible issue that might arise when introducing linkers of different lengths is that other factors, such as hydrophobicity, will also be altered. To address this issue, linkers of similar length but of different chemical structures will be compared (e.g. BMH vs BM(PEG)2). Furthermore, since these linkers are non-cleavable a control construct will be generated similar to dfTAT however not linked via disulfide bonds (eg. CK(TMR)TAT can be conjugated to I-CH2-CO-K(TMR)TAT. This construct will not contain a cleavable

disulfide bond but will have approximately the same linker length between the two monomer TAT copies). Currently, the BMOE-linked CK(TMR)TAT has been generated and shows efficient cellular penetration activity (Chapter 2), however further quantitative studies are required to compare it's efficiency to dfTAT.

3) The effect of linker and fluorophore position

dfTAT was synthesized with the CysLys(TMR) groups at the N-terminus. A working hypothesis is that the disulfide bond formed brings two Lys(TMR) moieties in close proximity, creating a hydrophobic "warhead" attached to two hydrophilic peptides. Whether this configuration is important for cell penetration is unknown. Test will be required to test the working hypothesis by shuffling the position of the Cys and Lys(TMR) residues.

As part of my thesis work, I have generated many of the reagents shown in Figure 5-2 below. Future work will be required to test the working hypothesis mentioned above and compare the efficiency of these modified peptides in comparision to the dfTAT prototype.

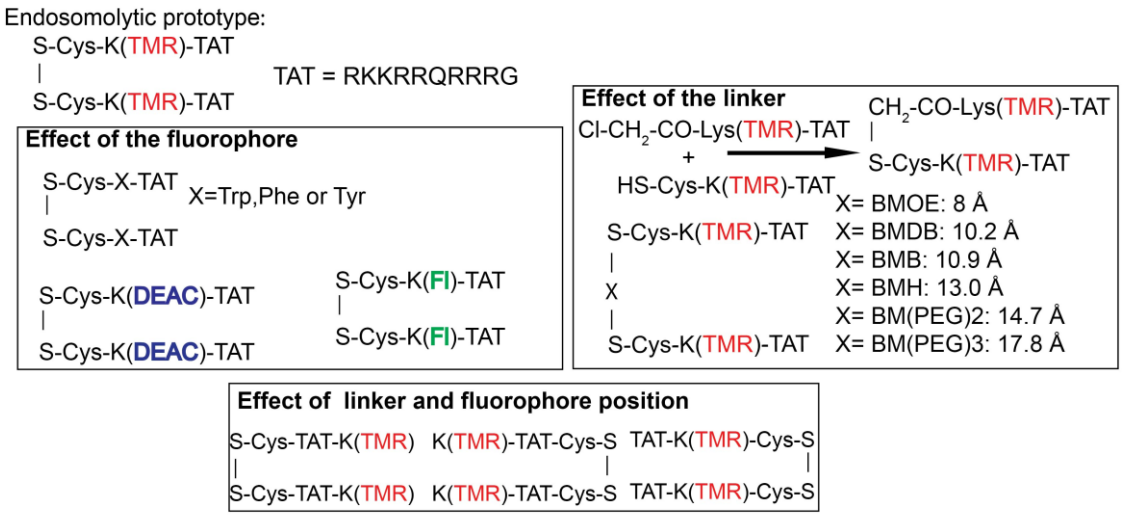

Figure 5-2 Design of future dfTAT analogues.

REFERENCES

1. Pan, C., Lu, B., Chen, H. & Bishop, C.E. Reprogramming human fibroblasts using HIV-1 TAT recombinant proteins OCT4, SOX2, KLF4 and c-MYC. *Molecular Biology Reports* **37**, 2117-2124 (2010).

2. Kim, T.K. & Eberwine, J.H. Mammalian cell transfection: the present and the future. *Analytical and Bioanalytical Chemistry* **397**, 3173-3178 (2010).

3. McNeil, P.L., Murphy, R.F., Lanni, F. & Taylor, D.L. A method for incorporating macromolecules into adherent cells. *J Cell Biol* **98**, 1556-1564 (1984).

4. Ortiz, D., Baldwin, M.M. & Lucas, J.J. Transient correction of genetic defects in cultured animal cells by introduction of functional proteins. *Mol Cell Biol* **7**, 3012-3017 (1987).

5. Chakrabarti, R., Wylie, D.E. & Schuster, S.M. Transfer of monoclonal antibodies into mammalian cells by electroporation. *J Biol Chem* **264**, 15494-15500 (1989).

6. Prior, T.I., FitzGerald, D.J. & Pastan, I. Barnase toxin: a new chimeric toxin composed of pseudomonas exotoxin A and barnase. *Cell* **64**, 1017-1023 (1991).

7. Prior, T.I., FitzGerald, D.J. & Pastan, I. Translocation mediated by domain II of Pseudomonas exotoxin A: transport of barnase into the cytosol. *Biochemistry* **31**, 3555-3559 (1992).

8. Renneisen, K., Leserman, L., Matthes, E., Schroder, H.C. & Muller, W.E. Inhibition of expression of human immunodeficiency virus-1 in vitro by antibody-targeted liposomes containing antisense RNA to the env region. *J Biol Chem* **265**, 16337-16342 (1990).

9. van den Boorn, J.G., Schlee, M., Coch, C. & Hartmann, G. SiRNA delivery with exosome nanoparticles. *Nat Biotechnol* **29**, 325-326 (2011).

10. Kaczmarczyk, S.J., Sitaraman, K., Young, H.A., Hughes, S.H. & Chatterjee, D.K. Protein delivery using engineered virus-like particles. *Proc Natl Acad Sci U S A* **108**, 16998-17003 (2011).

11. Fawell, S. et al. Tat-mediated delivery of heterologous proteins into cells. *Proc Natl Acad Sci U S A* **91**, 664-668 (1994).

12. Patel, L.N., Zaro, J.L. & Shen, W.C. Cell penetrating peptides: intracellular pathways and pharmaceutical perspectives. *Pharm Res* **24**, 1977-1992 (2007).

13. Frankel, A.D. & Pabo, C.O. Cellular uptake of the tat protein from human immunodeficiency virus. *Cell* **55**, 1189-1193 (1988).

14. Green, M. & Loewenstein, P.M. Autonomous functional domains of chemically synthesized human immunodeficiency virus tat trans-activator protein. *Cell* **55**, 1179-1188 (1988).

15. Mann, D.A. & Frankel, A.D. Endocytosis and targeting of exogenous HIV-1 Tat protein. *EMBO J* **10**, 1733-1739 (1991).

16. Vivès, E., Brodin, P. & Lebleu, B. A Truncated HIV-1 Tat Protein Basic Domain Rapidly Translocates through the Plasma Membrane and Accumulates in the Cell Nucleus. *Journal of Biological Chemistry* **272**, 16010-16017 (1997).

17. Bechara, C. & Sagan, S. Cell-penetrating peptides: 20 years later, where do we stand? *FEBS Letters* **587**, 1693-1702 (2013).

18. Milletti, F. Cell-penetrating peptides: classes, origin, and current landscape. *Drug Discovery Today* **17**, 850-860 (2012).

19. Nishikawa, M. et al. Induction of Tumor-specific Immune Response by Gene Transfer of Hsp70-cell-penetrating Peptide Fusion Protein to Tumors in Mice. *Mol Ther* **18**, 421-428 (2009).

20. Deshayes, S., Morris, M.C., Divita, G. & Heitz, F. Interactions of amphipathic CPPs with model membranes. *Biochimica et Biophysica Acta (BBA) - Biomembranes* **1758**, 328-335 (2006).

21. Derossi, D., Joliot, A.H., Chassaing, G. & Prochiantz, A. The third helix of the Antennapedia homeodomain translocates through biological membranes. *Journal of Biological Chemistry* **269**, 10444-10450 (1994).

22. Pooga, M., Hällbrink, M., Zorko, M., Langel, U. & lo Cell penetration by transportan. *The FASEB Journal* **12**, 67-77 (1998).

23. Morris, M.C., Depollier, J., Mery, J., Heitz, F. & Divita, G. A peptide carrier for the delivery of biologically active proteins into mammalian cells. *Nat Biotech* **19**, 1173-1176 (2001).

24. Montrose, K., Yang, Y., Sun, X., Wiles, S. & Krissansen, G.W. Xentry, a new class of cell-penetrating peptide uniquely equipped for delivery of drugs. *Sci. Rep.* **3** (2013).

25. Crombez, L. et al. A New Potent Secondary Amphipathic Cell-penetrating Peptide for siRNA Delivery Into Mammalian Cells. *Mol Ther* **17**, 95-103 (2008).

26. Lorents, A. et al. Cell-penetrating Peptides Split into Two Groups Based on Modulation of Intracellular Calcium Concentration. *Journal of Biological Chemistry* **287**, 16880-16889 (2012).

27. Munyendo, W.L., Lv, H., Benza-Ingoula, H., Baraza, L.D. & Zhou, J. Cell Penetrating Peptides in the Delivery of Biopharmaceuticals. *Biomolecules* **2**, 187-202 (2012).

28. Li, W., Nicol, F. & Szoka Jr, F.C. GALA: a designed synthetic pH-responsive amphipathic peptide with applications in drug and gene delivery. *Advanced Drug Delivery Reviews* **56**, 967-985 (2004).

29. Oehlke, J. et al. Cellular uptake of an α-helical amphipathic model peptide with the potential to deliver polar compounds into the cell interior non-endocytically. *Biochimica et Biophysica Acta (BBA) - Biomembranes* **1414**, 127-139 (1998).

30. Taylor, B.N. et al. Noncationic Peptides Obtained From Azurin Preferentially Enter Cancer Cells. *Cancer Research* **69**, 537 (2009).

31. Schafmeister, C.E., Po, J. & Verdine, G.L. An All-Hydrocarbon Cross-Linking System for Enhancing the Helicity and Metabolic Stability of Peptides. *Journal of the American Chemical Society* **122**, 5891-5892 (2000).

32. Wender, P.A. et al. The design, synthesis, and evaluation of molecules that enable or enhance cellular uptake: peptoid molecular transporters. *Proc Natl Acad Sci U S A* **97**, 13003-13008 (2000).

33. Mitchell, D.J., Kim, D.T., Steinman, L., Fathman, C.G. & Rothbard, J.B. Polyarginine enters cells more efficiently than other polycationic homopolymers. *J Pept Res* **56**, 318-325 (2000).

34. Futaki, S. et al. Arginine-rich peptides. An abundant source of membrane-permeable peptides having potential as carriers for intracellular protein delivery. *J Biol Chem* **276**, 5836-5840 (2001).

35. Richard, J.P. et al. Cell-penetrating peptides. A reevaluation of the mechanism of cellular uptake. *J Biol Chem* **278**, 585-590 (2003).

36. Vives, E., Richard, J.P., Rispal, C. & Lebleu, B. TAT peptide internalization: seeking the mechanism of entry. *Curr Protein Pept Sci* **4**, 125-132 (2003).

37. Thoren, P.E. et al. Uptake of analogs of penetratin, Tat(48-60) and oligoarginine in live cells. *Biochem Biophys Res Commun* **307**, 100-107 (2003).

38. Luedtke, N.W., Carmichael, P. & Tor, Y. Cellular uptake of aminoglycosides, guanidinoglycosides, and poly-arginine. *J Am Chem Soc* **125**, 12374-12375 (2003).

39. Shin, M.C. et al. Cell-penetrating peptides: achievements and challenges in application for cancer treatment. *Journal of biomedical materials research. Part A* **102**, 575-587 (2014).

40. Lee, Y.-J., Erazo-Oliveras, A. & Pellois, J.-P. Delivery of macromolecules into live cells by simple co-incubation with a peptide. *Chembiochem : a European journal of chemical biology* **11**, 325-330 (2010).

41. Kim, D.T. et al. Introduction of soluble proteins into the MHC class I pathway by conjugation to an HIV tat peptide. *J Immunol* **159**, 1666-1668 (1997).

42. Nagy, A. Cre recombinase: the universal reagent for genome tailoring. *Genesis* **26**, 99-109 (2000).

43. Kim, D. et al. Generation of Human Induced Pluripotent Stem Cells by Direct Delivery of Reprogramming Proteins. *Cell Stem Cell* **4**, 472-476 (2009).

44. Takahashi, K. & Yamanaka, S. Induction of Pluripotent Stem Cells from Mouse Embryonic and Adult Fibroblast Cultures by Defined Factors. *Cell* **126**, 663-676 (2006).

45. Ramakrishna, S. et al. Gene disruption by cell-penetrating peptide-mediated delivery of Cas9 protein and guide RNA. *Genome Res* **24**, 1020-1027 (2014).

46. Horvath, P. & Barrangou, R. CRISPR/Cas, the Immune System of Bacteria and Archaea. *Science* **327**, 167 (2010).

47. Wiedenheft, B., Sternberg, S.H. & Doudna, J.A. RNA-guided genetic silencing systems in bacteria and archaea. *Nature* **482**, 331-338 (2012).

48. Hemmi, H. et al. A Toll-like receptor recognizes bacterial DNA. *Nature* **408**, 740-745 (2000).

49. Wagner, H. Toll meets bacterial CpG-DNA. *Immunity* **14**, 499-502 (2001).

50. Gaj, T., Guo, J., Kato, Y., Sirk, S.J. & Barbas, C.F. Targeted gene knockout by direct delivery of zinc-finger nuclease proteins. *Nat Meth* **9**, 805-807 (2012).

51. Liu, J., Gaj, T., Patterson, J.T., Sirk, S.J. & Barbas, C.F., 3rd Cell-penetrating peptide-mediated delivery of TALEN proteins via bioconjugation for genome engineering. *PLoS One* **9**, e85755 (2014).

52. Whitehead, K.A., Langer, R. & Anderson, D.G. Knocking down barriers: advances in siRNA delivery. *Nat Rev Drug Discov* **8**, 129-138 (2009).

53. Glover, D.J., Lipps, H.J. & Jans, D.A. Towards safe, non-viral therapeutic gene expression in humans. *Nat Rev Genet* **6**, 299-310 (2005).

54. Eguchi, A. et al. Efficient siRNA delivery into primary cells by a peptide transduction domain-dsRNA binding domain fusion protein. *Nat Biotechnol* **27**, 567-571 (2009).

55. Lebleu, B. et al. Cell penetrating peptide conjugates of steric block oligonucleotides. *Advanced Drug Delivery Reviews* **60**, 517-529 (2008).

56. Kole, R., Vacek, M. & Williams, T. Modification of alternative splicing by antisense therapeutics. *Oligonucleotides* **14**, 65-74 (2004).

57. Krutzfeldt, J. et al. Silencing of microRNAs in vivo with 'antagomirs'. *Nature* **438**, 685-689 (2005).

58. Kilk, K. et al. Targeting of antisense PNA oligomers to human galanin receptor type 1 mRNA. *Neuropeptides* **38**, 316-324 (2004).

59. Wolf, Y. et al. Structural Requirements for Cellular Uptake and Antisense Activity of Peptide Nucleic Acids Conjugated with Various Peptides. *Biochemistry* **45**, 14944-14954 (2006).

60. Shiraishi, T., Pankratova, S. & Nielsen, P.E. Calcium Ions Effectively Enhance the Effect of Antisense Peptide Nucleic Acids Conjugated to Cationic Tat and Oligoarginine Peptides. *Chemistry & Biology* **12**, 923-929 (2005).

61. Schwarze, S.R., Ho, A., Vocero-Akbani, A. & Dowdy, S.F. In vivo protein transduction: delivery of a biologically active protein into the mouse. *Science* **285**, 1569-1572 (1999).

62. McCormick, F. Cancer gene therapy: fringe or cutting edge? *Nat Rev Cancer* **1**, 130-141 (2001).

63. Hupp, T.R., Sparks, A. & Lane, D.P. Small peptides activate the latent sequence-specific DNA binding function of p53. *Cell* **83**, 237-245 (1995).

64. Snyder, E.L., Meade, B.R., Saenz, C.C. & Dowdy, S.F. Treatment of terminal peritoneal carcinomatosis by a transducible p53-activating peptide. *PLoS Biol* **2**, E36 (2004).

65. Michl, J. et al. PNC-28, a p53-derived peptide that is cytotoxic to cancer cells, blocks pancreatic cancer cell growth in vivo. *Int J Cancer* **119**, 1577-1585 (2006).

66. Hosotani, R. et al. Trojan p16 peptide suppresses pancreatic cancer growth and prolongs survival in mice. *Clin Cancer Res* **8**, 1271-1276 (2002).

67. Araki, D. et al. Cell-penetrating D-isomer peptides of p53 C-terminus: long-term inhibitory effect on the growth of bladder cancer. *Urology* **75**, 813-819 (2010).

68. Perea, S.E. et al. Antitumor Effect of a Novel Proapoptotic Peptide that Impairs the Phosphorylation by the Protein Kinase 2 (Casein Kinase 2). *Cancer Research* **64**, 7127 (2004).

69. Jo, D., Liu, D., Yao, S., Collins, R.D. & Hawiger, J. Intracellular protein therapy with SOCS3 inhibits inflammation and apoptosis. *Nat Med* **11**, 892-898 (2005).

70. Graham, S.H., Chen, J. & Clark, R.S. Bcl-2 family gene products in cerebral ischemia and traumatic brain injury. *J Neurotrauma* **17**, 831-841 (2000).

71. Rizzuti, M., Nizzardo, M., Zanetta, C., Ramirez, A. & Corti, S. Therapeutic applications of the cell-penetrating HIV-1 Tat peptide. *Drug Discov Today* **20**, 76-85 (2015).

72. Puri, V. et al. Cholesterol modulates membrane traffic along the endocytic pathway in sphingolipid-storage diseases. *Nat Cell Biol* **1**, 386-388 (1999).

73. Hirose, H. et al. Transient Focal Membrane Deformation Induced by Arginine-rich Peptides Leads to Their Direct Penetration into Cells. *Molecular Therapy* **20**, 984-993 (2012).

74. Jiang, T. et al. Tumor imaging by means of proteolytic activation of cell-penetrating peptides. *Proceedings of the National Academy of Sciences of the United States of America* **101**, 17867-17872 (2004).

75. Derossi, D. et al. Cell internalization of the third helix of the Antennapedia homeodomain is receptor-independent. *J Biol Chem* **271**, 18188-18193 (1996).

76. Lundin, P. et al. Distinct uptake routes of cell-penetrating peptide conjugates. *Bioconjug Chem* **19**, 2535-2542 (2008).

77. Jones, A.T. & Sayers, E.J. Cell entry of cell penetrating peptides: tales of tails wagging dogs. *J Control Release* **161**, 582-591 (2012).

78. Trehin, R., Krauss, U., Beck-Sickinger, A.G., Merkle, H.P. & Nielsen, H.M. Cellular uptake but low permeation of human calcitonin-derived cell penetrating peptides and Tat(47-57) through well-differentiated epithelial models. *Pharm Res* **21**, 1248-1256 (2004).

79. Foerg, C., Ziegler, U., Fernandez-Carneado, J., Giralt, E. & Merkle, H.P. Differentiation restricted endocytosis of cell penetrating peptides in MDCK cells corresponds with activities of Rho-GTPases. *Pharm Res* **24**, 628-642 (2007).

80. Barany-Wallje, E., Gaur, J., Lundberg, P., Langel, U. & Graslund, A. Differential membrane perturbation caused by the cell penetrating peptide Tp10 depending on attached cargo. *FEBS Lett* **581**, 2389-2393 (2007).

81. Tunnemann, G. et al. Cargo-dependent mode of uptake and bioavailability of TAT-containing proteins and peptides in living cells. *FASEB J* **20**, 1775-1784 (2006).

82. Fischer, R., Waizenegger, T., Köhler, K. & Brock, R. A quantitative validation of fluorophore-labelled cell-permeable peptide conjugates: fluorophore and cargo dependence of import. *Biochimica et Biophysica Acta (BBA) - Biomembranes* **1564**, 365-374 (2002).

83. Duchardt, F., Fotin-Mleczek, M., Schwarz, H., Fischer, R. & Brock, R. A comprehensive model for the cellular uptake of cationic cell-penetrating peptides. *Traffic* **8**, 848-866 (2007).

84. Ter-Avetisyan, G. et al. Cell Entry of Arginine-rich Peptides Is Independent of Endocytosis. *Journal of Biological Chemistry* **284**, 3370-3378 (2009).

85. Magzoub, M., Gr, auml & slund, A. Cell-penetrating peptides: small from inception to application. *Quarterly Reviews of Biophysics* **37**, 147-195 (2004).

86. Berlose, J.P., Convert, O., Derossi, D., Brunissen, A. & Chassaing, G. Conformational and associative behaviours of the third helix of antennapedia homeodomain in membrane-mimetic environments. *Eur J Biochem* **242**, 372-386 (1996).

87. Pouny, Y., Rapaport, D., Mor, A., Nicolas, P. & Shai, Y. Interaction of antimicrobial dermaseptin and its fluorescently labeled analogues with phospholipid membranes. *Biochemistry* **31**, 12416-12423 (1992).

88. Lee, M.T., Hung, W.C., Chen, F.Y. & Huang, H.W. Many-body effect of antimicrobial peptides: On the correlation between lipid's spontaneous curvature and pore formation. *Biophysical Journal* **89**, 4006-4016 (2005).

89. Sun, D., Forsman, J., Lund, M. & Woodward, C.E. Effect of arginine-rich cell penetrating peptides on membrane pore formation and life-times: a molecular simulation study. *Physical Chemistry Chemical Physics* **16**, 20785-20795 (2014).

90. Conner, S.D. & Schmid, S.L. Regulated portals of entry into the cell. *Nature* **422**, 37-44 (2003).

91. Mayor, S. & Pagano, R.E. Pathways of clathrin-independent endocytosis. *Nat Rev Mol Cell Biol* **8**, 603-612 (2007).

92. Fischer, R., Fotin-Mleczek, M., Hufnagel, H. & Brock, R. Break on through to the other side-biophysics and cell biology shed light on cell-penetrating peptides. *Chembiochem* **6**, 2126-2142 (2005).

93. Doherty, G.J. & McMahon, H.T. Mechanisms of endocytosis. *Annu Rev Biochem* **78**, 857-902 (2009).

94. Plapied, L., Duhem, N., des Rieux, A. & Preat, V. Fate of polymeric nanocarriers for oral drug delivery. *Curr Opin Colloid In* **16**, 228-237 (2011).

95. Sakai, N. & Matile, S. Anion-mediated transfer of polyarginine across liquid and bilayer membranes. *J Am Chem Soc* **125**, 14348-14356 (2003).

96. Nakase, I., Takeuchi, T., Tanaka, G. & Futaki, S. Methodological and cellular aspects that govern the internalization mechanisms of arginine-rich cell-penetrating peptides. *Adv Drug Deliv Rev* **60**, 598-607 (2008).

97. Favretto, M.E., Wallbrecher, R., Schmidt, S., van de Putte, R. & Brock, R. Glycosaminoglycans in the cellular uptake of drug delivery vectors - bystanders or active players? *J Control Release* **180**, 81-90 (2014).

98. Tumova, S., Woods, A. & Couchman, J.R. Heparan Sulfate Chains from Glypican and Syndecans Bind the Hep II Domain of Fibronectin Similarly Despite Minor Structural Differences. *Journal of Biological Chemistry* **275**, 9410-9417 (2000).

99. Richard, J.P. et al. Cellular uptake of unconjugated TAT peptide involves clathrin-dependent endocytosis and heparan sulfate receptors. *J Biol Chem* **280**, 15300-15306 (2005).

100. Futaki, S., Nakase, I., Tadokoro, A., Takeuchi, T. & Jones, A.T. Arginine-rich peptides and their internalization mechanisms. *Biochem Soc Trans* **35**, 784-787 (2007).

101. Suzuki, T. et al. Possible existence of common internalization mechanisms among arginine-rich peptides. *J Biol Chem* **277**, 2437-2443 (2002).

102. Ziegler, A. & Seelig, J. Binding and clustering of glycosaminoglycans: a common property of mono- and multivalent cell-penetrating compounds. *Biophys J* **94**, 2142-2149 (2008).

103. Fuchs, S.M. & Raines, R.T. Pathway for polyarginine entry into mammalian cells. *Biochemistry* **43**, 2438-2444 (2004).

104. Nakase, I. et al. Interaction of Arginine-Rich Peptides with Membrane-Associated Proteoglycans Is Crucial for Induction of Actin Organization and Macropinocytosis†. *Biochemistry* **46**, 492-501 (2006).

105. Kawaguchi, Y. et al. Syndecan-4 Is a Receptor for Clathrin-Mediated Endocytosis of Arginine-Rich Cell-Penetrating Peptides. *Bioconjugate Chemistry* **27**, 1119-1130 (2016).

106. Fuki, I.V., Iozzo, R.V. & Williams, K.J. Perlecan Heparan Sulfate Proteoglycan: A NOVEL RECEPTOR THAT MEDIATES A DISTINCT PATHWAY FOR LIGAND CATABOLISM. *Journal of Biological Chemistry* **275**, 25742-25750 (2000).

107. Argyris, E.G. et al. The perlecan heparan sulfate proteoglycan mediates cellular uptake of HIV-1 Tat through a pathway responsible for biological activity. *Virology* **330**, 481-486 (2004).

108. Lambaerts, K., Wilcox-Adelman, S.A. & Zimmermann, P. The signaling mechanisms of syndecan heparan sulfate proteoglycans. *Current Opinion in Cell Biology* **21**, 662-669 (2009).

109. Beckett, K., Franch-Marro, X. & Vincent, J.-P. Glypican-mediated endocytosis of Hedgehog has opposite effects in flies and mice. *Trends in Cell Biology* **18**, 360-363 (2008).

110. Madani, F. et al. Mechanisms of Cellular Uptake of Cell-Penetrating Peptides. *Journal of Biophysics* **2011** (2011).

111. Kaplan, I.M., Wadia, J.S. & Dowdy, S.F. Cationic TAT peptide transduction domain enters cells by macropinocytosis. *J Control Release* **102**, 247-253 (2005).

112. Nakase, I. et al. Cellular uptake of arginine-rich peptides: roles for macropinocytosis and actin rearrangement. *Mol Ther* **10**, 1011-1022 (2004).

113. Fotin-Mleczek, M. et al. Cationic cell-penetrating peptides interfere with TNF signalling by induction of TNF receptor internalization. *J Cell Sci* **118**, 3339-3351 (2005).

114. Erazo-Oliveras, A., Muthukrishnan, N., Baker, R., Wang, T.Y. & Pellois, J.P. Improving the endosomal escape of cell-penetrating peptides and their cargos: strategies and challenges. *Pharmaceuticals (Basel)* **5**, 1177-1209 (2012).

115. Wadia, J.S., Stan, R.V. & Dowdy, S.F. Transducible TAT-HA fusogenic peptide enhances escape of TAT-fusion proteins after lipid raft macropinocytosis. *Nat Med* **10**, 310-315 (2004).

116. Fittipaldi, A. et al. Cell membrane lipid rafts mediate caveolar endocytosis of HIV-1 Tat fusion proteins. *J Biol Chem* **278**, 34141-34149 (2003).

117. Gump, J.M., June, R.K. & Dowdy, S.F. Revised Role of Glycosaminoglycans in TAT Protein Transduction Domain-mediated Cellular Transduction. *Journal of Biological Chemistry* **285**, 1500-1507 (2010).

118. Swanson, J.A. & Watts, C. Macropinocytosis. *Trends in Cell Biology* **5**, 424-428 (1995).

119. Meier, O. et al. Adenovirus triggers macropinocytosis and endosomal leakage together with its clathrin-mediated uptake. *The Journal of Cell Biology* **158**, 1119 (2002).

120. Mishra, A. et al. Translocation of HIV TAT peptide and analogues induced by multiplexed membrane and cytoskeletal interactions. *Proceedings of the National Academy of Sciences* **108**, 16883-16888 (2011).

121. Swanson, J.A. Shaping cups into phagosomes and macropinosomes. *Nat Rev Mol Cell Biol* **9**, 639-649 (2008).

122. Stoorvogel, W., Oorschot, V. & Geuze, H.J. A novel class of clathrin-coated vesicles budding from endosomes. *The Journal of Cell Biology* **132**, 21-33 (1996).

123. Fridolfsson, H.N., Roth, D.M., Insel, P.A. & Patel, H.H. Regulation of intracellular signaling and function by caveolin. *The FASEB Journal* **28**, 3823-3831 (2014).

124. Gruenberg, J., Griffiths, G. & Howell, K.E. Characterization of the early endosome and putative endocytic carrier vesicles in vivo and with an assay of vesicle fusion in vitro. *J Cell Biol* **108**, 1301-1316 (1989).

125. Gruenberg, J. The endocytic pathway: a mosaic of domains. *Nat Rev Mol Cell Biol* **2**, 721-730 (2001).

126. Stenmark, H. Rab GTPases as coordinators of vesicle traffic. *Nat Rev Mol Cell Biol* **10**, 513-525 (2009).

127. Griffiths, G., Hoflack, B., Simons, K., Mellman, I. & Kornfeld, S. The mannose 6-phosphate receptor and the biogenesis of lysosomes. *Cell* **52**, 329-341 (1988).

128. Kobayashi, T. et al. A lipid associated with the antiphospholipid syndrome regulates endosome structure and function. *Nature* **392**, 193-197 (1998).

129. Matsuo, H. et al. Role of LBPA and Alix in multivesicular liposome formation and endosome organization. *Science* **303**, 531-534 (2004).

130. Roth, S.L. & Whittaker, G.R. Promotion of vesicular stomatitis virus fusion by the endosome-specific phospholipid bis(monoacylglycero)phosphate (BMP). *FEBS Letters* **585**, 865-869 (2011).

131. Le Blanc, I. et al. Endosome-to-cytosol transport of viral nucleocapsids. *Nat Cell Biol* **7**, 653-664 (2005).

132. Yang, S.-T., Zaitseva, E., Chernomordik, L.V. & Melikov, K. Cell-Penetrating Peptide Induces Leaky Fusion of Liposomes Containing Late Endosome-Specific Anionic Lipid. *Biophysical Journal* **99**, 2525-2533 (2010).

133. Xu, H. & Ren, D. Lysosomal Physiology. *Annual review of physiology* **77**, 57-80 (2015).

134. Lee, Y.J., Datta, S. & Pellois, J.P. Real-time fluorescence detection of protein transduction into live cells. *J Am Chem Soc* **130**, 2398-2399 (2008).

135. Gillmeister, M.P., Betenbaugh, M.J. & Fishman, P.S. Cellular Trafficking and Photochemical Internalization of Cell Penetrating Peptide Linked Cargo Proteins: A Dual Fluorescent Labeling Study. *Bioconjug Chem* **22**, 556-566 (2011).

136. Appelbaum, Jacob S. et al. Arginine Topology Controls Escape of Minimally Cationic Proteins from Early Endosomes to the Cytoplasm. *Chemistry & Biology* **19**, 819-830 (2012).

137. Burlina, F., Sagan, S., Bolbach, G. & Chassaing, G. A direct approach to quantification of the cellular uptake of cell-penetrating peptides using MALDI-TOF mass spectrometry. *Nat. Protocols* **1**, 200-205 (2006).

138. Paramelle, D. et al. A Straightforward Approach for Cellular-Uptake Quantification. *Angewandte Chemie International Edition* **49**, 8240-8243 (2010).

139. Loison, F. et al. A ubiquitin-based assay for the cytosolic uptake of protein transduction domains. *Mol Ther* **11**, 205-214 (2005).

140. Falnes, P.Ø., Wesche, J. & Olsnes, S. Ability of the Tat Basic Domain and VP22 To Mediate Cell Binding, but Not Membrane Translocation of the Diphtheria Toxin A-Fragment. *Biochemistry* **40**, 4349-4358 (2001).

141. Thorén, P.E.G. et al. Membrane Binding and Translocation of Cell-Penetrating Peptides†. *Biochemistry* **43**, 3471-3489 (2004).

142. Tiriveedhi, V. & Butko, P. A Fluorescence Spectroscopy Study on the Interactions of the TAT-PTD Peptide with Model Lipid Membranes. *Biochemistry* **46**, 3888-3895 (2007).

143. Ruzza, P., Biondi, B., Marchiani, A., Antolini, N. & Calderan, A. Cell-Penetrating Peptides: A Comparative Study on Lipid Affinity and Cargo Delivery Properties. *Pharmaceuticals* **3**, 1045-1062 (2010).

144. Lee, Y.-J., Johnson, G. & Pellois, J.-P. Modeling of the Endosomolytic Activity of HA2-TAT Peptides with Red Blood Cells and Ghosts. *Biochemistry* **49**, 7854-7866 (2010).

145. Leventis, P.A. & Grinstein, S. The Distribution and Function of Phosphatidylserine in Cellular Membranes. *Annual Review of Biophysics* **39**, 407-427 (2010).

146. Cahill, K.E. Molecular Electroporation and the Transduction of Oligoarginines. *Biophysical Journal* **98**, 83a.

147. Tünnemann, G. et al. Live-cell analysis of cell penetration ability and toxicity of oligo-arginines. *Journal of Peptide Science* **14**, 469-476 (2008).

148. El-Sayed, A., Futaki, S. & Harashima, H. Delivery of Macromolecules Using Arginine-Rich Cell-Penetrating Peptides: Ways to Overcome Endosomal Entrapment. *The AAPS Journal* **11**, 13-22 (2009).

149. Lönn, P. et al. Enhancing Endosomal Escape for Intracellular Delivery of Macromolecular Biologic Therapeutics. *Scientific Reports* **6**, 32301 (2016).

150. Erbacher, P., Roche, A.C., Monsigny, M. & Midoux, P. Putative Role of Chloroquine in Gene Transfer into a Human Hepatoma Cell Line by DNA/Lactosylated Polylysine Complexes. *Experimental Cell Research* **225**, 186-194 (1996).

151. Ciftci, K. & Levy, R.J. Enhanced plasmid DNA transfection with lysosomotropic agents in cultured fibroblasts. *Int J Pharm* **218**, 81-92 (2001).

152. Caron, N.J., Quenneville, S.P. & Tremblay, J.P. Endosome disruption enhances the functional nuclear delivery of Tat-fusion proteins. *Biochem Biophys Res Commun* **319**, 12-20 (2004).

153. Shiraishi, T. & Nielsen, P.E. Enhanced delivery of cell-penetrating peptide-peptide nucleic acid conjugates by endosomal disruption. *Nat Protoc* **1**, 633-636 (2006).

154. Forgac, M. Vacuolar ATPases: rotary proton pumps in physiology and pathophysiology. *Nat Rev Mol Cell Biol* **8**, 917-929 (2007).

155. Wharton, S.A., Martin, S.R., Ruigrok, R.W., Skehel, J.J. & Wiley, D.C. Membrane fusion by peptide analogues of influenza virus haemagglutinin. *J Gen Virol* **69 (Pt 8)**, 1847-1857 (1988).

156. Michiue, H. et al. The NH2 terminus of influenza virus hemagglutinin-2 subunit peptides enhances the antitumor potency of polyarginine-mediated p53 protein transduction. *J Biol Chem* **280**, 8285-8289 (2005).

157. Erazo-Oliveras, A. et al. Protein delivery into live cells by incubation with an endosomolytic agent. *Nat Meth* **11**, 861-867 (2014).

158. Cabantous, S., Terwilliger, T.C. & Waldo, G.S. Protein tagging and detection with engineered self-assembling fragments of green fluorescent protein. *Nat Biotechnol* **23**, 102-107 (2005).

159. Cabantous, S. & Waldo, G.S. In vivo and in vitro protein solubility assays using split GFP. *Nat Methods* **3**, 845-854 (2006).

160. Maiolo, J.R., Ottinger, E.A. & Ferrer, M. Specific Redistribution of Cell-Penetrating Peptides from Endosomes to the Cytoplasm and Nucleus upon Laser Illumination. *Journal of the American Chemical Society* **126**, 15376-15377 (2004).

161. Matsushita, M. et al. Photo-acceleration of protein release from endosome in the protein transduction system. *FEBS Letters* **572**, 221-226 (2004).

162. Srinivasan, D. et al. Conjugation to the cell-penetrating peptide TAT potentiates the photodynamic effect of carboxytetramethylrhodamine. *PLoS One* **6**, e17732 (2011).

163. Muthukrishnan, N., Johnson, G.A., Erazo-Oliveras, A. & Pellois, J.P. Synergy Between Cell-Penetrating Peptides and Singlet Oxygen Generators Leads to Efficient Photolysis of Membranes. *Photochemistry and photobiology* (2012).

164. Choi, Y., McCarthy, J.R., Weissleder, R. & Tung, C.-H. Conjugation of a Photosensitizer to an Oligoarginine-Based Cell-Penetrating Peptide Increases the Efficacy of Photodynamic Therapy. *ChemMedChem* **1**, 458-463 (2006).

165. Endoh, T., Sisido, M. & Ohtsuki, T. Spatial regulation of specific gene expression through photoactivation of RNAi. *Journal of Controlled Release* **137**, 241-245 (2009).

166. Lee, Y.C. et al. Binding of synthetic oligosaccharides to the hepatic Gal/GalNAc lectin. Dependence on fine structural features. *Journal of Biological Chemistry* **258**, 199-202 (1983).

167. Mammen, M., Choi, S.-K. & Whitesides, G.M. Polyvalent Interactions in Biological Systems: Implications for Design and Use of Multivalent Ligands and Inhibitors. *Angewandte Chemie International Edition* **37**, 2754-2794 (1998).

168. Kiessling, L.L., Gestwicki, J.E. & Strong, L.E. Synthetic multivalent ligands in the exploration of cell-surface interactions. *Current Opinion in Chemical Biology* **4**, 696-703 (2000).

169. Sung, M., Poon, G.M. & Gariepy, J. The importance of valency in enhancing the import and cell routing potential of protein transduction domain-containing molecules. *Biochim Biophys Acta* **1758**, 355-363 (2006).

170. Torchilin, V.P., Rammohan, R., Weissig, V. & Levchenko, T.S. TAT peptide on the surface of liposomes affords their efficient intracellular delivery even at low temperature and in the presence of metabolic inhibitors. *Proceedings of the National Academy of Sciences* **98**, 8786-8791 (2001).

171. Torchilin, V.P. TAT peptide-modified liposomes for intracellular delivery of drugs and DNA. *Cell Mol Biol Lett* **7**, 265-267 (2002).

172. Torchilin, V.P. et al. Cell transfection in vitro and in vivo with nontoxic TAT peptide-liposome-DNA complexes. *Proc Natl Acad Sci U S A* **100**, 1972-1977 (2003).

173. Tseng, Y.L., Liu, J.J. & Hong, R.L. Translocation of liposomes into cancer cells by cell-penetrating peptides penetratin and tat: a kinetic and efficacy study. *Mol Pharmacol* **62**, 864-872 (2002).

174. Zhao, M., Kircher, M.F., Josephson, L. & Weissleder, R. Differential conjugation of tat peptide to superparamagnetic nanoparticles and its effect on cellular uptake. *Bioconjug Chem* **13**, 840-844 (2002).

175. Koch, A.M., Reynolds, F., Merkle, H.P., Weissleder, R. & Josephson, L. Transport of surface-modified nanoparticles through cell monolayers. *Chembiochem* **6**, 337-345 (2005).

176. Lewin, M. et al. Tat peptide-derivatized magnetic nanoparticles allow in vivo tracking and recovery of progenitor cells. *Nat Biotechnol* **18**, 410-414 (2000).

177. Kircher, M.F. et al. In vivo high resolution three-dimensional imaging of antigen-specific cytotoxic T-lymphocyte trafficking to tumors. *Cancer Res* **63**, 6838-6846 (2003).

178. Phelan, A., Elliott, G. & O'Hare, P. Intercellular delivery of functional p53 by the herpesvirus protein VP22. *Nat Biotechnol* **16**, 440-443 (1998).

179. Johnson, C.R., Morin, P.E., Arrowsmith, C.H. & Freire, E. Thermodynamic analysis of the structural stability of the tetrameric oligomerization domain of p53 tumor suppressor. *Biochemistry* **34**, 5309-5316 (1995).

180. Lee, W. et al. Solution structure of the tetrameric minimum transforming domain of p53. *Nat Struct Biol* **1**, 877-890 (1994).

181. Kawamura, K.S., Sung, M., Bolewska-Pedyczak, E. & Gariepy, J. Probing the impact of valency on the routing of arginine-rich peptides into eukaryotic cells. *Biochemistry* **45**, 1116-1127 (2006).

182. Wang, J. et al. Grb10, a positive, stimulatory signaling adapter in platelet-derived growth factor BB-, insulin-like growth factor I-, and insulin-mediated mitogenesis. *Mol Cell Biol* **19**, 6217-6228 (1999).

183. Chen, M., Won, D.J., Krajewski, S. & Gottlieb, R.A. Calpain and mitochondria in ischemia/reperfusion injury. *J Biol Chem* **277**, 29181-29186 (2002).

184. Kang, H., DeLong, R., Fisher, M.H. & Juliano, R.L. Tat-Conjugated PAMAM Dendrimers as Delivery Agents for Antisense and siRNA Oligonucleotides. *Pharmaceutical Research* **22**, 2099-2106 (2005).

185. Juliano, R.L. Intracellular delivery of oligonucleotide conjugates and dendrimer complexes. *Ann N Y Acad Sci* **1082**, 18-26 (2006).

186. Pantos, A., Tsiourvas, D., Nounesis, G. & Paleos, C.M. Interaction of functional dendrimers with multilamellar liposomes: design of a model system for studying drug delivery. *Langmuir* **21**, 7483-7490 (2005).

187. Kim, J.B. et al. Enhanced transfection of primary cortical cultures using arginine-grafted PAMAM dendrimer, PAMAM-Arg. *J Control Release* **114**, 110-117 (2006).

188. Medina, S.H. & El-Sayed, M.E. Dendrimers as carriers for delivery of chemotherapeutic agents. *Chem Rev* **109**, 3141-3157 (2009).

189. Sheldon, K., Liu, D., Ferguson, J. & Gariepy, J. Loligomers: design of de novo peptide-based intracellular vehicles. *Proc Natl Acad Sci U S A* **92**, 2056-2060 (1995).

190. Singh, D., Kiarash, R., Kawamura, K., LaCasse, E.C. & Gariepy, J. Penetration and intracellular routing of nucleus-directed peptide-based shuttles (loligomers) in eukaryotic cells. *Biochemistry* **37**, 5798-5809 (1998).

191. Kawamura, K.S. et al. In vivo generation of cytotoxic T cells from epitopes displayed on peptide-based delivery vehicles. *J Immunol* **168**, 5709-5715 (2002).

192. Singh, D., Bisland, S.K., Kawamura, K. & Gariepy, J. Peptide-based intracellular shuttle able to facilitate gene transfer in mammalian cells. *Bioconjug Chem* **10**, 745-754 (1999).

193. Dawson, P.E., Muir, T.W., Clark-Lewis, I. & Kent, S.B. Synthesis of proteins by native chemical ligation. *Science* **266**, 776 (1994).

194. Angeles-Boza, A.M., Erazo-Oliveras, A., Lee, Y.J. & Pellois, J.P. Generation of endosomolytic reagents by branching of cell-penetrating peptides: tools for the delivery of bioactive compounds to live cells in cis or trans. *Bioconjug Chem* **21**, 2164-2167 (2010).

195. Rudolph, C. et al. Application of novel solid lipid nanoparticle (SLN)-gene vector formulations based on a dimeric HIV-1 TAT-peptide in vitro and in vivo. *Pharm Res* **21**, 1662-1669 (2004).

196. Lee, S.J., Yoon, S.H. & Doh, K.O. Enhancement of gene delivery using novel homodimeric tat peptide formed by disulfide bond. *J Microbiol Biotechnol* **21**, 802-807 (2011).

197. Elmquist, A. & Langel, U. In vitro uptake and stability study of pVEC and its all-D analog. *Biol Chem* **384**, 387-393 (2003).

198. Purkayastha, N. et al. Enantiomeric and diastereoisomeric (mixed) L/ D-octaarginine derivatives - a simple way of modulating the properties of cell-penetrating peptides. *Chem Biodivers* **10**, 1165-1184 (2013).

199. Verdurmen, W.P. et al. Preferential uptake of L- versus D-amino acid cell-penetrating peptides in a cell type-dependent manner. *Chem Biol* **18**, 1000-1010 (2011).

200. Khafagy, E.-S. et al. Efficiency of cell-penetrating peptides on the nasal and intestinal absorption of therapeutic peptides and proteins. *International Journal of Pharmaceutics* **381**, 49-55 (2009).

201. Rennert, R., Wespe, C., Beck-Sickinger, A.G. & Neundorf, I. Developing novel hCT derived cell-penetrating peptides with improved metabolic stability. *Biochimica et Biophysica Acta (BBA) - Biomembranes* **1758**, 347-354 (2006).

202. Chorev, M. & Goodman, M. Recent developments in retro peptides and proteins--an ongoing topochemical exploration. *Trends Biotechnol* **13**, 438-445 (1995).

203. Chorev, M. The partial retro-inverso modification: a road traveled together. *Biopolymers* **80**, 67-84 (2005).

204. Fischer, P.M. The design, synthesis and application of stereochemical and directional peptide isomers: a critical review. *Curr Protein Pept Sci* **4**, 339-356 (2003).

205. Li, C. et al. Limitations of peptide retro-inverso isomerization in molecular mimicry. *J Biol Chem* **285**, 19572-19581 (2010).

206. Brugidou, J., Legrand, C., Mery, J. & Rabie, A. The retro-inverso form of a homeobox-derived short peptide is rapidly internalised by cultured neurones: a new basis for an efficient intracellular delivery system. *Biochem Biophys Res Commun* **214**, 685-693 (1995).

207. Lyu, P.C., Sherman, J.C., Chen, A. & Kallenbach, N.R. Alpha-helix stabilization by natural and unnatural amino acids with alkyl side chains. *Proc Natl Acad Sci U S A* **88**, 5317-5320 (1991).

208. Jones, S. & Howl, J. Charge delocalisation and the design of novel mastoparan analogues: enhanced cytotoxicity and secretory efficacy of [Lys5, Lys8, Aib10]MP. *Regul Pept* **121**, 121-128 (2004).

209. Chen, F., Ma, B., Yang, Z.C., Lin, G. & Yang, D. Extraordinary metabolic stability of peptides containing alpha-aminoxy acids. *Amino Acids* **43**, 499-503 (2012).

210. Ma, Y., Yang, D., Ma, Y. & Zhang, Y.H. Novel cell-penetrating peptides based on alpha-aminoxy acids. *Chembiochem* **13**, 73-79 (2012).

211. Potocky, T.B., Menon, A.K. & Gellman, S.H. Effects of conformational stability and geometry of guanidinium display on cell entry by beta-peptides. *J Am Chem Soc* **127**, 3686-3687 (2005).

212. Youngblood, D.S., Hatlevig, S.A., Hassinger, J.N., Iversen, P.L. & Moulton, H.M. Stability of cell-penetrating peptide-morpholino oligomer conjugates in human serum and in cells. *Bioconjug Chem* **18**, 50-60 (2007).

213. Foged, C. et al. Cellular uptake and membrane-destabilising properties of alpha-peptide/beta-peptoid chimeras: lessons for the design of new cell-penetrating peptides. *Biochim Biophys Acta* **1778**, 2487-2495 (2008).

214. Jing, X. et al. Membrane adsorption and binding, cellular uptake and cytotoxicity of cell-penetrating peptidomimetics with alpha-peptide/beta-peptoid backbone: effects of hydrogen bonding and alpha-chirality in the beta-peptoid residues. *Biochim Biophys Acta* **1818**, 2660-2668 (2012).

215. Farrera-Sinfreu, J., Giralt, E., Castel, S., Albericio, F. & Royo, M. Cell-penetrating cis-gamma-amino-l-proline-derived peptides. *J Am Chem Soc* **127**, 9459-9468 (2005).

216. Lattig-Tunnemann, G. et al. Backbone rigidity and static presentation of guanidinium groups increases cellular uptake of arginine-rich cell-penetrating peptides. *Nat Commun* **2**, 453 (2011).

217. Rothbard, J.B. et al. Arginine-rich molecular transporters for drug delivery: role of backbone spacing in cellular uptake. *J Med Chem* **45**, 3612-3618 (2002).

218. Qian, Z. et al. Early endosomal escape of a cyclic cell-penetrating peptide allows effective cytosolic cargo delivery. *Biochemistry* **53**, 4034-4046 (2014).

219. Lian, W., Jiang, B., Qian, Z. & Pei, D. Cell-permeable bicyclic peptide inhibitors against intracellular proteins. *J Am Chem Soc* **136**, 9830-9833 (2014).

220. Craik, D.J., Swedberg, J.E., Mylne, J.S. & Cemazar, M. Cyclotides as a basis for drug design. *Expert Opin Drug Discov* **7**, 179-194 (2012).

221. Gould, A., Ji, Y., Aboye, T.L. & Camarero, J.A. Cyclotides, a novel ultrastable polypeptide scaffold for drug discovery. *Current Pharmaceutical Design* **17**, 4294-4307 (2011).

222. Fominaya, J., Bravo, J. & Rebollo, A. Strategies to stabilize cell penetrating peptides for in vivo applications. *Ther Deliv* **6**, 1171-1194 (2015).

223. Holm, T. et al. Retro-inversion of certain cell-penetrating peptides causes severe cellular toxicity. *Biochim Biophys Acta* **1808**, 1544-1551 (2011).

224. Najjar, K., Erazo-Oliveras, A. & Pellois, J.-P. Delivery of Proteins, Peptides or Cell-impermeable Small Molecules into Live Cells by Incubation with the Endosomolytic Reagent dfTAT. e53175 (2015).

225. Hussain, A.F. et al. Targeted Delivery of Dendritic Polyglycerol–Doxorubicin Conjugates by scFv-SNAP Fusion Protein Suppresses EGFR+ Cancer Cell Growth. *Biomacromolecules* **14**, 2510-2520 (2013).

226. Takeuchi, T. et al. Direct and Rapid Cytosolic Delivery Using Cell-Penetrating Peptides Mediated by Pyrenebutyrate. *ACS Chemical Biology* **1**, 299-303 (2006).

227. Sakakibara, D. et al. Protein structure determination in living cells by in-cell NMR spectroscopy. *Nature* **458**, 102-105 (2009).

228. Schwarze, S.R., Hruska, K.A. & Dowdy, S.F. Protein transduction: unrestricted delivery into all cells? *Trends in Cell Biology* **10**, 290-295 (2000).

229. Dietz, G.P.H. & Bδhr, M. Delivery of bioactive molecules into the cell: the Trojan horse approach. *Molecular and Cellular Neuroscience* **27**, 85-131 (2004).

230. Pan, C., Lu, B., Chen, H. & Bishop, C. Reprogramming human fibroblasts using HIV-1 TAT recombinant proteins OCT4, SOX2, KLF4 and c-MYC. *Molecular Biology Reports* **37**, 2117-2124 (2010).

231. Gratton, J. et al. Cell-permeable peptides improve cellular uptake and therapeutic gene delivery of replication-deficient viruses in cells and in vivo. *Nat Med* **9**, 357 - 362 (2003).

232. Massignani, M. et al. Enhanced Fluorescence Imaging of Live Cells by Effective Cytosolic Delivery of Probes. *PLoS One* **5**, e10459 (2010).

233. Erazo-Oliveras, A., Muthukrishnan, N., Baker, R., Wang, T.Y. & Pellois, J.P. Improving the Endosomal Escape of Cell-Penetrating Peptides and Their Cargos: Strategies and Challenges. *Pharmaceuticals* **5**, 1177-1209 (2012).

234. Hoyer, J., Schatzschneider, U., Schulz-Siegmund, M. & Neundorf, I. Dimerization of a cell-penetrating peptide leads to enhanced cellular uptake and drug delivery. *Beilstein Journal of Organic Chemistry* **8**, 1788-1797 (2012).

235. Eguchi, A. et al. Efficient siRNA delivery into primary cells by a peptide transduction domain-dsRNA binding domain fusion protein. *Nat Biotech* **27**, 567-571 (2009).

236. Austin, C.D. et al. Oxidizing potential of endosomes and lysosomes limits intracellular cleavage of disulfide-based antibody–drug conjugates. *Proceedings of the National Academy of Sciences of the United States of America* **102**, 17987-17992 (2005).

237. Dominska, M. & Dykxhoorn, D.M. Breaking down the barriers: siRNA delivery and endosome escape. *Journal of Cell Science* **123**, 1183-1189 (2010).

238. Koivusalo, M. et al. Amiloride inhibits macropinocytosis by lowering submembranous pH and preventing Rac1 and Cdc42 signaling. *The Journal of Cell Biology* **188**, 547-563 (2010).

239. Johnson, L.S., Dunn, K.W., Pytowski, B. & McGraw, T.E. Endosome acidification and receptor trafficking: bafilomycin A1 slows receptor externalization by a mechanism involving the receptor's internalization motif. *Molecular Biology of the Cell* **4**, 1251-1266 (1993).

240. Vercauteren, D. et al. The Use of Inhibitors to Study Endocytic Pathways of Gene Carriers: Optimization and Pitfalls. *Mol Ther* **18**, 561-569 (2010).

241. Rejman, J., Bragonzi, A. & Conese, M. Role of Clathrin- and Caveolae-Mediated Endocytosis in Gene Transfer Mediated by Lipo- and Polyplexes. *Mol Ther* **12**, 468-474 (2005).

242. Sun, X. et al. Development of SNAP-Tag Fluorogenic Probes for Wash-Free Fluorescence Imaging. *Chembiochem* **12**, 2217-2226 (2011).

243. Johnson, J.R., Kocher, B., Barnett, E.M., Marasa, J. & Piwnica-Worms, D. Caspase-Activated Cell-Penetrating Peptides Reveal Temporal Coupling Between Endosomal Release and Apoptosis in an RGC-5 Cell Model. *Bioconjug Chem* **23**, 1783-1793 (2012).

244. Wadia, J.S., Stan, R.V. & Dowdy, S.F. Transducible TAT-HA fusogenic peptide enhances escape of TAT-fusion proteins after lipid raft macropinocytosis. *Nat Med* **10**, 310-315 (2004).

245. Csaszar, E. et al. An automated system for delivery of an unstable transcription factor to hematopoietic stem cell cultures. *Biotechnol Bioeng* **103**, 402-412 (2009).

246. Amsellem, S. et al. Ex vivo expansion of human hematopoietic stem cells by direct delivery of the HOXB4 homeoprotein. *Nat Med* **9**, 1423-1427 (2003).

247. Krosl, J. et al. In vitro expansion of hematopoietic stem cells by recombinant TAT-HOXB4 protein. *Nat Med* **9**, 1428-1432 (2003).

248. Will, E. et al. HOXB4 Inhibits Cell Growth in a Dose-Dependent Manner and Sensitizes Cells Towards Extrinsic Cues. *Cell cycle* **5**, 14-22 (2006).

249. Muthukrishnan, N., Johnson, G.A., Lim, J., Simanek, E.E. & Pellois, J.P. TAT-mediated photochemical internalization results in cell killing by causing the release of calcium into the cytosol of cells. *Biochim Biophys Acta* **1820**, 1734-1743 (2012).

250. Marino, J. et al. Lysosomal and mitochondrial permeabilization mediates zinc(II) cationic phthalocyanine phototoxicity. *The International Journal of Biochemistry & Cell Biology* **45**, 2553-2562 (2013).

251. Pourahmad, J., Hosseini, M.-J., Eskandari, M.R., Shekarabi, S.M. & Daraei, B. Mitochondrial/lysosomal toxic cross-talk plays a key role in cisplatin nephrotoxicity. *Xenobiotica* **40**, 763-771 (2010).

252. Yang, M. et al. Lysosomal membrane permeabilization: Carbon nanohorn-induced reactive oxygen species generation and toxicity by this neglected mechanism. *Toxicology and Applied Pharmacology* **280**, 117-126 (2014).

253. Bird, P.I., Trapani, J.A. & Villadangos, J.A. Endolysosomal proteases and their inhibitors in immunity. *Nat Rev Immunol* **9**, 871-882 (2009).

254. Scharf, B. et al. Annexin A2 binds to endosomes following organelle destabilization by particulate wear debris. *Nat Commun* **3**, 755 (2012).

255. Tung, C.-H., Mueller, S. & Weissleder, R. Novel Branching Membrane Translocational Peptide as Gene Delivery Vector. *Bioorganic & Medicinal Chemistry* **10**, 3609-3614 (2002).

256. Peitz, M., Pfannkuche, K., Rajewsky, K. & Edenhofer, F. Ability of the hydrophobic FGF and basic TAT peptides to promote cellular uptake of recombinant Cre recombinase: A tool for efficient genetic engineering of mammalian genomes. *Proceedings of the National Academy of Sciences* **99**, 4489-4494 (2002).

257. Pellois, J.P. & Muir, T.W. A ligation and photorelease strategy for the temporal and spatial control of protein function in living cells. *Angewandte Chemie* **44**, 5713-5717 (2005).

258. Boukamp, P. et al. Normal keratinization in a spontaneously immortalized aneuploid human keratinocyte cell line. *The Journal of Cell Biology* **106**, 761-771 (1988).

259. Woods, L.K. et al. Comparison of Four New Cell Lines from Patients with Adenocarcinoma of the Ovary. *Cancer Research* **39**, 4449-4459 (1979).

260. Jiang, N., Bénard, C.Y., Kébir, H., Shoubridge, E.A. & Hekimi, S. Human CLK2 Links Cell Cycle Progression, Apoptosis, and Telomere Length Regulation. *Journal of Biological Chemistry* **278**, 21678-21684 (2003).

261. Gonzalez-Vallina, R. et al. Lipoprotein and apolipoprotein secretion by a newborn piglet intestinal cell line (IPEC-1), Vol. 271. (1996).

262. Hunt, M.E., Scherrer, M.P., Ferrari, F.D. & Matz, M.V. Very Bright Green Fluorescent Proteins from the Pontellid Copepod <italic>Pontella mimocerami</italic>. *PLoS One* **5**, e11517 (2010).

263. Wessel, D. & Flügge, U.I. A method for the quantitative recovery of protein in dilute solution in the presence of detergents and lipids. *Analytical Biochemistry* **138**, 141-143 (1984).

264. Najjar, K., Erazo-Oliveras, A., Brock, D.J., Wang, T.-Y. & Pellois, J.-P. An l- to d-Amino Acid Conversion in an Endosomolytic Analog of the Cell-penetrating

Peptide TAT Influences Proteolytic Stability, Endocytic Uptake, and Endosomal Escape. *Journal of Biological Chemistry* **292**, 847-861 (2017).

265. Zorko, M. & Langel, Ü. Cell-penetrating peptides: mechanism and kinetics of cargo delivery. *Advanced Drug Delivery Reviews* **57**, 529-545 (2005).

266. Gupta, B., Levchenko, T.S. & Torchilin, V.P. Intracellular delivery of large molecules and small particles by cell-penetrating proteins and peptides. *Advanced Drug Delivery Reviews* **57**, 637-651 (2005).

267. Stewart, M.P. et al. In vitro and ex vivo strategies for intracellular delivery. *Nature* **538**, 183-192 (2016).

268. Munyendo, W.L.L., Lv, H., Benza-Ingoula, H., Baraza, L.D. & Zhou, J. Cell Penetrating Peptides in the Delivery of Biopharmaceuticals. *Biomolecules* **2**, 187-202 (2012).

269. Palm, C., Jayamanne, M., Kjellander, M. & Hällbrink, M. Peptide degradation is a critical determinant for cell-penetrating peptide uptake. *Biochimica et Biophysica Acta (BBA) - Biomembranes* **1768**, 1769-1776 (2007).

270. Elmquist, A. & Langel, Ü. in Biological Chemistry, Vol. 384 387 (2003).

271. Lindgren, M.E., HÄLlbrink, M.M., Elmquist, A.M. & Langel, Ü. Passage of cell-penetrating peptides across a human epithelial cell layer in vitro. *Biochemical Journal* **377**, 69-76 (2004).

272. Pujals, S., Sabidó, E., Tarragó, T. & Giralt, E. all-D proline-rich cell-penetrating peptides: a preliminary in vivo internalization study. *Biochemical Society Transactions* **35**, 794-796 (2007).

273. Youngblood, D.S., Hatlevig, S.A., Hassinger, J.N., Iversen, P.L. & Moulton, H.M. Stability of Cell-Penetrating Peptide−Morpholino Oligomer Conjugates in Human Serum and in Cells. *Bioconjug Chem* **18**, 50-60 (2007).

274. Wender, P.A. et al. The design, synthesis, and evaluation of molecules that enable or enhance cellular uptake: Peptoid molecular transporters. *Proceedings of the National Academy of Sciences of the United States of America* **97**, 13003-13008 (2000).

275. Mitchell, D.J., Steinman, L., Kim, D.T., Fathman, C.G. & Rothbard, J.B. Polyarginine enters cells more efficiently than other polycationic homopolymers. *The Journal of Peptide Research* **56**, 318-325 (2000).

276. Derossi, D. et al. Cell Internalization of the Third Helix of the Antennapedia Homeodomain Is Receptor-independent. *Journal of Biological Chemistry* **271**, 18188-18193 (1996).

277. Pujals, S., Fernández-Carneado, J., Ludevid, M.D. & Giralt, E. D-SAP: A New, Noncytotoxic, and Fully Protease Resistant Cell-Penetrating Peptide. *ChemMedChem* **3**, 296-301 (2008).

278. Olson, E.S. et al. In vivo characterization of activatable cell penetrating peptides for targeting protease activity in cancer. *Integrative biology : quantitative biosciences from nano to macro* **1**, 382-393 (2009).

279. Brugidou, J., Legrand, C., Mery, J. & Rabie, A. The Retro-inverso Form of a Homeobox-Derived Short Peptide Is Rapidly Internalized by Cultured Neurons: A New Basis for an Efficient Intracellular Delivery System. *Biochemical and Biophysical Research Communications* **214**, 685-693 (1995).

280. Mueller, J., Kretzschmar, I., Volkmer, R. & Boisguerin, P. Comparison of Cellular Uptake Using 22 CPPs in 4 Different Cell Lines. *Bioconjug Chem* **19**, 2363-2374 (2008).

281. Verdurmen, Wouter P.R. et al. Preferential Uptake of L- versus D-Amino Acid Cell-Penetrating Peptides in a Cell Type-Dependent Manner. *Chemistry & Biology* **18**, 1000-1010 (2011).

282. Tunnemann, G. et al. Live-cell analysis of cell penetration ability and toxicity of oligo-arginines. *Journal of peptide science : an official publication of the European Peptide Society* **14**, 469-476 (2008).

283. Erazo-Oliveras, A. et al. The Late Endosome and Its Lipid BMP Act as Gateways for Efficient Cytosolic Access of the Delivery Agent dfTAT and Its Macromolecular Cargos. *Cell chemical biology* **23**, 598-607 (2016).

284. Fretz, Marjan M. et al. Temperature-, concentration- and cholesterol-dependent translocation of L- and D-octa-arginine across the plasma and nuclear membrane of CD34+ leukaemia cells. *Biochemical Journal* **403**, 335-342 (2007).

285. Peitz, M., Pfannkuche, K., Rajewsky, K. & Edenhofer, F. Ability of the hydrophobic FGF and basic TAT peptides to promote cellular uptake of recombinant Cre recombinase: a tool for efficient genetic engineering of mammalian genomes. *Proc Natl Acad Sci U S A* **99**, 4489-4494 (2002).

286. Colpitts, T.M., Moore, A.C., Kolokoltsov, A.A. & Davey, R.A. Venezuelan equine encephalitis virus infection of mosquito cells requires acidification as well as

mosquito homologs of the endocytic proteins Rab5 and Rab7. *Virology* **369**, 78-91 (2007).

287. Bucci, C., Thomsen, P., Nicoziani, P., McCarthy, J. & van Deurs, B. Rab7: A Key to Lysosome Biogenesis. *Molecular Biology of the Cell* **11**, 467-480 (2000).

288. Kobayashi, T. et al. Late endosomal membranes rich in lysobisphosphatidic acid regulate cholesterol transport. *Nat Cell Biol* **1**, 113-118 (1999).

289. Kobayashi, T., Startchev, K., Whitney Andrew, J. & Gruenberg, J. Localization of Lysobisphosphatidic Acid-Rich Membrane Domains in Late Endosomes. *Biological Chemistry* **382**, 483-485 (2001).

290. Piper, R.C. & Katzmann, D.J. Biogenesis and Function of Multivesicular Bodies. *Annual Review of Cell and Developmental Biology* **23**, 519-547 (2007).

291. Duchardt, F., Fotin-Mleczek, M., Schwarz, H., Fischer, R. & Brock, R. A Comprehensive Model for the Cellular Uptake of Cationic Cell-penetrating Peptides. *Traffic* **8**, 848-866 (2007).

292. Tamai, M. et al. IN VITRO AND IN VIVO INHIBITION OF CYSTEINE PROTEINASES BY EST, A NEW ANALOG OF E-64. *Journal of Pharmacobio-Dynamics* **9**, 672-677 (1986).

293. Vidard, L., Rock, K.L. & Benacerraf, B. The generation of immunogenic peptides can be selectively increased or decreased by proteolytic enzyme inhibitors. *The Journal of Immunology* **147**, 1786-1791 (1991).

294. Poon, G.M. & Gariepy, J. Cell-surface proteoglycans as molecular portals for cationic peptide and polymer entry into cells. *Biochemical Society Transactions* **35**, 788-793 (2007).

295. Al-Taei, S. et al. Intracellular traffic and fate of protein transduction domains HIV-1 TAT peptide and octaarginine. Implications for their utilization as drug delivery vectors. *Bioconjug Chem* **17**, 90-100 (2006).

296. Nishi, K. & Saigo, K. Cellular Internalization of Green Fluorescent Protein Fused with Herpes Simplex Virus Protein VP22 via a Lipid Raft-mediated Endocytic Pathway Independent of Caveolae and Rho Family GTPases but Dependent on Dynamin and Arf6. *Journal of Biological Chemistry* **282**, 27503-27517 (2007).

297. Wang, T.-Y. et al. Membrane oxidation enables the cytosolic entry of polyarginine cell-penetrating peptides. *Journal of Biological Chemistry* (2016).

298. Kosuge, M., Takeuchi, T., Nakase, I., Jones, A.T. & Futaki, S. Cellular internalization and distribution of arginine-rich peptides as a function of extracellular peptide concentration, serum, and plasma membrane associated proteoglycans. *Bioconjug Chem* **19**, 656-664 (2008).

299. Thompson, D.B., Cronican, J.J. & Liu, D.R. Engineering and identifying supercharged proteins for macromolecule delivery into mammalian cells. *Methods Enzymol* **503**, 293-319 (2012).

300. Freire, J.M., Santos, N.C., Veiga, A.S., Da Poian, A.T. & Castanho, M.A. Rethinking the capsid proteins of enveloped viruses: multifunctionality from genome packaging to genome transfection. *FEBS J* **282**, 2267-2278 (2015).

301. Tanaka, G. et al. CXCR4 Stimulates Macropinocytosis: Implications for Cellular Uptake of Arginine-Rich Cell-Penetrating Peptides and HIV. *Chemistry & Biology* **19**, 1437-1446 (2012).

APPENDIX A

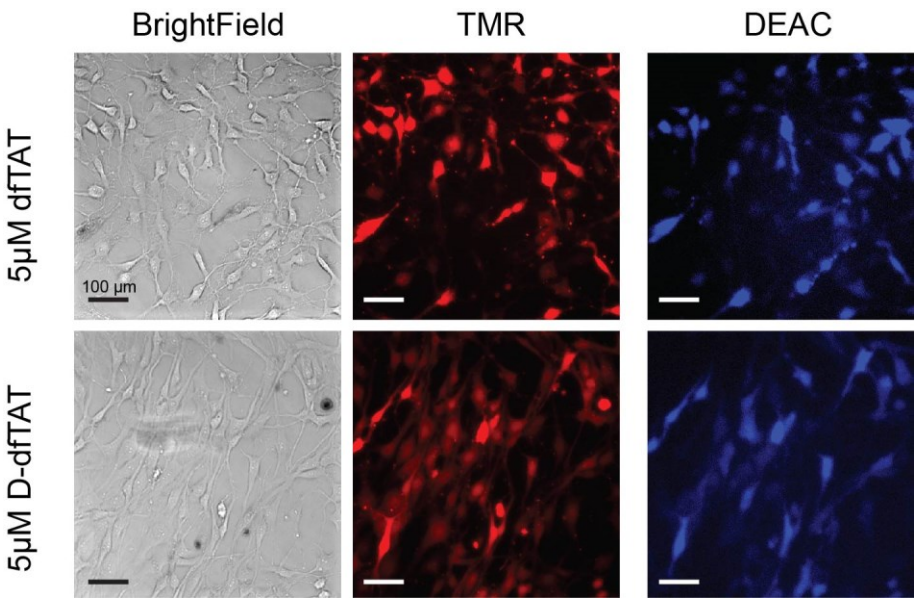

Figure A-1 D-dfTAT similar to dfTAT can efficiently delivery the DEAC-k5 peptide into the cytosolic space of MCH58 cells. MCH58 cell were co-incubated with dfTAT or D-dfTAT (5 μM) in presence of DEAC-k5 (10 μM). Cells were washed and then imaged using a 20X objective. Scale bars, 100 μm.

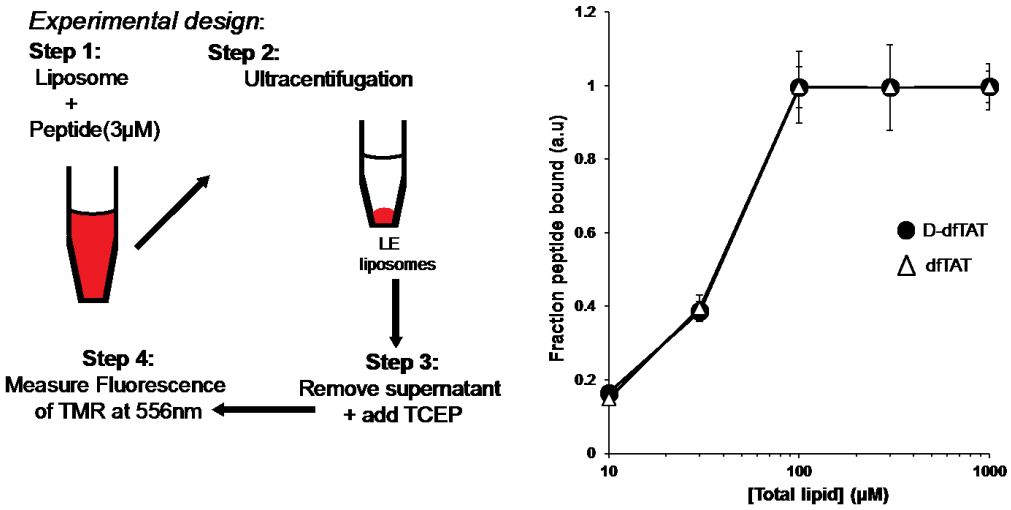

Figure A-2 Comparison of the affinity of dfTAT and D-dfTAT to LE MLVs. L.E MLVs at various concentrations were incubated with either peptide at 3 μM. The samples were spun down at 87,000 RPM and the fluorescence signal in the supernatant corresponding to the unbound peptide was quantified.

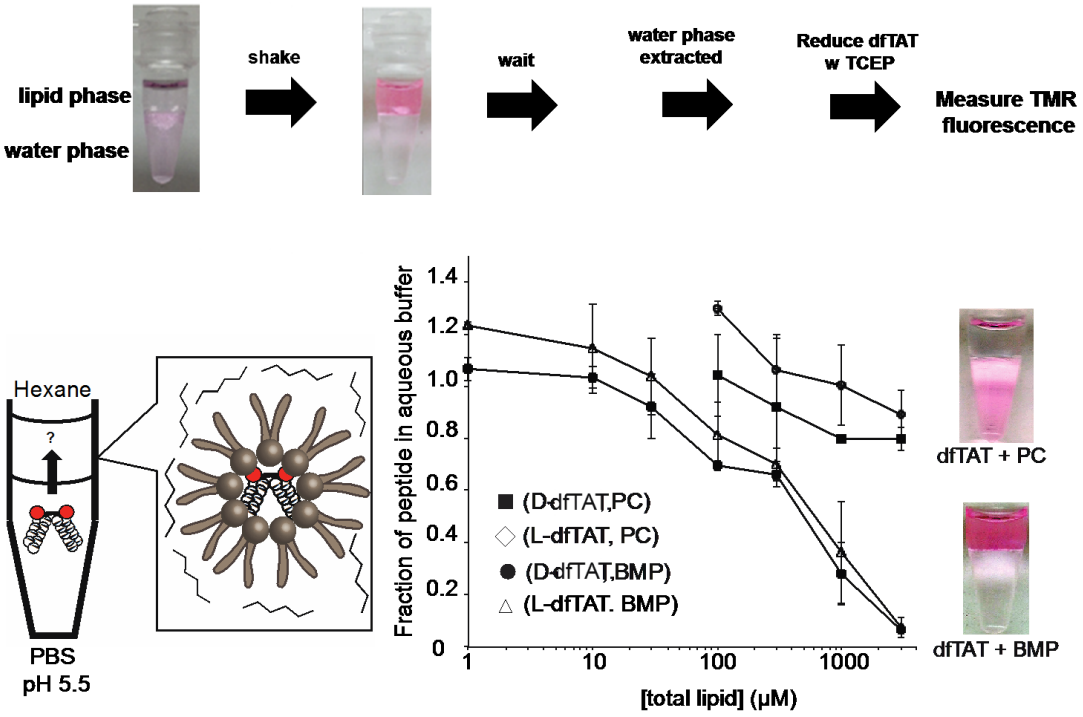

Figure A-3 BMP-mediated partitioning of dfTAT and D-dfTAT into hexanes. dfTAT or D-dfTAT (3 μM) was incubated in a phosphate buffer (pH 5.5) and the lipids PC or PG dissolved in hexanes at various concentrations were added. The fraction of peptide that remain in the aqueous phase upon mixing was measured by fluorescence spectroscopy.

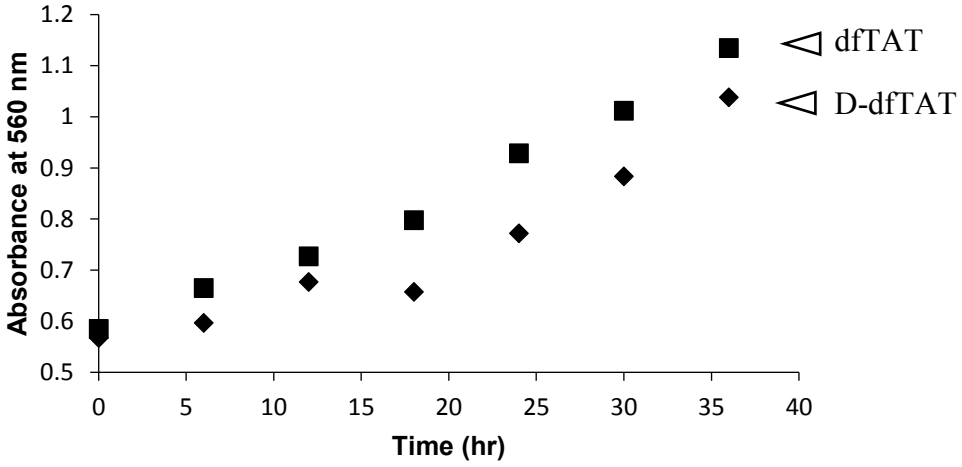

Figure A-4 D-dfTAT does not impact cellular proliferation of HeLa cells after cytosolic delivery. Proliferation assays. HeLa cells were incubated with 5 μM dfTAT or D-dfTAT for 1h. Cells were then incubated in growth media (DMEM/10%FBS) and cellular proliferation was monitored over a period of 36 h using a MTT assay.

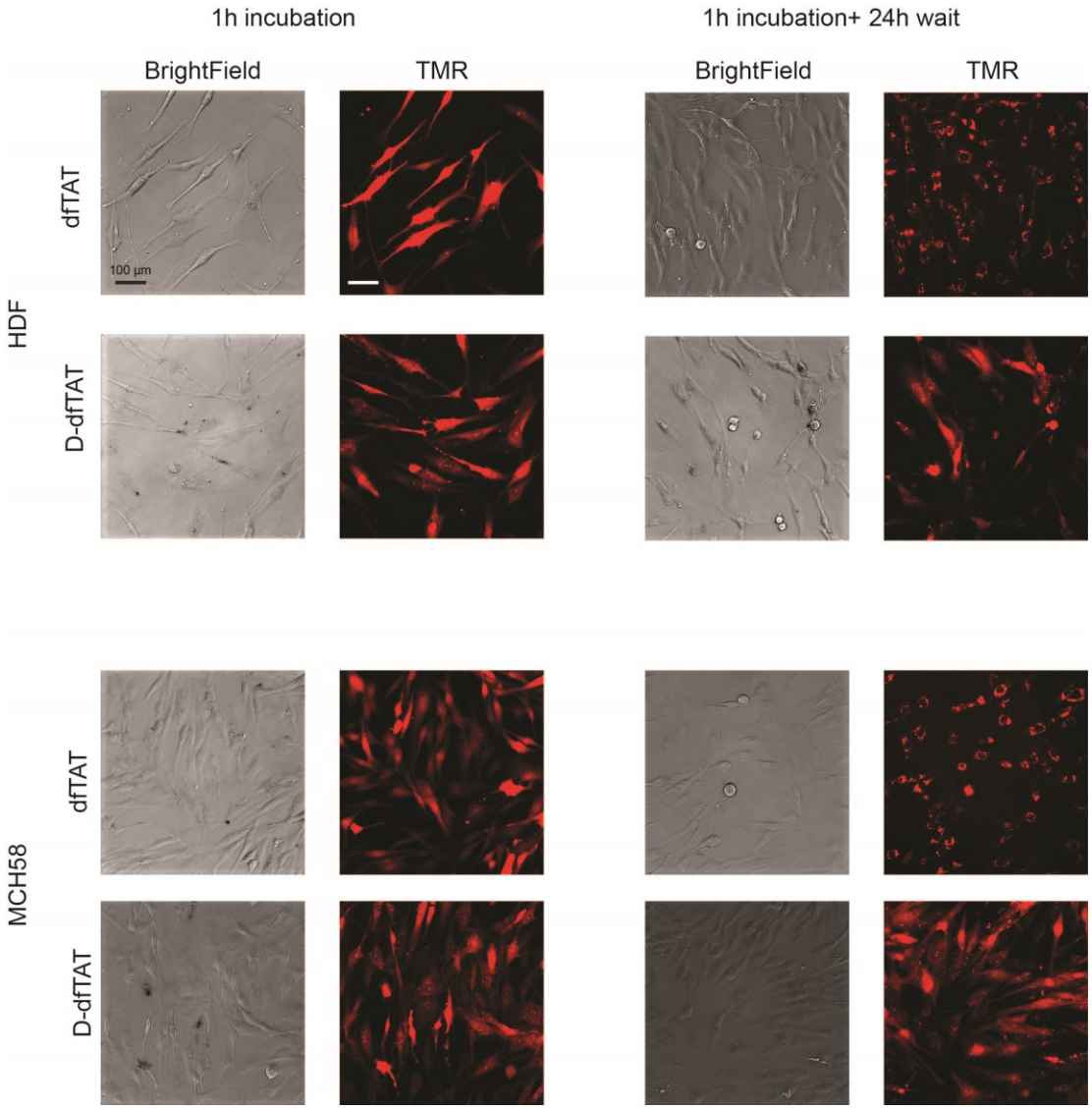

Figure A-5 Images for the RNA-seq analysis of HDF and MCH58 cells treated with D-dfTAT or dfTAT (5µM) in L-15 for 1 h. HDF and MCH58 cell were incubated with dfTAT or D-dfTAT (5 µM). Cells were washed and then either immediately imaged or returned to the incubator and images 24 h post-delivery. Scale bars, 100 µm.